Modeling and analysis of cell population dynamics: application to the early development of ovarian follicles

THÈSE

présentée et soutenue publiquement le 26 Septembre 2019

pour l'obtention du

Doctorat de Sorbonne Université
(mention mathématiques appliquées)

par

Frédérique ROBIN

Après l'avis favorable des rapporteurs :
  M. Jan HASENAUER *(Universität Bonn)*
  M. Marc HOFFMAN *(Université Paris-Dauphine)*

COMPOSITION DU JURY :

Rapporteur	M. Marc HOFFMAN	Université Paris-Dauphine
Examinateur	M. Nicolas CHAMPAGNAT	INRIA Nancy Grand-Est IECL, Université de Lorraine
Examinateur	Mme Marie DOUMIC	INRIA Paris LJLL, Sorbonne Université
Examinateur	M. Pierre GABRIEL	Université de Versailles St-Quentin-en-Yvelines
Examinateur	Mme Béatrice LAROCHE	INRA Jouy en Josas
Directeur de thèse	Mme Frédérique CLÉMENT	INRIA Saclay-Île de France
Directeur de thèse	M. Romain YVINEC	INRA Centre Val de Loire

Équipe-projet MƎDISIM
INRIA Saclay-Île de France

Abstract

This thesis aims to design and analyze population dynamics models dedicated to the dynamics of somatic cells during the early stages of ovarian follicle growth. The model behaviors are analyzed through theoretical and numerical approaches, and the calibration of parameters is performed by proposing maximum likelihood strategies adapted to our specific dataset. A non-linear stochastic model, that accounts for the joint dynamics of two cell types (precursors and proliferative), is dedicated to the activation of follicular growth. In particular, we compute the extinction time of precursor cells. A rigorous finite state projection approach is implemented to characterize the system state at extinction. A linear multitype age-structured model for the proliferative cell population is dedicated to the early follicle growth. The different types correspond here to the spatial cell positions. This model is of decomposable kind; the transitions are unidirectional from the first to the last spatial type. We prove the long-term convergence for both the stochastic Bellman-Harris model and the multi-type McKendrick-VonFoerster equation. We adapt existing results in a context where the Perron-Frobenius theorem does not apply, and obtain explicit analytical formulas for the asymptotic moments of cell numbers and stable age distribution. We also study the well-posedness of the inverse problem associated with the deterministic model.

keys-words: cell population dynamics; multi-type deterministic and stochastic renewal process; first hitting time; long time behavior; inverse problem; parameter calibration

Résumé

Cette thèse vise à concevoir et analyser des modèles de dynamique des populations dédiés à la dynamique des cellules somatiques durant les premiers stades de la croissance du follicule ovarien. Les comportements des modèles sont analysés par des approches théoriques et numériques, et les valeurs des paramètres sont calibrées en proposant des stratégies de maximum de vraisemblance adaptées à notre jeu de données spécifique. Un modèle stochastique non linéaire, qui tient compte de la dynamique conjointe entre deux types cellulaires (précurseur et prolifératif), est dédié à l'activation de la croissance folliculaire. Une approche rigoureuse de projection par états finis est mise en œuvre pour caractériser l'état du système à l'extinction et calculer le temps d'extinction des cellules précurseurs. Un modèle linéaire multi-type structuré en âge, appliquée à la population de cellules prolifératives, est dédié à la croissance folliculaire précoce. Les différents types correspondent ici aux positions spatiales des cellules. Ce modèle est de type décomposable ; les transitions sont unidirectionnelles du premier vers le dernier type. Nous prouvons la convergence en temps long du modèle stochastique de Bellman-Harris et de l'équation de McKendrick-VonFoerster multi-types. Nous adaptons les résultats existants dans le cas où le théorème de Perron-Frobenius ne s'applique pas, et nous obtenons des formules analytiques explicites pour les moments asymptotiques des nombres de cellules et de la distribution stationnaire en âge. Nous étudions également le caractère bien posé du problème inverse associé au modèle déterministe.

mots-clés: dynamique de populations cellulaires ; processus de renouvellement multi-type stochastique et déterministe ; premier temps d'atteinte ; comportement en temps long ; problème inverse ; calibration de paramètres

Acknowledgements

I would like to thank all the people who contributed to the success of this thesis and who helped me in writing this report.

First of all, I would like to thank my two thesis supervisors, Frédérique Clément and Romain Yvinec, for proposing this subject and guiding me throughout these three years. I would also like to thank my two reporters, Marc Hoffman and Jan Hasenauer, for reviewing my work and for their constructive comments. I also thank Nicolas Champagnat, Marie Doumic, Pierre Gabriel and Béatrice Laroche for agreeing to complete my thesis jury (and for their very prompt response!).

Many thanks to Danielle Monniaux and Véronique Cadoret for their enriching discussions on the ovarian follicle. Many thanks also to Marie Postel, for her support and patience during the building of the numerical scheme, and to Béatrice Laroche, for her help and discussion on the inverse problem. A special mention to the BIOS team, thank you for your warm welcome every time I was in Tours. Last but not least, a big thank you to the whole MΞDISIM team: your warm welcome has brightened up the part of my thesis I spent among you. I almost came to find some charms in mechanics!

Thank you to my friends and family, for whom the ovarian follicle has almost no mystery left! This thesis would not have had the same taste without my Touraine hosts, Sylvie and Jean: your hospitality and your making your house mine leaves me with many fond memories. I would also like to thank my parents and sister for their support in the distance from Toulouse. A second special mention for my older brother, for his support during these three years, even though they have not been easier for you. Finally, I would like to thank you from the bottom of my heart for your unwavering support, both emotional and scientific, thank you Thibaut for sharing this with me.

VI

Contents

Chapter I

Introduction

This thesis aims to model and analyze the cell population dynamics involved during the formation of a tissue which is a rare example of morphogenesis[1] taking place in a mammal adult organism: the ovarian follicle. Specifically, the stages of its development that we consider are tightly linked with issues addressed by developmental biology[2]. The main cellular mechanisms involved during the early stages of the development of the ovarian follicle are cell division and transition (differentiation). In the first section, we present a non-exhaustive list of models dedicated to represent cell population dynamics. In the second section, we present our biological object of study, the ovarian follicle. The last section is dedicated to the contributions and the outline of this thesis.

I.1   Modeling cell dynamics

Before introducing the cell dynamics models used in this thesis, we briefly explain our views on the general purpose and steps of the building of a model. A model of a system is a theoretical description that can help to understand how the system works, or how it might work[3]. Regarding the mathematical modeling of cell dynamics, it appears that the whole process follows the classical scheme of model-building:

1) analyze qualitatively (and sometimes quantitatively) the biological system under consideration,

2) choose the level of description (cell average solely or structured population by age, size, etc.) and the formalism (deterministic or stochastic),

3) propose a mathematical formalism to describe the phenomenon,

4) simulate and/or analyze the model (extinction times, long time behaviors, remarkable trajectories, etc.),

5) and confront the (mathematical) model with the biological situation.

---

[1]Morphogenesis: the origin and development of morphological characteristics. (*Oxford dictionnary definition*)
[2]The study of the processes by which organisms grow and develop.
[3]In the words of George Box: *"all models are wrong but some of them are useful"* [2].

These steps are the common thread of the analyses carried out in this thesis.

Unlike some tissue formation mechanisms such as tumor growth, few models have been proposed to represent the cell dynamics involved in the early development of an ovarian follicle. We mainly rely on the model introduced in [1], where the authors use a stochastic non-linear model structured in age (continuous variable) and space (discrete variable). Later, a scaling limit in space of this model was studied in [3] that will be detailed in Chapter 4. This model was the starting point for this thesis and is presented in details at the beginning of Chapter 3. To analyze some characteristic quantities (division time, cell flow), we reformulate this model in the framework of linear branching models (multi-type Bellman-Harris). In this section, we describe the models dedicated to cell population dynamics at different levels of description (cell average, structured cell average, cell based and structured cell based). We focus in particular on models that take into account age which were used during this thesis.

I.1.1   Cell average models *(used in Chapter 2 and 3)*

The simplest way to describe the changes in cell dynamics is to follow the total cell number along time. The natural associated mathematical formalism is the Ordinary Differential Equations system (ODEs), and the cell number dynamics is then described as a continuous function of time. We introduce the main models using the finite dimension differential system formalism to describe biological structures. We also present the modeling principles used during this thesis to represent the cell dynamics involved in the formation of an ovarian follicle.

The best-known (and simplest) model of population dynamics is likely to be the Malthus growth model, published in 1798 [4]. In this model, the change in speed of a growing population is proportional to the population size (see Table I.1). A generalized version of this model is the Birth–Death model, where the population growth speed depends on both the population, and time-dependent birth and death rates. The Malthus growth and Birth–Death models belong to the linear model category in which each individual cell is independent from the other cells. Since the ODE formalism only represents the total cell number, it may be unnatural to think about independency between cells. This property is a direct consequence of the additivity property verified by the linear ODE solution: suppose that we have a population of N_0 cells at time $t = 0$ following the Malthusian growth of parameter α. We consider the trajectory of each individual in the population and thus solve N_0 systems following the Malthus law of parameter α and starting from 1 cell. Each of these systems verifies $N(t) = e^{\alpha t}$, for all $t \geq 0$. Summing those N_0 systems (by additivity property of the linear ODE solution), we obtain that the total cell number is, for all time $t \geq 0$, the expected function $N(t) = N_0 e^{\alpha t}$, which is the trajectory of population following a Malthus growth and composed initially of N_0 cells.

The cell interactions are actually important mechanisms that allow the development of a tissue. These various mechanisms are generally the result of local events: for example, chemical factors exchanged to help develop a tissue or growth factors that are collected from the local cell environment to facilitate the tissue development. The integration of interaction phenomena leads to non-linear models that are often difficult to analyze or even simulate. With regard to the ODE formalism, the cell interactions can be represented by a non-local term consisting of nonlinear functions depending on the population size. For example, in the

Gompertz or Verhulst models, the population grows modulated by an intrinsic growth rate until it reaches a steady state K corresponding to the maximal capacity of the population (see Table I.1). Another case of cell interactions is treated in Chapter 2 where we propose a model dedicated to the ovarian follicle activation.

Model	ODE formalism	Parameters
Malthus	$m'(t) = \alpha m(t)$	α: Malthus parameter
Birth–Death	$m'(t) = (b(t) - d(t))m(t)$	$b(t)$: birth rate, $d(t)$: death rate
Gompertz model	$m'(t) = b \ln\left(\frac{K}{m(t)}\right) m(t)$	b: intrinstic birth rate, K: steady state
Verhulst model (logistic growth)	$m'(t) = r\left(1 - \frac{K}{m(t)}\right) m(t)$	r: intrinstic birth rate, K: steady state

Table I.1 – Instancies of some cell dynamics ODE models.

One may want to represent different cell types such as proliferative versus quiescent cells. This can be done with the compartmental models, which consist in decomposing the cell population into subcategories representing the selected cell types that explain the whole population dynamics. For example, the famous Lotka–Volterra model [5, 6], that represents birth and competition events occuring between two species, is a good example of compartmental model with interaction phenomena. As regards to cell dynamics, the biological ODE system models presented in [7, 8] aim to analyze the differentiation and proliferation of cells involved in the primary immune response. In [9], a model reproducing the sequence of divisions that a pool of progenitor cells undergoes during the neurogenesis phase is presented. In [10], a time-dependent compartmental model is proposed to describe the cellular changes in the somatic cells during the terminal phase of the ovarian follicle development. The model compartements represent the proliferative, the differentiated (exited from the cell-cycle) and the apoptotic cells.

Once the model is built, some dynamic characteristics can be inferred from its outputs such as the doubling time (for example, equals to $\ln(2)/\alpha$ for the Malthus growth model). Another way to characterize the trajectories of the built-model is to the search for some remarkable solutions such as the Exponentially Stable States.

a)   Exponentially stable state analysis: general theory

One can look for solutions of the form $t \mapsto Ne^{\lambda t}$. In particular, when λ is positive and maximal (Malthus parameter), such solutions are called the Exponentially Stable States (ESS) and $N \in \mathbb{R}^N$ is then called the stable state vector. The ESS indicates that the overall cell number evolves exponentially following a Malthusian growth.

Once a remarkable solution of a dynamical system has been found, it may be interesting to investigate to what extent this trajectory is representative of the system: do all the trajectories of the dynamical system converge towards this particular trajectory (attractive solution)? If so, after how long? A technique based on a function called entropy has been used to measure the difference between two solutions of a dynamical system over time. If this entropy function

has appropriate properties, then the convergence of the two solutions towards each other can be shown. This method is called the Generalized Relative Entropy (GRE) [11, 12]. We introduce below some elements to understand its application to the specific case of a finite dimensional system inspired by the work done in Section 6.3 of [12].

Suppose that the dynamics of the whole population $n(t) := (n_k(t))_{k \in [\![1,K]\!]}$ follows the ODE system:

$$\frac{d}{dt}n(t) = An(t), \quad n(t = 0; \theta) = n_0 \tag{I.1}$$

where $A \in M_K(\mathbb{R})^4$ is a positive matrix, i.e. for all $1 \leq i, j \leq K$, the element A_{ij} of matrix A verifies $A_{ij} > 0$. We can thus apply the Perron-Frobenius theorem (see [13] for the positive matrix case) and deduce that A has a first (maximum) eigenvalue $\lambda > 0$ associated with a positive right eigenvector $N \in \mathbb{R}^K$, and a positive left eigenvector $\phi \in \mathbb{R}^K$, such that:

$$\begin{cases} AN = \lambda N, & N_i > 0 \text{ for all } i \in [\![1, K]\!], \\ \phi A = \lambda \phi, & \phi_i > 0 \text{ for all } i \in [\![1, K]\!]. \end{cases}$$

The eigenvalue λ, called the Perron–Frobenius eigenvalue (or sometimes the Malthus parameter), is simple and both right and left eigenspaces associated with λ are one-dimensional. In addition, if

$$\sum_{k=1}^{K} N_k = \sum_{k=1}^{K} N_k \phi_k = 1,$$

then the triple (λ, N, ϕ) is unique.

To obtain the convergence of solutions to Eq. (I.1) towards a remarkable solution (here $t \mapsto Ne^{\lambda t}$), we use a Lyapunov function, i.e. a quantity that decreases along the trajectories of the equation being considered. For the linear system Eq. (I.1), the quantity

$$\mathcal{H}[x] := \sum_{k=1}^{K} \phi_k N_k H\left(\frac{x_k}{N_k}\right), \tag{I.2}$$

is classically used and called the Generalized Relative Entropy. Thus, to compare the trajectories solution of Eq. (I.1) to the ESS, the function x is the quantity $t \mapsto n(t)e^{-\lambda t}$, which allows a better control of the trajectory n with respect to time avoiding explosion when t goes to $+\infty$.

Proposition I.1 (Proposition 6.6, extract from [12])**.** *Let λ be the first (positive) eigenvalue associated with matrix A and H be a convex function on $\mathbb{R}$, then the solution to Eq. (I.1) satisfies*

$$\frac{d}{dt}\mathcal{H}[n(t)e^{-\lambda t}] \leq 0.$$

The use of the right and left eigenvectors N and ϕ, the convexity of function H and the positivity of matrix A are crucial to prove that the GRE decreases with respect to time. On the contrary, the positivity of the Malthus parameter λ is not required here to prove the GRE decays. In Chapter 3, we will deal with a case of non-positive matrix A.

From the decay of the entropy $\mathcal{H}[n(t)e^{-\lambda t}]$ with respect to time, one can deduce that the trajectory $t \mapsto n(t)e^{-\lambda t}$ approaches the right eigenvector N in a given norm. For example, taking $H(x) = x^2$, a convergence with square norm can then be deduced.

---

[4]$M_K(\mathbb{R})$ is the set of real square matrices of size K.

Proposition I.2 (Proposition 6.5, extract from [12])**.** *For any solution of the ODE* (I.1)*, we have*

$$\mu := \sum_{k=1}^{K} \phi_k n_k(t) e^{-\lambda t} = \sum_{k=1}^{K} \phi_k n_k(0),$$

$$\sum_{k=1}^{K} \phi_k |n_k(t)| e^{-\lambda t} \le \sum_{k=1}^{K} \phi_k |n_k(0)|,$$

and there is a constant $\kappa > 0$ such that

$$\sum_{k=1}^{K} \phi_k N_k \left(\frac{n_k(t)e^{-\lambda t} - \mu N_k}{N_k} \right)^2 \le \sum_{k=1}^{K} \phi_k N_k \left(\frac{n_k(0) - \mu N_k}{N_k} \right)^2 e^{-\kappa t}.$$

Thus, all the trajectories solution of the ODE (I.1) converge to the remarkable solution $t \mapsto N e^{\lambda t}$ at the exponentially speed of parameter κ up to a constant μ (that depends on the initial condition). The κ value can be estimated thanks to a discrete Poincaré inequality (see details in Lemma 6.2 in [14]).

According to Remark 6.2 of [12], it happens that the GRE approach holds also for $M-$matrices[5]. In the next part, we focus on the special case of nonnegative matrix, which is a case encoutered in Chapter 3.

b) Stable state analysis: illustration of a failure case of the general theory

We present in this part an example of ODE system for which the general theory of stable state analysis cannot be applied: suppose that a cell population dynamics is ruled by the ODE system below

$$\frac{d}{dt} n(t) = C n(t), C = \begin{pmatrix} b_1 - d_1 & 0 & \dots & 0 & 2K_{I \to 1} \\ K_{1 \to 2} & b_2 - d_2 & \dots & 0 & 0 \\ \vdots & \vdots & \ddots & \vdots & \vdots \\ 0 & 0 & \dots & b_{I-1} - d_{I-1} & 0 \\ 0 & 0 & \dots & K_{I-1 \to I} & b_I - d_I \end{pmatrix},$$

where $n(t) = (n_i(t))_{i \in [\![1,I]\!]}$. Each component n_i of the vector n represents the cell number in state i (the system contains $I \in \mathbb{N}$ states). The $b_i \in \mathbb{R}_+$, $i \in [\![1, I]\!]$, represent the birth rates while the $d_i \in \mathbb{R}_+$, $i \in [\![1, I]\!]$, are the death rates. The $K_{i \to i+1} \in \mathbb{R}_+$ terms are the transition rates from state i to state $i + 1$.

Since matrix C may be nonnegative, the stable state analysis presented above cannot be directly applied. Nevertheless, we can follow the general scheme and thus first turn to the existence of a maximal eigenvalue for matrix C. The Perron-Frobenius theorem tell us that:

Theorem I.1 (The Perron–Frobenius theorem, strong form (p.82 of [15]))**.** *Let $B \in M_n(\mathbb{R})$ be a nonnegative irreducible matrix. Then, the spectral radius $\rho(B)$[6] is a simple eigenvalue of B associated with positive eigenvectors. Moreover, $\rho(B) > 0$.*

---

[5]A $M-$matrix is a matrix whose off-diagonal entries are nonpositive ($Z-$matrix) with real part eigenvalues are nonnegative.

[6]We recall that the spectral radius of a matrix B is defined as $\rho(B) := \max_{k \in [\![1,n]\!]}\{|\lambda_k|\}$, where $\lambda_1, \cdots \lambda_n$ are the eigenvalues of matrix B.

We recall below the definition of a reducible matrix:

Definition I.1 (Reducible/irreducible matrix, p.30 of [15])**.** *A square matrix A is said reducible if there exists a nontrivial partition $\{1, \cdots, n\} = I \cup J$ such that $(i, j) \in I \times J$ implies $a_{ij} = 0$. In other words, a matrix A is said reducible if there exists a permutation matrix P such that PAP^{-1} is of block-triangular form:*

$$\begin{pmatrix} B & C \\ 0_{p,n-p} & D \end{pmatrix}$$

with $1 \geq p \geq n - 1$.
A matrix that is not reducible is called irreducible.

If $b_i > d_i$ and $K_{i \to i+1} > 0$ for all $i \in [\![1, I]\!]$, then matrix C is a nonnegative irreducible matrix. We can apply the Perron–Frobenius theorem and deduce that there exists a unique maximal eigenvalue associated with positive eigenvectors. Due to the existence of some null elements of matrix C, the proof of Proposition I.1 needs to be adapted.
If there exists $i \in [\![1, I]\!]$ such that $K_{i \to i+1} = 0$, then matrix C is reducible and the Perron–Frobenius theorem cannot be applied to prove the existence of a unique maximal eigenvalue (and its associated positive eigenvectors). We detail this situation below since it is encoutered in Chapter 3.
We assume that $I = 4$ and that only $K_{4 \to 1} = 0$ ($K_{i \to i+1} > 0$ for all $i \in [\![1, 3]\!]$). The cell number n is thus solution of

$$\frac{d}{dt}n(t) = \widetilde{C}n(t), \quad \widetilde{C} = \begin{pmatrix} b_1 - d_1 & 0 & 0 & 0 \\ K_{1 \to 2} & b_2 - d_2 & 0 & 0 \\ 0 & K_{2 \to 3} & b_3 - d_3 & 0 \\ 0 & 0 & K_{3 \to 4} & b_4 - d_4 \end{pmatrix}. \tag{I.3}$$

In this case, the eigenvalues can be directly read on matrix $\widetilde{C}$ diagonal (see Eq. (I.3)): note that the eigenvalues may be negative and the uniqueness of a maximum eigenvalue is not guaranteed without additional information on the parameters. For some parameter values, it may happen that the maximum eigenvalue has a multiplicity greater that one. In such a case, one can show by direct computation that the leading order of the solution of Eq. (I.3) is $t^\alpha e^{e^{\lambda t}}$ with α equals to the multiplicity of λ minus one. Hence, the ESS ansatz is not always valid for Eq. (I.3).
Supposing that, for the rest of the proof, the eigenvalue $\lambda = b_3 - d_3$ is the only maximum eigenvalue, we build the eigenvectors N and ϕ associated with matrix $\widetilde{C}$ ($\widetilde{C}N = \lambda N$ and $\phi\widetilde{C} = \lambda\phi$). The eigenvector N verifies the linear system

$$\begin{pmatrix} \lambda - b_1 + d_1 & 0 & 0 & 0 \\ K_{1 \to 2} & \lambda - b_2 + d_2 & 0 & 0 \\ 0 & K_{2 \to 3} & 0 & 0 \\ 0 & 0 & K_{3 \to 4} & \lambda - b_4 + d_4 \end{pmatrix} N = 0.$$

We thus obtain

$$\forall i \in \{1, 2\}, N_i = 0 \text{ and } K_{3 \to 4}N_3 + (\lambda - b_4 + d_4)N_4 = 0.$$

By using the classical normalization hypothesis for the eigenvectors ($\sum_{i=1}^{4} N_i = 1$), we fix uniquely N_3 and N_4.

On the other hand, the dual vector ϕ verifies

$$\begin{pmatrix} \lambda - b_1 + d_1 & K_{1\to 2} & 0 & 0 \\ 0 & \lambda - b_2 + d_2 & K_{2\to 3} & 0 \\ 0 & 0 & 0 & K_{3\to 4} \\ 0 & 0 & 0 & \lambda - b_4 + d_4 \end{pmatrix} \phi^T = 0.$$

We obtain a recurrence equation for ϕ_i, $i \in [\![1,4]\!]$:

$$\begin{cases} (\lambda - b_1 + d_1)\phi_1 + K_{1\to 2}\phi_2 = 0, \\ (\lambda - b_2 + d_2)\phi_2 + K_{2\to 3}\phi_3 = 0, \end{cases} \text{ and } \phi_4 = 0.$$

We fix in a unique way ϕ using the following renormalization hypothesis:

$$\sum_{i=1}^{4} \phi_i N_i = \phi_3 N_3 = 1.$$

One can consider an entropy approach to show the convergence of all trajectories n to the (intermediate) state $e^{\lambda t} N$. Since the left and right eigenvectors are not positive, the entropy function proposed in the usual theoretical framework (Eq. (I.2)) cannot be used in this case and must be adapted. We tackle this issue in Chapter 3 (in the more general context of infinite differential systems).

In this subsection, we have just seen that a first way to model and analyze a biological system consists in selecting suitable structuring states that are markers of a biological function (cell types) and that have a significant role in population dynamics. The result is a differential system with a finite size of K. When K becomes very large, the analysis of the model often becomes very complicated and finally calls for another formalism where the structuring states are described by continuous variables.

I.1.2 Structuring physiological variables at the population level *(used in Chapter 3 to 5)*

Structured population models first appeared almost two hundred years after the first average population models. The structuring state generally chosen corresponds either to a physiological characteristic that changes continuously over the life of the individual (size, age, size increment, etc.) or fixed at birth (genetic mutations). Some of those models were constructed from the discrete differential system by applying a method named continuum limit (see for instance [16, 17]). However, the models were built most of the time from scratch. During this thesis, we focus on age-dependent models and therefore present a non-exhaustive state-of-the-art of the different approaches considered in that case.

a) The McKendrick–VonFoerster and renewal equations

The age-structured models have the particularity of assuming two biological properties: the dynamic behavior of each individual is independent of that of his or her parents and an

individual's ability to reproduce or die does not depend on past experience [18]. The initial genesis of age-structured models is too complex to be described here, but the reader can refer to [19] for a complete presentation.

We solely introduce the partial differential equation (PDE) model named as McKendrick-VonFoerster (MK-VF) equation. First introduced by McKendrick in 1926 for demographic studies [20], it was reintroduced almost 30 years later by Von-Foerster in a cellular biology context without any link to the first model [21]. It is now known as the McKendrick–VonFoerster equation [19], and consists of a non-conservative transport equation with a non-local term at the boundary condition:

$$\begin{cases} \partial_t \rho(t,a) + \partial_a \rho(t,a) = -\delta(a)\rho(t,a) \\ \rho(t,0) = \int_0^{+\infty} \mu(a)\rho(t,a)da, \\ \rho(0,a) = \rho_0(a) \end{cases}$$

where δ and μ are continuous positive functions defined on $\mathbb{R}_+$ corresponding to the death and birth rates, respectively. The age-structured population is represented by the density function $\rho(t,\cdot) \in \mathbf{L}^1(\mathbb{R}_+)$. The initial condition ρ_0 is usually assumed to belong to the $\mathbf{L}^1(\mathbb{R}_+)$ space. Another classical assumption is often made on the death rate:

$$\lim_{a \to +\infty} \int_0^a \delta(s)ds = +\infty. \tag{I.4}$$

Hence, the probability that an individual is still alive at age a verifies $\exp(-\int_0^a \delta(s)ds)$ and assumption (I.4) guarantee that this individual eventually dies.

This model is a special case where the structuring variable evolves at the same speed as time. There exist other models representing the evolution of temporal variables such as maturation that do not evolve at the same speed as time (see for instance the cell maturation models [22, 23, 24]). Interestingly, the Leslie model [25] which corresponds to an age and time-discrete version of the MK–VF model was also proposed after the first introduction of the MK–VF. A retrospective link between these two models is proposed in [16] where the author uses the continuum limit to move from Leslie's model to the MK–VF model.

The MK–VF model is mainly a demographic model. In this thesis, we focus on its "cell model" counterpart known as the renewal equation. The renewal equation is a special case of the MK–VF where the death rate is linked to the birth rate:

$$\begin{cases} \partial_t \rho(t,a) + \partial_a \rho(t,a) = -b(a)\rho(t,a), \\ \rho(t,0) = 2\int_0^{+\infty} b(a)\rho(t,a)da, \\ \rho(0,a) = \rho_0(a), \end{cases} \tag{I.5}$$

where both ρ_0 and $\rho(t,\cdot)$ belongs to the $\mathbf{L}^1(\mathbb{R}_+)$ space. The function b is supposed to be positive and represents the division rate. It usually belongs to the $\mathcal{C}(\mathbb{R}_+)$ space (the set of continuous functions) but we also consider the case of non-negative functions belonging to the space $\mathcal{C}_c(\mathbb{R}_+)$ (the set of continuous compactly supported functions) in Chapter 5. In the same way as the MK–VF, the probability that an individual has not divided at age a verifies

$$\mathbb{P}[\tau \geq a] = \exp\left(-\int_0^a b(s)ds\right).$$

If one wants to model a population in which all cells eventually divide (non quiescent cells), the following hypothesis is necessary

$$\lim_{a \to +\infty} \int_0^a b(s)ds = +\infty. \tag{I.6}$$

Both the MK–VF and the renewal equation have been extensively studied and modified since their introduction. Regarding the theoretical studies, general results based on operator theory can be found in [26, 18]; [19, 27] provide analytical solutions using the method of characteristics. In the case of the renewal equation, this representation formula has the form

$$\rho(t,a) = \begin{cases} \rho_0(a-t) \exp\left(-\int_{a-t}^a b(s)ds\right) & \text{when } a \geq t \\ \rho(t-a,0) \exp\left(-\int_0^a b(s)ds\right) & \text{when } a \leq t. \end{cases} \tag{I.7}$$

(see the details of the proof in Chapter 5). Note that this formula still depends on the ρ function. However, this particular shape helps to design a numerical scheme [28]. Other methods are also available: escalator boxcar train (see for instance [29, 30]), finite-difference method (see for instance [31, 32]) and finite-volume method [33], presented in Chapter 3. A review of the main numerical schemes available for the age-structured equations can be found in [32].

More recently, studies have been done on measure solutions. They consider measure initial conditions such as Dirac mass instead of the classical $\mathbf{L}^1$ function. Such conditions allow to consider synchronized initial conditions and will be more widely discussed in Chapter 5. In [34, 35, 36, 37], the authors study the existence and uniqueness of such solutions while numerical approaches are proposed in [38, 39].

b)   The Lotka integral equation

Even before the first appearance of the age-structured PDE model, Sharpe and Lotka introduced in 1911 a model dedicated to the age distribution of a population [40]. Their aim was to represent the age fluctuation based on demographic observations: *"certain age-distributions will practically never occur"* [40]. This model links the number of births per unit time B to the fraction l of individuals surviving to age a :

$$B(t) = \int_0^t B(t-a)l(a)b(a)da.$$

The function b is the birth rate per capita for mother of age a. Based on the other observation that *"there must be a limiting stable type about which the actual distribution varies, and towards which it tends to return if through any agency disturbed therefrom"*, they assume an exponential solution $B(t) = Qe^{rt}$ and deduce the Fredholm integral equation, called the characteristic equation [41],

$$\int_0^t e^{-ra}l(a)b(a)da = 1.$$

Sharpe and Lotka laid the foundations for the well-known result of the convergence of all the trajectories to an exponential stable state, but did not provide any clues for the proof. The proof of this result was ultimately demonstrated in 1941 by Feller [42] and calls for tools belonging to the renewal theory approach. Another proof based on group theory was proposed

later in [41].

The true "renewal equation" term refers to the integral equation of the form

$$u(t) = g(t) + \int_0^t u(t-x)f(x)ds. \tag{I.8}$$

Eq. (I.8) is a linear Volterra equation of the second kind where f is sometimes called the kernel and g is a source term. This type of equation appears under different forms mainly in population theory, the theory of industrial replacement and self-renewing aggregates, and are usually analyzed and solved by Laplace transform techniques. The term renewal equation used above and referring to a MK–FV like equation is thus a little abusive although the two models are the same. A way to pass from the MK–FV equation to the Lotka integral can be found p.148 of [18]. It consists in injecting the representation formula obtained with the method of characteristics (Eq. (I.7)) into the boundary condition of PDE (I.5):

$$\rho(t,0) = \underbrace{2 \int_t^{+\infty} b(a)\rho_0(a-t) \exp\left(-\int_{a-t}^a b(s)ds\right) da}_{\text{source term}}$$

$$+ 2\int_0^t \rho(t-a,0) \underbrace{b(a)\exp\left(-\int_0^a b(s)ds\right)}_{\text{kernel}} da \tag{I.9}$$

In Chapter 5, we apply the same method to pass from a multi-type MK–FV like equation to the integral equation.

c) Stable state analysis

Again, one way to analyze the differential system is to look for remarkable solutions and then see if these particular solutions are attractive (i.e. any trajectory converges towards these solutions in long time). The range of remarkable solutions usually studied for differential systems of infinite dimension are the solutions with separable variables, and the renewal equation (I.5) does not deviate from the rule. We are therefore interested in the stationary age profile, anticipated by Sharpe and Lotka, $(t,a) \mapsto \hat{\rho}(a)e^{\lambda t}$: the stationary age profile is multiplied by exponential growth. One can obtain the well-known eigenvalue problem by injecting such a solution in Eq. (I.5):

$$\begin{cases} \dfrac{d}{da}\hat{\rho}(a) = -(b(a) + \lambda)\hat{\rho}(a), \\ \hat{\rho}(0) = 2\displaystyle\int_0^{+\infty} b(a)\hat{\rho}(a)da. \end{cases} \tag{I.10}$$

This non-local differential equation is easily solved by hand: for all $a \geq 0$,

$$\hat{\rho}(a) = \hat{\rho}(0)\exp\left(-\int_0^a (\lambda + b(s))ds\right). \tag{I.11}$$

The solution of Eq. (I.10) is expected to belong to the $\mathbf{L}_1(\mathbb{R}_+)$ space. A common assumption for that is that Eq. (I.6) is verified.

To analyze the convergence of the trajectories towards the stationary age profile, a generalized entropy method can again be used (see previous sub-section). Again, the dual problem will be necessary for building a weighted–$\mathbf{L}^1$ set in which convergence will be shown. We briefly recall here how to build such a problem. Let $\mathcal{L}$ the operator associated with Eq. (I.5) by: for any function $\rho(t,\cdot)$ solution of Eq. (I.5), $\partial_t\rho(t,\cdot) = \mathcal{L}\rho(t,\cdot)$. The dual operator $\mathcal{L}^D$ is then defined as: for any test function $\phi \in \mathcal{C}_c\left(\mathbb{R}_+\right)$,

$$< \mathcal{L}\rho(t,\cdot), \phi > = < \rho(t,\cdot), \mathcal{L}^D\phi > .^7$$

Hence, we deduce from Eq. (I.5) that for any $\phi \in \mathcal{C}_c\left(\mathbb{R}_+\right)$,

$$\int_0^{+\infty} \left(\mathcal{L}\rho(t,a)\right)\phi(a)da = -\int_0^{+\infty} \partial_a\rho(t,a)\phi(a)da - \int_0^{+\infty} b(a)\rho(t,a)\phi(a)da.$$

Applying an integration by part and using the boundary condition of Eq. (I.5), we deduce that

$$\int_0^{+\infty} \left(\mathcal{L}\rho(t,a)\right)\phi(a)da = \int_0^{+\infty} \rho(t,a)\left[\partial_a + (2\phi(0) - 1)b(a)\right]\phi(a)da$$

and conclude that $\mathcal{L}^D = \partial_a + (2\phi(0)-1)b(\cdot)$. The dual problem associated with the trajectory $\bar{\rho}(t,a) \mapsto \hat{\rho}(a)e^{\lambda t}$ therefore verifies

$$< \bar{\rho}(t,\cdot), \mathcal{L}^D\phi > = \lambda < \bar{\rho}(t,\cdot), \phi > = < \mathcal{L}\bar{\rho}(t,\cdot), \phi > .$$

The dual problem associated with the stationary problem (I.10) is thus defined as:

$$\frac{d}{da}\phi(a) - (\lambda + b(a))\phi(a) = -2\phi(0)b(a). \tag{I.12}$$

The uniqueness of the triplet $(\lambda, \hat{\rho}, \phi)$ in the continuous case is shown by a direct proof:

Theorem I.2 (Theorem extract from [43])**.** *Assume that b is a continuous non-negative function on $\mathbb{R}_+$ verifiying Eq.* (I.6)*. Then, there exists a unique triplet $(\lambda, \hat{\rho}, \phi)$ solution of the problems* (I.10)*-*(I.12) *such that*

$$\int_0^{+\infty} \hat{\rho}(a)da = \int_0^{+\infty} \hat{\rho}(a)\phi(a)da = 1.$$

In addition, both the eigenvalue λ and the eigenfunctions $\hat{\rho}$ and ϕ are positive.

Proof. The condition $\int_0^{+\infty} \hat{\rho}(a)da = 1$ ensures that $\hat{\rho}(0) \neq 0$. Hence, injecting Eq. (I.11) in the boundary condition of the eigenproblem, we deduce the characteristic equation

$$f(\lambda) := 2\int_0^{+\infty} b(a)\exp\left(-\int_0^a (\lambda + b(s)ds)\right)da = 1. \tag{I.13}$$

Since f is a stricly decreasing function satisfying $f(0) = 2$ and $\lim_{\lambda \to +\infty} f(\lambda) = 0$ (using the dominated convergence theorem), we obtain the uniqueness of the solution of $f(\lambda) = 1$ from the intermediate value theorem. It gives that $\hat{\rho}$ is unique thanks to the normalization condition $\int_0^{+\infty} \hat{\rho}(a)da = 1$. In addition, the solution of the dual problem (I.12) is classically

$$\phi(a) = 2\phi(0)\int_0^{+\infty} b(s)\exp(-\int_s^u (\lambda + b(u)du))ds.$$

The uniqueness is deduced from the normalization condition $\int_0^{+\infty} \hat{\rho}(a)\phi(a)da = 1$. □

---

[7] The scalar product $< \cdot, \cdot >$ is the $\mathbf{L}^1$–scalar product defined as $< f, g > = \int f(a)g(a)da$.

Note that Eq. (I.6) is a sufficient but not necessary assumption to obtain the existence of a positive eigenvalue λ. Indeed, if after a given age $A_{\max} \in \mathbb{R}_+$ cells do not divide, then we have

$$f(0) = 2\left[1 - \exp\left(-\int_0^{A_{\max}} b(s)ds\right)\right],$$

that could be less than 1. In that case, there exist no positive eigenvalue λ that verifies Eq. (I.13).

The renewal equation is one of the few examples of structured equations where a constructive method is applied to prove the existence and uniqueness of the triplet of eigenelements. In more complex cases such as ones involving either integro-differential equations (e.g. size equations [44] or for a review on the subject [12, 11]) or periodic PDEs (e.g. cell cycle [45]), the Krein–Rutman theorem is applied to obtain the same type of results. In these cases, explicit solutions are unknown and thus numerical solutions are constructed by the iterated power method (see [17, 46]).

Using the entropy function, similar to the entropy function (I.2) used in the finite dimension case, defined as, for $n \in \mathbf{L}_1(\mathbb{R}_+)$ and a convex function H defined on $\mathbb{R}_+$

$$\mathcal{H}[n] := \int_0^{+\infty} \phi(a)\hat{\rho}(a)H\left(\frac{n(a)}{\hat{\rho}(a)}\right)da,$$

one can deduce the exponential convergence:

Theorem I.3 (see [43]). *Suppose that there exists κ such that for all $a \geq 0$, $2b(a) \geq \kappa\frac{\phi(a)}{\phi(0)}$, then all the solutions of Eq. (I.5) satisfy*

$$\int_0^{+\infty} |\rho(t,a)e^{-\lambda t} - \mu\hat{\rho}(a)|\phi(a)da \leq e^{-\kappa t}\int_0^{+\infty} |\rho_0(a) - \mu\hat{\rho}(a)|\phi(a)da$$

where $\mu := \int_0^{+\infty} \phi(a)\rho_0(a)da$.

In this subsection, we have just seen how the level of description of a model dedicated to cell dynamics can be increased by including continuous structuring variables such as age. More and more models tend to combine several structuring variables together to explain cell dynamic behaviors, see for instance [47, 12, 48, 18]. A next natural step is to wonder whether the cell variability observed is important, or not, to describe the cell population dynamics. To that end, some people have enriched the deterministic models by representing the difference existing between cells with statistical approaches such as Non-Linear Mixed Effect models. These models aim to estimate the cell-specific parameters for each individual following a same behavioral law (see for instance [49, 50]). For others, part of the observed variability comes from our current inability to capture the full range of behaviors of each individual in a population and make it totally predictable. This part of variability, of lack of certainty about individual trajectories, is the motivation for stochastic models (see [51] *p.2: Why is stochastic modelling necessary?*). In particular, stochastic models allow to represent the dynamics of small size population where the uncertainty on each individual trajectory cannot be hidden by the whole population.

I.1.3 Cell-based level *(used in Chapter 2)*

We go back to our common thread: modeling and analyzing the cell number changes taking into account this time the incompleteness of our knowledge about the individual cell behaviors. Starting simple and assuming that our cell population is only dividing (pure birth process), we deduce that the total cell number at each division increases by $+1$, which makes us naturally introduce the building blocks of most of stochastics models: the counting processes.

Definition I.2 (Counting process, according to Definition 1.1 of [52])**.** *The process $N(t)$ is a counting process if $N(0) = 0$ and N is constant except for jumps of size $+1$.*

A counting process, as its name suggests, therefore counts the number of events (positive jumps) taking place during a given time interval. To clarify how these jumps occur, Definition I.2 may be supplemented as follows to correspond to the homogeneous Poisson process definition:

Definition I.3 (Homogeneous Poisson process, according to Definition 1.2 of [52])**.** *A counting process is a Poisson process if it satisfies the following conditions:*

1. *let t_k, $k = 0, \ldots, m$ be a time sequence, then the increments $N(t_k) - N(t_{k-1})$, for all $k = 1, \ldots, m$ are independent random variables.*

2. *for all $s \geq 0$, $N(t + s) - N(t)$ does not depend on t.*

Two fundamental properties of Poisson processes that are the starting point for many analyses and algorithms can be derived from this definition.

1) the number of events during a time interval $[t, s]$ follows a Poisson law of parameter λ: $\mathbb{P}[N(s) - N(t) = k] = \frac{(\lambda(s-t))^k}{k!} e^{-\lambda(s-t)}$ (see the proof of Theorem 1.3 of [52] for details).

2) the time jump law follows an exponential law $\mathcal{E}(\lambda)$ of parameter λ: for all $k \in \mathbb{N}^*$, let S_k be the time of the kth event, that is, the kth jump of N. We fix $S_0 = 0$ and then define the kth jump time $T_k := S_k - S_{k-1}$, for all $k \in \mathbb{N}^*$. Then, $T_k \sim \mathcal{E}(\lambda)$.[8]

A Poisson process of intensity λ verifies $N_t = \mathcal{Y}(\lambda t)$, where $\mathcal{Y}$ is a unit Poisson process. Property 1) fully characterizes the cell number N_t (e.g., the mean and variance cell number are equal to λt) while property 2) fully characterizes the time sequence ($S_k \sim \Gamma(k, \lambda)$). It should be noted that this first model involves a linear growth of cells, very far from the Malthusian model introduced previously, and allows the spontaneous generation!

The Poisson process can be improved in two ways: either by changing the time scale (i.e., the law of jump times) or the jump scale. With regard to cell dynamics, it is more natural to first try to modulate the time sequence S_k since the jumps size corresponds exactly to one division[9]. The leverage point for varying the sequence of jump times is the intensity of the

---

[8]The T_k law can be easily deduced from the law of the event number:

$$\mathbb{P}[T_k \leq t] = 1 - \mathbb{P}[T_k > t] = 1 - \mathbb{P}\left[N_{T_k} - N_{T_{k-1}} = 0\right] = 1 - e^{-\lambda t}.$$

[9]The jump size modulation leads to some well-known process such as the Brownian process.

Poisson process, that may depends at time t on the behavior of the counting process prior to time t or other stochastic inputs, usually the external noise or the environment, represented here by the stochastic process Z. For measurability issues, Z is assumed to be *càdlàg*[10]. Let $E \subset \mathbb{N}^d$ a state space, $D_E[0, \infty)$ the space of *càdlàg* and $D^c[0, \infty)$ the space of counting paths (zero at time zero and constant except for jumps $+1$). The intensity λ is required to satisfy the following condition (see Condition 1.9 of [52]):

$$\lambda : [0, +\infty) \times D_E[0, +\infty) \times D^c[0, +\infty) \to [0, +\infty)$$

is measurable, nonanticipating and $\int_0^t \lambda(s, z, v)ds < \infty$ for all $t \geq 0$, $z \in D_E[0, +\infty)$ and $v \in D^c[0, +\infty)$. We thus obtain the Poisson process of intensity λ

$$N_t = \mathcal{Y}\left(\int_0^t \lambda(s, Z_s, N_s)ds\right).$$

By drawing an analogy between the jump intensity and the event occurrence speed, we naturally come to propose a cell division model where the intensity is proportional to the population size (see Malthus' model presented in section I.1.1): $\lambda(s, Z, N) = \lambda N$, resulting in $N_t = \mathcal{Y}\left(\int_0^t \lambda N_s ds\right)$.

To finish with this round of modeling cell dynamics with Poisson processes, as with differential systems, we may want to build stochastic models that take into account several cellular mechanisms (division, death, transition) and/or cellular types (quiescent, proliferative, precursor, etc.). Such models can be designed by combining different counting processes modulated by different intensities. The whole cell number $X = (X_t)_{t \geq 0}$ consists then of a vector of m processes $(X_t = (X_t^m)_{m \in [\![1,M]\!]})$ corresponding to a given cell property (type), and process X follows a Stochastic Differential Equation (SDE):

$$X_t = X_0 + \sum_{m=1}^{M} \xi_m \mathcal{Y}_m\left(\int_0^t \lambda_m(X_s)ds\right), \tag{I.14}$$

where M is the total number of cell mechanisms (events), $\mathcal{Y}_m$ are M independent unit Poisson processes. Each cell event is represented by a vector ξ_m corresponding to the jump size (e.g., $+1$ for a division, -1 for a death, etc.) and an intensity λ_m corresponding to the speed of the mechanism. An example can be found in Chapter 2.

One way to analyze such processes is to use a characterization by another type of process, the martingales, defined as follows

Definition I.4 (Martingale definition, p.71 of [52])**.** *An $\mathbb{R}$-valued stochastic process M adapted to a filtration $\{\mathcal{F}_t\}$[11] is an $\{\mathcal{F}_t\}$-martingale if*

1) for all $t \geq 0$, $\mathbb{E}\left[|M_t|\right] < \infty$,

2) for all $t, r \geq 0$, $\mathbb{E}\left[M_{t+r}|\mathcal{F}_t\right] = M_t$ or equivalently, $\mathbb{E}\left[M_{t+r} - M_t|\mathcal{F}_t\right] = 0$.

The link between a martingale and the homogeneous Poisson process was first introduced by Watanabe in 1964:

---

[10] i.e., Z is right continuous with left limits at all $t > 0$.

[11] A filtration $\{\mathcal{F}_t\}$ is a representation of the information available about the process from the beginning up to a time $t \geq 0$. The reader can find more details about it p.71 in [52].

Theorem I.4 (Watanabe theorem, see Theorem 2.3 of [53]). *If N is a Poisson process with parameter λ, then $N_t - \lambda t$ is a martingale. Conversely, if N is a counting process and $N_t - \lambda t$ is a martingale, then N is a Poisson process with parameter λ.*

This link was then extended by Brémaud [54] to more complex processes (see SDE I.14 for instance). We quickly give (some) details about the procedure to adopt in the case where X is defined as a solution to an SDE (here SDE I.14). The first step consists in writing the infinitesimal generator A associated with the process, defined as, for all $x \in \mathcal{S}$, where $\mathcal{S} \subset \mathbb{N}^m$ is the state set,

$$Af(x) = \sum_{m=1}^{M} \lambda_m(x) \left(f(x + \xi_m) - f(x) \right), \tag{I.15}$$

for all bounded functions f. This operator fully characterizes the process. Under the assumption of sufficient regularity of the operator

Hypothesis I.1. *Assuming that, for all $m \in [\![1, M]\!]$,*

- *$\lambda_m(x) \geq 0$, for all $x \in \mathcal{S}$. (positive intensity)*

- *$\xi_m \in \mathbb{R}^d$ such that $x \in \mathcal{S}$ and $\lambda_m(x) > 0$ implies $x + \xi_m \in \mathcal{S}$. (additivity property)*

- *$x \in \mathcal{S}$, $\sum_{m=1}^{M} \lambda_m(x) < \infty$ (finite jump intensity)*

- *For f with finite support in $\mathcal{S}$ and A defined by Eq. (I.15), $\lim_{|x| \to +\infty} Af(x) = 0$.*

we get the martingale problem:

Definition I.5 (Martingale problem and minimal solution, see [52] p. 12). *A right continuous $\mathcal{S} \cup \{\infty\}$–valued stochastic process X is a solution of the martingale problem below for the operator A if there exists a filtration $\{\mathcal{F}_t\}$ such that for each f with finite support,*

$$f(X_t) - f(X_0) - \int_0^t Af(X_s)ds$$

is a $\{\mathcal{F}_t\}$–martingale.
Let $\tau_K := \inf\{t : |X_t| \geq K\}$ be a sequence of stopping times of process X and $\tau_\infty := \lim_{K \to +\infty} \tau_K$. If τ_∞ is finite with positive probability, then there may be more than one solution the martingale problem. If in addition to the martingale requirements, we require that $X_t = \infty$ for $t \geq \tau_\infty$, then we say that X is a minimal solution of the martingale problem.

There is a close link between the martingale problem and the SDE solution:

Theorem I.5 (Theorem 1.22 of [52]). *Under Hypothesis I.1, the solution of SDE (I.14) with $X_t = +\infty$ for all $t \geq \tau_\infty$ is the unique minimal solution of the martingale problem for A.*

a)   Link with the continuous time Markov chains

In the same way that Poisson processes are special cases of counting processes, they are also examples of continuous Markov chains.

Definition I.6 (Continuous-time Markov chains, Definition 2.1, chapter 8 of [54])**.** *The $\mathbb{R}$-valued stochastic process $\{X_t\}_{t\geq 0}$ is called a continuous-time Markov chain if for all states $i, j, i_1, \ldots i_k \in \mathcal{S}$, all times $t, s \geq 0$ and all time-points $s_1, \ldots, s_k \geq 0$ such that $s_l \leq s$ for all $l \in [\![1, k]\!]$,*

$$\mathbb{P}\left[X(t+s) = j | X(s) = i, X(s_1) = i_1, \ldots, X(s_k) = i_k\right] = \mathbb{P}\left[X(t+s) = j | X(s) = i\right],$$

whenever both sides are well-defined.

A continuous-time Markov chain is fully characterized by its associated transition semi-group[12] P given by, for all $s \geq 0$,

$$P(t) = \{p_{ij}(t)\}_{i,j\in\mathcal{S}} \text{ where } p_{ij}(t) = \mathbb{P}\left[X(t+s) = j | X(s) = i\right].$$

In the case of a homogeneous continuous-time Markov chain, the chain is in particular characterized by a time-independent operator: its infinitesimal generator $Q := \{q_{i,j}\}_{i,j\in\mathcal{S}}$, where $q_{i,j}$ are the local characteristics of the semigroup P (see Definition 2.3, p.335 of [54]). The matrix Q is thus sometimes defined as

$$Q := \lim_{h\searrow 0} \frac{P(h) - P(0)}{h}.$$

The process is then connected with the Kolmogorov equations:

- the backward Kolmogorov equation $P'(t) = QP(t)$.

- the forward Kolmogorov equation $P'(t) = P(t)Q$.

The backward Kolmogorov equation is classically used when the final condition is known (an extinction for example) while the forward equation is preferred when the initial condition is known. When they can be solved analytically, these equations give access to the analytical expression of the law of the whole process at any time.

The birth and death process.
The pure birth and death process is a pure[13] jump Markov process whose jump steps are equal to ± 1 and the transition rates are defined as follows: for all $i \in \mathbb{N}$,

$$\begin{cases} i \to i+1 & \text{at rate } \lambda_i, \\ i \to i-1 & \text{at rate } \mu_i, \end{cases}$$

where $(\lambda_i)_{i\in\mathbb{N}^*}$ and $(\mu_i)_{i\in\mathbb{N}^*}$ are two sequences of positive real numbers such that $\lambda_0 = \mu_0 = 0$ [55]. The birth and death process consists thus of jumps of size $+1$ (birth) at random times that follow the exponential law $\mathcal{E}(\lambda_i)$ and jumps of size -1(death) at random times that follow the exponential law $\mathcal{E}(\mu_i)$, where i is the current population size [56, 57, 55]. Although we have mainly used the Yule process that corresponds to the case where $\lambda_i = i\lambda$ and $\mu_i = 0$ in this thesis, we present some general results in the following.

---

[12]For example, the transition semi-group of a Poisson process of intensity λ is $p_{ij}(t) = e^{-\lambda t}\frac{(\lambda t)^{j-i}}{(j-i)!}$.

[13]The term "pure" means that there is neither drift or diffusion part in the process.

To obtain the law of the transition semi-group P, we start by writing the infinitesimal generator Q. For this step, we write the probabilities $\mathbb{P}[X(t+h) = j | X(t) = i]$ over a very small time interval h based on the behavioral law of our model. As far as the birth, we have

$$\mathbb{P}[\text{ jump } +1 \text{ during a time interval of length h } | X(t) = i] = 1 - e^{-\lambda_i h} \approx \lambda_i h + o(h).$$

Symmetrically, the probability of having a death within a small time interval h corresponds to a -1 jump in the process (with an exponential random law time $\mathcal{E}(\mu_i)$):

$$\mathbb{P}[\text{ jump -1 during a time interval of length h } | X(t) = i] = 1 - e^{-\mu_i h} \approx \mu_i h + o(h).$$

Assuming that the probability of having more than one event (birth or death) in a h time interval is very low (in the order of $o(h)$), one can write, for any $t \geq 0$,

$$\mathbb{P}[X(t+h) = i+1 | X(t) = i] = \lambda_i h + o(h), \quad \mathbb{P}[X(t+h) = i-1 | X(t) = i] = \mu_i h + o(h)$$
$$\text{and } \mathbb{P}[X(t+h) = i | X(t) = i] = 1 - (\lambda_i + \mu_i)h + o(h).$$

By the Markov property, we can take $t = 0$ and deduce the infinitesimal generator $Q = (q_{i,j})_{i,j\in\mathbb{N}}$ applying Definition a): for all $i \geq 0$,

$$q_{i,i-1} = \mu_i, \quad q_{i,i+1} = \lambda_i, \quad q_{i,i} = -(\lambda_i + \mu_i) \text{ and } q_{i,j} = 0 \text{ otherwise.}$$

We deduce the Kolmogorov forward equation for the birth-and-death process (see p.10 of [55]): for all $i, j \in \mathbb{N}$,

$$\frac{d}{dt} p_{i,j}(t) = \mu_{j+1} p_{i,j+1}(t) + \lambda_{j-1} p_{i,j-1}(t) - (\lambda_j + \mu_j) p_{i,j}(t)$$

and the Kolmogorov backward equation

$$\frac{d}{dt} p_{i,j}(t) = \mu_i p_{i-1,j}(t) + \lambda_i p_{i+1,j}(t) - (\lambda_i + \mu_i) p_{i,j}(t).$$

From these equations, we can deduce an equation verified by the probability measure π defined, for all $j \in \mathbb{N}$, by

$$\pi_j(t) := \mathbb{P}[X_t = j] = \sum_i \mathbb{P}[X_t = j | X_0 = i] \mathbb{P}[X_0 = i] = \sum_i \mathbb{P}[X_0 = i] \, p_{i,j}(t).$$

We thus deduce the forward Kolmogorov equation

$$\frac{d}{dt} \pi_j(t) = \mu_{j+1} \pi_{j+1}(t) + \lambda_{j-1} \pi_{j-1}(t) - (\lambda_j + \mu_j) \pi_j(t). \tag{I.16}$$

A classic first analysis then consists in looking at the stationary state of the process, i.e. looking for a vector $\bar{\pi}$ such as $\mu_{j+1}\bar{\pi}_{j+1} + \lambda_{j-1}\bar{\pi}_{j-1} - (\lambda_j + \mu_j)\bar{\pi}_j = 0$.
In some cases, the stationary state does not exist: the process may explode for instance. Another analysis then focuses on the extinction time T_0 (no more cells in the system). The probability to see an extinction in a finite time starting from i cells, is defined as $w_i = \mathbb{P}[T_0 < \infty | X_0 = i]$ and verifies the equation $\lambda_i w_{i+1} - (\lambda_i + \mu_i)w_i + \mu_i w_{i-1} = 0$ (that is deduced from the backward Kolmogorov equation, see p.11 of [55] for details). The extinction (or not) of the process almost surely in finite time is a well-known result and depends on the convergence of the series $\sum_{k\geq 1} \frac{\mu_1 \cdots \mu_k}{\lambda_1 \cdots \lambda_k}$ (see Theorem 2.5 of [55] for details). As far as the

binary branching process (linear birth and death rates: $\mu_i = \mu i$ and $\lambda_i = \lambda i$), this results is: if $\lambda < \mu$, then the probability of extinction in finite time ω verifies

$$\omega_j = \frac{\lambda^j}{\mu^j \left(1 + \sum_{n=1}^{\infty} (\frac{\lambda}{\mu})^n\right)}.$$

The condition $\lambda < \mu$ implies that death dominates reproduction so that the number of individuals does not diverge at long times.

In special cases, the Kolmogorov equation (I.16) can be solved. For example, one can show that the law of cell numbers of a Yule process, starting from n_0 cells at time $t = 0$, follows a binomial negative law of parameter $p = e^{\lambda t}$ and $n = n_0$ by solving the Kolmogorov forward equation. Additional examples are provided in Table I.2.

	Kolmogorov forward equ.	**X_t law**
Homogeneous Birth $(\lambda_i = \lambda \setminus \mu_i = 0)$	$\pi_i'(t) = \lambda\left[\pi_{i-1} - \pi_i(t)\right]$ $\pi_1(0) = 1$	$\pi_n(t) = e^{-\lambda t}\frac{(\lambda t)^n}{n!}$ (X_t follows a Poisson law $\mathcal{P}(\lambda t)$)
Yule process $(\lambda_i = i\lambda \setminus \mu_i = 0)$	$\pi_i'(t) = \lambda\left[(i-1)\pi_{i-1} - i\pi_i(t)\right]$ $\pi_1(0) = 1$	$\pi_n(t) = e^{-\lambda t}(1 - e^{-\lambda t})^{n-1}$ (X_t follows a Geometric law $\mathcal{G}(e^{\lambda t})$ with support in $\mathbb{N}^*$)
Pure Birth $(\lambda_i = i\lambda \setminus \mu_i = 0)$	$\pi_i'(t) = \lambda\left[(i-1)\pi_{i-1} - i\pi_i(t)\right]$ $\pi_{n_0}(0) = 1$	$\pi_n(t) = \binom{n-1}{n_0-1}e^{-\lambda n_0 t}(1 - e^{-\lambda t})^{n-n_0}$ (X_t follows a Binomial negative law $\mathcal{BN}(n_0, e^{\lambda t})$)
Pure Death $(\lambda_i = 0 \setminus \mu_i = \mu i)$	$\pi_i'(t) = \mu\left[(i+1)\pi_{i+1} - i\pi_i(t)\right]$ $\pi_{n_0}(0) = 1$	$\pi_n(t) = \binom{n}{n_0}e^{-\mu n t}(1 - e^{-\mu t})^{n_0-n}$ (X_t follows a Binomial law $\mathcal{B}(n_0, e^{-\mu t})$)

Table I.2 – **Birth and Death process laws**. We consider different examples of the Kolmogorov forward equation (I.16), starting either with one cell ($\pi_1(0) = 1$) or several ($\pi_{n_0}(0) = 1$).

However, it happens generally that the Kolmogorov (forward or backward) equation cannot be solved (unclosed system). For example, in the case of Eq. (I.16), the probability π_j (state j) is deduced from the probabilities π_{j+1} (state $j+1$) and π_{j-1} (state $j-1$). Without absorbing states or frontiers[14], the state $j+1$ is always required to compute the state j, for all $j \in \mathbb{N}$. Sometimes, the situation (studied) makes it possible to naturally introduce absorbing states, but this is quite rare! A domain closure method was developed about fifteen years ago to solve Kolmogorov's equations: the finite state projection. The validity of the finite state projection has already been proven in [58] and subsequent work. More recently, Thomas Kuntz's thesis work has tackled the characterization of a Markov chain exit from a domain (absorbing frontier) [59, 60]. This approach is detailed in Chapter 2 where we develop a rigorous method based on it to simulate hitting times (specifically, extinction times).

---

[14]A state i is absorbing if for all states $j \neq i$, $\pi_{i,j}(t) = 0$. An absorbing frontier is a connected set of absorbing states.

b) Simulation of the Poisson process

There are two main categories of algorithms for simulating Poisson processes:

- algorithms based on the Markov chain definition of the Poisson process. The most famous algorithm in this category is the Gillespie algorithm [61], which we introduce below and is used for the simulations in Chapter 2.

- algorithms based on the jump process definition (see for instance the next reaction method, p.59 [52]).

A detailed presentation of these algorithms can be found in Chapter 5 of [52].

The Gillespie algorithm [61], sometimes called Stochastic Simulation Algorithm (SSA), is a direct method that takes advantage of the Markov chain property satisfied by the Poisson process. Using the decomposition of the Poisson process $X = (X_t)_{t \geq 0}$ as the couple of processes (S_n, X_n) where S_n is the sequence of jump times of the process (see Definition I.3) and X_n is the embedded Markov chain associated with process X^{15}, the Gillespie algorithm proceeds by simulating the embedded Markov chain concurrently with the sequence of time jumps S_n. The embedded Markov chain, similar to a discrete time Markov chain, is simulated with the transition probabilities

$$p_{xy} = \left\{ \begin{array}{ll} \dfrac{\lambda_k(x)}{\sum_l \lambda_l(x)}, & \text{if } y = x + \xi_l, \\ 0, & \text{else.} \end{array} \right.$$

For example, starting from an initial cell population vector N_0, the next state $\widetilde{y}$ of the chain is simulated with the transition probabilities $(p_{N_0 y})_{y \in \mathcal{S}}$. The next jumptime is obtained by simulating an exponential random variable with parameter $\sum_l \lambda_l(x)$ (exponential law property[16]).

When event rates (division, transformation, etc.) are linear, there is another way to simulate the process taking advantage of the branching property induced by the linear rate. Such an algorithm was used during this thesis (see detailed Algorithm 3 in Appendix A.1).

c) The branching property

The basic assumption involved is that each cell in the process behaves identically and independently from the other cells (see 1.3 of [62]). A branching process representing the cell division can be described as follows (for more general results, see Chapter 4 of [63], Chapter 2 of [64] or Chapter 5 of [65]). A single ancestor cell is born at time $t = 0$ and does not divide until a random time τ, which is exponentially distributed with parameter b. At division, the cell divides into two daughter cells that behave independently from each other and in the same way as the ancestor cell. Hence, the two daughter cells of the first generation divide at a random exponentially distributed time with parameter b. Mathematically, this can be written as: let Z_t be the cell number at time t starting from one cell at time $t = 0$:

$$Z_t = \left\{ \begin{array}{ll} 1, & t < \tau, \\ Z_{t-\tau}^{(1)} + Z_{t-\tau}^{(2)}, & t \geq \tau, \end{array} \right. \tag{I.17}$$

---

[15] which can also be seen as the state chain of the process X.

[16] $\min_{i \in [\![1, I]\!]} \mathcal{E}(\lambda_i) = \mathcal{E}\left(\sum_{i=1}^{I} \lambda_i \right)$.

where $Z^{(1)}$ and $Z^{(2)}$ are identical and independent distributed (iid) copies of process Z. Hence, taking any cell from either process $Z^{(1)}$ or $Z^{(2)}$ gives rise to its own clones, which is a subprocess of the whole process $\{Z_t, t \geq 0\}$. Mathematically speaking, branching processes belong to a class of stochastic objects called "self-recurrent", introduced by Feller. Matters become a little more complicated if we allow particles of different types. The clones created by cells of different types are different, so the bookkeeping becomes more involved. However, the principle stays the same (see Chapter 3).

Generating function of the process The tool dedicated to the study of processes verifying the branching property is the generating function.
Let $s \in [0,1]$. Following [66], we define the generating function $F[s;t]$ associated with our stochastic process defined by Eq. (I.17):

$$F[s;t] := \mathbb{E}\left[s^{Z_t}|Z_0 = 1\right] = \sum_{k \in \mathbb{N}} s^k \mathbb{P}\left[Z_t = k|Z_0 = 1\right]. \tag{I.18}$$

The renewal equation verified by the generating function F is obtained by writting first a renewal equation for the probability $\mathbb{P}\left[Z_t = k|Z_0 = 1\right]$. In the same way as the Kolmogorov equations, this equation is obtained by writing the events occurring from the initial time $t = 0$ up to time t: i) no division has occurred at time t, ii) a division has taken place before time t:

$$\mathbb{P}\left[Z_t = k|Z_0 = 1\right] = \delta_{k,1}\mathbb{P}\left[\tau \geq t\right] + \int_0^t \mathbb{P}\left[Z_{t-y} = k|Z_0 = 1\right] f(y)dy,$$

where f is the density function of the exponential law: $f(t) = be^{-bt}$. After a few calculation steps (see details in Appendix A.1.3), we deduce a renewal equation for F:

$$F[s;t] = se^{-bt} + \int_0^t F[s;t-y]^2 be^{-by}dy.$$

Differentiating this expression with respect to time, we obtain that

$$\partial_t F[s;t] = -b\left[F[s;t] - F[s;t]^2\right],$$

which is a Riccati equation whose solution is known in that case:

Theorem I.6 (Solution of a Riccati equation, see Theorem 4.2 of [63])**.** *The solution of the differential equation*

$$\frac{d}{dt}F(t) = f(t)F(t) + hF(t)^2,$$

where $f \in C^0([0,+\infty))$ and $h \in \mathbb{R}$, with initial condition $F(0)$, is the uniquely defined function $F \in C^1([0,+\infty))$:

$$F(t) = \frac{F(0)e^{\int_0^t f(u)du}}{1 - hF(0)\int_0^t e^{\int_0^u f(s)ds}du}.$$

Applying Theorem I.6, we deduce that for all $s \in [0,1]$, $F[s;t] = \frac{s}{s+(1-s)e^{bt}}$, which corresponds to the generating function of the geometric law $\mathcal{G}(e^{bt})$, consistent with the Table results I.2.

Decomposable branching process. In this thesis, we have focused on a rather particular category of processes: the decomposable processes (see Chapter 3). In this type of process, a population is decomposed into a countable number of $J \in \mathbb{N}$ categories. Immediately after the division of a mother-cell from category j (at a category-dependent rate), the two new-born daughter cells change from their mother's category to another one according to given probabilities (mutation, immigration, etc.). The specificity of decomposable processes comes from the fact that daughter cells can only "choose" their categories from a subset of $[\![1, J]\!]$: $[\![j, J]\!]$. The decomposable processes have been particularly studied by Vatutin and Sagitov, see for example [67, 68, 69, 70]. In these studies, the authors are mainly interested in Galton-Watson-type processes[17] modeling immigration phenomena between several islands, sometimes integrating environmental effects on the migration probabilities. In Chapter 3, we analyze age-dependent branching processes.

I.1.4 Structuring physiological variables at the individual level *(used in Chapter 3)*

The integration of structuring physiological variables at the individual level has been the subject of much research since the middle of the 20th century. Concerning models dedicated to cell dynamics, two categories of techniques stand out: the moment-generating functions and the Poisson point measure.

a) The moment-generating functions

One of the first models that incorporates a structuring variable at the individual level is the Bellman-Harris model, which emerged from the collaboration between Theodore E. Harris and Richard Bellman [71, 72]. Introduced in [71], this model focuses on the dynamics of cell number[18] at time $t \geq 0$. At a random time τ given by the G distribution function ($G(t) := \mathbb{P}[\tau \leq t]$), a cell is transformed into n cells (in the case of a division, $n = 2$). It is assumed that G is a cumulative distribution for which $G(0) = 0$ and $G(+\infty) = 1$. Using an approach based on generating functions, the authors derive a renewal equation verified by the generating function $F[\mathbf{s}; t]$ defined in (I.18). Analyses are then carried out, including one on asymptotic behavior using Feller's work [42] on renewal equations. This model was later extended by Charles Mode [73, 74] and Kenny S. Crump [75, 76] to multi-type populations, a detailed version of which is provided in Chapter 3.

Using the same definition as Markov branching processes, we introduce Z_t the cell number at time t, starting with one cell at time $t = 0$:

$$Z_t = \begin{cases} 1, & t < \tau, \\ Z_{t-\tau}^{(1)} + Z_{t-\tau}^{(2)}, & t \geq \tau, \end{cases} \tag{I.19}$$

where τ follows an G distributed law and $Z^{(1)}$ and $Z^{(2)}$ are iid, identical to process Z. Using the generating function (see details in Chapter 3), one can deduce a renewal equation for the mean cell number:

Theorem I.7 (Expectation, Chapter VI, section 15 of [65])**.** *Let G be a probability distribution for which $G(0) = 0$ and G is continuous on the right. Then, the expectation*

---

[17]In discrete Markov processes, the events take place at discrete times $n \in \mathbb{N}$.

[18]The authors use the term "particles" in the article, since the model was designed for a more general context (biology, physics or chemistry).

$M(t) := \mathbb{E}[Z_t]$ *defined in Eq.* (I.19) *satistifies the renewal equation*

$$M(t) = 1 - G(t) + 2\int_0^t M(t-u)dG(u), \qquad (I.20)$$

where dG is the density function associated with the probability distribution G. M is bounded on each finite t-interval and is the only solution of Eq.(I.20) having this property.

Note that the renewal equation Eq.(I.20) is the same as the Lotka equation (Eq. (I.9)) deduced from the MK–VF equation in the special case of cell division. Using a Laplace transform method, one can determine from Eq.(I.20) the Laplace transform of M:

$$M^*(s) := \int_0^{+\infty} e^{-st}M(t)dt = \frac{1 - \int_0^{+\infty} e^{-st}dG(t)}{s\left[1 - 2\int_0^{+\infty} e^{-st}dG(t)\right]}$$

for all $s \in \mathbb{R}$ such that M^* exists. In most cases, the Laplace transform of M^* cannot explicitly be inversed and M can be calculated only by numerical or series methods [65]. In constrast, the asymptotic behavior of $M(t)$ when t goes to $+\infty$ can be determined in most cases by applying results on the integral equation thanks to renewal theory. For example, if G has good properties such as not being lattice:

Definition I.7 (Lattice distribution definition, Definition 17.1 of [65])**.** *A distribution G is a Δ-lattice distribution if it is constant excepts for jumps that are located at positive integer multiples of some positive number Δ, and if Δ is the largest such number.*

Theorem I.8 (Asymptotic behavior of M, extract from Theorem 17.1 [65].)**.** *Let λ be defined as the positive root of*

$$2\int_0^{+\infty} e^{-\lambda t}dG(t) = 1. \qquad (I.21)$$

If G is not a lattice distribution then

$$M(t) \sim n_1 e^{\lambda t}, \quad t \to +\infty,$$

where $n_1 = \frac{1}{4\lambda \int_0^{+\infty} te^{-\lambda t}dG(t)}$.

Note that the constant λ, sometimes called the Malthus parameter, is solution of the characteristic equation Eq. (I.13) met earlier. Note that the existence of a positive root of Eq. (I.21) can be deduced with the same arguments as the ones provided for Eq. (I.13).

One may also want to analyze the age distribution of the branching process (I.19). One way for that consists in studying the random variable $Z(t,a)$ corresponding to the number of cells at time t of age $\leq a$. Using again generating functions (see Chapter 3 or section 21.1 of [65]), one can show that $M(t,a) = \mathbb{E}[Z(t,a)]$ follows the renewal equation

$$M(a,t) = [1 - G(t)]\mathbb{1}_{[0,a]}(t) + 2\int_0^t M(a,t-y)dG(y).$$

Theorem I.9 (Asymptotic mean age distribution, Theorem 24.1 of [65])**.** *Suppose that G is not a lattice distribution, that there exists a real λ solution of the characterisitic equation Eq. (I.21) and that $\int_0^{+\infty} te^{-\lambda t}dG(t) < \infty$, then for each $a \in \mathbb{R}_+$,*

$$M(a,t) \sim n_1 e^{\lambda t}A(a), \quad t \to +\infty,$$

where n_1 if defined in Theorem I.8 and $A(a) := 2\lambda \int_0^a e^{-\lambda t}[1 - G(t)]\,dt$.

The method of generating functions seen above is efficient when the process is linear (each cell divides or transforms itself independently from the others). It is a generic method that can also be applied in more general situations: for example, in [77], the authors consider the case where the lifetime of a cell in the system, as well as the number of its children, depends on the other cells (sisters).

Another formalism, developed at the end of the 20th century, emerged to help analyze cell-based models, especially ones with interactions: the Poisson point measures.

b) The Poisson point measure

The counting measure presented above (Definition I.2) can be enriched by adding physiological or structural individual specificities. Using our example of a population of cells that divide at an age-dependent rate, the counting measure allows us to enumerate the cells characterized here by their age (continuous structuring variable):

$$\nu_t = \sum_{i=1}^{N_t} \delta_{a_i(t)},$$

where N_t stands for the total cell number in the population. Each cell $i \in [\![1, N_t]\!]$ of the population is therefore represented by a Dirac mass in $a_i(t)$ corresponding to its age.

The counting measure $\nu = (\nu_t)_{t \geq 0}$ enriched with a structuring variable is a measure-valued process in the finite point measure space $\mathcal{M}$, where

$$\mathcal{M} := \{\sum_{i=1}^{n} \delta_{x_i} : n \geq 0, \quad x_1, ..., x_n \in \mathcal{X}\}$$

where $\mathcal{X} \subset \mathbb{R}^d$ and δ_x is the Dirac measure at x. Such a formalism was first introduced in a biological modeling context in [78] where the authors focus on the spatial dynamics of non-moving individuals (plants) regulated by death and birth phenomena. In particular, the birth of new plants is the result of a local dispersion of seeds, produced by a mother plant, that instantly become mature individuals. This formalism was later exploited mainly for ecological purposes, and led to models following population dynamics where individuals reproduce asexually, age, interact and die, see for example (non-exhaustive!) [79, 80, 81, 55]. Some applications have also been considered for growth-fragmentation models [82].

In the following, we present an example of the use of the Poisson point measure process based on the founder article [78] and the book [55](especially, Chapter 2). Suppose that our population dynamics verifies the following assumptions:

1. at the initial time $t = 0$, the initial cell population is a measure of the space $\mathcal{M}$, possibly random.

2. Each cell $i \in [\![1, N_t]\!]$ divides according to an exponential clock (hence the term Poisson) at a rate of $b(a_i(t))$.

The pathwise description of the $\mathcal{M}$-valued stochastic process ν can be given using Poisson point measures. Under the appropriate assumptions of regularity on the jump rates (usually bounded, i.e. $b(a) \leq \bar{b}$), it can be shown that the process ν is a solution of the stochastic differential equation (SDE) governed by the elementary Poisson measure $Q(ds, di, d\theta)$ of intensity

$ds \otimes \#dk \otimes d\theta^{19}$, where ds and $d\theta$ are Lebesgue measures on $\mathbb{R}_+$ and $\#dk = \sum_{i\geq 1} \delta_i(dk)$ is a counting measure on $\mathbb{N}^*$:

$$\nu_t = \nu_0 + \int_0^t \int_0^{+\infty} \mathbb{1}_{k \leq N_{s-}} \left(2\delta_{t-s} - \delta_{a_k(t-s)+t-s} \right) \mathbb{1}_{\theta \leq b(\nu_{s-})} Q(ds, dk, d\theta). \qquad (\text{I.22})$$

Analysis of the process paths ruled by Poisson point measures

The analysis of the process paths ruled by Poisson point measures uses stochastic calculus techniques. The reader may refer to [83](specifically, Chapter 13 for an overview of those techniques for biologically inspired models), [55] (Chapter 6) and [84].

Sometimes the process is first defined as the solution of an SDE, as is done in particular in [55] (specifically, Definition 6.2 and Proposition 6.3 in Chapter 6), and also in this manuscript (Chapter 3). We suppose in the following that process ν is defined as the solution of SDE (I.22). The first step to analyze the process then consists in writing the associated infinitesimal generator by integrating test functions $f \in \mathcal{C}_b^1(\mathbb{R}_+, \mathbb{R}_+)$ against the measure process ν_t:

$$< f, \nu_t > = \int_{\mathbb{R}_+} f(a)\nu_t(da) = \sum_{i=1}^{N_t} f(a_i).$$

Then, we apply Ito's formula[20] for all functions $F \in \mathcal{C}^1(\mathbb{R}_+, \mathbb{R}_+)$ to deduce the infinitesimal generator $\mathcal{G}F[< f, \nu_t >]$ associated with process ν_t. Once the equivalence between the generator and the SDE solution has been shown, the following martingale problem can be deduced by writing process $< f, \nu_t >$, for all f functions, as the sum of its compensator and a martingale (and taking $F(x) = x$, see Theorem 13.12 and 13.14 in [83] for details):

$$< f, \nu_t > \quad = \quad < f, \nu_0 > \quad + \quad \underbrace{\int_0^t < \mathcal{L}^D f, \nu_s > ds}_{\text{compensator}} \quad + \quad M_t^\phi, \qquad (\text{I.23})$$

where $\mathcal{L}^D$ is the operator defined by $\mathcal{L}^D f = f' - bf + 2bf(0)$ which is the dual operator associated with the renewal equation (see subsection I.1.2), and M_t^ϕ is a càdlàg $(\mathcal{F}_t)_{t\geq 0}$-martingale starting at time $t = 0$. Then, we deduce Dynkin's formula by taking the expectation:

$$\mathbb{E}\left[< f, \nu_t > \right] = \mathbb{E}\left[< f, \nu_0 > \right] + \mathbb{E}\left[\int_0^t < \mathcal{L}^D f, \nu_s > ds \right].$$

A sufficient condition for Dynkin's formula to hold is: for all positive functions $f \in \mathcal{C}^1(\mathbb{R}_+)$, for all measures $\nu \in \mathcal{M}$, there exists a constant C such that:

$$| < \mathcal{L}^D f, \nu > | \leq C(1+ < f, \nu >)$$

(see details in Theorem 13.16 of [83]). The asymptotic behavior can be deduced from the martingale problem above (eq. (I.23)):

Theorem I.10 (Positive martingale and eigenfunction, Theorem 13.18 of [83]). *Let q_r be a positive eigenfunction of $\mathcal{L}^D$ corresponding to the eigenvalue r. Then, $Q_r(t) = e^{-rt} < q_r, \nu_t >$ is a positive martingale.*

---

[19]The sign $\otimes$ refers to the outer product.
[20]See details in the Appendix chapter A.1.2

If r is the Malthus parameter and satisfies the characteristic equation

$$2 \int_0^\infty e^{-rs} b(s) e^{-\int_0^s b(u) du} ds = 1 \qquad (I.24)$$

then the eigenfunction q_r corresponds to the eigenfunction ϕ encountered in subsection I.1.2. The asymptotic behavior of process ν_t can be deduced:

Theorem I.11 (Asymptotic behavior, Theorem 13.20 of [83]). *Suppose that there exists a positive constant λ solution of the characteristic equation* (I.24) *and let ϕ be its associated eigenfunction (positive). The process $W_t = e^{-\lambda t} < \phi, \nu_t >$ is a positive square integrable martingale, and therefore converges almost surely and in $\mathbf{L}^2$ to a non-degenerate limit $W \geq 0$ such that $\mathbb{E}[W] = \phi(\nu_0) > 0$ and $\mathbb{P}[W > 0] > 0$.*

We have just seen that the eigenproblem of the renewal equation helps to deduce the asymptotic behavior of process ν. It turns out that the stochastic process ν and the renewal equation are more tightly linked.

Link between the Poisson point measure and the PDE. In [82], the authors used other techniques based on the martingale problem and Dynkyn formula to tackle the growth-fragmentation-death model case. They obtain an explicit link between the adjoint operator of the growth-fragmentation-death PDE and its stochastic process counterpart. As regards to the birth process, one can apply the Fubini theorem under suitable assumptions (for instance, the division rate b is bounded), and deduce that

$$\mathbb{E}[< f, \nu_t >] = \mathbb{E}[< f, \nu_0 >] + \int_0^t \mathbb{E}\left[< \mathcal{L}^D f, \nu_s > ds\right].$$

Since both the operator L and the expectation are linear operators, we can write that $\mathbb{E}\left[< \mathcal{L}^D f, \nu_s >\right] = \mathcal{L}^D \mathbb{E}[< f, \nu_s >]$ and deduce the MK–FV equation.

Using another approach based on the law of large numbers, the authors expressed in [85] the link existing between the MK–VF equation and the stochastic Birth–Death process. They first show that the sequence $Z_t^n = \frac{1}{n} Z_t$ converge when n goes to infinity to a deterministic measure $\eta_t \in \mathcal{M}_F(\mathbb{R}_+^d)$[21] and deduce:

Proposition I.3 (Based on Proposition 3.4 of [85]). *If η_0 admits a density $\rho_0 \in \mathbf{L}^1(\mathbb{R}_+)$, then for every $t \in \mathbb{R}_+$, η_t admits a density ρ_t which is solution of the MK–VF equation.*

This method was then extended to the case of age- and trait-structured population models in [85].

I.1.5   Data and model matching *(used in Chapter 2, 3 and 5)*

The confrontation of a model with data is a key event in the life of the model. This crucial step makes it possible to validate the relevance of using a model in a given context (here biological). If this step is successful, "model predictions" on the dataset can be made in the sense that hidden dataset information such as mean division time can be found, and sometimes

---

[21]the set of finite measures on $\mathbb{R}^d$.

participate in extrapolating experimental results. The adequacy between a model and a dataset is achieved through a quantitative approach: the model parameters are estimated through the minimization of a cost function, and a measure is proposed for the validity of the predictive power of the model over the dataset. In other words, such a measure quantifies how well the model with the estimated parameters fits the data[22].

Let us suppose that we are interested in the cell dynamics of a population composed of K cellular types. The dynamics of the whole population $N(t;\theta) := (N_k(t;\theta))_{k\in[\![1,K]\!]}$ follows the ODE system:

$$\frac{d}{dt}N(t;\theta) = f(N(t;\theta),\theta), \quad N(t=0;\theta) = N_0 \tag{I.25}$$

where $\theta := (\theta_l)_{l\in[\![1,L]\!]} \in \Theta \subseteq \mathbb{R}^L$ is a parameter vector of size L, and f is a known function and assumed to be sufficiently regular such that Eq. (I.25) has a unique solution (Cauchy-Lipschitz theorem). Since the function f is known, the dynamics of N is totally dependent on the value of the parameter θ (and, in some cases, on the initial condition N_0). To estimate the parameters (not directly observable) of the model, the ODE system (I.25) is supplemented by experimental observations and represented by the following observable function g such that

$$y(t_i;\theta) = g(N(t_i;\theta),\theta) + \varepsilon_i,$$

where $y(t_i;\theta)$, $i \in [\![1,I]\!]$ are the I discrete-time observables (at time t_i) of the population vector N performed with a measurement error ϵ_i. The experimental measurements can be the total cell counts ($g(N,\theta) = \sum_{k=1}^{K} N_k$), partial counts ($g(N,\theta) = \sum_{k\in\tilde{K}} N_k$, with $\tilde{K} \subset K$) or cell counts for each type ($g(N,\theta) = N$). The observable function can sometimes depends on additional parameters such as scaling or offset parameters included in θ [86].

The difference between the experimental data $y^\dagger := (y^\dagger(t_i))_{i\in[\![1,I]\!]}$ and the observables $y(\theta) := (y(t_i;\theta))_{i\in[\![1,I]\!]}$ predicted by the model is measured by the likelihood function (cost function) classically defined as

$$\mathcal{L}(\theta|y^\dagger) := \mathbb{P}\left[y(\theta) = y^\dagger|\theta\right] = \prod_{i\in[\![1,I]\!]} \mathbb{P}\left[y(t_i;\theta) = y^\dagger(t_i)|\theta\right]. \tag{I.26}$$

It is more convenient to use the negative log-likelihood function $\mathcal{L}^{\log}(\theta|y^\dagger) := -\log(\mathcal{L}(\theta|y^\dagger))$. In the case of an ODE system model, the measurement error ε_i associated with each measurement $y^\dagger(t_i)$ is generally modeled by a normal centered distribution: $\varepsilon_i \sim \mathcal{N}(0,\sigma_i^2)$[23]. The cost function is then commonly a weighted sum of squared residuals.

The maximum likelihood estimator is then defined as

$$\hat{\theta} := \arg\max_{\theta\in\Theta} \mathcal{L}(\theta|y^\dagger) = \arg\min_{\theta\in\Theta} \mathcal{L}^{\log}(\theta|y^\dagger). \tag{I.27}$$

The $\hat{\theta}$ estimator is the parameter for which the conditional probability that the experimental observations are equal to the observations predicted by the model is the highest. This does not guarantee that $\hat{\theta}$ is the true value $\hat{\theta}^*$. The mere estimator $\hat{\theta}$ must therefore be associated with a measurement of the parameter uncertainty for the model prediction to be relevant. For each parameter θ_l, $l \in [\![1,L]\!]$, its associated uncertainty measurement is given by the

---

[22]For instance, one can apply the Akaike Information Criteria (AIC) to compate nested submodels.

[23]In the case where the y measure is a vector of dimension D, it is also assumed that each measure is independent. The measurement error ε_i follows then a normal centered distribution of diagonal covariance matrix $V \in \mathbb{R}^{D\times D}$ such that $[V]_{dd} = \sigma_{dd}^2$.

confidence interval $[\sigma_l^-, \sigma_l^+]$ of confidence level $1 - \alpha$. This means that the true value $\hat{\theta}_l^*$ belongs to the confidence interval with probability $1 - \alpha$.

The construction of such confidence intervals can be done using a method widely recognized as robust and based on the Likelihood Ratio (LR) test, see for instance [87, 88, 89, 90]. The LR test is a statistical test used for comparing the goodness of fit of two models: a null model (null hypothesis) against an alternative model. Using the likelihood definition (I.26) and MLE definition (I.27), we define classically the following LR statistic (see for instance [90, 86]):

$$\lambda(\theta) := \frac{\mathcal{L}(\hat{\theta}|y^\dagger)}{\mathcal{L}(\theta|y^\dagger)},$$

where $\theta \in \Theta$. To construct the pointwise likelihood-based confidence interval of parameter θ_i, we first introduce its partial maximum likelihood estimate:

$$\hat{\theta}|\,[\theta_i = x] := \arg \min_{\theta \in \Theta; \theta_i = x} \mathcal{L}^{\log}(\theta|y^\dagger).$$

According to [90], the asymptotic distribution of λ verifies, under the null hypothesis, $-2\log(\lambda) \sim \chi^2(df)$, where df is the number of parameters considered[24]. Here, since we want to build a confidence interval for parameter θ_i, $df = 1$.

The confidence interval of parameter θ_i is thus defined as:

$$\{x \in Supp(\theta_i) |-2\log\left(\lambda(\hat{\theta}|\,[\theta_i = x])\right) < \Delta_\alpha\} \subset \mathbb{R},$$

where the threshold Δ_α is the $1 - \alpha$ quantile of the $\chi^2(1)$ distribution. We recall that $\mathcal{L}^{\log}(x) := -\log(\mathcal{L}(x))$ and thus deduce the following confidence interval:

$$\{x \in Supp(\theta_i) |-2\left(\mathcal{L}^{\log}(\hat{\theta}) - \mathcal{L}^{\log}(\hat{\theta}|\,[\theta_i = x])\right) < \Delta_\alpha\} \subset \mathbb{R}.$$

In the case of a finite dimension differential system, the numerical estimation of both the MLE and confidence intervals can be performed efficiently using Matlab D2D software [91]. This was done in Chapter 3. The likelihood approach can also be applied in the case of infinite dimension systems to infer the model parameters. For example, in [92], the authors solve an inverse problem through a non-parametric approach based on maximum-likelihood and Bayesian estimation on a special multi-type MK–VF like model to study cell proliferation in vivo and in vitro[25]. Another approach for parameter estimation is either to solve numerically an inverse problem (non-parametric approach) [93, 94, 95] or prescribe a shape to the parameters (parametric approach), see for instance [96]. If the cell population has reached the exponential steady state before the start of the experiment, the stable state can be used, as in [97] where the authors reconstruct the division rate from the intermitotic time distribution measurements.

Depending on the quality and quantity of the data, it may be difficult to determine the MLE or confidence intervals, and minimization algorithms (usually gradient descent) do not converge. These difficulties may stem from structural or practical non-identifiability described in [86] and defined as

---

[24]In particular, when the error law follows a Gaussian law, $-2\log(\lambda)$ follows exactly a $\chi^2(1)$.

[25]In this model, the type corresponds to a cell lineage and in addition to age, the authors consider another structuring variable: the concentration of a division marker.

- structural identifiability: assuming ideal measurements, with arbitrarily many and perfectly chosen measurement time points t_i and absence of measurements errors ($\varepsilon_i = 0$), a parameter θ_i is structurally identifiable if it is uniquely estimable from the model observables $y(t_i; \theta)$. In other words, the structural identifiability corresponds to the injectivity of an inverse problem: given two observations y and $\tilde{y}$, a parameter θ is structurally identifiable if

$$y(t_i; \theta) = \tilde{y}(t_i; \tilde{\theta}) \Rightarrow \theta = \tilde{\theta}.$$

- practical identifiability: a parameter θ_i is practically identifiable if its confidence interval is a compact set.

The practical identifiability depends thus on the quality and quantity of the data, and the accurancy of the estimators can be improved by increasing the number of experimental points. On the contrary, the structural identifiability is a data-free property that solely depends on the model and the type of observations (e.g., mean cell number)[26]. Indeed, in some cases, this quantitative increase in data does not lead to practical identifiability of a parameter [98]. In these cases, the problem is often related to qualitative rather than quantitative factors. It is in particular the case of microscopic parameters that cannot be deduced solely from macroscopic observation. One way to avoid these problems is to look at the theoretical inverse problem (structural identifiability), which aims to verify whether it is possible to deduce the uniqueness of the model parameters based on observable data (cell counts, for example) and additional information (initial conditions, knowledge of certain parameters).

As example, in the case of the Malthus growth, a theoretical inverse problem can be: supposing that m is known for all $t \geq 0$, can we recover uniquely the Malthus parameter α [98]? We can easily show that this inverse problem is well-posed: supposing that there exist two functions m_1 and m_2 that verify the Malthus growth equation with parameter α_1 and α_2, respectively, such that $m_1(t) = m_2(t)$ for all t, we have:

$$\frac{d}{dt}m_1(t) = \frac{d}{dt}m_2(t) \Rightarrow \alpha_1 m_1(t) = \alpha_2 m_1(t) \Rightarrow \alpha_1 = \alpha_2.$$

This is a perfect example where additional information is not required. In constrast, one can show that the (theoretical) inverse problem: "supposing that m is known for all $t \geq 0$ and verifies the birth-death model, can we recover uniquely the birth and death rates?" is not well-posed. Indeed, even considering a simple case where the birth and death rate are constant, we obtain:

$$\frac{d}{dt}m_1(t) = \frac{d}{dt}m_2(t) \Rightarrow (b_1 - d_1)m_1(t) = (b_2 - d_2)m_1(t) \Rightarrow b_1 - d_1 = b_2 - d_2.$$

The relation $b_1 - d_1 = b_2 - d_2$ needs to be completed with additional information to deduce the well-posedness. Usually, either the death or birth rate is assumed to be known.
For more complex ODE systems, the theoretical inverse problem is usually solved on a case-by-case basis: for example by using linear algebra tools [33] or, for first and second order differential equations, a technique called collage which is based on a fixed point method applied to the Picard operator [99, 100]. In the case of PDE, the theoretical inverse problems,

---

[26]Considering ideal measurements, [86] proposes a likelihood-based definition which appears to be a useful tool when theoretical structural identifiability approaches fail. This definition is: a parameter θ_i is structurally identifiable if its estimator $\hat{\theta}_i$ is the only maximum of the likelihood function $\mathcal{L}$.

intending to recover model functions, such as the death or division rate, from observable model outputs are most of the time model-specific. For example, in the case of the age-structured PDE model, most of the methods take advantage of the renewal property of this equation to solve the inverse problem [94, 95, 93, 101, 96] (see details in Chapter 5). The use of the eigenproblem is a rare example of method that can be applied to solve the inverse problem (structural and practical identifiability) in many situations: age-structured model [97], size-structured model [14, 44], etc. However this approach assumes that the observed data reaches the steady state.

Check the structural identifiability property (or solve a theoretical inverse problem) is a relevant approach that should be applied even before considering statistic models to fit parameters with data. This question has been addressed all along this thesis and is the subject of an entire chapter (5) as well as an element of Chapter 3.

I.2 Introduction to the early development of the ovarian follicle

The development of ovarian follicles is a rare example of morphogenesis taking place in a adult mammalian organism [102]. Like many morphogenesis processes, their formation and growth are the result of the finely regulated biological mechanisms that we describe below.

I.2.1 The dynamics of follicle growth

The ovarian follicles are the basic anatomical and functional units of the ovaries (Figure I.1, left-panel). In mammals, the main function of the ovary is to produce one or more fertile oocytes (egg cells) at each ovulation and to create a hormonal environment conducive to the eventual start of a pregnancy. The ovarian hormones also have non reproductive actions. The maturation of the oocytes, named oogenesis, is a long and discontinuous developmental process initiated during the fetal life that goes on throughout the individual's life. The proper development of the oocyte is supported by a somatic structure sheltering it; together they form the ovarian follicle[27]. This somatic structure provides the oocyte with the necessary environment for its growth and acquisition of the capability to be fertilized and proceed to a fetal development.

a) The ovarian reserve of primordial follicles

The formation of the oocyte pool during the fetal life precedes the formation of the first follicles in the primordial stage. The primordial follicles consist of an oocyte surrounded by a single layer of somatic cells with a flattened shape [104]. The order of magnitude of the initial cell number varies from ten to about fifty. Such a variability is inherited from the mechanism underlying the formation of primordial follicles [105, 102], which assemble from the fragmentation of multi-oocyte structures (the germ cell cysts) and retrieve more or less (somatic) cells.

In mammals, the number of primordial follicles available for a female throughout her reproductive life is fixed once and for all, during those critical periods (oocyte and follicle formations) [104]. The size of the ovarian reserve of primordial follicles is extremely variable between individuals of the same species belonging or not to different strains [106]. Despite its

---

[27]*Folliculus* means "little bag" in Latin.
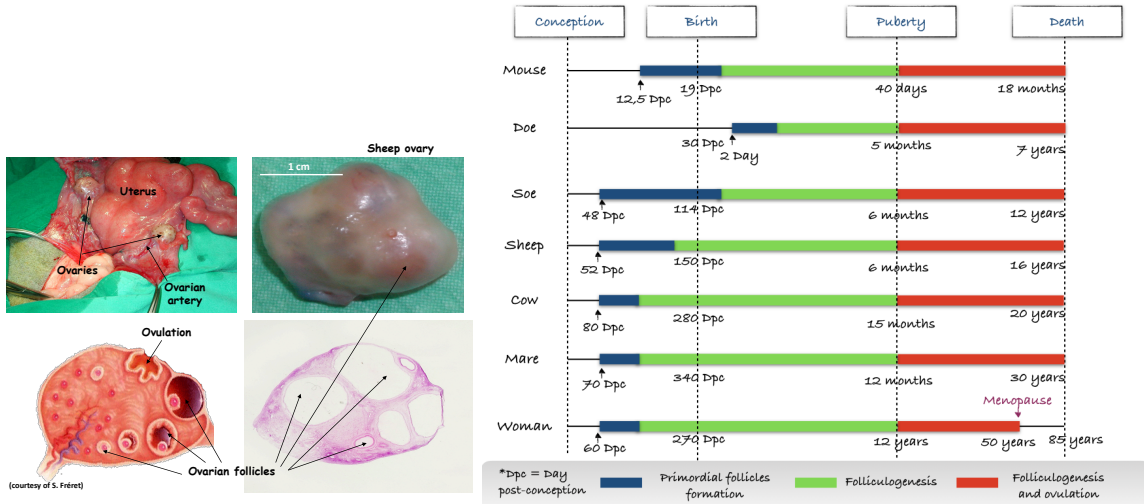
Fig. I.1 **Ovary and folliculogenesis.** *Left-panel: anatomy and histology of the ovary (courtesy of Danielle Monniaux). Top-left panel: overview of the genital tract; top-right panel: external view of an ovary after ovariectomy; bottom-left: schematic view of an ovarian section; bottom-right: histological slice of an ovary. Right-panel: main steps of folliculogenesis during the lifespan of an individual for different mammals species, adaptation of Figure 1 in [103].*

undeniable importance, an accurate estimate of the size of an individual's reserve of primordial follicles remains difficult to obtain due to the lack of proper experimental observation means.
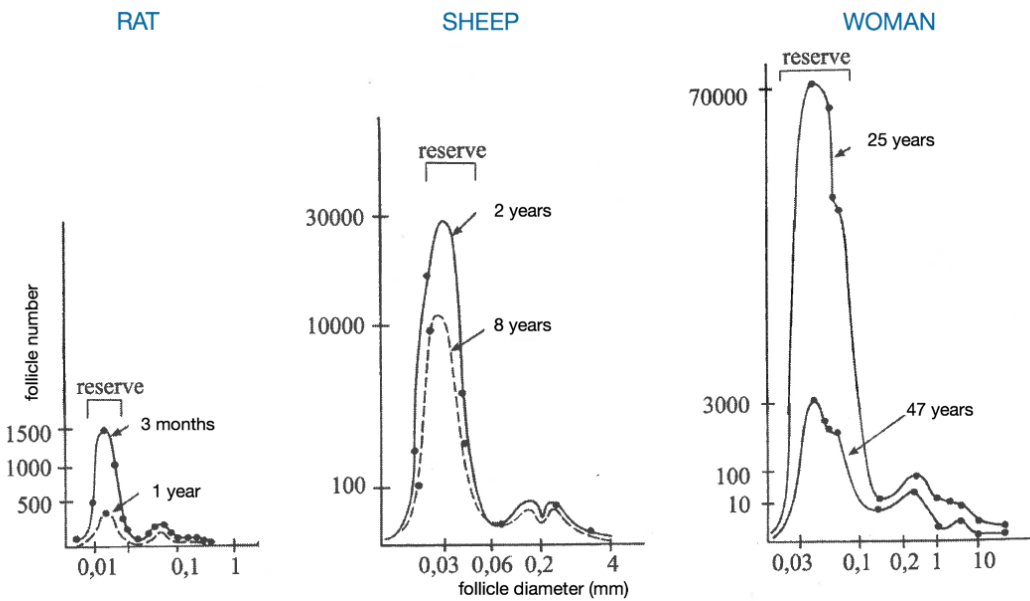
Fig. I.2 *Contributions of the different follicle categories to the total number of ovarian follicles in three species at different ages, extracted from [107] p.320.*

Once formed, the primordial follicles may begin to grow immediately or become quiescent. In the latter case, they will either degenerate or resume their growth up to ten years later [104, 108]. At any given moment in an individual's life, only a small proportion of primordial follicles enter growth (see the decreasing amplitude in the age-dependent distribution in Figure I.2) leading to a decrease in the size of the ovarian reserve of primordial follicles as the individual ages. The number of follicles that leave the primordial follicles reserve varies according to the species: about 10 per day in rats before puberty, 1 to 3 in ewes and about 20 in 20-year-old women [107]. In most mammals, death occurs before the reserve is completely exhausted. The human species and some primates are examples where this phenomenon usually happens the other way around: the reproductive life is shorter than the lifespan (menopause, see Figure I.1).

Not all primordial follicles grow and not all growing follicles reach the final stage of ovulatory follicles. For example, in women, of the few million primordial follicles present at 5 months of gestation, only about 450 follicles will be used for the ovulatory menstrual cycles in the normal human reproductive lifespan [109]. Before puberty, all the growing follicles degenerate through a process called atresia. A tiny proportion (about 0.01 %) of follicles which start growing after puberty manage to ovulate in adults and the rest disappear by atresia.

The frequency with which primordial follicles will exit their quiescent state and start growing is a key factor in maintaining an individual's fertility and a defective management of the ovarian reserve of primordial follicles can have serious consequences on it [109, 110]. For example, the early exhaustion of the ovarian reserve is one of the causes of human sterility (we speak of POF: premature ovarian failure) and can be caused by spontaneous genetic mutations, or chemical or radiation treatments [111]. The initial size and management of the ovarian reserve of primordial follicles is a highly variable phenomenon between individuals, of the same species or not, and may be affected by external environmental factors (pesticides, drugs). The exhaustion of the ovarian reserve is also regulated by internal regulations involving the growing follicles themselves. For example, the anti-Müllerian hormone (AMH) secreted by the growing follicles inhibits the activation of primordial follicles and slows down the growth of small follicles [112].

Some evolutionary strategies have been developed to ensure an individual's fertility despite the initially small size of the ovarian reserve of primordial follicles. For example, ewes of the Booroola genotype, which carry a naturally occurring mutation, have a lower reserve of primordial follicles than non-carrier ewes at birth, yet their ovaries contain two to three times more primordial follicles in adulthood [113]. This difference is offset by a different strategy in managing the reserve of primordial follicles. The Booroola genotype has a more economic behavior: the rate of follicle activation is lower. This difference between these two genotypes is studied in Chapter 2.

In the following section, we describe the mechanisms occuring during the growth of a follicle once it has been activated.

b)   Folliculogenesis stages

The follicle development, namely folliculogenesis, is a multistage morphogenesis process involving both growth and functional maturation that can be divided into two main phases: the basal phase of follicle development, the longest (around 75% of the development time),

which is under the control of ovarian growth factors, and the terminal phase, which is under the control of the pituitary gonadotropins (hormones) (see Figure I.3 and Table I.3). In all the mammalian species, the first steps of follicle development are comparable from the primordial follicle stage (30–50 μm) up to the apparition of a fluid-filled cavity called the antrum (at 200–250 μm of follicular diameter) in the small growing follicle.

Species	Development time (day)		Follicle diameter (mm)		
	Total	From follicles with antrum	Primordial follicle	Antrum formation	Ovulation
Mouse	19 to 22	3 to 4	0.03 to 0.05	≈ 0.2	0.6 to 0.8
Doe	97	10	0.03 to 0.05	≈ 0.2	6 to 7
Sheep	180	44	0.03 to 0.05	≈ 0.2	7 to 11
Cow	ND	22 to 42	0.03 to 0.05	≈ 0.2	10 to 20
Mare	120	35	0.03 to 0.05	≈ 0.2	45
Woman	> 200	50	0.03 to 0.05	≈ 0.2	20

Table I.3 – **Follicular development times and follicular diameters during certain stages of folliculogenesis in different mammals.** (Table based on Tables 1 and 2 of [103]).

The activation of primordial (quiescent) follicles is characterized by three main processes[28] [114]: (i) an irreversible transition of the somatic cell phenotype, characterized by a change in their shape, from flattened (quiescent cells) to cuboidal (proliferative cells); (ii) an increase in the number of somatic cells by cell division and (iii) the awakening and associated enlargement of the oocyte. The activation phase ends when all somatic cells have transitioned, at which time the mono-layer developmental stage is completed [115], and somatic cells will go on proliferating and building up several concentric layers [115].

During the main part of the basal phase, the follicle growth is the result of a joint increase in both the oocyte size and the number of surrounding somatic cells. The oocyte growth and cell proliferation are coupled by a close molecular dialogue established between the oocyte and the somatic cells. Growth factors derived from somatic cells (KIT Ligand) promote the growth of the oocyte and in turn those from the oocyte (BMP15, GDF9) influence the somatic cell proliferation. The morphological evolution of a follicle at this stage results from a finely balanced equilibrium between the growth rate of the oocyte and the proliferation rate of the follicular cells determining, for a given follicular diameter, the size of the oocyte, and the number of somatic cells and layers. This equilibrium is compromised in the case of some natural genetic mutations (observed and studied particularly in sheep species) or mutations induced experimentally (Knock-Out (KO) in mice). Depending on the molecular target of these mutations, the unbalance between growth and proliferation leads to either large oocytes surrounded by fewer cells (example of the FecB mutation in Booroola ewes, associated with an increase in the number of ovulations), or on the contrary to small oocytes buried in a dense mass of follicular cells (example of the inhibin KO in mice) [106].

At the beginning of the basal phase of the follicle development, from the primary stage to the preantral stage, the ovarian follicle grows as a compact cell aggregate with a spherical shape. In sheep, the somatic cell population doubles some 10–12 times and the cell layer number grows from one up to four-six layer [1]. In the multi-layered follicle about $200\mu m$ diameter (Table I.3), fluid-filled cavities appear and merge to form a single large cavity called

---

[28]In Chapter 2, we consider whether those three processes are sequential or not.
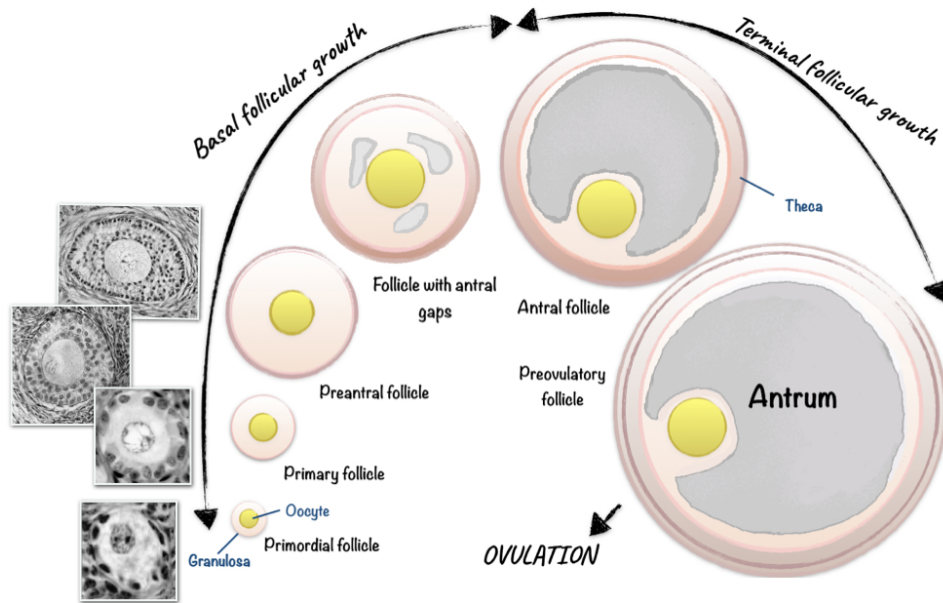
Fig. I.3   **Main steps of follicle development**. *Growing follicles exit the pool of quiescent primordial follicles. The primordial to primary stage transition is characterized by a morphological change of somatic cells: from a flattened shape, they adopt a round shape (cuboidal). During the basal phase, somatic cells proliferate while the maximal diameter of the oocyte is reached. During the terminal phase, cells proliferation slows down and follicle growth is mainly due to the antrum inflation. The vascularized theca appears at the pre-antral stage and has a role in maintaining the structure of the follicle. Between the pre-antral stage and the antral stage, small cavities filled with liquid appear within the somatic tissue, then merge to form a large cavity: the antrum. The pictures are histological sections of ovarian follicles in the compact growth phase (courtesy of Danielle Monniaux).*

the antrum. Up to this stage, the follicular development is mainly controlled by local ovarian factors. When it enters the final development phase, the follicle becomes dependent on the supply of pituitary hormones: the Follicle-stimulating hormone (FSH) and Luteinizing hormone (LH). The transition from the basal to the terminal phase corresponds thus to a functional change of the follicle: to continue its growth, the follicle needs an FSH hormonal support. In some mammalian species, this functional change appears after the appearance of the antrum cavity while in others like the rodents it appears at the time of the antrum formation.

I.2.2   Dataset presentation

The dataset used throughout this work was provided to us by Kenneth McNatty and is partially published in [116, 117]. The dataset consists of morphological measurements of follicles

performed by histology on ovaries from 120– and 135–day-old sheep fetuses (cf Figure I.4): follicle and oocyte diameter, cell number, layer number, presence or absence of an antrum. The sheep used in this study are of the Romney strain. The dataset is subdivided into two subsets corresponding to two different genotypes: the "wild-type" genotype and the "mutant" Booroola (BB) genotype. Morphodynamic differences are observed between these two genotypes. During fetal development, the primordial follicles appear later in BB, as well as the subsequent developmental stages. At the end of the compact phase, oocytes are larger and there are fewer cells in BB. The alteration of follicle development observed in Booroola genotype comes from a natural mutation affecting the receptor to growth factor BMP15 [106].
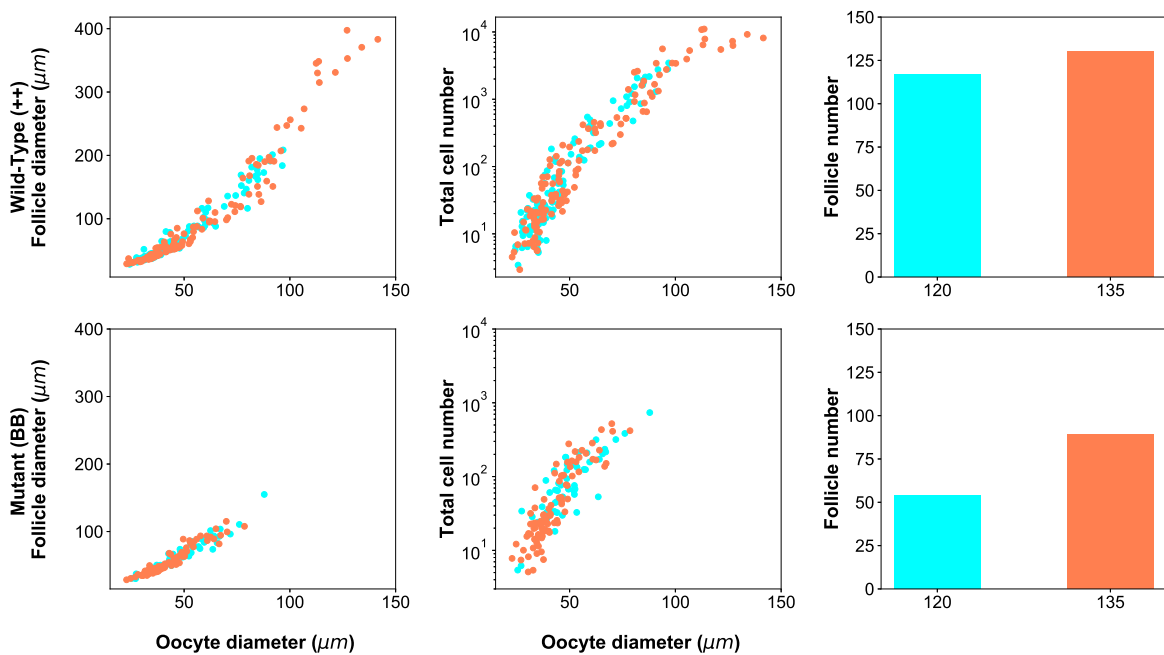
Fig. I.4 **Dataset presentation** [116]. *The blue points represent the 120–days old fetuses while the orange ones correspond to the 135–days old fetuses.*

The measurement of morphological characteristics of ovarian follicles is an invasive procedure [116]. The ovaries are removed from 120– and 135–day-old fetuses, then sectioned (slices of $20\mu m$ thickness) and fixed with a chemical agent. To perform the measurements (diameter, number of layers, etc.), experimentalists select the optical plane passing through the oocyte nucleolus (see for instance Figure I.5). Cells are counted from this optical plane. This 2D cell number can be used to assess the whole 3D cell number from stereological techniques (see details in [116]). We do not have access to temporal information associated with the morphological measures. We dwell on a particular feature of our dataset, the follicle type, that we describe in more details below.

a)   Follicle types in early development

Follicles (in basal growth phase) were classified according to a system, first introduced by [118] for the mouse and adapted for the bovine species in [119, 116]. It is based on morphological criteria (somatic cell shapes, number of layers and presence of an antrum) that can easily be

Fig. I.5 ***Histological slice of an ovary with different types of follicles****. Courtesy of Danielle Monniaux.*

observed on histological slices (see Figure I.5) and includes six categories:

- Type 1: primordial quiescent follicles (one layer of flattened somatic cells),

- Type 1A: transitory follicles (one layer with a mixture of flattened and cuboidal somatic cells),

- Type 2: primary follicles (from one to less than two complete layers of cuboidal somatic cells),
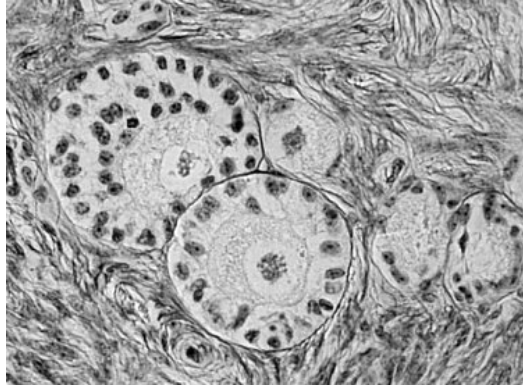
- Type 3: small preantral follicles (from two to less than four complete layers of cuboidal somatic cells),

- Type 4: large preantral follicles (from four to less than six complete layers of cuboidal somatic cells),

- Type 5: small antral follicles (more than five layers of cuboidal somatic cells and a fully formed antrum).

Figure I.6 presents the number of follicles of different types observed in our dataset. There are some differences in the distribution of follicle types according to the genotype, due to the later apparition of follicles in BB ewes. There are only very few primordial follicles already formed at 120 day of age in the Mutant genotype. Newly formed follicles have not reached the Type 4 and 5 at 120– or 135– days of age in Mutant genotype. In the following chapters, we have used most of the types present in the dataset: Type 1, 1A and 2 are used to model the activation phase (Chapter 2), and Type 2 to 4 are used for the compact growth phase modeling (Chapter 3).

b) Kinetics information: dataset building of Chapter 3 and Chapter 4

In complement to the dataset, we use information, presented in [121, 122, 120], on the times of appearance of the different follicular types during the fetal life (see Figure I.7):

- at day 100, most of the observed follicles were at the primordial stage (Type 1, quiescent) and few of them were at the primary stage (Type 2).
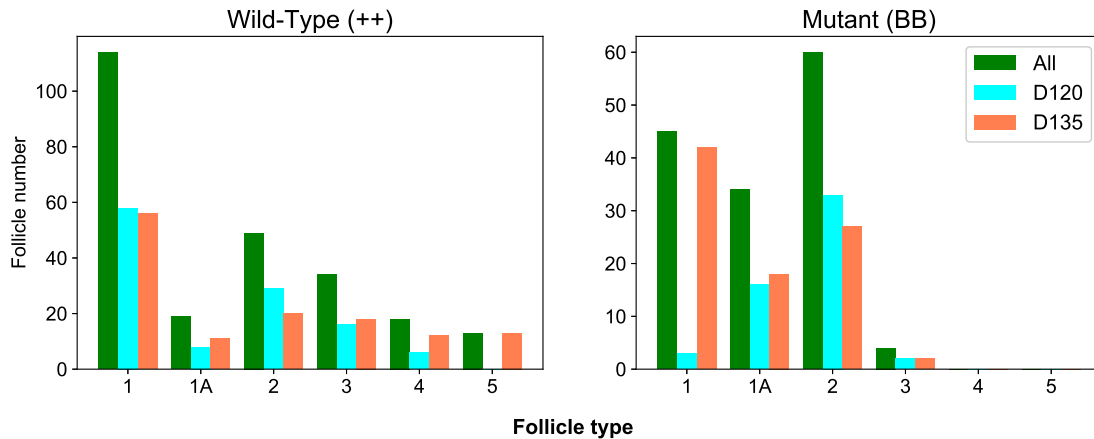
Fig. I.6   ***Follicle types in dataset [116]***. *Follicle distribution according to follicle types.*

- at day 120, most of the observed follicles were at the primordial stage and few of them were at higher stages (the most advanced have three somatic cell layers, Type 3 follicles).

- at day 135, most of the observed follicles were still at the primordial stage and some of them reach the early antral stage (Type 4).

From these data, we deduce the minimal transit times: it takes 20 days to go from a Type 2 to a Type 3 follicle, and 15 more days to go from a Type 3 to a Type 4. Due to the delay in follicle development observed for the Mutant genotype (BB), we do not have information for the third time point (t = 35). Our study therefore has focused only on the Wild-Type genotype and we build a new dataset with the following criteria:

- category "t=0": Type 2 follicles,

- category "t=20": Type 3 follicles with three complete layers,

- category "t=35": Type 4 follicles.

Our three categories correspond thus to relative time categories: "t=0", "t=20" and "t=35" are not real times but transit times (between specific follicles categories).
We obtain the dataset of 101 follicles presented in Figure I.8 (red, blue and green points) that is used in Chapter 3 to calibrate the model dedicated to the compact growth phase. Note that some follicles with the same oocyte diameter were not selected, due to the restrictive criterion on the Type 3 follicles.

c)   Dataset building of Chapter 2

The dataset dedicated to the activation of the ovarian follicles used in Chapter 2 is built with Type 1, Type 1A and Type 2 follicles of both the Mutant and Wild-Type genotypes from the original dataset. We select the healthy (properly formed) follicles of Type 1, all the Type 1A follicles and early Type 2 follicles corresponding to follicles with a single layer.
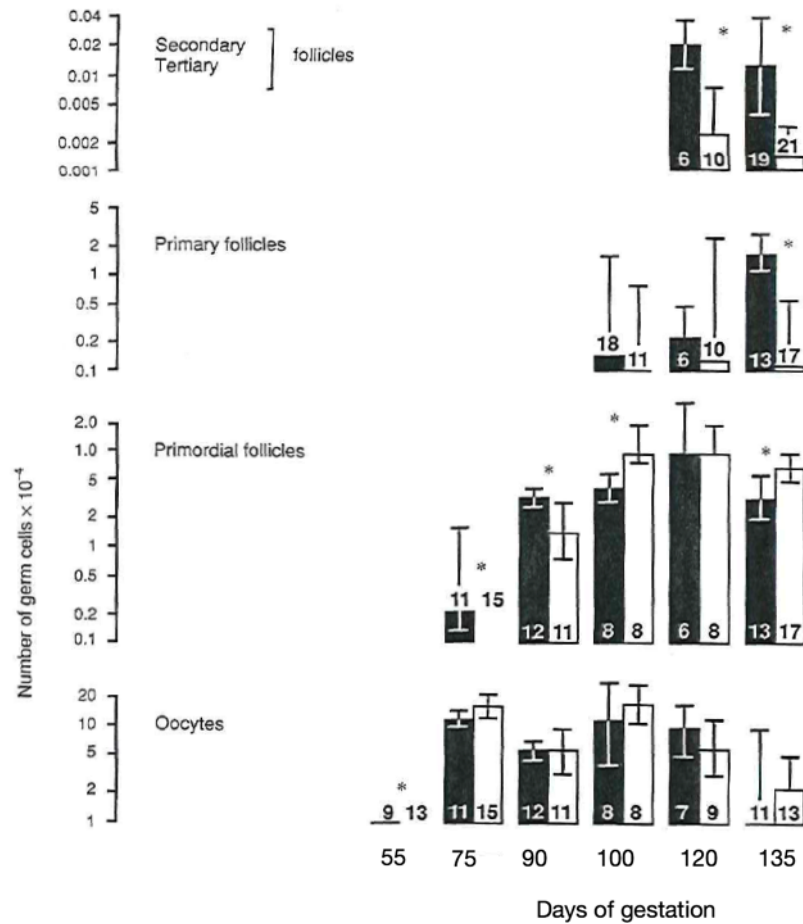
Fig. I.7 **Number of secondary and tertiary follicles, primary follicles, primordial follicles and oocytes per ovary in sheep fetuses with respect to the specific day of gestation**. *Extract from Figure 3 in [120]. The values given (scale bars on the left) are geometric means plotted on a log scale and vertical bars are the 95% confidence intervals. The number associated with each histogram refer to the number of fetuses. The star sign '∗' indicates significant differences between the genotypes (□: Booroola genotype, ■: Wild-Type genotype).*
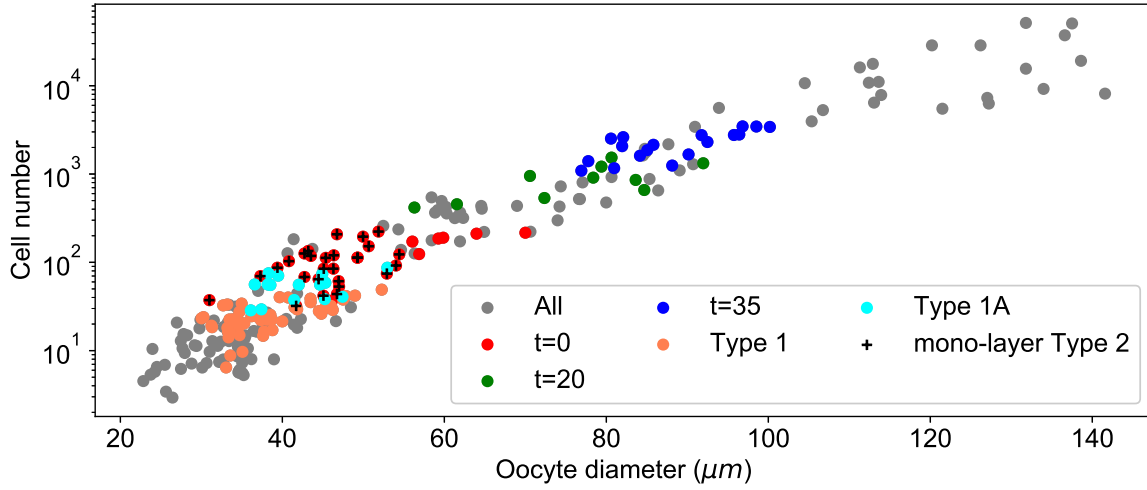
Fig. I.8 ***Initial Wild-Type and extracted datasets.*** *We extract from the original dataset, partially presented in [116], two datasets: one dedicated to the compact growth phase (red, green and blue points) and one dedicated to the activation phase (coral and cyan points, and cross sign +). The gray points represent the follicles of the original dataset that do not belong to any of the selected datasets.*

The oocyte size, as well as the ratio between the initial oocyte diameter and the cell number, inherited from the time of formation of the oocyte, has to be sufficient to start their development [105], and the activated follicles are thus the "properly formed" ones.
To select these follicles among the whole Type 1 follicles, we use the information, gathered in [123, 102] to design appropriate criteria.[29] Only properly formed follicles will be able to get activated. The oocyte size, as well as the ratio between the initial oocyte diameter and the cell number, inherited from the time of formation of the follicle have to be high enough.

We thus first fix the following thresholds on the minimal follicle diameter (34μm), minimal oocyte diameter (24μm) and minimal number of cells (fifteen). In addition, we introduce the notion of cell coverage of the oocyte to select the follicles with a good balance between the initial oocyte diameter and the cell number. We introduce the coefficient e_O that represents the average contact length between a somatic cell and the oocyte:

$$e_O = \frac{\pi d_O}{N_g^s} \tag{I.28}$$

where d_O is the oocyte diameter and N_g^s is the number of cells counted on the largest section. We compute the e_O coefficient for each follicle in our dataset (see Figure I.9). Note that considering an oocyte diameter of $24\mu m$ and a cell number of fifteen (as indicated in [123]), we obtain a coefficient e_O equal to $5\mu m$, which is a lower bound of the values obtained from our dataset. The oocyte diameter of $24\mu m$ is also lower than the minimal oocyte diameter in our dataset.

Finally, we consider the following critera to select the activated follicles as well as the "newly" Type 2 follicles:

---

[29]This study was performed on histological sections of follicles of Romanov and Ile-de-France strains.
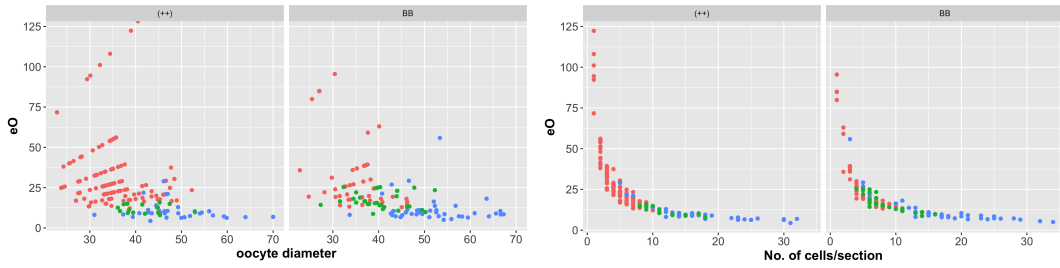
Fig. I.9 **Coefficient** e_O. *Using Formula (I.28), we compute the cell coverage for each follicle of the dataset introduced in section I.2.2, for both the Wild-Type genotype (++) or the Booroola genotype (BB). Left-panel: cell coverage coefficient e_O with respect to the oocyte diameter; right-panel: cell coverage coefficient e_O with respect to the cell number. The coral points represent the Type 1 follicles, the green ones, the Type 1A and the blue points, the Type 2 follicles.*

[C1] The maximal cell coverage of the oocyte is $e_O \leq 25\mu m$. Since the somatic cell diameter is about 10-12μm, we assume that the cell coverage e_O cannot exceed twice this value, so that cells remain in contact.

[C2] The oocyte diameter verifies $d_O \leq 55\mu m$.

The remaining follicles, that do not verify these criteria, are assumed to be unable to pursue their development.

Applying the above criteria ([C1] and [C2]), we construct the dataset used for the calibration of the follicle activation model: the Wild-Type dataset consists of 90 data points while the BB dataset consists of 81 data points. The dataset for the Wild-Type genotype corresponds to the coral and cyan points, and cross sign points in Figure I.8. We can observe that the two datasets overlap each other on the mono-layer Type 2 follicles.

I.3   Contributions and outline of the dissertation

The objective of this thesis is to design models dedicated to the early growth phase of the ovarian follicle, and analyze them using complementary formal and numerical approaches. Few models have been proposed to represent the dynamics of somatic cells involved in the development of an ovarian follicle. Most of the models tackle the terminal phase aspect of the folliculogenesis [10, 24, 22, 23], where the cell proliferation is under the control of hormones (FSH). Reviews on this aspect can be found in [124, 125]. To our knowledge, only one model is dedicated to the somatic cells dynamics modeling during the basal phase: introduced in [1], this model is a nonlinear stochastic age- and spatially-structured model dedicated to the dynamics of both the somatic cells and the oocyte. This article has been the starting point for this thesis and is presented in more detail at the beginning of Chapter 3.

During this thesis, two models representing the somatic cell dynamics shaping the ovarian follicle were proposed: one deals with the sequence of events occurring just after the initiation of follicle growth while the other is dedicated to the compact phase of follicular development. For each model, using data presented in the subsection I.2.2 above, quantitative analyses were conducted to complement the qualitative analyses. We also proceed for

each model to parameter calibration by proposing strategies adapted to our time-free dataset.
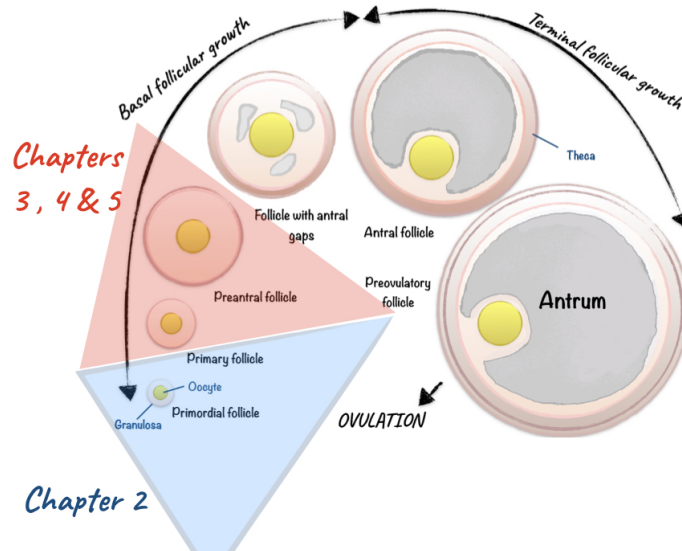
Fig. I.10   ***Chapter presentation.***

In Chapter 2, we investigate the sequence of somatic cell events occurring just after follicle activation. We introduce a nonlinear stochastic model accounting for the joint dynamics of two cell types, either precursor or proliferative cells. The initial precursor cell population transitions progressively to a proliferative cell population, by both spontaneous and self-amplified processes. In the mean time, the proliferative cell population may start either a linear or exponential growing phase. A key issue is to determine whether cell proliferation is concomitant or posterior to cell transition, and to assess both the time needed for all precursor cells to complete transition and the corresponding increase in the cell number with respect to the initial cell number. Using the probabilistic theory of first passage times, we design a numerical scheme based on a rigorous Finite State Projection and coupling techniques to assess the mean extinction time and the cell number at extinction time. We also obtain analytical formulas for an approximating branching process. We calibrate the model parameters using an exact likelihood approach using both experimental and in-silico datasets. We carry out a comprehensive comparison between the initial model and a series of submodels, which help to select the critical cell events taking place during activation. We finally interpret these results from a biological viewpoint.

In Chapter 3, we analyze a multitype age-dependent model for cell populations subject to unidirectional motion in both a stochastic and deterministic framework. Cells are distributed into successive layers; they may divide and move irreversibly from one layer to the next. We adapt results on the large-time convergence of PDE systems and branching processes to our context, where the Perron–Frobenius theorem cannot be applied. We derive explicit analytical formulas for the asymptotic cell number moments, and the stable age distribution. We illustrate these results numerically and apply them to the study of the morphodynamics of ovarian follicles. We prove the structural parameter identifiability of our model in the case

of age independent division rates. Using a set of experimental biological data (Wild-Type genotype solely), we estimate the model parameters to fit the changes in the cell numbers in each layer during the early stages of follicle development.

In Chapter 4, we present an additional work following that presented in Chapter 3. We present another approach to represent the compact growth of an ovarian follicle using the pre-existing Hele-Shaw model and other free boundary problems.

Finally, in Chapter 5, we study a multiscale inverse problem associated with a multi-type model for age structured cell populations. In the single type case, the model is a McKendrick–VonFoerster like equation with a mitosis-dependent death rate and potential migration at birth. In the multi-type case, the migration term results in an unidirectional motion from one type to the next, so that the boundary condition at age 0 contains an additional extrinsic contribution from the previous type. We consider the inverse problem of retrieving microscopic information (the division rates and migration proportions) from the knowledge of macroscopic information (total number of cells per layer), given the initial condition. We first show the well-posedness of the inverse problem in the single type case using a Fredholm integral equation derived from the characteristic curves, and we use a constructive approach to obtain the lattice division rate, considering either a synchronized or non-synchronized initial condition. We take advantage of the unidirectional motion to decompose the whole model into nested submodels corresponding to self-renewal equations with an additional extrinsic contribution. We again derive a Fredholm integral equation for each submodel and deduce the well-posedness of the multi-type inverse problem. In each situation, we illustrate numerically our theoretical results.

Chapter II

Stochastic nonlinear model for somatic cell population dynamics during ovarian follicle activation

This chapter is based on
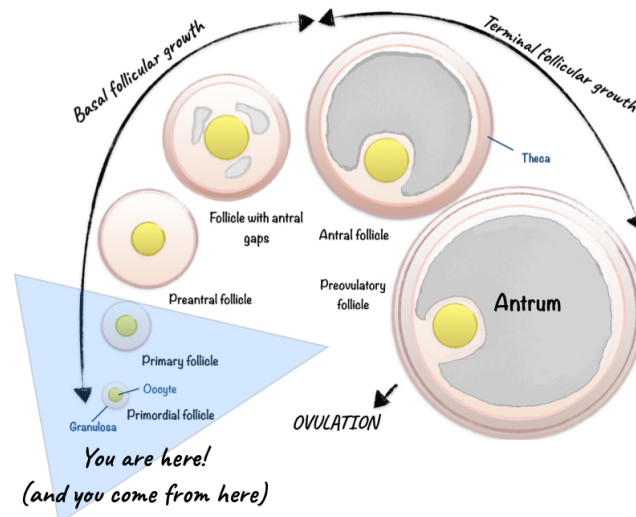
In mammals, the number of oocytes (egg cells) available for a female throughout her reproductive life is fixed once for all, during the fetal or perinatal period [104]. Dormant oocytes are sheltered within somatic structures called ovarian follicles, which remain in a quiescent state until they get activated and undergo a longstanding process of growth and

maturation ending by ovulation (release of a fertilizable oocyte). Growth initiation is asynchronous among follicles, so that all developmental stages can be observed in the ovaries at a given time, and follicles can remain quiescent for as long as tens of years [108].

In the earliest stages of development, ovarian follicles are made up of the oocyte and a single layer of surrounding somatic cells. The initial cell number is on the order of ten or several of tens according to the species and is quite variable between follicles. Such a variability is inherited from the mechanism underlying the formation of primordial follicles [105, 102], which assemble from the fragmentation of multi-oocyte structures (the germ cell cysts) and retrieve more or less (somatic) cells.

The activation of primordial (quiescent) follicles is characterized by three main processes [114]: (i) an irreversible transition of the somatic cell phenotypes, characterized by a change in their shape, from flattened (precursor cells) to cuboidal (proliferative cells); (ii) an increase in the number of somatic cells by cell division and (iii) the awakening and associated enlargement of the oocyte. The activation phase is ended when all somatic cells have transitioned, at which time the mono-layer developmental stage is completed, and somatic cells will go on proliferating and build up several concentric layers [115].

In this work, we focus on the sequence of events occurring just after the initiation of follicle growth. A key issue is to determine whether cell proliferation is concomitant or posterior to cell shape change, and to assess both the time needed for all precursor cells to complete transition and the corresponding increase in the cell number with respect to the initial cell number.

We introduce a model based on a formalism of cell population dynamics accounting for both cell transition and division. Within such a formalism, linear models have been built up on the branching property, disregarding cellular interactions [63, 65], while nonlinear models have accounted for interactions among different cell populations (e.g., typically, a feedback from differentiated cells onto precursor cells) either to ensure homeostasis, as in dynamical models for blood cells [127, 128, 129], or to achieve a proper developmental sequence, as in dynamical models for neural cells [9]. On our side, we are interested in assessing the duration of the activation process, and in ordering the events taking place during activation. A natural concept in probability theory to investigate these issues is the first passage time theory [130, 131], which aims to characterize the statistics of random events related to some particular outcomes. The analysis of first passage times are becoming more and more popular in mathematical biology [132, 133], to quantify random times needed to reach a given final state, such as population extinction for instance. Typically, the parameters of cell dynamics models are calibrated using time series of cell counts sorted into different cell types [134, 135]. In contrast, in the case of early folliculogenesis, we only have the number of cells. Indeed, precursor and proliferative cell numbers are not available directly as a function of time, but only in relation with other morphological variables such as the oocyte and follicle diameters [119, 136, 116, 137], so that we lack kinetic information. Yet, thanks to the discrete-time embedded Markov chain, we could apply here classical statistical tools like the maximum likelihood [51], and related parameter identifiability concept [138], by using the information on the state space alone.

Our model allows us to study the joint dynamics of the precursor cells F and proliferative cells C within a single follicle, whose populations are ruled by four types of possible cell events. Two cell events occur at the expense of the precursor cells, which are consumed during their transition : (i) $\mathcal{R}_1$ is the spontaneous transition of precursor cells into proliferative cells, whose rate $\alpha_1 F$ is linearly proportional to the number of precursor cells; (ii) $\mathcal{R}_2$ is the auto-

amplified transition of precursor cells into proliferative cells, which occurs at rate $\beta_1 \frac{FC}{F+C}$. This event represents the feedback of proliferative cells onto the transition of the precursor cells. Two other cell events increase the proliferative cell population without affecting the precursor cell population: (i) $\mathcal{R}_3$ is an asymmetric division of precursor cells F (giving rise to one precursor cell and one proliferative cell), which occurs at rate $\alpha_2 F$; (ii) $\mathcal{R}_4$ is a symmetric division of the proliferative cells C (giving rise to two proliferative cells), which occurs at rate γC.

These four cell events are the building blocks of our main model $\mathcal{M}_{FC}$, which is summarized below :

$$
\begin{array}{rccl}
 & \text{Cell events} & \text{Rate} & \\
\mathcal{R}_1: & (F,C) \to (F-1, C+1), & \alpha_1 F, & \\
\mathcal{R}_2: & (F,C) \to (F-1, C+1), & \beta_1 \frac{FC}{F+C}, & (\mathcal{M}_{FC}) \\
\mathcal{R}_3: & (F,C) \to (F, C+1), & \alpha_2 F, & \\
\mathcal{R}_4: & (F,C) \to (F, C+1), & \gamma C.
\end{array}
$$

Cell events $\mathcal{R}_1$ and $\mathcal{R}_4$ constitute the fundamental ingredients involved in the activation process. We also consider two additional cell events, $\mathcal{R}_3$ and $\mathcal{R}_4$, which are not only intended to enrich the model behavior, but are also substantiated by biological observations.

Cell event $\mathcal{R}_3$ considers that flattened (precursor) cells may divide before transition, which is consistent with experimental studies where KI67 staining (a marker of cell cycle progression) was detected in some flattened cells [139]. Since the number of flattened cells is non increasing, one can envisage the existence of self-renewing asymmetric divisions in flattened cells, giving birth to one proliferative cell (and keeping the precursor cell number unchanged).

Cell event $\mathcal{R}_2$ accounts for a possibly auto-amplified acceleration in cell shape transitions, which could result from the molecular mechanisms underlying follicle activation and establishing a dialog between the oocyte and somatic cells [140]. In brief, the initiation signal (mTORC1) is first perceived by somatic cells [141], which then start stimulating the oocyte through specific signaling pathways (KIT-Ligand cytokine). In turn, once activated, the oocyte signals to the somatic cells through factors of the TGFβ family [142] (mainly GDF9 and BMP15). This molecular dialog settles a positive feedback loop, which can be represented by an auto-amplified transition rate. In sheep, there exist natural mutations affecting this molecular dialog (disruption of either the GDF9 or BMP15 ligand, or the receptor to BMP15). Introducing cell event $\mathcal{R}_2$ can help to investigate possible differences in the activation process in wild-type compared to mutant strains. More specifically, we have access to experimental cell numbers (courtesy of Ken McNatty) obtained either from a wild-type strain (Ile-de-France) or a mutant strain for BMP15R (Booroola), whose follicle development is known to be clearly different in the multi-layer stages [116], especially as far as cell dynamics. Whether cell dynamics is also affected during the mono-layer stage remains unclear [143], which is an additional motivation for this work.

All the reactions rates (α_1, β_1, α_2 and γ) are non-negative. At initial time, there are only precursor cells, and the initial condition is chosen as a random positive integer variable, in consistency with the observed biological variability.

In the following, we will use different submodels derived from the full model $\mathcal{M}_{FC}$, by removing either one or several cell events (hence setting to zero the corresponding parameter values β_1, α_2 and/or γ). We will name these submodels by explicitly mentioning the remaining events. For instance, model $(\mathcal{R}_1, \mathcal{R}_3)$ consists only of the spontaneous cell transition event and asymmetric cell division ($\beta_1 = \gamma = 0$), while model $(\mathcal{R}_1, \mathcal{R}_4)$ is composed of the spontaneous cell transition event and asymmetric cell division ($\beta_1 = \alpha_2 = 0$).

Model $\mathcal{M}_{FC}$ can be mathematically formulated either with Ordinary Differential Equations (ODEs) or Continuous time Markov chain (CTMC) [144].

The stochastic description is especially appropriate when dealing with a small number of cells. Even if the cell numbers in activating follicles are small, a deterministic formulation of model $\mathcal{M}_{FC}$ can still be convenient to get insight into the transient behavior of the cell populations and the parameter influence on the model outputs. Using the stochastic version of model $\mathcal{M}_{FC}$, we can illustrate the dynamics of both the precursor and proliferative cells (Figure II.1). The C population grows as the F population decreases until extinction (top-left panel), and the proportion of proliferative cells $p_C := \frac{C}{F+C}$ increases monotonously from 0 to 1 (bottom-left panel). In the (C, F) phase plane (top-right panel), we can observe that the number of precursor cells remains constant (aligned red or black points on the horizontal line (k, F), $k \in \mathbb{N}$) whenever there is a division event ($\mathcal{R}_3$ or $\mathcal{R}_4$). In contrast, whenever there is a transition event ($\mathcal{R}_1$ or $\mathcal{R}_2$), the number of precursor cells decreases by one, as illustrated by the jump from the current line $((k, F), k \in \mathbb{N})$ to the lower one $((k, F-1), k \in \mathbb{N})$. Hence, in this simulation, we observe a sequence of transition and division events (which appear to be here mainly spontaneous transitions $\mathcal{R}_1$ and asymmetric divisions $\mathcal{R}_3$ due to the specific parameter choice). If we are only given the sequence of events types (i.e. sequence of state visiting by the chain) in this plane, we cannot discriminate $\mathcal{R}_1$ from $\mathcal{R}_2$, neither $\mathcal{R}_3$ from $\mathcal{R}_4$. Note that, depending on the initial condition, some parts of the phase plane cannot be reached. The trajectories can also be observed in the (C, p_C) phase plane (bottom-right panel). In this case, the trajectories remain on the curves parameterized by $((k, \frac{k}{F+k}), k \in \mathbb{N})$ if a division event ($\mathcal{R}_3$ or $\mathcal{R}_4$) occurs, whereas they move to the upper curves parameterized by $((k, \frac{k}{F-1+k}), k \in \mathbb{N})$ whenever a transition event ($\mathcal{R}_1$ or $\mathcal{R}_2$) occurs.

The manuscript is organized as follows. After introducing the mathematical definitions in Section 2, we analyze both the deterministic and stochastic versions of model $\mathcal{M}_{FC}$ in Section 3. In subsection 3.1, we obtain the analytical solutions of the deterministic model, and explore the parameter influence on the model outputs. Subsection 3.2 deals with the Markov chain formulation of model $\mathcal{M}_{FC}$. In the linear case ($\beta_1 = 0$), we obtain analytical formulas for the mean extinction time. In the nonlinear case, we design a numerical scheme based on a rigorous Finite State Projection (see [58, 59]) and coupling techniques to assess the mean extinction time. In both cases, we study the sensitivity of the extinction time, as well as the cell number at extinction time, with respect to the parameter values. In section 4, using the embedded Markov chain, we calibrate the parameters of the different submodels and full model $\mathcal{M}_{FC}$ from our experimental, time-free datasets, and analyze the practical identifiability in each case. From data-fitting, we manage to retrieve hidden kinetic information and provide some biological interpretations of out results. We conclude in section 5.

II.1 Model definition

Markov chain formulation

On a probability space $(\Omega, \mathcal{F}, \mathbb{P})$, let the initial number of precursor (flattened) cells F_0 be a positive integer random variable. The population of precursor cells F and proliferative
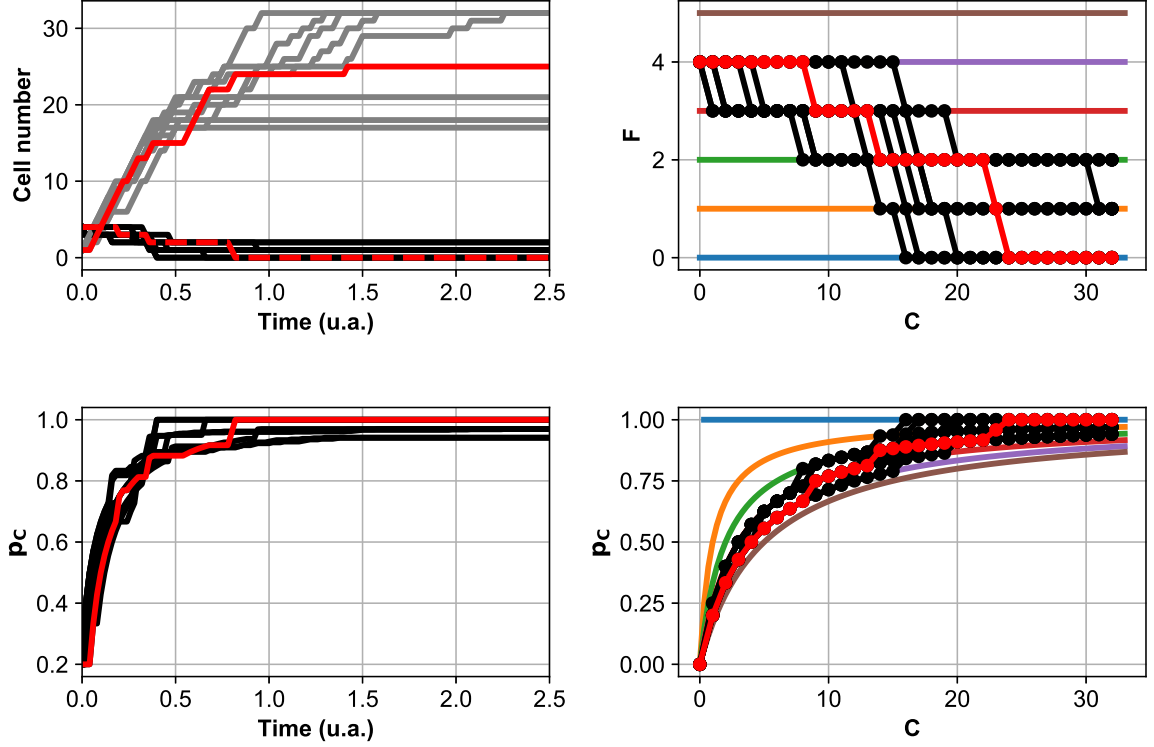
Fig. II.1 ***Illustration of the dynamics generated by model*** $\mathcal{M}_{FC}$***.*** *The dynamics of the precursor and proliferative cells are computed using a Gillespie SSA algorithm [145] with the parameter values:* $\alpha_1 = 1$, $\beta_1 = 0.01$, $\alpha_2 = 10$, $\gamma = 0.001$ *and a deterministic initial condition* $F(0) = 4$*. In each panel, the black or gray lines represent 9 different trajectories of the process and the red line corresponds to one specific trajectory. Top-left panel: Number of precursor* F *(black lines) and proliferative* C *(gray lines) cells as a function of time. Bottom-left panel: Proportion* p_C *of proliferative cells as a function of time. Top-right panel: Number of precursor cells* F *as a function of the number proliferative cells* C*. Bottom-right panel: Proportion of proliferative cells* p_C *as a function of the number of proliferative cells* C*.*

(cuboidal) cells C follows the Stochastic Differential Equation (SDE) below:

$$F_t = F_0 - \mathcal{Y}_1 \left(\int_0^t \alpha_1 F_s ds \right) - \mathcal{Y}_2 \left(\int_0^t \beta_1 \frac{F_s C_s}{F_s + C_s} ds \right),$$

$$C_t = \mathcal{Y}_1 \left(\int_0^t \alpha_1 F_s ds \right) + \mathcal{Y}_2 \left(\int_0^t \beta_1 \frac{F_s C_s}{F_s + C_s} ds \right)$$

$$+ \mathcal{Y}_3 \left(\int_0^t \alpha_2 F_s ds \right) + \mathcal{Y}_4 \left(\int_0^t \gamma C_s ds \right). \quad \text{(II.1)}$$

where $\mathcal{Y}_i$, for all $i = 1, 2, 3, 4$, are mutually independent standard Poisson processes. $X = (X_t)_{t \geq 0}$, with $X_t := (F_t, C_t)$ for all $t \geq 0$, denotes the solution of (II.1). $(\mathcal{F}_t)_{t \geq 0}$ denotes the canonical filtration generated by the process X.

We can also see X as a continuous-time Markov chain with countable state space $\mathcal{S} :=$

$\mathbb{N}^2 \backslash \{(0,0)\}$ and transition matrix $Q := (q(x,y))_{x,y \in \mathcal{S}}$, with for all $(f,c) \in \mathcal{S}$,

$$q((f,c),(f-1,c+1)) = \alpha_1 f + \beta_1 \frac{fc}{f+c},$$
$$q((f,c),(f,c+1)) = \alpha_2 f + \gamma c.$$

We recall that Q is linked to the infinitesimal generator $\mathcal{L}$ by the Dynkin's formula (Theorem 2.2, p.380, [54]):

$$\mathcal{L}g(x) = \sum_{y \in \mathcal{S}, y \neq x} q(y,x)g(y) - q(x)g(x), \text{ where } q(x) = \sum_{y \in \mathcal{S}, y \neq x} q(x,y).$$

Thus, the infinitesimal generator $\mathcal{L}$ of X is given by

$$\mathcal{L}g(f,c) = (\alpha_1 f + \beta_1 \frac{fc}{f+c}) [g(f-1,c+1) - g(f,c)]$$
$$+ (\alpha_2 f + \gamma c) [g(f,c+1) - g(f,c)],$$

for all g bounded functions and for all $(f,c) \in \mathcal{S}$.

In the whole study, we will need the following hypotheses:

Hypothesis II.1. *The spontaneous activation rate α_1 is positive.*

Hypothesis II.2. *The initial condition F_0 is L_2-integrable.*

For specific results, we will also need an additional hypothesis:

Hypothesis II.3. *The spontaneous activation rate α_1 is strictly greater than the proliferation rate γ: $\alpha_1 > \gamma$.*

With Hypothesis II.2, we apply Theorem 1.22 of [52] (p.12-13) and deduce that the process M_t^g defined as

$$M_t^g := g(X_t) - g(X_0) - \int_0^t \mathcal{L}g(X_s)ds \tag{II.2}$$

is a $\mathcal{F}_t$-martingale, for all $t \geq 0$.

Note that the F process is a non-negative decreasing process. To study the hitting time of the state $F = 0$, we introduce the following definition

Definition II.1. *Let τ^{F_0} be the extinction time of the precursor cell population F*

$$\tau^{F_0} := \inf\{t \geq 0; \quad F_t = 0 | F_0\}.$$

The number of proliferative cells C at $t = \tau^{F_0}$ is $C_{\tau^{F_0}}$.

Mean-field formulation

To get some insight into the model, we describe the mean-field version of the model $\mathcal{M}_{FC}$, given by the set of ODE below:

$$\begin{cases} \frac{d}{dt}f(t) = -\alpha_1 f(t) - \beta_1 f(t)\frac{c(t)}{f(t)+c(t)}, \\ \frac{d}{dt}c(t) = (\alpha_1 + \alpha_2)f(t) + \beta_1 f(t)\frac{c(t)}{f(t)+c(t)} + \gamma c(t), \end{cases} \tag{II.3}$$

with the initial condition $(f(0),c(0)) = (f_0,0)$, with $f_0 \in \mathbb{R}_+$.

II.2 Model analysis

In this section we analyze the cell dynamics of the precursor and proliferative cells both for the deterministic and stochastic versions of model $\mathcal{M}_{FC}$. We start by solving analytically the deterministic formulation, and investigate the effect of each parameter on the model outputs. Then, we study the mean extinction time of the precursor cell population and the number of proliferative cells at that time.

II.2.1 Analysis of the deterministic model

From the ODE sytem (II.3), we deduce the change in the proliferative cell proportion $p_C(t) := \frac{c(t)}{f(t)+c(t)}$:

$$\frac{d}{dt}p_C(t) = \alpha_1 + \alpha_2 - (\alpha_1 + 2\alpha_2 - \beta_1 - \gamma)p_C(t) + (\alpha_2 - \beta_1 - \gamma)p_C(t)^2$$
$$= (\alpha_2 - \beta_1 - \gamma)(p_C(t) - 1)(p_C(t) - \frac{\alpha_1 + \alpha_2}{\alpha_2 - \beta_1 - \gamma}). \quad \text{(II.4)}$$

From ODEs (II.3) and (II.4), using the classical method of separation of variables, we can compute the analytical expressions for the proliferative cell proportion $p_C(t)$, proliferative cell number $c(t)$ and precursor cell number $f(t)$:

Proposition II.1. *The solution of the ODE system* (II.3) *is, for all $t \geq 0$,*

$$f(t) = f_0 \exp\left(-\alpha_1 t - \beta_1 \int_0^t p_C(s)ds\right),$$
$$c(t) = f_0 \left(\exp\left(\alpha_2 t + (\gamma - \alpha_2)\int_0^t p_C(s)ds\right) - \exp\left(-\alpha_1 t - \beta_1 \int_0^t p_C(s)ds\right)\right).$$

In addition, the solution of ODE (II.4) *is*

$$p_C(t) = \frac{1 - \exp\left(-(\alpha_1 + \beta_1 + \gamma)t\right)}{1 - \frac{\alpha_2 - \beta_1 - \gamma}{\alpha_1 + \alpha_2}\exp\left(-(\alpha_1 + \beta_1 + \gamma)t\right)}. \quad \text{(II.5)}$$

Remark II.1. *The total cell number verifies*

$$n(t) := f(t) + c(t) = f_0 \exp\left(\alpha_2 t + (\gamma - \alpha_2)\int_0^t p_C(s)ds\right).$$

As the proliferative cell proportion p_C converges to 1, the total cell number grows exponentially, first at rate α_2 and then at rate γ.

We illustrate the changes in the state variables along time on Figure II.2, for different parameter configurations corresponding to different submodels. The transition kinetics of the precursor cells can either follow an exponential decay when β_1 is zero (or much smaller than α_1), or a sharper transition when β_1 is larger than α_1, with a sigmoid-like shape and an inflexion point (top-left panel). The growth kinetics of the proliferative cells can be characterized by three types of behavior (top-middle and top-right panels):

- a saturated growth with steadily decreasing speed with submodels $(\mathcal{R}_1)$ and $(\mathcal{R}_1, \mathcal{R}_3)$,

- an exponential growth as long as $\gamma > 0$ with submodel $(\mathcal{R}_1, \mathcal{R}_4)$,

- a logistic growth when the feedback term is strong enough (submodel $(\mathcal{R}_1, \mathcal{R}_2)$).

The growth kinetics of the total cell number behaves accordingly (bottom-right panel), with three possible patterns: exponential growth, saturated growth for submodel $(\mathcal{R}_1)$, and steadiness for submodel $(\mathcal{R}_1, \mathcal{R}_2)$. Finally, the proportion p_C (bottom-left panel) may either increase in a saturated manner (with steadily decreasing speed, submodels $(\mathcal{R}_1)$ and $(\mathcal{R}_1, \mathcal{R}_3)$), or in a sigmoid-like manner (with a change in the acceleration sign) if β_1 or γ are high enough. The inflexion point of $t \mapsto p_C(t)$ can be computed from the analytical solution (II.5):

$$\bar{p}_C = \frac{\alpha_1 + 2\alpha_2 - (\beta_1 + \gamma)}{2\alpha_2 - 2(\beta_1 + \gamma)}.$$

Note that according to the observed variables, the submodels cannot be distinguished from one another, or, alternatively, different parameter values (within a same submodel) may lead to identical outputs. Indeed, the changes in the precursor cell population are independent of parameters α_2, γ, and, more strikingly, parameters β_1 and γ cannot be separated in the analytical solution (II.5), leading to the same kinetic patterns as long as the combination $\gamma + \beta_1$ remains unchanged.

From Proposition II.1, we deduce that p_C is a strictly increasing function, hence we can invert the p_C function and deduce that $\forall t \in \mathbb{R}_+, \exists! p \in [0, 1)$, such that

$$t(p) = p_C^{-1}(p) = \frac{-1}{(\alpha_1 + \beta_1 + \gamma)} \ln\left(\frac{1 - p}{1 - p^{\frac{\alpha_2 - \beta_1 - \gamma}{\alpha_1 + \alpha_2}}} \right).$$

II.2.2 Analysis of the extinction of the precursor cell population

To simplify the proofs, we will consider in the following that the initial condition is a deterministic value $f_0 \in \mathbb{N}^*$. All the proofs can be generalized to the random F_0 case by conditioning by the law of F_0.

a) Analytical expressions in the linear case

When β_1 is zero, the process X is linear, and we can compute the law of the extinction time. In the case when, in addition, either α_2 or γ is zero, or both are zero, the mean number of proliferative cells at extinction time can also be computed.
In this subsection we will write $X_t^L = (F_t^L, C_t^L)$ the solution of the SDE (II.1) when $\beta_1 = 0$ and $\tau_L^{f_0}$ the associated extinction time of the population F_t^L:

$$\tau_L^{f_0} := \inf\{t; \quad F_t^L = 0 | f_0\}. \tag{II.6}$$

Note that the F^L process is independent of the C^L process. The jumping times T_k of F^L, for all $k \in [\![0, f_0 - 1]\!]$, are given by

$$T_{k+1} := T_k + \mathcal{E}\left(\alpha_1(f_0 - k)\right), \tag{II.7}$$

with $T_0 = 0$ by convention. Note that $T_{f_0} = \tau_L^{f_0}$.
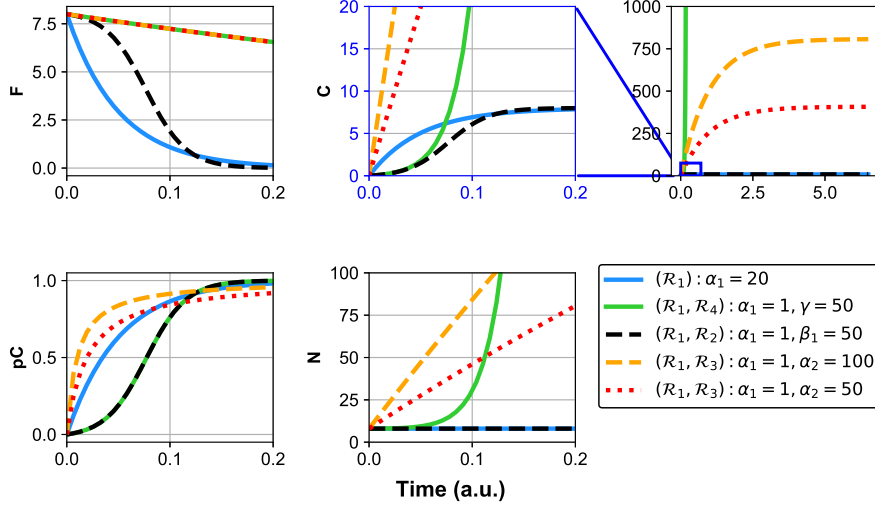
Fig. II.2 ***Parameter influence on the outputs of the deterministic model.***
*From ODEs (II.3) and (II.4), we compute numerically (using the Python solver
odeint from the package scipy.integrate), for different parameter values, the different
model outputs as a function of time. Top-left panel: precursor cell number $f(t)$.
Top-middle panel: proliferative cell number $c(t)$, with a zoom insert in the top-right
panel. Bottom-left panel: proliferative cell proportion $p_C(t)$. Bottom-middle panel:
total cell number $n(t)$. The legend insert specifies the (non-zero) parameter values
corresponding to each submodel and the color code. Blue line: submodel $(\mathcal{R}_1)$ with
$\alpha_1 = 20$; green line: submodel $(\mathcal{R}_1, \mathcal{R}_4)$ with $\alpha_1 = 1$ and $\gamma = 50$; black dashed
line: submodel $(\mathcal{R}_1, \mathcal{R}_2)$ with $\alpha_1 = 1$ and $\beta_1 = 50$; orange dashed line: submodel
$(\mathcal{R}_1, \mathcal{R}_3)$ with $\alpha_1 = 1$ and $\alpha_2 = 100$; red dotted line: submodel $(\mathcal{R}_1, \mathcal{R}_3)$ with $\alpha_1 = 1$
and $\alpha_2 = 50$. In each case, the initial number of precursor cells is fixed to $f_0 = 8$.*

Proposition II.2 (F_t^L and $\tau_L^{f_0}$ laws)**.** *Under Hypothesis II.1 and for all $t \geq 0$, $F_t^L | F_0 = f_0$
follows a binomial law with parameters $(n, p) = (f_0, e^{-\alpha_1 t})$, and the extinction time $\tau_L^{f_0}$, de-
fined by formula (II.6), follows a generalized Erlang law (or hypo-exponential law) of density:*

$$f_{\tau_L^{f_0}}(t) = \alpha_1 f_0 e^{-\alpha_1 t}(1 - e^{-\alpha_1 t})^{f_0 - 1} \mathbb{1}_{[0, +\infty[}(t),$$

such that $\mathbb{E}\left[\tau_L^{f_0}\right] = \dfrac{1}{\alpha_1} \displaystyle\sum_{k=1}^{f_0} \dfrac{1}{k}.$

Proof. Let $t \geq 0$ and $f \in [\![0, f_0]\!]$. Since F_t is autonomous and is a pure death process, we can
directly write the following forward Kolmogorov equation: for all $f \in [\![0, f_0]\!]$,

$$\frac{d}{dt}\mathbb{P}\left[F_t^L = f | F_0 = f_0\right] =$$
$$\alpha_1(f+1)\mathbb{P}\left[F_t^L = f+1 | F_0 = f_0\right] - \alpha_1 f \mathbb{P}\left[F_t^L = f | F_0 = f_0\right]. \quad \text{(II.8)}$$

Solving by recurrence (II.8), we deduce that, for all $f \in [\![0, f_0]\!]$,

$$\mathbb{P}\left[F_t^L = f | F_0 = f_0\right] = \binom{f_0}{f}(e^{-\alpha_1 t})^f (1 - e^{-\alpha_1 t})^{f_0 - f}.$$

Note that $\mathbb{P}[F_t = 0|F_0 = f_0] = (1 - e^{-\alpha_1 t})^{f_0}$ which converges to 1 when t goes to infinity. Hence, the process F^L extincts almost surely (a.s.) when t goes to infinity, hence $\tau_L^{f_0} < \infty$. Before computing the law of $\tau_L^{f_0}$, we can directly obtain its mean using the recursive expression (II.7):

$$\mathbb{E}\left[\tau_L^{f_0}\right] = \sum_{k=0}^{f_0-1} \mathbb{E}\left[T_{k+1} - T_k\right] = \sum_{k=0}^{f_0-1} \mathbb{E}\left[\mathcal{E}\left(\alpha_1(f_0 - k)\right)\right] = \frac{1}{\alpha_1} \sum_{k=1}^{f_0} \frac{1}{k}.$$

Then, using the same recursive expression (II.7), we deduce that $\tau_L^{f_0}(= T_{f_0})$ follows a generalized Erlang law whose density function is:

$$f_{\tau_L^{f_0}}(t) = \mathbb{1}_{t\geq 0} \sum_{i=0}^{f_0-1} \prod_{j\neq i, j=0}^{f_0-1} \frac{f_0 - j}{i - j} \alpha_1(f_0 - i)e^{-\alpha_1(f_0-i)t}. \tag{II.9}$$

Due to the specific form of the exponential rate in Eq. (II.9), we can simplify it further. As $\prod_{j\neq i, j=0}^{f_0-1} (f_0 - j) = \frac{f_0!}{f_0 - i}$ and

$$\prod_{j\neq i, j=0}^{f_0-1} (i - j) = \prod_{j=0}^{i-1}(i - j) \times \prod_{j=i+1}^{f_0-1} (i - j)$$

$$= i!(-1)^{f_0-1-i} \prod_{j=1}^{f_0-1-i} j = (-1)^{f_0-1-i}i!(f_0 - 1 - i)!,$$

we deduce

$$f_{\tau_L^{f_0}}(t) = \alpha_1 \mathbb{1}_{t\geq 0} \sum_{i=0}^{f_0-1} \frac{f_0!}{i!(f_0 - 1 - i)!}(-1)^{f_0-1-i}e^{-\alpha_1(f_0-i)t}$$

$$= \alpha_1 f_0 e^{-\alpha_1 t}\mathbb{1}_{t\geq 0} \sum_{i=0}^{f_0-1} \binom{f_0 - 1}{i}(-e^{-\alpha_1 t})^{f_0-i-1}$$

$$= \alpha_1 f_0 e^{-\alpha_1 t}(1 - e^{-\alpha_1 t})^{f_0-1}\mathbb{1}_{t\geq 0}.$$

$\square$

Figure II.3 illustrates both the precursor cell distribution at different times (left panel) and the extinction time distribution of precursor cells (right panel) in the linear model $(\mathcal{R}_1, \mathcal{R}_3, \mathcal{R}_4)$. Thanks to the analytical solutions, one can easily compute a confidence interval for the extinction time. For instance, we compute the time $t = t_{0.95}$ for which extinction has occurred with probability 0.95,

$$\mathbb{P}[F_{t_{0.95}} = 0|F_0 = f_0] = 1 - e^{-\alpha_1 f_0 t_{0.95}} \geq 0.95 \Rightarrow t_{0.95} \geq -\frac{\ln(0.05)}{\alpha_1 f_0} \approx \frac{3}{\alpha_1 f_0}.$$

We now study the mean number of proliferative cells at the extinction time. We define the stochastic processes $C^{k,j}$, for $(k, j) \in \mathbb{N} \times \mathbb{N}$, as independent and identically distributed Yule processes. We recall that the Yule process can be seen as the solution of

$$C_t^{0,0} = 1 + \mathcal{Y}\left(\gamma \int_0^t C_s^{0,0}ds\right),$$
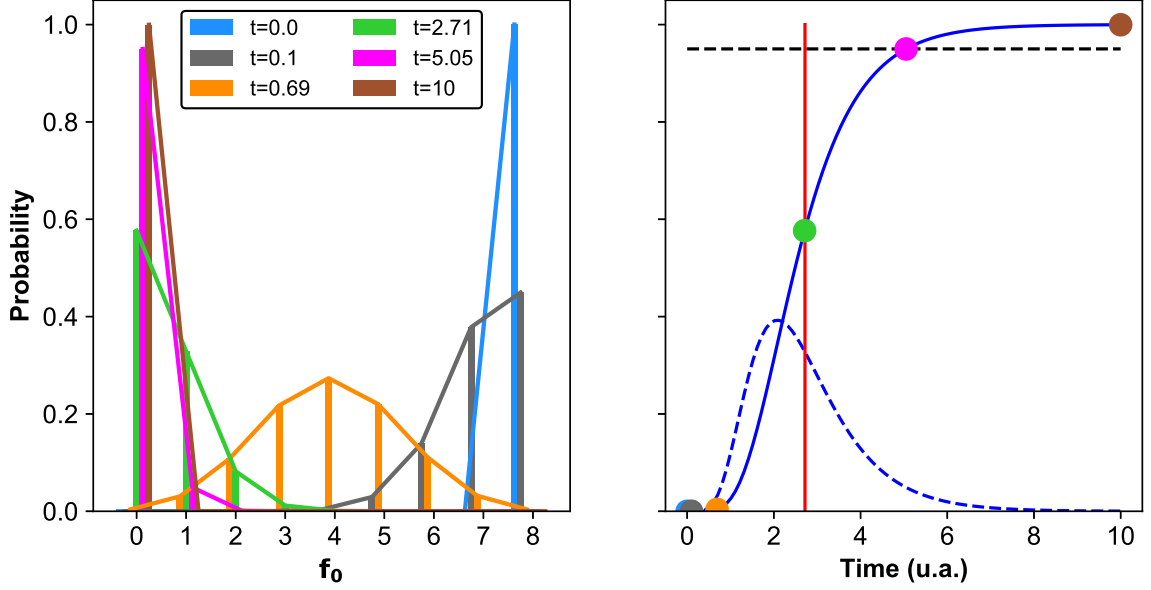
Fig. II.3 **Illustration of Proposition II.2**. *Left-panel: Distribution of the random variable F_t^L (binomial law) given the initial value $F_0 = 8$. Each colored bar plot/line corresponds to a different time (t=0,0.1,0.69,2.71,5.05, 10), see color code in the legend insert. Right-panel: Extinction time of the precursor cells. The blue solid line is the cumulative distribution function of the extinction time $\tau_L^{f_0}$, while the blue dashed line is the probability density function. The vertical red line indicates the mean extinction time value. The horizontal black dashed line indicates the 95% confidence level. The colored points indicate the time points corresponding to the legend insert. In both panels, $\alpha_1 = 1$.*

where $\mathcal{Y}$ is a Poisson process.

Since the process C_t^L is linear, hence is a branching process, it can be written as the sum of independent and identically distributed elementary processes $C^{k,j}$ (cell lineages, see Figure II.4): for all $t \geq 0$,

$$C_t^L = \underbrace{\sum_{k=1}^{F_0} C_{t-T_k^0}^{k,0} \mathbb{1}_{t \geq T_k^0}}_{\text{cell lineages generated by cell event } \mathcal{R}_1} + \underbrace{\sum_{k=0}^{F_0-1} \sum_{j=1}^{N_k(t)} C_{t-T_k^j}^{k,j} \mathbb{1}_{t \geq T_k^j}}_{\text{cell lineages generated by cell event } \mathcal{R}_3}, \qquad (\text{II.10})$$

where we define, for all $k \in [\![1, f_0]\!]$,

- $T_k^0 := T_k$ (with T_k given by equation (II.7)), the k-th jumping time of the cell event $\mathcal{R}_1$ of $\mathcal{M}_{FC}$.

- $N_k(t)$, the number of occurrences of cell event $\mathcal{R}_3$ between T_k and T_{k+1}, for $t \geq T_k$. Note that

$$N_k(t) = \mathcal{Y}_3 \left(\alpha_2 \int_0^{t \wedge T_{k+1}} F_s^L ds \right) - \mathcal{Y}_3 \left(\alpha_2 \int_0^{T_k} F_s^L ds \right). \qquad (\text{II.11})$$

- for all $j \in [\![1, N_k(t)]\!]$,

$$T_k^j := T_k^{j-1} + \mathcal{E} \left(\alpha_2(f_0 - k) \right), \qquad (\text{II.12})$$

the j-th jumping time of the cell event $\mathcal{R}_3$ occurring between the two random times T_k and T_{k+1}.
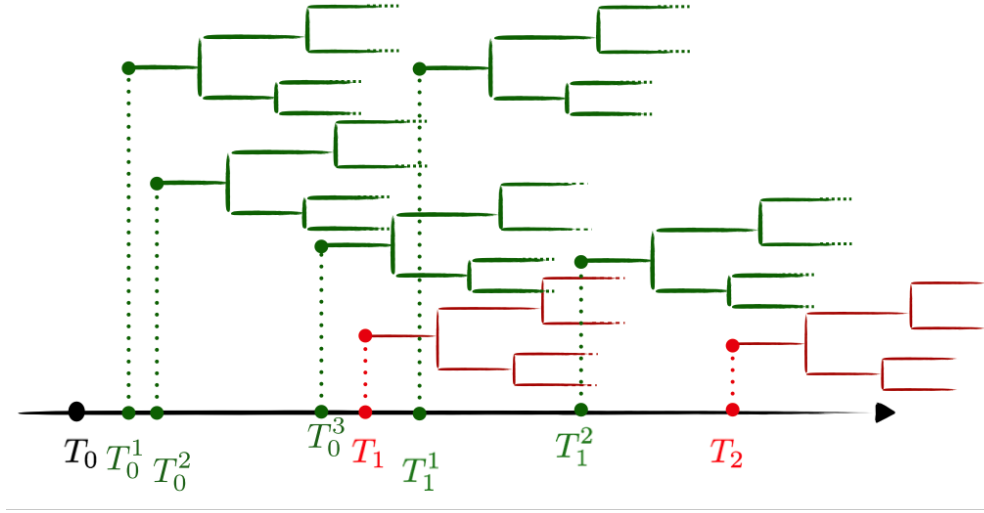
Fig. II.4 **Jumping times and cell lineages.** *Each cell lineage represents schematically the random process $C^{k,j}$, arising either from the cell event $\mathcal{R}_1$ (green trees) or $\mathcal{R}_2$ (red trees), for the linear version of model $\mathcal{M}_{FC}$ (submodel $(\mathcal{R}_1, \mathcal{R}_3, \mathcal{R}_4)$). For all $k \in [\![0, f_0]\!]$, the random times T_k are defined by equation (II.7) and, for all $j \in [\![1, N_k(t)]\!]$ where $N_k(t)$ is given by equation (II.11), the random times T_k^j are defined by equation (II.12). The times of the subsequent symmetric division events following the T_k^j and T_k times are represented at arbitrary time points.*

According to Proposition II.2, $\tau_L^{f_0}$ is a.s. finite. To take the expectation of C_t^L at time $t = \tau_L^{f_0}$, we check that $\mathbb{E}\left[C_{\tau_L^{f_0} - T_k^j}^{k,j} \right] < \infty$, for all k and j. For all $t \geq 0$, $C_t^{k,j}$ is L_1−integrable (as a Yule process) with $\mathbb{E}\left[C_t^{k,j} \right] = e^{\gamma t}$. Note that

$$I := \int_0^{+\infty} e^{\gamma t} f_{\tau_L^{f_0}}(t) dt = \alpha_1 f_0 \int_0^t e^{(\gamma - \alpha_1)t}(1 - e^{-\alpha_1 t})^{f_0 - 1} dt$$

$$= \alpha_1 F_0 \sum_{i=0}^{f_0 - 1} \binom{f_0 - 1}{i} \int_0^{+\infty} e^{(\gamma - \alpha_1(i+1))t} dt.$$

If Hypothesis II.3 holds, $I < \infty$ and, since $C^{k,j}$ is a positive increasing process, we deduce:

$$\mathbb{E}\left[C_{\tau_L^{f_0} - T_k^j}^{k,j} \right] \leq \mathbb{E}\left[C_{\tau_L^{f_0}}^{k,j} \right] = I < \infty.$$

Then, taking the expectation of (II.10) at time $t = \tau_L^{f_0}$, we obtain:

$$\mathbb{E}\left[C_{\tau_L^{f_0}}^L \right] = \sum_{k=1}^{f_0} \mathbb{E}\left[C_{\tau_L^{f_0} - T_k^0}^{k,0} \right] + \sum_{k=0}^{f_0 - 1} \mathbb{E}\left[\sum_{j=1}^{N_k(\tau_L^{f_0})} C_{\tau_L^{f_0} - T_k^j}^{k,j} \right]. \tag{II.13}$$

In some cases, the latter formulas can be used to obtain the first moment of $C_{\tau_L^{f_0}}^L$.

Proposition II.3 (First moment of $C^L_{\tau^{f_0}_L}$). *1. Under Hypothesis II.1, and supposing that γ is zero,*

$$\mathbb{E}\left[C^L_{\tau^{f_0}_L}\right] = f_0(1 + \frac{\alpha_2}{\alpha_1}).$$

2. Under Hypotheses II.1 and II.3, and supposing that α_2 is zero,

$$\mathbb{E}\left[C^L_{\tau^{f_0}_L}\right] = 1 + \alpha_1 \sum_{k=1}^{f_0-1}(f_0-k)\sum_{i=0}^{f_0-k-1}\binom{f_0-k-1}{i}\frac{(-1)^{i+1}}{\gamma-\alpha_1(i+1)}.$$

Proof. When γ is zero, then for all $t \geq 0$, for all $k \in [\![1, f_0]\!]$ and for all $j \in [\![1, N_k(\tau^{f_0}_L)]\!]$, $C^{k,j}_t = 1$. We deduce directly from Eq. (II.13) that

$$\mathbb{E}\left[C^L_{\tau^{f_0}_L}\right] = f_0 + \sum_{k=0}^{f_0-1}\mathbb{E}\left[N_k(\tau^{f_0}_L)\right]. \tag{II.14}$$

From Eq. (II.11), we have

$$\mathbb{E}\left[N_k(\tau^{f_0}_L)\right] = \mathbb{E}\left[\mathcal{Y}_3\left(\alpha_2\int_0^{T_{k+1}}F^L_s ds\right) - \mathcal{Y}_3\left(\alpha_2\int_0^{T_k}F^L_s ds\right)\right]$$

$$= \mathbb{E}\left[\mathcal{Y}_3\left(\alpha_2\int_{T_k}^{T_{k+1}}F^L_s ds\right)\right] = \mathbb{E}\left[\alpha_2\int_{T_k}^{T_{k+1}}F^L_s ds\right],$$

by Poisson process property. Since for all $t \in [T_k, T_{k+1})$, $F^L_t = f_0-k$, we deduce $\mathbb{E}\left[N_k(\tau^{f_0}_L)\right] = \mathbb{E}[\alpha_2(f_0-k)(T_{k+1}-T_k)]$. Using (II.7), we deduce that $\mathbb{E}\left[N_k(\tau^{f_0}_L)\right] = \frac{\alpha_2(f_0-k)}{\alpha_1(f_0-k)} = \frac{\alpha_2}{\alpha_1}$ and conclude with (II.14).

When α_2 is zero, $N_k(t)$ is null for all $t \geq 0$, hence we deduce directly from (II.13) that

$$\mathbb{E}\left[C^L_{\tau^{f_0}_L}\right] = \sum_{k=1}^{f_0}\mathbb{E}\left[C^{k,0}_{\tau^{f_0}_L-T_k}\right]. \tag{II.15}$$

Since $T_{f_0} = \tau^{f_0}_L$, we have $C^{f_0,0}_{\tau^{f_0}_L-T_{f_0}} = 1$. Let $k \in [\![1, f_0-1]\!]$. Since $\tau^{f_0}_L-T_k \overset{(law)}{=} \sum_{i=k+1}^{f_0}\mathcal{E}\left(\alpha_1(f_0-i+1)\right) \overset{(law)}{=} \sum_{i=1}^{f_0-k}\mathcal{E}\left(\alpha_1 i\right)$, using Proposition II.2, we deduce that the density function of $\tau^{f_0}_L - T_k$ is

$$f_{\tau^{f_0}_L-T_k}(t) = \alpha_1(f_0-k)e^{-\alpha_1 t}(1-e^{-\alpha_1 t})^{f_0-k-1}\mathbb{1}_{t\geq 0}.$$

Then, conditioning $C^{k,0}_{\tau^{f_0}_L-T_k}$ by the law of $\tau^{f_0}_L - T_k$, we deduce first

$$\mathbb{E}\left[C^{k,0}_{\tau^{f_0}_L-T_k}\right] = \int_0^{+\infty}\mathbb{E}\left[C^{k,0}_t\right]f_{\tau^{f_0}_L-T_k}(t)dt,$$

then, since $\mathbb{E}\left[C_t^{k,0}\right] = e^{\gamma t}$,

$$\mathbb{E}\left[C_{\tau_L^{f_0}-T_k}^{k,0}\right] = \alpha_1(f_0-k)\int_0^{+\infty} e^{(\gamma-\alpha_1)t}(1-e^{-\alpha_1 t})^{f_0-k-1}dt$$

$$= \alpha_1(f_0-k)\sum_{i=0}^{f_0-k-1}\binom{f_0-k-1}{i}\int_0^{+\infty}(-1)^i e^{(\gamma-\alpha_1(i+1))t}dt$$

$$= \alpha_1(f_0-k)\sum_{i=0}^{f_0-k-1}\binom{f_0-k-1}{i}\frac{(-1)^{i+1}}{\gamma-\alpha_1(i+1)},$$

which ends the proof using (II.15).   □

The influence of each parameter on the mean number of proliferative cells at the extinction time, $\mathbb{E}\left[C_{\tau_L^{f_0}}^L\right]$, for the linear model $(\mathcal{R}_1, \mathcal{R}_3, \mathcal{R}_4)$, are illustrated in Figure II.5. We observe that $C_{\tau_L^{f_0}}^L$ grows without bound as the symmetric division rate γ approaches α_1 (submodel $(\mathcal{R}_1, \mathcal{R}_4)$), while it grows linearly as a function of the asymmetric division rate α_2 (submodel $(\mathcal{R}_1, \mathcal{R}_3)$). Both behaviors are consistent with the deterministic results (Figure II.2).

Remark II.2. *In the case when both $\alpha_2 > 0$ and $\gamma > 0$, a simple analytical formula cannot be obtained for the first moment of $C_{\tau_L^{f_0}}^L$ since it is tricky to deal with expectation in the second term of relation* (II.10)*.*
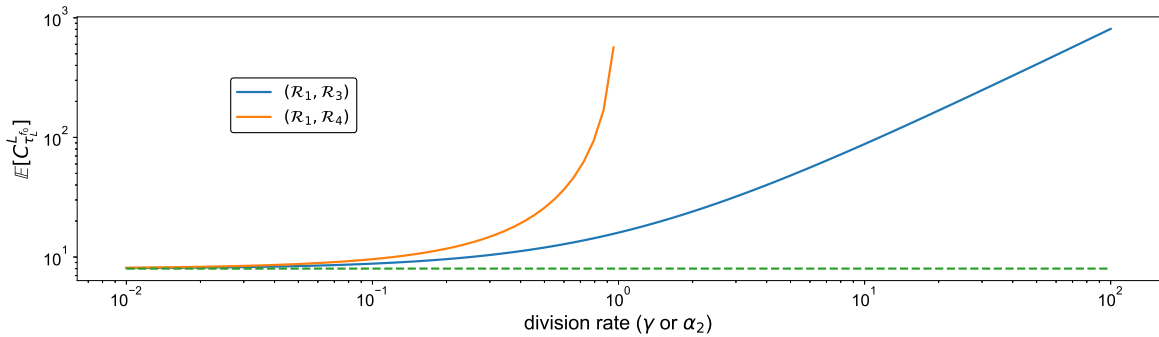
Fig. II.5   ***Illustration of Proposition II.3.*** *Mean number of proliferative cells at the extinction time, $\mathbb{E}\left[C_{\tau_L^{f_0}}^L\right]$ for different parameter values. Orange line: $\mathbb{E}\left[C_{\tau_L^{f_0}}^L\right]$ with respect to γ in submodel $(\mathcal{R}_1, \mathcal{R}_4)$ $(\alpha_2 = 0)$. Blue line: $\mathbb{E}\left[C_{\tau_L^{f_0}}^L\right]$ with respect to α_2 in submodel $(\mathcal{R}_1, \mathcal{R}_3)$ $(\gamma = 0)$. Green dashed line: both α_2 and γ are zero, hence $\mathbb{E}\left[C_{\tau_L^{f_0}}^L\right] = f_0 = 8$. In all cases, $\alpha_1 = 1$.*

b)   Upper bound of the stochastic model

In the general case, we cannot obtain analytical expressions for the extinction time, and we will rather use numerical simulations. To control the numerical error, we need a tractable

upper bound of the stochastic model introduced in Eq. (II.1), which is obtained in this sub-section.

Let $\mathcal{L}_F^{sup}$ and $\mathcal{L}_C^{sup}$ be the following operators:

$$\mathcal{L}_F^{sup}\phi(f) = \alpha_1 f \left[\phi(f-1) - \phi(f)\right],$$
$$\mathcal{L}_C^{sup}\phi(c) = \left[(\alpha_1 + \beta_1 + \alpha_2)f_0 + \gamma c\right]\left[\phi(c+1) - \phi(c)\right].$$

for all ϕ bounded functions, for all $f, c \in \mathbb{N}$.
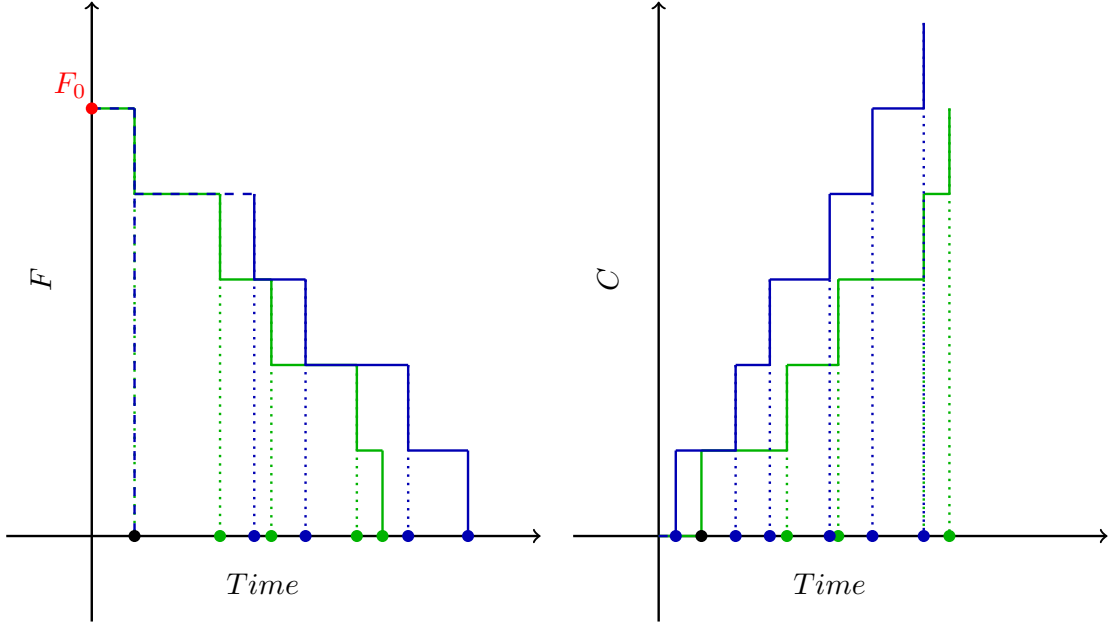
Fig. II.6 *Schematic trajectories of the coupled processes (F^{sup}, C^{sup}) and $X = (F, C)$. Left panel: number of precursor cells F (in green) and upper bound F^{sup} (in blue). Right panel: number of proliferative cells C (in green) and upper bound C^{sup} (in blue).*

Proposition II.4 (Coupling)**.** *For the X process, there exist processes F^{sup} and C^{sup} of generator $\mathcal{L}_F^{sup}$ and $\mathcal{L}_C^{sup}$, respectively, such that for all $t \in \mathbb{R}_+$, $F_t^{sup} \geq F_t$ and $C_t^{sup} \geq C_t$ a.s.*

Figure II.6 illustrates (schematically) the upper bound (F^{sup}, C^{sup}) of the process $X = (F, C)$ solution of model $\mathcal{M}_{FC}$. This upper bound is obtained from an appropriate coupling of both processes, which may or may not jump together, and which are such that when $F^{sup} = F$ (resp. $C^{sup} = C$), the process F^{sup} (resp. C^{sup}) jumps after (resp. before) the process F (resp. C), which ensures keeping the order $F^{sup} \geq F$ (resp. $C^{sup} \geq C$). The coupling is explicit in the proof of Proposition II.4. We define F^{sup} and C^{sup} as the solutions of the SDEs:

$$F_t^{sup} = f_0 - \mathcal{Y}_1 \left(\alpha_1 \int_0^t F_s^{sup} ds\right),$$

$$C_t^{sup} = \mathcal{Y}_1\left(\alpha_1 f_0 t\right) + \mathcal{Y}_2\left(\beta_1 f_0 t\right) + \mathcal{Y}_3\left(\alpha_2 f_0 t\right) + \mathcal{Y}_4\left(\gamma \int_0^t C_s^{sup} ds\right), \quad \text{(II.16)}$$

where the Poisson processes $(\mathcal{Y}_i)_{i=1..4}$ are the same as those in Eq. (II.1). By additivity of independent Poisson processes, we deduce that the infinitesimal generator of F^{sup} and C^{sup} are $\mathcal{L}_F^{sup}$ and $\mathcal{L}_C^{sup}$, respectively.

Remark II.3. *The C^{sup} process is linear, as the C^L process introduced in subsection a). It turns out that the C^{sup} process yields a much more tractable analytical expression to control the mean number of proliferative cells at the extinction time.*

To prove the upper bound for the C process, we first start by a lemma.

Lemma II.1. *For $i = 1, 2, 3$, let $(U_k^i)_{k \geq 0}$ be the sequences of jumping times associated with the counting processes*

$$t \;\mapsto\; \mathcal{Y}_1\left(\int_0^t \alpha_1 F_s ds\right), \quad t \;\mapsto\; \mathcal{Y}_2\left(\int_0^t \beta_1 \frac{F_s C_s}{F_s + C_s} ds\right), \quad and \quad t \;\mapsto\; \mathcal{Y}_3\left(\int_0^t \alpha_2 F_s ds\right)$$

respectively, and, for $i = 1, 2, 3$, let $(V_k^i)_{k \geq 0}$ be the sequences of jumping times associated with the counting processes

$$t \mapsto \mathcal{Y}_1\left(\alpha_1 f_0 t\right), \; t \mapsto \mathcal{Y}_2\left(\beta_1 f_0 t\right), \; and \; t \mapsto \mathcal{Y}_3\left(\alpha_2 f_0 t\right)$$

respectively. We also define the process $Z_t^U := \sum_{i=1}^{3} \sum_{k \geq 1} \mathbb{1}_{\{U_k^i \leq t\}}$ and the process $Z_t^V := \sum_{i=1}^{3} \sum_{k \geq 1} \mathbb{1}_{\{V_k^i \leq t\}}$. For all $t \geq 0$,

$$Z_t^U \leq Z_t^V, \;\; a.s. \tag{II.17}$$

Proof. (Proof of Lemma II.1) By definition of a standard Poisson process, there exists a sequence of jumping times $(S_k^i)_{k \geq 0}$ for each $i = 1, 2, 3$ such that

$$\mathcal{Y}_i(t) = \sum_{k \geq 1} \mathbb{1}_{\{S_k^i \leq t\}}.$$

By definition of $(S_k^i)_{k \geq 0}$ and $(U_k^i)_{k \geq 0}$, for each $i = 1, 2, 3$ and for all $k \geq 0$, we have

$$\int_{U_k^1}^{U_{k+1}^1} \alpha_1 F_s ds = S_{k+1}^1 - S_k^1, \tag{II.18}$$

$$\int_{U_k^2}^{U_{k+1}^2} \beta_1 \frac{F_s C_s}{F_s + C_s} ds = S_{k+1}^2 - S_k^2,$$

$$\int_{U_k^3}^{U_{k+1}^3} \alpha_2 F_s ds = S_{k+1}^3 - S_k^3, \tag{II.19}$$

Also, by definition of $(S_k^i)_{k \geq 0}$ and $(V_k^i)_{k \geq 0}$, for each $i = 1, 2, 3$ and for all $k \geq 0$, we have

$$V_{k+1}^1 - V_k^1 = \frac{S_{k+1}^1 - S_k^1}{\alpha_1 f_0}, \quad V_{k+1}^2 - V_k^2 = \frac{S_{k+1}^2 - S_k^2}{\beta_1 f_0}$$

$$and \; V_{k+1}^3 - V_k^3 = \frac{S_{k+1}^3 - S_k^3}{\alpha_2 f_0}. \tag{II.20}$$

From (II.18)-(II.19), we obtain

$$S_{k+1}^1 - S_k^1 \le \alpha_1 f_0(U_{k+1}^1 - U_k^1), \; S_{k+1}^2 - S_k^2 \le \beta_1 f_0(U_{k+1}^2 - U_k^2)$$
$$\text{and } S_{k+1}^3 - S_k^3 \le \alpha_2 f_0(U_{k+1}^3 - U_k^3). \quad \text{(II.21)}$$

Combining (II.20) and (II.21) , we conclude that for each $i = 1, 2, 3$

$$V_{k+1}^i - V_k^i \le U_{k+1}^i - U_k^i.$$

We obtain that, for all $t \ge 0$, $Z_t^U \le Z_t^V$ a.s. , by counting process definition. $\qquad \square$

We can now proceed to the proof of Proposition II.4.

Proof. (Proof of Proposition II.4) The C and C^{sup} processes start from the same state: $C_0 = C_0^{\text{sup}} = 0$. By Poisson process definition and since C verifies Eq. (II.1), we have

$$C_t = Z_t^U + \mathcal{Y}_4 \left(\gamma \int_0^t C_s ds \right). \quad \text{(II.22)}$$

In the same way, since C^{sup} verifies (II.16), we have

$$C_t^{\text{sup}} = Z_t^V + \mathcal{Y}_4 \left(\gamma \int_0^t C_s^{\text{sup}} ds \right). \quad \text{(II.23)}$$

Let Q be the first time when the C^{sup} and C processes are distinct:

$$Q := \inf \left(t \ge 0, C_t^{\text{sup}} \ne C_t \right),$$

and, let R_Q, be the first time when the C^{sup} and C processes meet again:

$$R_Q := \inf \left(t \ge Q, C_t^{\text{sup}} = C_t \right).$$

Note that at $t = Q$, $\mathcal{Y}_4 \left(\gamma \int_0^t C_s ds \right) = \mathcal{Y}_4 \left(\gamma \int_0^t C_s^{\text{sup}} ds \right)$. Since C and C^{sup} have jumps of size one, between Q and R_Q, one of the two processes stays necessarily over the other one. Using inequality (II.17) and equations (II.22) and (II.23), we deduce that for all $t \in (Q, R_Q)$,

$$C_t^{\text{sup}} > C_t.$$

Hence, for all $t \in (Q, R_Q)$,

$$\mathcal{Y}_4 \left(\gamma \int_0^t C_s^{\text{sup}} ds \right) \ge \mathcal{Y}_4 \left(\gamma \int_0^t C_s ds \right).$$

From this and from inequality (II.17), we deduce that for all $t \in (0, R_Q)$,

$$C_t^{\text{sup}} \ge C_t.$$

By strong Markov property, we conclude that the above inequality is valid for all times $t \in \mathbb{R}_+$.
In the same way as in Eq. II.6, we obtain the upper bound for the F process. Using the same notation as above, we can write that

$$F_t = f_0 - \sum_{k \ge 1} \mathbb{1}_{\{U_k^2 \le t\}} - \mathcal{Y}_1 \left(\alpha_1 \int_0^t F_s ds \right).$$

Let Q^F be the first time when the F^{sup} and F processes are distinct:

$$Q^F := \inf\left(t \geq 0, F_t^{\text{sup}} \neq F_t\right),$$

and, let $R_{Q^F}^F$, be the first time when the F^{sup} and F processes meet again:

$$R_{Q^F}^F := \inf\left(t \geq Q^F, F_t^{\text{sup}} = F_t\right).$$

Note that at $t = Q^F$, $\mathcal{Y}_1\left(\alpha_1 \int_0^t F_s ds\right) = \mathcal{Y}_1\left(\alpha_1 \int_0^t F_s^{\text{sup}} ds\right)$. Since F and F^{sup} have jumps of size one, between Q^F and $R_{Q^F}^F$, one of the two processes stays necessarily over the other one. Hence, we deduce that for all $t \in (0, R_{Q^F}^F)$,

$$F_t^{\text{sup}} \geq F_t.$$

By strong Markov property, we conclude that the above inequality is valid for all times $t \in \mathbb{R}_+$. $\qquad\square$

We now assess the first moment of the extinction time of the upper bound process. In the same way, we define τ^{sup} as

$$\tau^{sup} := \inf\left\{t, F_t^{sup} = 0 | F_0^{\text{sup}} = f_0\right\}.$$

Proposition II.5 (First moment of $C_{\tau^{sup}}^{\text{sup}}$)**.** *Under Hypotheses II.1 and II.3, we have:*

- *if $\gamma > 0$:*

$$\mathbb{E}\left[C_{\tau^{sup}}^{sup}\right] = \frac{(\alpha_1 + \beta_1 + \alpha_2)f_0}{\gamma}\left[\alpha_1 f_0 \sum_{k=0}^{f_0-1}\binom{f_0-1}{k}(-1)^{k+1}\frac{1}{\gamma - \alpha_1(k+1)} - 1\right] \quad \text{(II.24)}$$

- *if $\gamma = 0$:*

$$\mathbb{E}\left[C_{\tau^{sup}}^{sup}\right] = \frac{\alpha_1 + \beta_1 + \alpha_2}{\alpha_1}f_0\sum_{i=1}^{f_0}\frac{1}{i}. \quad \text{(II.25)}$$

Proof. Since τ^{sup} and C^{sup} are independent, we deduce by conditioning with respect to τ^{sup} that

$$\mathbb{E}\left[C_{\tau^{sup}}^{sup}\right] = \int_0^{+\infty}\mathbb{E}\left[C_t^{sup}\right]f_{\tau^{sup}}(t)dt, \quad \text{(II.26)}$$

where $f_{\tau^{sup}}$ is the density probability of τ^{sup}.
First, we suppose that $\gamma > 0$. Hence, C^{sup} is a birth process with immigration and we use the classical result that C_t^{sup} follows a negative binomial law $\mathcal{BN}\left(\frac{\alpha_1+\beta_1+\alpha_2}{\gamma}f_0, e^{-\gamma t}\right)$. In particular, for all $t \geq 0$,

$$\mathbb{E}\left[C_t^{sup}\right] = \frac{\alpha_1 + \beta_1 + \alpha_2}{\gamma}f_0(e^{\gamma t} - 1). \quad \text{(II.27)}$$

Since F^{sup} is linear, we apply Proposition II.2 and obtain

$$f_{\tau^{sup}}(t) = \alpha_1 f_0 e^{-\alpha_1 t}(1 - e^{-\alpha_1 t})^{f_0-1}\mathbb{1}_{[0,+\infty)}(t). \quad \text{(II.28)}$$

Then, using (II.27) and (II.28), we deduce from (II.26) that

$$\mathbb{E}\left[C_{\tau^{sup}}^{sup}\right] = \alpha_1 \frac{\alpha_1 + \beta_1 + \alpha_2}{\gamma} f_0^2 \int_0^\infty (e^{\gamma t} - 1)e^{-\alpha_1 t}(1 - e^{-\alpha_1 t})^{f_0 - 1} dt < \infty$$

under Hypothesis II.3. We have

$$\alpha_1 f_0 \int_0^\infty e^{-\alpha_1 t}(1 - e^{-\alpha_1 t})^{f_0 - 1} dt = \left[(1 - e^{-\alpha_1 t})^{f_0}\right]_0^\infty = 1, \tag{II.29}$$

and

$$\int_0^\infty e^{(\gamma - \alpha_1)t}(1 - e^{-\alpha_1 t})^{f_0 - 1} dt = \sum_{k=0}^{f_0 - 1} \binom{f_0 - 1}{k}(-1)^k \int_0^\infty e^{(\gamma - \alpha_1(k+1))t} dt$$

$$= \sum_{k=0}^{f_0 - 1} \binom{f_0 - 1}{k}(-1)^{k+1} \frac{1}{\gamma - \alpha_1(k+1)}. \tag{II.30}$$

From Eq. (II.29) and (II.30), we deduce relation (II.24).

If $\gamma = 0$, then C^{sup} is a pure immigration process and follows a Poisson law $\mathcal{P}\left((\alpha_1 + \beta_1 + \alpha_2)f_0 t\right)$ at time $t \geq 0$. Using the same approach, we obtain that

$$\mathbb{E}\left[C_{\tau^{\text{sup}}}^{\text{sup}}\right] = \int_0^{+\infty} (\alpha_1 + \beta_1 + \alpha_2) f_0 t f_{\tau^{\text{sup}}}(t) dt = (\alpha_1 + \beta_1 + \alpha_2) f_0 \mathbb{E}\left[\tau^{\text{sup}}\right].$$

We obtain Eq. (II.25) using Proposition II.2. □

We immediately deduce the following corollary

Corollary II.1. *Under Hypothesis II.1, we have* $\mathbb{E}\left[\tau^{f_0}\right] < \infty$. *In addition, under Hypothesis II.3, we have* $\mathbb{E}\left[C_{\tau^{f_0}}\right] < \infty$.

Proof. Since, according to Proposition II.4, for all $t \geq 0$, $F_t^{\text{sup}} \geq F_t$, we first deduce that, necessarily, $\tau^{\text{sup}} \geq \tau^{f_0}$. Then, since, according to Proposition II.2, $\mathbb{E}\left[\tau^{\text{sup}}\right] < \infty$, we can conclude that $\mathbb{E}\left[\tau^{f_0}\right] < \infty$.

In the same way, since C^{sup} and C are both increasing processes, we obtain from Proposition II.4, that

$$C_{\tau^{\text{sup}}}^{\text{sup}} \geq C_{\tau^{\text{sup}}} \geq C_{\tau^{f_0}}.$$

Using Proposition II.5, we conclude that $\mathbb{E}\left[C_{\tau^{f_0}}\right] < \infty$. □

c) Numerical scheme for the mean extinction time and mean number of proliferative cells at the extinction time

Let the domain $\mathcal{D}$ be defined as

$$\mathcal{D} := [\![1, f_0]\!] \times \mathbb{N}. \tag{II.31}$$

We can compute the moment of τ^{f_0} and $C_\tau^{f_0}$ using the martingale problem (II.2). We introduce the following problem: find the value $g(f_0, 0)$ where g is solution of

$$\forall (f, c) \in \mathcal{D}, \quad \mathcal{L}g(f, c) = \alpha \text{ and } g(0, c) = g_0(c), \forall c \in \mathbb{N} \tag{II.32}$$

where the g_0 function and α scalar are to be chosen according to whether we want to obtain $\mathbb{E}\left[\tau^{f_0}\right]$ or $\mathbb{E}\left[C_{\tau^{f_0}}\right]$.

1. For $\mathbb{E}\left[\tau^{f_0}\right]$, we take, for all $c \in \mathbb{N}$, $g_0(c) = 0$ and $\alpha = -1$.

2. For $\mathbb{E}\left[C_{\tau^{f_0}}\right]$, we take, for all $c \in \mathbb{N}$, $g_0(c) = c$ and $\alpha = 0$.

We detail formally why $\mathbb{E}\left[\tau^{f_0}\right] = g(f_0, 0)$. Instantiating the martingale problem (II.2) at time $t = \tau^{f_0}$ and taking the expectation, we obtain:

$$\mathbb{E}\left[g(X_{\tau^{f_0}})\right] = \mathbb{E}\left[g(X_0)\right] - \mathbb{E}\left[\int_0^{\tau^{f_0}} \mathcal{L}g(X_s)ds\right].$$

Note that, for all $s \in (0, \tau^{f_0})$, $X_s \in \mathcal{D}$. Since $\alpha = -1$, $\mathcal{L}g = -1$ for all $(f, c) \in \mathcal{S}$, and, since $g(X_{\tau^{F_0}} = (0, C_{\tau^{f_0}})) = 0$, we deduce that $\mathbb{E}\left[\tau^{f_0}\right] = \mathbb{E}\left[g(X_0)\right] = g(f_0, 0)$.

Actually, the martingale problem (II.2) is only valid for compactly supported functions, which is not necessarily the case for g. Nevertheless, we are going to show directly that the solution of system (II.32) on a truncated domain converges to $\mathbb{E}\left[\tau^{f_0}\right]$. The truncated problem is also motivated by numerical issues.

We can notice that system (II.32), which is similar to the Kolmogorov backward equation, is unclosed, and there exists no analytical solution. We can obtain a numerical estimate for the scalar $g(f_0, 0)$ using a domain truncation method, as proposed in [58, 59].

Domain truncation method

We introduce the killed chain Z, similar to X on $\mathcal{D}$, whose transition matrix $Q^Z := (q^Z(x, y))_{x, y \in \mathcal{S}}$ coincides with Q on $\mathcal{D}$:

$$q^Z(x, y) = q(x, y), \forall x \in \mathcal{D}, y \in \mathcal{S}, \text{ and } q^Z(x, y) = 0, \forall x \notin \mathcal{D}, y \in \mathcal{S}.$$

Lemma 2.4 of [59] ensures us that the chains X and Z are identical up to the first exit time from domain $\mathcal{D}$, i.e. at time $t = \tau^{f_0}$.

In a second step, we introduce the truncated state space $\mathcal{S}^r$ (following [59]), defined as: for all $r \in \mathbb{N}^*$,

$$S^r := [\![0, f_0]\!] \times [\![0, r]\!] \cup \{(0, r+1), (1, r+1)\} \setminus \{(0, 0)\} \tag{II.33}$$

and the truncated domain $\mathcal{D}^r := S^r \cap \mathcal{D}$.

We also construct the Markov chain Z^r, similar to Z on domain $\mathcal{D}^r$ and killed outside $\mathcal{D}^r$. The chains Z and Z^r are identical up to the first exit time from domain $\mathcal{D}^r$,

$$\tau_r^{f_0} := \inf\left(t \text{ such that } Z_t^r \notin \mathcal{D}^r\right) = \tau^{f_0} \wedge \tau_{\mathcal{S}^r},$$

$$\text{where } \tau_{\mathcal{S}^r} := \inf\left(t \text{ such that } Z_t^r \notin \mathcal{S}^r\right). \tag{II.34}$$

We include the state $(0, r+1), (1, r+1)$ in domain S^r to ensure that $\tau_{\mathcal{S}^r} \neq \tau^{f_0}$. In Figure II.7 we draw the different domains $\mathcal{D}, S^r, \mathcal{D}^r$, and we sketch typical trajectories of the X process and the auxiliary processes that we have defined on each domain, namely Z and Z^r. The Z (resp. Z^r) process coincides with X as long as X stays in domain $\mathcal{D}$ (resp. $\mathcal{D}^r$) and is stopped when X leaves domain $\mathcal{D}$ (resp. $\mathcal{D}^r$).

Since $\mathcal{S}^r$ is a strictly increasing sequence of sets such that $\cup_r \mathcal{S}^r = \mathcal{S}$, $\tau_{\mathcal{S}_r}$ goes to infinity a.s. when r goes to infinity. Since, according to Corollary II.1, $\tau^{f_0} < +\infty$, $\tau_r^{f_0}$ converges to τ^{f_0} a.s. when r goes to infinity. Using that C is an increasing process, we also deduce the a.s. convergence of the sequence of random variables $C_{\tau_r^{f_0}}$ to $C_{\tau^{f_0}}$ when r goes to infinity.

We show in the next proposition that the convergence holds in mean for both $\tau_r^{f_0}$ and $C_{\tau_r^{f_0}}$.
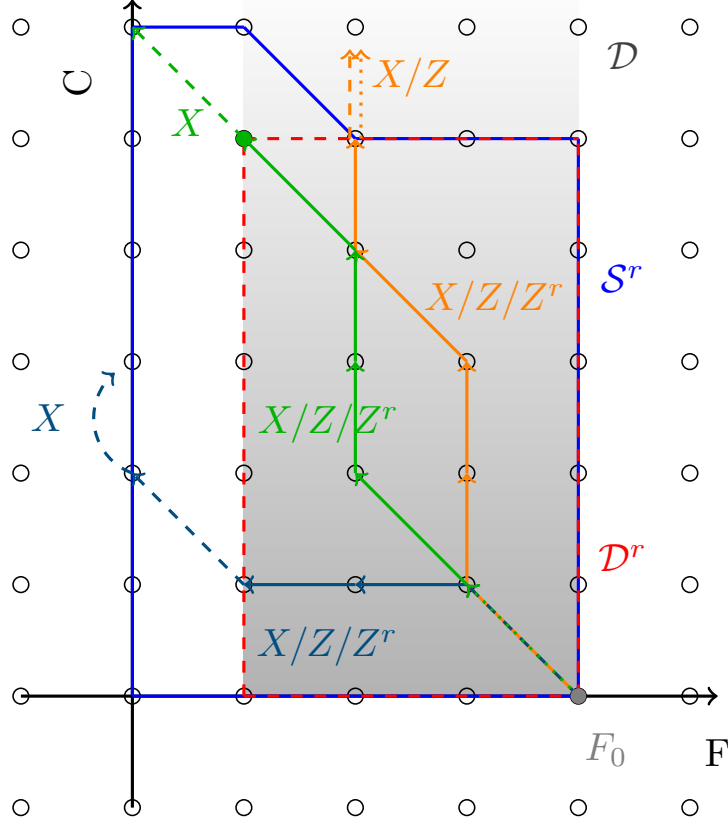
Fig. II.7 **Domains and processes used in the finite state projection method, related to Proposition II.6.** *In shaded gray, we plot the infinite domain $\mathcal{D}$ defined in Eq. (II.31). The solid blue line delimits the boundary of domain $\mathcal{S}^r$, defined in Eq. (II.33). The red dashed line delimits the boundary of domain $\mathcal{D}^r$, corresponding to the intersection of $\mathcal{D}$ and $\mathcal{S}^r$. The blue, green and orange lines illustrate three typical trajectories of the processes X, Z, Z^r.*

Proposition II.6 (Domain truncation relative error)**.** *Let $p \in \mathbb{N}^*$, such that $\mathbb{E}[(C_{\tau^{f_0}})^p] < \infty$, and, let $r \in \mathbb{R}_+^*$ and $\epsilon_r := \frac{\mathbb{E}[(C_{\tau^{f_0}})^p]}{r^p}$. Then, we have*

$$\frac{|\mathbb{E}\left[\tau^{f_0}\right] - \mathbb{E}\left[\tau_r^{f_0}\right]|}{\mathbb{E}\left[\tau^{f_0}\right]} \le \epsilon_r \ \text{ and } \ \frac{|\mathbb{E}\left[C_{\tau_{f_0}}\right] - \mathbb{E}\left[C_{\tau_{f_0}^r}\right]|}{\mathbb{E}\left[C_{\tau_{f_0}}\right]} \le \epsilon_r.$$

Proof. We combine the study of $\tau_r^{f_0}$ and $C_{\tau_r^{f_0}}$ by introducing $h(\tau_r^{f_0})$, where the h function is either $h(x) = x$ or $h(x) = C_x$. According to Corollary II.1, we get $\mathbb{E}\left[h(\tau_r^{f_0})\right] < \infty$ for both cases. As $\mathbb{P}\left[\tau_{\mathcal{S}_r} = \tau^{f_0}\right] = 0$, we can write that

$$\mathbb{P}\left[\tau_r^{f_0} = \tau^{f_0}\right] = 1 - \mathbb{P}\left[\tau_r^{f_0} = \tau_{\mathcal{S}_r}\right]. \tag{II.35}$$

Conditioning $\mathbb{E}\left[h(\tau_r^{f_0})\right]$ with respect to $\tau_r^{f_0}$ and using its definition (see (II.34)), we deduce:

$$\mathbb{E}\left[h(\tau_r^{f_0})\right]$$
$$= \mathbb{E}\left[h(\tau_r^{f_0})|\tau_r^{f_0} = \tau^{f_0}\right] \mathbb{P}\left[\tau_r^{f_0} = \tau^{f_0}\right] + \mathbb{E}\left[h(\tau_r^{f_0})|\tau_r^{f_0} = \tau_{\mathcal{S}_r}\right] \mathbb{P}\left[\tau_r^{f_0} = \tau_{\mathcal{S}_r}\right]$$
$$= \mathbb{E}\left[h(\tau^{f_0})\right] \mathbb{P}\left[\tau_r^{f_0} = \tau^{f_0}\right] + \mathbb{E}\left[h(\tau_{\mathcal{S}_r})\right] \mathbb{P}\left[\tau_r^{f_0} = \tau_{\mathcal{S}_r}\right].$$

We have $\tau^{f_0} \geq \tau_r^{f_0}$ for all $r \geq 0$. Hence, $h(\tau^{f_0}) \geq h(\tau_r^{f_0})$ and we obtain:

$$|\mathbb{E}\left[h(\tau^{f_0})\right] - \mathbb{E}\left[h(\tau_r^{f_0})\right]| = \mathbb{E}\left[h(\tau^{f_0})\right] \left(1 - \mathbb{P}\left[\tau_r^{f_0} = \tau^{f_0}\right]\right) - \mathbb{E}\left[h(\tau_{\mathcal{S}_r})\right] \mathbb{P}\left[\tau_r^{f_0} = \tau_{\mathcal{S}_r}\right].$$

From equation (II.35), we deduce first

$$|\mathbb{E}\left[h(\tau^{f_0})\right] - \mathbb{E}\left[h(\tau_r^{f_0})\right]| = \left(\mathbb{E}\left[h(\tau^{f_0})\right] - \mathbb{E}\left[h(\tau_{\mathcal{S}_r})\right]\right) \mathbb{P}\left[\tau_r^{f_0} = \tau_{\mathcal{S}_r}\right],$$

then

$$\frac{|\mathbb{E}\left[h(\tau^{f_0})\right] - \mathbb{E}\left[h(\tau_r^{f_0})\right]|}{\mathbb{E}\left[h(\tau^{f_0})\right]} \leq \mathbb{P}\left[\tau_r^{f_0} = \tau_{\mathcal{S}_r}\right].$$

Note that $\mathbb{P}\left[\tau_r^{f_0} = \tau_{\mathcal{S}_r}\right] = \mathbb{P}\left[C_{\tau_r^{f_0}} = r\right] = \mathbb{P}\left[C_{\tau_r^{f_0}} \geq r\right]$. Since C is increasing, $C_{\tau_r^{f_0}} \leq C_{\tau^{f_0}}$, hence we obtain

$$\mathbb{P}\left[\tau_r^{f_0} = \tau_{\mathcal{S}_r}\right] \leq \mathbb{P}\left[C_{\tau^{f_0}} \geq r\right].$$

Finally, Chebychev inequality give us that,

$$\mathbb{P}\left[\tau_r^{f_0} = \tau_{\mathcal{S}_r}\right] \leq \frac{\mathbb{E}[(C_{\tau^{f_0}})^p]}{r^p},$$

which ends the proof. $\qquad\qquad\qquad\qquad\qquad\qquad\qquad\qquad\qquad\qquad\qquad\qquad$ $\square$

Pseudo-code

According to Proposition II.4, we first have that

$$C_{\tau_{F_0}} \leq C_{\tau^{\sup}}^{\sup} \text{ a.s. },$$

then together with Proposition II.6 for $p = 1$, we obtain

$$\frac{|\mathbb{E}\left[\tau^{f_0}\right] - \mathbb{E}\left[\tau_r^{f_0}\right]|}{\mathbb{E}\left[\tau^{f_0}\right]} \leq \frac{A}{r} \text{ and } \frac{|\mathbb{E}\left[C_{\tau_{f_0}}\right] - \mathbb{E}\left[C_{\tau_{f_0}^r}\right]|}{\mathbb{E}\left[C_{\tau_{f_0}}\right]} \leq \frac{A}{r},$$

where, if $\gamma > 0$,

$$A = \frac{(\alpha_1 + \alpha_2 + \beta_1)f_0}{\gamma} \left[\alpha_1 f_0 \sum_{k=0}^{f_0 - 1} \binom{f_0 - 1}{k} (-1)^{k+1} \frac{1}{\gamma - \alpha_1(k+1)} - 1\right] \qquad (\text{II.36})$$

or, if $\gamma = 0$,

$$A = \frac{\alpha_1 + \beta_1 + \alpha_2}{\alpha_1} f_0^2 \sum_{i=0}^{f_0 - 1} \binom{f_0 - 1}{i} \frac{(-1)^i}{(i+1)^2}. \qquad (\text{II.37})$$

We design the following algorithm to compute a numerical estimate of $g(f_0, 0)$:

Fix f_0, g_0, α, the parameter set $\theta = (\alpha_1, \alpha_2, \beta_1, \gamma)$ and the tolerance error ϵ;
Compute $r = \frac{A}{\epsilon}$ from equation (II.36) or equation (II.37) ;
Initialize $g_r(f, r) = 0$ for all $f \in [\![0, f_0]\!]$;
for c *from* $r - 1$ *to* 0 **do**
$\quad$ $g_r(0, c) \leftarrow g_0(c)$;
$\quad$ **for** f *from* 1 *to* f_0 **do**
$\quad\quad$ $g_r(f, c) \leftarrow \dfrac{-\alpha + (\alpha_1 f + \beta_1 \frac{fc}{f+c})g_r(f-1, c+1) + (\gamma c + \alpha_2 f)g_r(f, c+1)}{\gamma c + (\alpha_1 f + \beta_1 \frac{fc}{f+c}) + \alpha_2 f}$;
$\quad$ **end**
end
Return $g_r(f_0, 0)$;

Algorithm 1: Numerical estimate of $g(f_0, 0)$

We apply Algorithm 1 to explore the influence of parameters on both the mean extinction time of the precursor cells, $\mathbb{E}\left[\tau^{f_0}\right]$, and the mean number of proliferative cells at that time, $\mathbb{E}\left[C_{\tau f_0}\right]$ for the nonlinear model.

On the left panel of Figure II.8, we can observe that $\mathbb{E}\left[\tau^{f_0}\right]$ decreases like a logistic function with respect to β_1 (in log scale), with a sharp transition for $\beta_1 \approx \alpha_1$. When β_1 tends to zero ($\beta_1 \ll \alpha_1 = 1$), the mean extinction time $\mathbb{E}\left[\tau^{f_0}\right]$ converges to $\mathbb{E}\left[\tau_L^{f_0}\right]$. On the contrary, when β_1 is large ($\beta_1 \gg \alpha_1$), the mean extinction time $\mathbb{E}\left[\tau^{f_0}\right]$ converges to $\mathbb{E}\left[\mathcal{E}\left((\alpha_1 + \alpha_2)f_0\right)\right] = \frac{1}{(\alpha_1 + \alpha_2)f_0}$, which corresponds to the mean time of the first event (in other words, when β_1 is large, cell event $\mathcal{R}_2$ becomes instantaneous). The various parameter configurations shown in this panel lead to the conclusion that the parameter that affects the most the mean extinction time $\mathbb{E}\left[\tau^{f_0}\right]$ is the auto-amplified transition rate β_1, while the division rates α_2 and γ have relatively less effect. Moreover, it is clear from the analytical solutions of the linear model, that the initial number of precursor cells f_0 and the spontaneous transition rate α_1 have a major impact on $\mathbb{E}\left[\tau^{f_0}\right]$.

A logistic-shaped function is observed as well for $\mathbb{E}\left[C_{\tau f_0}\right]$ (middle panel of Figure II.8) when β_1 is tuned (log scale), with a sharp transition around $\beta_1 \approx \alpha_1$. When β_1 is small, cells have time to divide before extinction (leading to a higher level of $\mathbb{E}\left[C_{\tau f_0}\right]$) while when β_1 is large, the main cell event is $\mathcal{R}_2$ and few cells can divide before extinction, the limit value being $f_0 + \frac{\alpha_2}{\alpha_1 + \alpha_2}$ when $\beta_1 \to \infty$.

On the right panel of Figure II.8, we plot the mean number of proliferative cells at the extinction time as a function of the mean extinction time, when β_1 is tuned. These two quantities appear to be roughly linearly correlated, with a slope that depends on the other parameter values. The inserted zoom around $(0, f_0)$ shows that submodel $(\mathcal{R}_1, \mathcal{R}_2, \mathcal{R}_3)$ can surprisingly lead to a higher mean number of proliferative cells than submodel $(\mathcal{R}_1, \mathcal{R}_2, \mathcal{R}_4)$ (with unchanged α_2 and γ values). This phenomenon arises for a large β_1 value (and small mean extinction time). In such a case, an asymmetric division in submodel $(\mathcal{R}_1, \mathcal{R}_2, \mathcal{R}_3)$ may arise before a spontaneous transition (with probability $\frac{\alpha_2}{\alpha_1 + \alpha_2}$), while a symmetric division in submodel $(\mathcal{R}_1, \mathcal{R}_2, \mathcal{R}_4)$ can only arise after a first spontaneous transition, yet is unlikely to occur for large β_1 and fast extinction. However, for small feedback rate β_1, the possibility of symmetric divisions leads to significantly more proliferative cells at the extinction time, as expected.
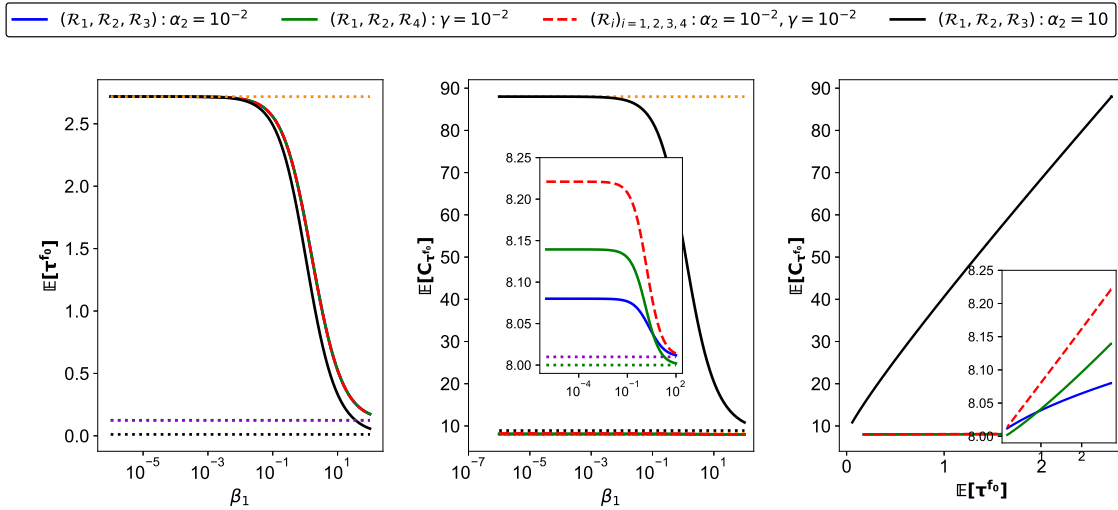
Fig. II.8 *Mean extinction time and mean number of proliferative cells at the extinction time. Using Algorithm 1 with $\epsilon = 10^{-2}$, we compute the mean extinction time and the mean number of proliferative cells at the extinction time. Left panel: mean extinction time as a function of β_1. Middle panel: mean number of proliferative cells at the extinction time as a function of β_1. Right panel: Mean number of proliferative cells as a function of the mean extinction time, when β_1 varies. In each panel, we use four different parameter configurations as follows. In all cases, $f_0 = 8$ and $\alpha_1 = 1$. Black solid line: submodel $(\mathcal{R}_1, \mathcal{R}_2, \mathcal{R}_3)$ with $\alpha_2 = 10$. Blue solid line: submodel $(\mathcal{R}_1, \mathcal{R}_2, \mathcal{R}_3)$ with $\alpha_2 = 0.01$. Green solid line: submodel $(\mathcal{R}_1, \mathcal{R}_2, \mathcal{R}_4)$ with $\gamma = 0.01$. Red dashed line: model $\mathcal{M}_{FC}$ with $\alpha_2 = \gamma = 0.01$. The orange dotted horizontal lines represent the mean extinction time and number of proliferative cells at the extinction time when $\beta_1 = 0$ (applying formulas in Proposition II.3 or, for submodel $(\mathcal{R}_1, \mathcal{R}_3, \mathcal{R}_4)$, simulating the stochastic process). The remaining colored dotted horizontal lines correspond to the mean extinction time and number of proliferative cells at the extinction time when $\beta_1 \to \infty$. The legend insert on the top of the panels specifies the color code. Dotted red: model $(\mathcal{R}_1, \mathcal{R}_2, \mathcal{R}_3, \mathcal{R}_4)$; blue: model $(\mathcal{R}_1, \mathcal{R}_2, \mathcal{R}_3)$ with $\alpha_2 = 0.01$; green: model $(\mathcal{R}_1, \mathcal{R}_2, \mathcal{R}_4)$; black: model $(\mathcal{R}_1, \mathcal{R}_2, \mathcal{R}_3)$ with $\alpha_2 = 10$. For the mean extinction time, the blue and red dotted lines are superimposed.*

II.3 Parameter calibration

In this section, we calibrate the model parameters using a likelihood approach. We first describe the available experimental dataset, as well as in-silico datasets that we use as a benchmark for our methodology. Then we derive a likelihood function based on the embedded Markov chain from the underlying continuous-time Markov process. We explain how this likelihood is specifically adapted to the data, which are time-free measurements of cell numbers. Finally, we both present the estimation results for each submodel derived from model ($\mathcal{M}_{FC}$) and carry out a comprehensive comparison between the different models. In addition, we manage to retrieve hidden kinetic information and assess transit times with given confidence intervals, thanks to a practical parameter identifiability analysis as proposed in [138].

II.3.1 Dataset description

Experimental dataset

Follicles undergoing the activation process have been classified according to three types [119, 136, 116, 137]. Primordial follicles (Type I or B) have either not yet or just initiated activation; they are composed of a single layer of flattened cells surrounding the oocyte. Primary follicles (Type II or C) have completed initiation; they only contain cuboidal (transitioned) somatic cells organized in less than two layers (this means that some follicles are strictly mono-layered, while in others an extra partially fulled layer is being built-up). In between Types I and II lies a class of transitory follicles (Type IA or B/C), with a mixture of flattened and cuboidal cells coexisting within a single layer. The progression from Type I to Type II is accompanied with a more or less pronounced increase in the total cell number (flattened plus cuboidal cells) and enlargement in the oocyte (and follicle) diameter (see bottom-right panel of Figure II.9).

We have made use of a dataset acquired in sheep fetuses [116, 117] (courtesy of Ken McNatty), which provides us with precursor and proliferative cell numbers in a sample of follicles distributed into the three activation steps. The dataset is subdivided into two subsets corresponding to two different sheep strains : the "wild-type" Romney strain and the "mutant" Booroola strain. The latter is characterized by a natural mutation affecting the receptor to growth factor BMP15 and resulting in the alteration of follicle development (see the Introduction section).

We denote respectively by $\mathbf{x}^{WT}$ and $\mathbf{x}^{M}$ the Wild-Type and Mutant subsets such that, for $l \in \mathbf{B} := \{WT, M\}$:

$$\mathbf{x}^l = (x_i)_{i \in [\![1, N^l]\!]},$$

where N^l is either 90 (Wild-Type) or 81 (Mutant), and each element x_i is a vector consisting of the number of precursor and proliferative cells. More specifically, the measures consist of the cell numbers counted on the largest 2D cross-section of histologically fixed follicles of type I, IB or II. This 2D number can be correlated with the total 3D cell number from standard stereological considerations [116]. In order to deal with a final cell number as close as possible to the number reached at the first time when all flattened cells have transitioned to cuboidal cells (hence to the extinction time in the model), we have only retained the strictly mono-layered type II follicles. Yet, due to the oocyte enlargement and the resulting
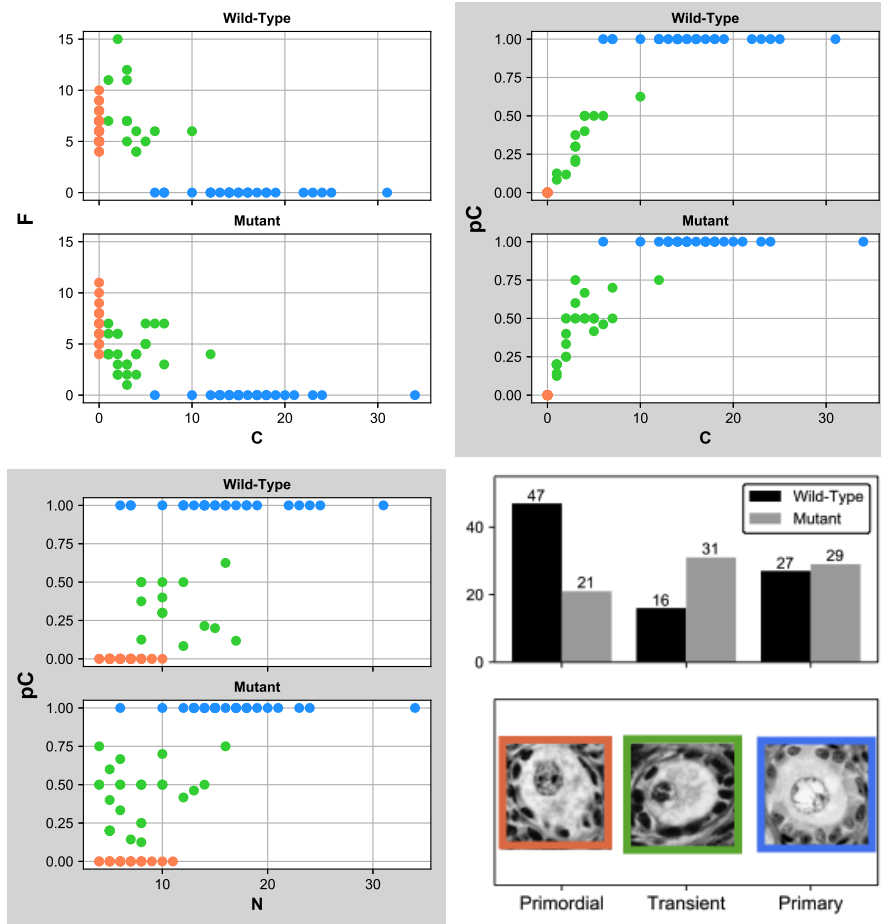
Fig. II.9 **Description of the experimental dataset**. *Top-left, top-right and bottom-left panels: experimental data points projected onto three different phase planes, respectively: (F,C), (C,p_c) and (N,p_C), for both the Wild-Type $(\mathbf{x}^{WT})$ and Mutant $(\mathbf{x}^M)$ subsets. Red points: primary follicles, green points: transitory follicles, blue points: primary follicles. Bottom-right panel: histological slices illustrating the different steps of activation (from left to right: primordial, transitory and primary follicles). Experimental dataset: courtesy of Ken McNatty; histological images: courtesy of Danielle Monniaux.*

increased capacity of the first layer, one cannot preclude that a significant amount of cuboidal cells have been generated after the end of the transition period.

Figure II.9 illustrates the repartition of the data points according to the follicle type and sheep strain in each phase plane (C, F) (C, p_C), (N, p_C).

In silico datasets

In addition to the experimental dataset, we have constructed in silico datasets generated from the simulation of five different submodels: $(\mathcal{R}_1, \mathcal{R}_3)$, $(\mathcal{R}_1, \mathcal{R}_4)$, $(\mathcal{R}_1, \mathcal{R}_2, \mathcal{R}_3)$, $(\mathcal{R}_1, \mathcal{R}_2, \mathcal{R}_4)$ and $(\mathcal{R}_1, \mathcal{R}_3, \mathcal{R}_4)$. We recall that the different submodels are named by the reactions which have corresponding positive reaction rates. All the submodels considered are thus nested models, or reduced model compared to the full model $(\mathcal{M}_{FC})$. For each submodel, we select two

parameter sets differing by contrasted values in the division rates α_2 or γ and/or transition rate β_1. We obtain the corresponding 10 datasets by simulating $1,000$ trajectories from the SDE (II.1), with the Gillespie algorithm [61], starting from the initial condition $(F_0, 0)$ at time $t = 0$ up to the time when $C(t) = 31$ (the value $C(t) = 31$ corresponds to the maximal number of cuboidal cells observed in the experimental dataset). The initial random variable F_0 follows a truncated Poisson law of parameter μ (see Eq.(II.40)). For each trajectory, we select randomly one point (f, c) among the state space points reached by the trajectory, so that each in-silico datasets is composed of $N = 1,000$ points. We choose a uniform distribution despite p_C values exceeding 0.50 are rarely observed (see Figure II.9). The parameter values are summarized in Table II.1.

		α_1	β_1	α_2	γ	μ
$(\mathcal{R}_1, \mathcal{R}_3)$	Dataset $\mathbf{x}^{(\mathcal{R}_1, \mathcal{R}_3), 1}$	1	0	0.7	0	5
	Dataset $\mathbf{x}^{(\mathcal{R}_1, \mathcal{R}_3), 2}$	1	0	0.007	0	5
$(\mathcal{R}_1, \mathcal{R}_4)$	Dataset $\mathbf{x}^{(\mathcal{R}_1, \mathcal{R}_4), 1}$	1	0	0	0.7	5
	Dataset $\mathbf{x}^{(\mathcal{R}_1, \mathcal{R}_4), 2}$	1	0	0	0.007	5
$(\mathcal{R}_1, \mathcal{R}_2, \mathcal{R}_3)$	Dataset $\mathbf{x}^{(\mathcal{R}_1, \mathcal{R}_2, \mathcal{R}_3), 1}$	1	0.01	0.07	0	5
	Dataset $\mathbf{x}^{(\mathcal{R}_1, \mathcal{R}_2, \mathcal{R}_3), 2}$	1	100	0.07	0	5
$(\mathcal{R}_1, \mathcal{R}_3, \mathcal{R}_4)$	Dataset $\mathbf{x}^{(\mathcal{R}_1, \mathcal{R}_3, \mathcal{R}_4), 1}$	1	0	0.007	0.7	5
	Dataset $\mathbf{x}^{(\mathcal{R}_1, \mathcal{R}_3, \mathcal{R}_4), 2}$	1	0	0.007	0.07	5
$(\mathcal{R}_1, \mathcal{R}_2, \mathcal{R}_4)$	Dataset $\mathbf{x}^{(\mathcal{R}_1, \mathcal{R}_2, \mathcal{R}_4), 1}$	1	0.01	0	0.07	5
	Dataset $\mathbf{x}^{(\mathcal{R}_1, \mathcal{R}_2, \mathcal{R}_4), 2}$	1	100	0	0.07	5

Table II.1 – **Parameter sets used to generate the in silico datasets**

We note

$$\mathbf{S} := \{((\mathcal{R}_1, \mathcal{R}_3), i), i = 1, 2\} \cup \{((\mathcal{R}_1, \mathcal{R}_4), i), i = 1, 2\} \cup \{((\mathcal{R}_1, \mathcal{R}_2, \mathcal{R}_3), i), i = 1, 2\}$$
$$\cup \{((\mathcal{R}_1, \mathcal{R}_2, \mathcal{R}_4), i), i = 1, 2\} \cup \{((\mathcal{R}_1, \mathcal{R}_3, \mathcal{R}_4), i), i = 1, 2\}$$

the set of all the in silico datasets.

In the sequel (see in particular Figure II.11 and II.12) these datasets will be used as benchmark tools for the parameter identifiability study and the statistical comparison between the submodels (and complete model). In any case, the set of estimated parameters will match the set of cell events included in the model used to generate the in silico dataset. For instance, we will estimate the values of parameters α_2 and γ on the two datasets generated from submodel $(\mathcal{R}_1, \mathcal{R}_3, \mathcal{R}_4)$.

II.3.2 Likelihood method

Since the experimental dataset is made of time-free observations, we are going to confront the model to the data using only the information on some state space values taken by the process, without their corresponding time information. This notion is intrinsically related to the embedded Markov chain which we detail below. We will use this Markov chain to

compute a likelihood function. Note that the proliferative cell population increases by one cell at each event ($\mathcal{R}_1$, $\mathcal{R}_2$, $\mathcal{R}_3$ or $\mathcal{R}_4$), while the precursor cell population can either remain constant ($\mathcal{R}_3$ or $\mathcal{R}_4$) or decrease by one ($\mathcal{R}_1$ or $\mathcal{R}_2$). The proliferative cell population C can thus be used as an event counter. Indeed, as a continuous-time Markov process, X (defined in Eq. II.1) can be decomposed into an embedded Markov chain $(F_n, C_n)_{n \in \mathbb{N}}$ and a sequence of random time jumps $(\tau_n)_{n \in \mathbb{N}}$ with

$$\tau_{n+1} = \tau_n + \mathcal{E}\left((\alpha_1 + \alpha_2)F_n + \beta_1 \frac{F_n C_n}{F_n + C_n} + \gamma C_n \right), \quad \tau_0 = 0.$$

Note that the sequence of time jumps $(\tau_n)_{n \in \mathbb{N}}$ corresponds exactly to the sequence of time jumps associated with process C, and

$$C(t) = \sum_{n \in \mathbb{N}} \mathbb{1}_{\tau_n \leq t}, \quad C_n = n.$$

Thus, given that $C_n = n$ is deterministic, it is clear that the precursor cell population F_n (alone) is also a (non-homogeneous) Markov chain. To clarify the link with the data, we will index the embedded chain F_n by the number of proliferative cells c, rather than by the number of events that occurred: let F_c be the random variable corresponding to the number of precursor cells given that there are $c \in \mathbb{N}$ proliferative cells. According to the dichotomy between the two division events ($\mathcal{R}_3$, $\mathcal{R}_4$) and the two transition events ($\mathcal{R}_1$, $\mathcal{R}_2$), we deduce the law of F_c at the "pseudo-time" $C = c$ from the law of F_{c-1} at the "pseudo-time" $C = c-1$ as follows: for all $(f, c) \in \mathcal{S}$,

$$\mathbb{P}\left[F_c = f\right] = \underbrace{q_{f+1,f}(c-1)\mathbb{P}\left[F_{c-1} = f+1\right]}_{\text{transition}} + \underbrace{q_{f,f}(c-1)\mathbb{P}\left[F_{c-1} = f\right]}_{\text{asymmetric/symmetric division}}, \quad \text{(II.38)}$$

where

$$q_{f+1,f}(c) = \frac{\alpha_1(f+1) + \beta_1 \frac{(f+1)c}{f+1+c}}{(\alpha_2 + \alpha_1)(f+1) + \gamma c + \beta_1 \frac{(f+1)c}{f+1+c}},$$

$$q_{f,f}(c) = \frac{\alpha_2 f + \gamma c}{(\alpha_2 + \alpha_1)f + \gamma c + \beta_1 \frac{fc}{f+c}}. \quad \text{(II.39)}$$

Hence $(F_c)_{c \in \mathbb{N}}$ is a non-homogeneous discrete time Markov chain. Notice that the law of $C_{\tau^{F_0}}$, the number of proliferative cells at the extinction time of the precursor cells, corresponds to the law of the first "pseudo-time" c such that $F_c = 0$, e.g. $C_{\tau^{F_0}} = \inf\{c \in \mathbb{N}^*, F_c = 0\}$. Hence, one can use the same estimates (Eq. (II.36) or Eq. (II.37)) used in the previous section to analyze the law of $C_{\tau^{F_0}}$, or to reconstruct a numerical approximation of the mean of $C_{\tau^{F_0}}$.

In addition to Eq. (II.38), to compute the law of (F_c), we need to specify an initial condition F_0. We suppose that the initial number of precursor cells follows a truncated Poisson law of parameter $\mu \in \mathbb{R}_+$ defined as, for all $f \in \mathbb{N}^*$,

$$\mathbb{P}\left[F_0 = f\right] = \frac{\mu^f}{(e^\mu - 1)f!}. \quad \text{(II.40)}$$

Then, we can use Eq. (II.38) to compute $\mathbb{P}[F_c = f]$ by recurrence from the initial probability vector $(\mathbb{P}[F_0 = i])_{i \in [\![0, c+f]\!]}$. Hence, we have built a discrete time Markov chain $(F_c)_{c \in \mathbb{N}}$ from model ($\mathcal{M}_{FC}$) adapted to our time-free observations.

As can be seen from Eq. (II.39), the timescale cannot be inferred, so that we fix arbitrarily $\alpha_1 = 1$, whatever the dataset, to obtain dimensionless parameters. The time unit of the remaining parameters is thus relative to the timescale of one spontaneous transition event. As far as the experimental and in silico datasets, except α_1, the estimated parameter values may depend on the specific dataset (experimental or in silico), which we highlight by the following notations for the parameter sets: $\theta^l = (\beta_1^l, \alpha_2^l, \gamma^l, \mu^l) \in \Theta \subset (\mathbb{R}_+)^3 \times [1, +\infty)$, $l \in \mathbf{B} \cup \mathbf{S}$.

Finally, we suppose that all data points are independent of one another, and that the observations are free of measurement errors, and we ignore inter-individual variability.

We obtain the following likelihood function for both the experimental and in silico datasets: for $l \in \mathbf{B} \cup \mathbf{S}$,

$$\mathcal{L}(\mathbf{x}^l; \theta) := \mathbb{P}\left[\mathbf{x}^l | \theta\right] = \prod_{i=1}^{N^l} \mathbb{P}\left[F_{c_i} = f_i | \theta\right].$$

For each submodel $m \in \{(\mathcal{R}_1, \mathcal{R}_4), (\mathcal{R}_1, \mathcal{R}_3), ...\}$ described in the previous section, the optimal parameter values are given by the maximum likelihood estimator $\hat{\theta}_m^l$ (MLE), which we compute by minimizing the negative log-likelihood, for $l \in \mathbf{B} \cup \mathbf{S}$:

$$\hat{\theta}_m^l := \arg\min_{\theta \in \Theta^m} \left(-\log\left(\mathcal{L}(\mathbf{x}^l; \theta)\right)\right),$$

where Θ^m is a subset of Θ constructed by fixing all the parameter sets related to the non-present events to the singletons $\{0\}$: for instance, in submodel $(\mathcal{R}_1, \mathcal{R}_4)$, we have $\Theta^{(\mathcal{R}_1, \mathcal{R}_4)} = \{0\} \times \{0\} \times \mathbb{R}_+ \times [1, +\infty)$.

To compute the minimum, we use a derivative-free optimization algorithm: the Differential Evolution (DE) algorithm [146]. In the following, we describe the whole procedure for the complete model $m = (\mathcal{R}_1, \mathcal{R}_2, \mathcal{R}_3, \mathcal{R}_4)$ with the experimental dataset ($l \in \mathbf{B}$). The algorithm starts from an initial population in which each individual is represented by a set of real numbers $(\beta_1, \alpha_2, \gamma, \mu)$. Then, the population evolves along successive generations by mutation and recombination processes. At each generation, the likelihood function is used to assess the fitness of the individuals, and only the best individuals are kept in the population. We have set the intrinsic optimization parameters as follows: the initial population has a size of 20 individuals, and the probability of mutation and crossing-over equals to 0.8 and 0.7 respectively. The starting individual parameter sets are defined on a log scale, and drawn from a uniform distribution on $\Theta = [-6, 6]^3 \times [0, 1.5]$. The algorithm was run over 1,000 iterations. To analyze the parameter identifiability, we follow the practical approach based on the profile likelihood estimate (PLE), see for instance [138]. Specifically, we compute the PLE around the MLE $\hat{\theta}_m^l = \left(\widehat{\beta_1}_m^l, \widehat{\alpha_2}_m^l, \widehat{\gamma}_m^l, \widehat{\mu}_m^l\right)$ for each ith component $\hat{\theta}_{m,i}^l$, $i \in [\![1, 4]\!]$, as follows. We design a grid G_i around the best parameter value $\hat{\theta}_{m,i}^l$ with a fixed step size (see Table II.5 in Appendix II.5.1 for details), and re-optimize the remaining parameters using the DE algorithm with the same optimization parameters (mut=0.8, crossp=0.7, popsize=20, its = 1,000) and initial parameter sets defined on a log scale, and drawn from a uniform distribution on $[-6, 6]^3$ for parameters β_1, α_2 and γ, and on $[-1 + \log(\hat{\mu}_m^l), \log(\hat{\mu}_m^l) + 1]$ for parameter μ. For each parameter $\hat{\theta}_{m,i}^l$, we obtain a MLE vector $\hat{\theta}_m^l | [\theta_{m,i}^l = x]$, with $x \in G_i$:

$$\hat{\theta}_m^l | [\theta_{m,i}^l = x] := \arg\min_{\theta \in \Theta^m, \theta_{m,i}^l = x} \left(-\log\left(\mathcal{L}(\mathbf{x}^l; \theta)\right)\right),$$

and its associated PLE (vector) $\mathcal{L}(\mathbf{x}^l; \hat{\theta}_m^l | \theta_{m,i}^l)$.

Finally, the pointwise likelihood-based confidence intervals are constructed thanks to the likelihood ratio test, following [138]; for each estimated parameter $\hat{\theta}_{m,i}^l$, we select all the parameters $\theta_{m,i}^l = x$ such that:

$$\log\left(\mathcal{L}(x; \hat{\theta}_m^l)\right) - \log\left(\mathcal{L}(x; \theta | [\theta_{m,i}^l = x])\right) < 0.5 * \Delta_\alpha,$$

where $\Delta_{0.95} = \chi^2(0.95, 1) = 3.84$ is the 0.95-quantile of the χ^2 law with 1 degree of freedom.

II.3.3   Fitting results

In this subsection, we calibrate the model parameters for several submodels derived from model ($\mathcal{M}_{FC}$):

- two-event submodels, including the spontaneous transition event together with either the asymmetric ($\mathcal{R}_1, \mathcal{R}_3$) or symmetric division ($\mathcal{R}_1, \mathcal{R}_4$);

- three-event submodels, including both the spontaneous and auto-amplified transition events, together with either the asymmetric ($\mathcal{R}_1, \mathcal{R}_2, \mathcal{R}_3$) or symmetric ($\mathcal{R}_1, \mathcal{R}_2, \mathcal{R}_4$) division event;

- the full model ($\mathcal{R}_1, \mathcal{R}_2, \mathcal{R}_4, \mathcal{R}_4$)

In all cases the parameter ruling the initial condition, μ, is estimated.

We follow the procedure described in subsection II.3.2 to fit the parameters on the experimental subsets $\mathbf{x}^{WT}$ and $\mathbf{x}^M$ and in-silico datasets introduced in subsection II.3.1.

a)   Two-event submodels

The fitting results for submodels ($\mathcal{R}_1, \mathcal{R}_3$) and ($\mathcal{R}_1, \mathcal{R}_4$) are shown in Figure II.10. For both the Wild-Type and Mutant subsets, a visual inspection shows that submodel ($\mathcal{R}_1, \mathcal{R}_4$) leads to a "direct" transition, followed by prolonged cell proliferation after precursor cell extinction, while with submodel ($\mathcal{R}_1, \mathcal{R}_3$), there is a higher probability that the total number of cells increases before precursor cell extinction. This observation is consistent with the fitting results of the in-silico datasets.

In Figure II.11, we show the PLE for each estimated parameter. Both the initial condition parameter μ (orange solid lines) and asymmetric division rate α_2 (green solid line) are practically identifiable (in the sense given in [138]), while parameter γ (blue solid line) is only partially practically identifiable in most cases. From the in silico dataset analyses, we observe that both parameters α_2 ($\mathcal{R}_3$) and γ ($\mathcal{R}_4$) are practically identifiable and close to their expected values (less than one $log10$ of difference) when the parameters are of the same order of magnitude than α_1 (Datasets $\mathbf{x}^{(\mathcal{R}_1, \mathcal{R}_3),1}$ and $\mathbf{x}^{(\mathcal{R}_1, \mathcal{R}_4),1}$). In contrast, a small parameter value compared to α_1 leads to a biased parameter estimate, with a huge shift between the estimated and true parameter values (roughly a two $log10$ difference).

b)   Three-event submodels and complete model

We turn now to the analysis of three-event submodels ($\mathcal{R}_1, \mathcal{R}_2, \mathcal{R}_3$), ($\mathcal{R}_1, \mathcal{R}_2, \mathcal{R}_4$) and ($\mathcal{R}_1, \mathcal{R}_3, \mathcal{R}_4$)) and the complete model (($\mathcal{R}_1, \mathcal{R}_2, \mathcal{R}_3, \mathcal{R}_4$). Qualitatively, the fitting results for submodel
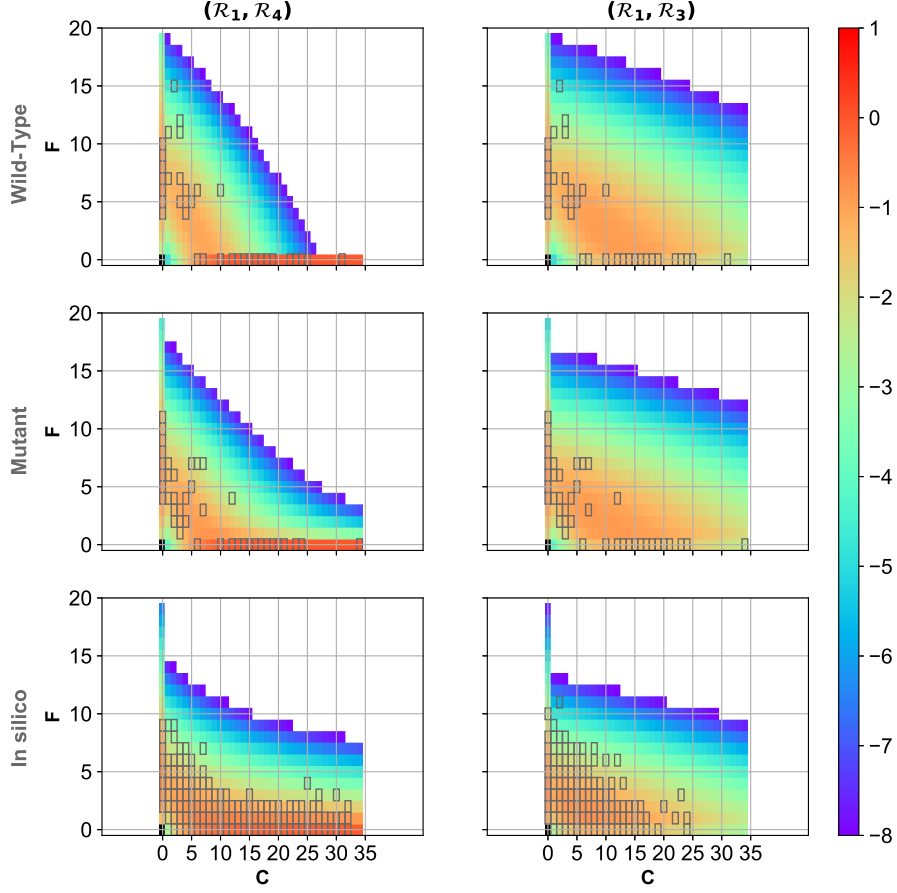
Fig. II.10 ***Two-event submodels: Best fit trajectories.*** *Using Formula II.38, we compute each probability* $\mathbb{P}\left[F_c = f\right]$ *for submodel* $(\mathcal{R}_1, \mathcal{R}_4)$ *with the MLE parameter set* $\hat{\theta}_m^l$, $l \in \{WT, M, ((\mathcal{R}_1, \mathcal{R}_4), 1)\}$ *(left panels), and submodel* $(\mathcal{R}_1, \mathcal{R}_3)$ *with the MLE parameter set* $\hat{\theta}_m^l$, $l \in \{WT, M, ((\mathcal{R}_1, \mathcal{R}_3), 1)\}$ *(right panels). Each dark gray square corresponds to a data point in the datasets* $\mathbf{x}^l$, $l \in \{WT, M, ((\mathcal{R}_1, \mathcal{R}_4), 1), ((\mathcal{R}_1, \mathcal{R}_3), 1)\}$.

$(\mathcal{R}_1, \mathcal{R}_2, \mathcal{R}_3)$ are similar to those for submodel $(\mathcal{R}_1, \mathcal{R}_3)$ (data not-shown); they are characterized by a high probability to produce ten or more proliferative cells before the precursor cell extinction. The fitting results for submodels $(\mathcal{R}_1, \mathcal{R}_2, \mathcal{R}_4)$ and $(\mathcal{R}_1, \mathcal{R}_3, \mathcal{R}_4)$, as well as for the complete model are rather similar to submodel $(\mathcal{R}_1, \mathcal{R}_4)$; they are characterized by direct cell transition with very little concomitant cell proliferation, followed by prolonged cell proliferation after precursor cell extinction. The fitting results for the complete model are shown in the top panel of Figure II.13 for both the Wild-type and Mutant subsets. We notice that in the Mutant case, there is a tendency to produce more proliferative cells.

The PLEs for each dataset and each parameter are presented in Figure II.12 for the three-event submodels and Figure II.13 for the complete model. The corresponding parameter values and confidence intervals for the Wild-Type and Mutant subsets are given in Tables II.3 and II.4 in the Appendix. As observed for the two-event submodels, in each case, the initial condition parameter μ (orange solid lines) is always practically identifiable, and its fitted value is close to the true one for the in silico datasets. In contrast, all other parameters
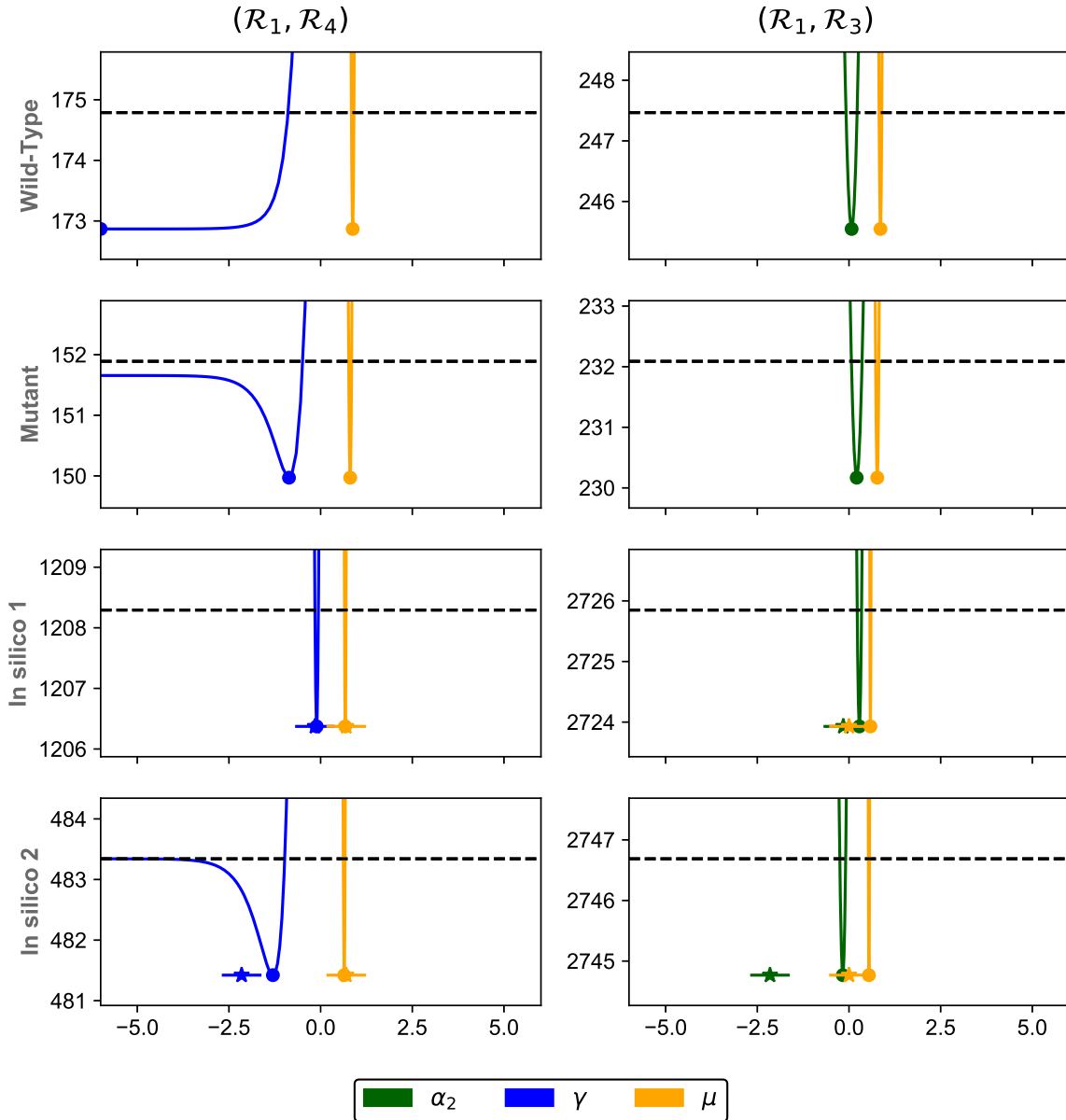
Fig. II.11 **Two-event submodels: PLE.** *Each panel represents the PLE, in log10 scale, obtained from the experimental (top panels) and in silico datasets (bottom panels), and either submodel $(\mathcal{R}_1, \mathcal{R}_4)$ (left panels) or $(\mathcal{R}_1, \mathcal{R}_3)$ (right panels). The dashed black line represents the 95%-statistical threshold, while each point represents the optimum value of the likelihood. Orange solid lines: PLE values $\mathcal{L}(\mathbf{x}^l; \hat{\theta}_m^l | \mu)$; blue solid lines: PLE values $\mathcal{L}(\mathbf{x}^l; \hat{\theta}_{(\mathcal{R}_1, \mathcal{R}_4)}^l | \gamma)$; green solid line: PLE values $\mathcal{L}(\mathbf{x}^l; \hat{\theta}_{(\mathcal{R}_1, \mathcal{R}_3)}^l | \alpha_2)$. The colored points are the associated MLE $\hat{\theta}_m^l$. In the bottom panels, the star symbols are the expected (true) parameter values (see Table II.1).*

have a lack of identifiability. Specifically, the asymmetric division rate α_2 is practically not identifiable for submodel $(\mathcal{R}_1, \mathcal{R}_2, \mathcal{R}_3)$ with the experimental subsets, while it is identifiable
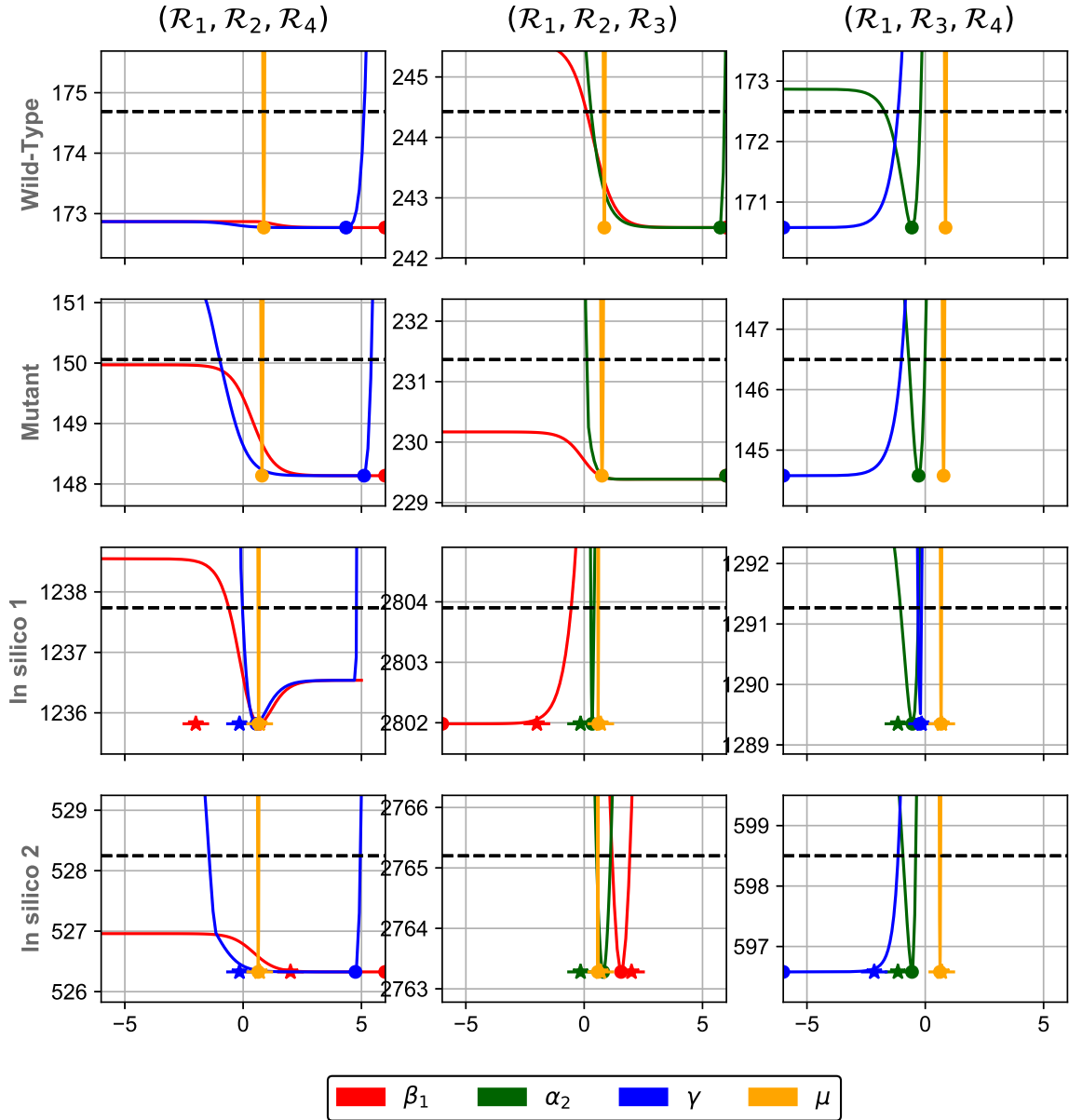
Fig. II.12 **Three-event submodels: PLE.** *Each panel represents the PLE, in log10 scale, obtained from the experimental (top panels) and in silico datasets (bottom panels), and either submodel $(\mathcal{R}_1, \mathcal{R}_2, \mathcal{R}_4)$ (left panels), $(\mathcal{R}_1, \mathcal{R}_2, \mathcal{R}_3)$ (center panels), or $(\mathcal{R}_1, \mathcal{R}_3), \mathcal{R}_4)$ (right panels). The dashed black line represents the 95%-statistical threshold, while each point represents the optimum value of the likelihood. Orange solid lines: PLE values $\mathcal{L}(\mathbf{x}^l; \hat{\theta}_m^l | \mu)$; blue solid lines: PLE values $\mathcal{L}(\mathbf{x}^l; \hat{\theta}_m^l | \gamma)$; green solid lines: PLE values $\mathcal{L}(\mathbf{x}^l; \hat{\theta}_m^l | \alpha_2)$; red solid lines: PLE values $\mathcal{L}(\mathbf{x}^l; \hat{\theta}_m^l | \beta_1)$. The colored points are the associated MLE $\hat{\theta}_m^l$. In the bottom panels, the star symbols are the expected (true) parameter values (see Table II.1).*

with the in-silico datasets (although the estimated values are slightly biased), which indicates that more data can indeed help to improve parameter identifiability. Interestingly, when the asymmetric division event is combined with the symmetric division event (submodel $(\mathcal{R}_1, \mathcal{R}_3, \mathcal{R}_4)$) rather than with the auto-amplified transition (submodel $(\mathcal{R}_1, \mathcal{R}_2, \mathcal{R}_3)$), the asymmetric division rate γ becomes identifiable in the experimental subsets, which reveals complex parameter dependencies between the asymmetric division rate α_2 and auto-amplified transition rate β_1. In the complete model, only a very broad confidence interval (3-5 logs) can be obtained for α_2. In most cases, a finite confidence interval for the symmetric division rate γ cannot be inferred from the experimental data, we can just get an upper-bound. The fitting results obtained with the models including event $\mathcal{R}_4$ suggest a possible explanation: since the transition and proliferation events are rather uncoupled, and occur sequentially (first transition, then proliferation), the proliferation rate can just be constrained to be small enough so that proliferation does almost not take place before cell precursor extinction. After precursor cell extinction, the only possible remaining event is the symmetric division event $\mathcal{R}_4$, whose timescale cannot be constrained by the time-free data. This explanation is confirmed by the dependencies of β_1 on γ for submodel $(\mathcal{R}_1, \mathcal{R}_2, \mathcal{R}_4)$, shown in Figure II.17 in the Appendix. The optimum value $\widehat{(\beta_1)}_m^l|\gamma$, computed from the PLE of γ (minimizing the likelihood with γ fixed, see the blue lines in the top panels of Figure II.12 and bottom panels of Figure II.13), increases linearly with γ as soon as the symmetric division rate gets upper than 1 (hence greater than α_1). Finally, the self-amplified transition rate β_1 is not-identifiable in most cases, and even not constrained by any upper-bound for the experimental subsets. We note that in the complete model, the self-amplified transition rate β_1 is constrained to be greater than $\approx 10^{0.66}$ in the Wild-type case, while it is unconstrained in the Mutant case (with a slightly higher probability around $10^{0.44}$).

c) Comparison of models

We now perform the comparison between the different nested submodels with either two or three cell events and the complete model ($\mathcal{M}_{FC}$).

The AIC and BIC analyses performed to compare the submodels are summarized in Table II.2. We use mainly this criterium as a rigorous tool even if some parameters are not identifiable. The AIC and BIC criteria suggest that the best model associated with the Wild-Type subset is the complete model, while the best model associated with the Mutant subset is the three-event linear submodel $(\mathcal{R}_1, \mathcal{R}_3, \mathcal{R}_4)$.

The reader can refer to [147] (Chapter 6) for a detailed presentation of the rule of thumb, classically used to analyze the $\Delta_i^{AIC} := AIC_i - AIC_{\min}$ and $\Delta_i^{BIC} = BIC_i - BIC_{\min}$ values, where i is the index of the ith model. For the Wild-Type subset, both ΔAIC and ΔBIC suggest that a suitable alternative ($2 < \Delta < 7$) to the complete model are models $(\mathcal{R}_1, \mathcal{R}_4)$, and $(\mathcal{R}_1, \mathcal{R}_3, \mathcal{R}_4)$, while model $(\mathcal{R}_1, \mathcal{R}_2, \mathcal{R}_4)$ is less relevant ($7 < \Delta < 9$) and the remaining models $(\mathcal{R}_1, \mathcal{R}_3)$, $(\mathcal{R}_1, \mathcal{R}_2, \mathcal{R}_3)$ can be safely ruled out ($\Delta > 10$). For the Mutant subset, the complete model is almost as probable ($\Delta AIC < 2$) as the best model $(\mathcal{R}_1, \mathcal{R}_3, \mathcal{R}_4)$, while models $(\mathcal{R}_1, \mathcal{R}_4)$ and $(\mathcal{R}_1, \mathcal{R}_2, \mathcal{R}_4)$ are less relevant ($6 < \Delta < 9$) and models $(\mathcal{R}_1, \mathcal{R}_3)$, $(\mathcal{R}_1, \mathcal{R}_2, \mathcal{R}_3)$ can be safely ruled out as well ($\Delta > 10$). These results are confirmed by the AIC and BIC weight analyzes. For each dataset and criterion (AIC or BIC), we order the AIC/BIC weights from the highest to the lowest values and sum them up. We retain as acceptable all the models such that the sum is upper than the p-value 0.95. The AIC-based selection retains the linear $(\mathcal{R}_1, \mathcal{R}_3, \mathcal{R}_4)$ and complete models for both the Wild-Type and

Mutant subsets (in both cases, p-value = 0.97), whereas the BIC-based selection retains the two linear models $(\mathcal{R}_1, \mathcal{R}_4)$ and $(\mathcal{R}_1, \mathcal{R}_3, \mathcal{R}_4)$ and the complete model (WT p-value = 0.97, M p-value = 0.96).

It is expected that even reaction $\mathcal{R}_4$ is crucial to better fit the data points on the C axis ($F = 0$). Both rejected submodels $(\mathcal{R}_1, \mathcal{R}_3)$, $(\mathcal{R}_1, \mathcal{R}_2, \mathcal{R}_3)$ have indeed a negative log-likelihood far away from the other models, which all includes event $\mathcal{R}_4$. As illustrated in Figure II.10, if event $\mathcal{R}_4$ is present, as in submodel $(\mathcal{R}_1, \mathcal{R}_4)$, the proliferative cells can keep dividing after the extinction of the precursor cells (line $f = 0$). Once the precursor cell number reaches zero for a given c, all remaining points $(0, c')$ for $c' \geq c$ are reached with probability one, which results in a comparatively low contribution of all $(0, c)$ data points to the negative log-likelihood. In contrast, if event $\mathcal{R}_4$ is not present, as in submodel $(\mathcal{R}_1, \mathcal{R}_3)$, the process stops as soon as the precursor cell population F gets extinct, which prevents the likelihood of all $(0, c')$ points from being close to one (they rather take all intermediate values).

Model	WILD-TYPE			MUTANT		
	$-\log \mathcal{L}(\theta; \mathbf{x})$	AIC	BIC	$-\log \mathcal{L}(\theta; \mathbf{x})$	AIC	BIC
$(\mathcal{R}_1, \mathcal{R}_4)$	172.87	349.74 $w = 0.02$ $\Delta = 7.6$	354.74 $w = 0.15$ $\Delta = 3.0$	149.97	303.94 $w = 0.08$ $\Delta = 8.8$	308.73 $w = 0.03$ $\Delta = 6.4$
$(\mathcal{R}_1, \mathcal{R}_3)$	245.54	495.09 $w < 10^{-10}$ $\Delta \gg 10$	500.09 $w < 10^{-10}$ $\Delta \gg 10$	230.17	464.34 $w < 10^{-10}$ $\Delta \gg 10$	469.13 $w < 10^{-10}$ $\Delta \gg 10$
$(\mathcal{R}_1, \mathcal{R}_2, \mathcal{R}_4)$	172.77	351.54 $w = 0.008$ $\Delta = 9.44$	359.04 $w < 10^{-10}$ $\Delta = 7.4$	148.14	302.27 $w = 0.02$ $\Delta = 7.1$	309.46 $w = 0.02$ $\Delta = 7.1$
$(\mathcal{R}_1, \mathcal{R}_2, \mathcal{R}_3)$	242.51	491.02 $w < 10^{-10}$ $\Delta \gg 10$	498.52 $w < 10^{-10}$ $\Delta \gg 10$	229.44	464.89 $w < 10^{-10}$ $\Delta \gg 10$	472.07 $w < 10^{-10}$ $\Delta \gg 10$
$(\mathcal{R}_1, \mathcal{R}_3, \mathcal{R}_4)$	170.58	347.16 $w = 0.07$ $\Delta = 5.0$	354.66 $w = 0.15$ $\Delta = 3.0$	144.58	295.15 $w = 0.64$	302.34 $w = 0.81$
$(\mathcal{R}_i)_{i \in [\![1,4]\!]}$	167.05	342.10 $w = 0.90$	351.68 $w = 0.68$	144.24	296.48 $w = 0.33$ $\Delta = 1.3$	306.06 $w = 0.12$ $\Delta = 3.7$

Table II.2 – **Model comparison analysis.** For each experimental subset and each submodel, we compute both the Akaike information criterion (AIC) and Bayesian information criterion (BIC), the AIC and BIC differences $\Delta_i^{AIC} := AIC_i - AIC_{\min}$ and $\Delta_i^{BIC} = BIC_i - BIC_{\min}$, and the corresponding Akaike and Bayesian weights $w_i^{AIC} = \frac{\exp(-0.5\Delta_i^{AIC})}{\sum_{k=1}^{6} \exp(-0.5\Delta_k^{AIC})}$ and $w_i^{BIC} = \frac{\exp(-0.5\Delta_i^{BIC})}{\sum_{k=1}^{6} \exp(-0.5\Delta_k^{BIC})}$ following the formulas provided in [147] (Chapter 2 and 3).

II.3.4 Model prediction

In this subsection, we use the fitted parameter sets $\hat{\theta}_m^l$ and the parameter values $\hat{\theta}_m^l | \hat{\theta}_{m,i}^l$, for which the PLE is below the 95% threshold of the best models (the two linear submodels $(\mathcal{R}_1, \mathcal{R}_4)$ and $(\mathcal{R}_1, \mathcal{R}_3, \mathcal{R}_4)$ and the complete model) to infer information on the experimental subsets.

a)   Distribution of the initial condition

In the previous section, we have observed that the initial condition parameter μ is the unique parameter to be practically identifiable in all cases, and that it is fitted to similar values from one submodel to another (see Table II.2). Parameter μ can be either estimated from the whole experimental subsets, as the other parameters, or, alternatively, from the cell number of the primordial follicles only. For all $l \in \mathbf{B}$, let $\mathbf{x}_{ini}^l$ be the subset composed of the sole primordial follicles:

$$\mathbf{x}_{ini}^l := \{(f_i, c_i) \in \mathbf{x}^l \text{ such that } c_i = 0, i \in [\![1, N^l]\!]\}.$$

We recall here that F_0 is assumed to follow a truncated Poisson law of parameter μ (see Eq. (II.40)). We use again a classical maximum likelihood approach, associated with the experimental dataset $\mathbf{x}_{ini}^l$. From the likelihood function

$$\mathcal{L}_{ini}(\mathbf{x}_{ini}^l; \mu) := \prod_{i \in [\![1, N^l]\!]:c_i=0} \frac{\mu^{f_i}}{(e^\mu - 1)f_i!},$$

we deduce the MLE $\hat{\mu}_{ini}^l$, for all $l \in \mathbf{B}$,

$$\hat{\mu}_{ini}^l := \arg\min_{\mu \geq 1} \left(-\log\left(\mathcal{L}_{ini}(\mathbf{x}_{ini}^l; \mu)\right) \right).$$

The law F_0 with parameter $\hat{\mu}_{ini}^l$ is thus inferred solely from the primordial follicle data, while the law F_0 with parameter $\hat{\mu}^l$ is inferred using also the transitory and primary follicle data. In Figure II.14, we compare for each subset WT or M the distributions derived from model $(\mathcal{R}_1, \mathcal{R}_4)$, $(\mathcal{R}_1, \mathcal{R}_3, \mathcal{R}_4)$ and $(\mathcal{R}_1, \mathcal{R}_2, \mathcal{R}_3, \mathcal{R}_4)$, using either only the primordial follicle data or the complete follicle data. From the top panels of Figure II.14, we observe that in all cases, there is an overestimation of the part of the distribution corresponding to $\mathbb{P}[F_0 \leq 5]$, which suggests that the model for the initial condition should be a more truncated Poisson distribution for the low values of F_0. As expected, using more information leads to narrowing down the uncertainties, hence the confidence intervals are smaller when the whole data are used (for all models and subsets considered). More surprisingly, we observe a shift of approximately one cell in average, in opposite directions for the Wild-Type and Mutant subset: for the Wild-Type subset, the mean cell number is found to be greater when the whole data are used, while for the Mutant subset, the mean cell number is found to be smaller (for all three models considered). In details, the confidence intervals for the Mutant subset using the whole data superimposes totally or partially to the confidence intervals using only the primordial follicle data, with an overlap of 100% for model $(\mathcal{R}_1, \mathcal{R}_4)$, 65% for model $(\mathcal{R}_1, \mathcal{R}_2, \mathcal{R}_3, \mathcal{R}_4)$, and 50% for model $(\mathcal{R}_1, \mathcal{R}_3, \mathcal{R}_4)$. In the Wild-Type subset, the confidence intervals are more disjoint, with an overlap of 64% for model $(\mathcal{R}_1, \mathcal{R}_2, \mathcal{R}_3, \mathcal{R}_4)$, 25% for model $(\mathcal{R}_1, \mathcal{R}_3, \mathcal{R}_4)$, and no overlap at all for model $(\mathcal{R}_1, \mathcal{R}_4)$.

b)   Proliferative cell proportion: reconstruction of time

In Figure II.15, we represent the predicted change in the proliferative cell proportion with respect to time. These predictions are derived from the deterministic formula Eq. (II.5) for each model, using the parameter values obtained from the identifiability analysis, for which the PLE is below the 95% threshold. In both the Wild-Type and Mutant cases, despite

the uncertainty affecting the model parameters for the two linear submodels (left and right upper panels), the dynamics just exhibit small uncertainties: the proportion of proliferative cells reaches 50%-70% in one time unit, which corresponds to the time unit of a single spontaneous transition event. This might due partly to the fact that parameter γ is partially identifiable and is estimated to relatively low values. In contrast, the lack of parameter identifiability of the complete model results in a huge uncertainty on the dynamics, that can be up to 5 order of magnitude faster than a single spontaneous transition event: the proportion of proliferative cells reaches 50% between 10^{-6} and 1 time unit. Indeed, cell event $\mathcal{R}_2$ (controlled by parameter β_1) can speed up the transition dynamics, and cell event $\mathcal{R}_3$ (controlled by parameter α_2) can trigger the transition, leading to a possible fast activation which avoids the bottleneck of the spontaneous transition timescale ($\alpha_1 = 1$). No clear timescale separation between the Wild-type and Mutant dynamics can be revealed, although some parameter combinations are compatible with a faster transition in the Wild-Type case than in the Mutant case.

c) Mean extinction time, mean number of cells at the extinction time and mean number of division events before extinction

In Figure II.16, we represent the mean number of proliferative cells, $\mathbb{E}\left[C_{\tau^{F_0}}\right]$, as a function of the extinction time $\mathbb{E}\left[\tau^{F_0}\right]$, and the mean number of division events before extinction, $\mathbb{E}\left[C_{\tau^{F_0}} - F_0\right]$, as predicted from the selected (sub)models $(\mathcal{R}_1, \mathcal{R}_4)$, $(\mathcal{R}_1, \mathcal{R}_3, \mathcal{R}_4)$ and $(\mathcal{R}_1, \mathcal{R}_2, \mathcal{R}_3, \mathcal{R}_4)$. These predictions are obtained from a direct stochastic simulation of the trajectories of each model (with Gillespie algorithm, or SSA)[1], using the parameter values obtained from the identifiability analysis, for which the PLE is below the 95% threshold. For each subset (Wild-Type or Mutant), the predicted mean number of proliferative cells at the extinction time is similar in each submodels and lies between 8 and 10 cells. Interestingly, the predicted mean number of proliferative cells at the extinction time is approximately 6-8 cells lower than the empirical mean number of proliferative cells obtained directly from the primary follicle data set $\{x^l, \text{ such that } f = 0\}$ (Figure II.16, top panels). This observation is consistent with the trajectory analysis performed from Figure II.10 for submodel $(\mathcal{R}_1, \mathcal{R}_4)$ and Figure II.13 for the complete model, from which we have concluded that the activation process follows with high probability a trajectory reaching state $f = 0$ with a low cell number, and characterized by direct transition and very little concomitant cell proliferation.

Similarly, the mean number of division events before the extinction time is approximately 5-7 cells lower than the increase in the mean empirical number of cells between the primordial follicle datasets and primary follicle datasets (Figure II.16, bottom panels). The mean extinction time of the two linear submodels $(\mathcal{R}_1, \mathcal{R}_4)$ and $(\mathcal{R}_1, \mathcal{R}_3, \mathcal{R}_4)$ depends only on the initial condition and is estimated to a value around 2.5 a.u. with a small uncertainty, similarly as in Figure II.15. In contrast, the complete model yields a larger uncertainty on the mean extinction time, with a confidence interval between 10^{-6} and 0.5 a.u. for the Wild-Type subset, and between 10^{-6} and 2.5 a.u. for the Mutant subset, consistently with the prediction on the dynamics of the proliferative cell proportion (Figure II.15).

---

[1]We use here the direct simulation rather than Algorithm 1, because the parameter range explored by the symmetric division rate γ in the PLE exceeds the bound $\gamma < \alpha_1$ required by Algorithm 1. A finer upper-bound of the proliferative cell population in the nonlinear process (taking into account event $\mathcal{R}_2$ for instance) would be required to use a finite state projection method when $\gamma > \alpha_1$.

d) Biological interpretation

From the primordial follicle data, we have found that the mean initial number of precursor cells $\hat{\mu}_{ini}^{WT}$ for the Wild-Type subset is about the same as $\hat{\mu}_{ini}^{M}$ for the Mutant. Moreover, the prediction on the total number of proliferative cells at the end of the activation phase, $\mathbb{E}\left[C_{\tau}^{F_0}\right]$, is also very similar in the Wild-Type and Mutant cases. The observed shift in opposite directions for the mean initial cell number inferred from the MLE of the dynamical models ($\hat{\mu}_m^{WT} \approx \hat{\mu}_{ini}^{WT} + 1$ and $\hat{\mu}_m^M \approx \hat{\mu}_{ini}^M - 1$) is thus compensated for by the differences in cell dynamics. The number of divisions during the transition is smaller in the Wild-Type than in the Mutant subset ($\mathbb{E}[C_\tau - F_0] \approx 2$ in Wild-Type, $\mathbb{E}[C_\tau - F_0] \approx 4$ in Mutant), as a result of a global difference between the MLE parameters: the order of magnitude of the division rates are closer to that of the transition rates in the Mutant compared to the Wild-Type subset. In overall, we conclude from our extensive datafitting analysis that the Wild-Type subset exhibits a clearer separation of dynamics during follicle activation (first cell transition, then cell proliferation), while in the Mutant cell proliferation could occur at a substantial rate before precursor cell extinction. We note that this conclusion has to be tempered by the sparse character of our experimental dataset. In particular, a detailed examination of the experimental data reveals that the four data points available for transitory follicles in the Wild-Type subset correspond to a clearly higher number of precursor cells than any of the primordial follicles, which certainly impacts our results. In contrast, the Mutant subset contains transitory follicles with significantly fewer precursor cells than the primary follicles.

Finally, we highlight that the β_1-free linear submodel $(\mathcal{R}_1, \mathcal{R}_3, \mathcal{R}_4)$ performs as well as, and even better than the complete model $(\mathcal{M}_{FC})$ $(\mathcal{R}_i)_{i \in [\![1,4]\!]}$ in Mutant compared to Wild-Type ewes, which is compatible with the functional hypotheses applicable to the BMP15R mutation. Indeed, one could speculate that the diminished BMP15 signaling would hamper the molecular dialog between the oocyte and somatic cells after follicle activation triggering, so that the auto-amplified cell event would barely occur in the Mutant group.

II.4 Conclusion

In this work, we have introduced a stochastic nonlinear cell population model to study the sequence of events occurring just after the initiation of follicle growth. We have characterized the dynamics of precursor and proliferative cell populations according to the parameter values, for both the stochastic model and its deterministic mean-field counterpart. We have studied in details the extinction time of the precursor cell population, and designed an algorithm to compute numerically both the mean extinction time and mean number of proliferative cells at the extinction time. The algorithm is based on a domain truncation similar to the Finite State Projection (FSP) method proposed in [58, 59]. The FSP approach aims to approximate the law of the process at a given time by solving a truncated version of the Kolmogorov forward system. We have adapted the FSP algorithm to solve the infinite recurrence relation satisfied by the extinction time moments. We have found a consistent spatial boundary to solve the closure problem, thanks to a coupling technique and tractable upper-bound process. The numerical cost of the algorithm is deeply related to the proper choice of the upper-bound processes. As we have noticed in section II.3, a finer approximation would be required to compute the mean extinction time and mean number of proliferative cells at the extinction time using the FSP method when dealing with a broader range of parameters (and in particular the case $\alpha_1 < \gamma < \beta_1$).

This algorithm has nevertheless allowed us to investigate the parameter influence on the precursor cell extinction time and number of proliferative cells at the end of the follicle activation phase. The auto-amplified transition rate β_1 exerts a critical control on the mean extinction time, with a sharp timescale reduction when β_1 exceeds the spontaneous cell transition α_1, while the division rates (α_2, γ) have relatively less effect. The effect of the auto-amplification process is probably dependent on the specific parameterization of the cell event rates chosen in this work, yet our findings bring interesting insight into the mechanisms underlying follicle activation; nonlinear feedbacks mediated through cell-to-cell communication certainly play a role, and our estimation results have shown that any impairment of this feedback would change drastically the kinetics of follicle activation.

Moreover, our results can be useful to understand the variability in the cell numbers among ovarian follicles at the end of the activation phase, which can be used as initial conditions for models describing the following stages of follicle development [1, 148].

We have performed the parameter calibration in a special context of time-free data. It turns out that the proliferative cell dynamics can be seen as a clock for the whole process, and that the embedded Markov chain is better adapted to the time-free data than the continuous-time model. We have used the embedded Markov chain to define a proper likelihood function and a statistically rigorous framework. The likelihood function has allowed us to perform an extensive data fitting analysis, using the very useful concept of profile likelihood estimate. This analysis sheds light onto several aspects of the activation of ovarian follicles. First, the transition scenario, where cell proliferation is mostly posterior to cell transition, and the cell number increase is moderate, seems to be predominant versus a more proliferative scenario. While the question is still open, it seems likely that cell transition is favored in the Wild-Type strain compared to the Booroola mutant strain. With the available experimental dataset, we have yet not managed to make a clear distinction between, on one side, a progressive transition with a steady net flux from flattened to cuboidal cells, and, on the other side, an auto-catalytic transition with an ever increasing flux all along the activation phase.

Beyond our application in female reproductive biology, we believe that the modeling approach presented here can have a more generic interest in cell kinetics related issues, especially when a small number of cells is involved. Also, from the mathematical biology viewpoint, the analysis performed on the extinction time, combining theoretical (coupling) and numerical (finite state projection) tools may have an interest for first passage time studies in stochastic processes.

II.5 Appendix

II.5.1 MLE parameter sets

Model	β_1	α_2	γ	μ
$(\mathcal{R}_1, \mathcal{R}_4)$	/	/	10^{-6} $\in (0; 0.12]$	7.49 $\in [7.05; 7.83]$
$(\mathcal{R}_1, \mathcal{R}_3)$	/	1.18 $\in [0.67; 1.57]$	/	7.22 $\in [6.81; 7.83]$
$(\mathcal{R}_1, \mathcal{R}_2, \mathcal{R}_4)$	$10^6 \in \mathbb{R}$	/	$10^{4.35}$ $\in (0; 10^{5.03}]$	7.45 $\in [7.05; 7.83]$
$(\mathcal{R}_1, \mathcal{R}_2, \mathcal{R}_3)$	10^6 $\in [1.52; +\infty)$	$10^{5.75}$ $\in [2.00; 10^{5.88}]$	/	7.07 $\in [5.15; 6.35]$
$(\mathcal{R}_1, \mathcal{R}_3, \mathcal{R}_4)$	/	0.27 $\in [0.022; 0.52]$	10^{-6} $\in (0; 0.068]$	7.20 $\in [6.69; 7.69]$
$(\mathcal{R}_1, \mathcal{R}_2, \mathcal{R}_3, \mathcal{R}_4)$	10^6 $\in [4.64; +\infty)$	$10^{4.78}$ $\in [0.87; 10^{5.27}]$	10^{-6} $\in (0; 10^{4.67}]$	7.06 $\in [6.58; 7.56]$

Table II.3 – Wild-Type parameter sets

Model	β_1	α_2	γ	μ
$(\mathcal{R}_1, \mathcal{R}_4)$	/	/	0.14 $\in (0; 0.28]$	6.40 $\in [5.93; 6.81]$
$(\mathcal{R}_1, \mathcal{R}_3)$	/	1.63 $\in [1.26; 2.20]$	/	5.91 $\in [5.34; 6.35]$
$(\mathcal{R}_1, \mathcal{R}_2, \mathcal{R}_4)$	10^6 $\in \mathbb{R}$	/	$10^{5.11}$ $\in [0.12; 10^{5.39}]$	6.26 $\in [5.72; 6.81]$
$(\mathcal{R}_1, \mathcal{R}_2, \mathcal{R}_3)$	10^6 $\in \mathbb{R}$	10^6 $\in [1.52; +\infty)$	/	5.57 $\in [5.15; 6.35]$
$(\mathcal{R}_1, \mathcal{R}_3, \mathcal{R}_4)$	/	0.52 $\in [0.21; 0.91]$	10^{-6} $\in (0, 0.98]$	5.94 $\in [5.43; 6.54]$
$(\mathcal{R}_1, \mathcal{R}_2, \mathcal{R}_3, \mathcal{R}_4)$	2.81 $\in \mathbb{R}_+$	1.16 $\in [0.28; 10^{5.51}]$	10^{-6} $\in (0; 10^{4.9}]$	5.83 $\in [5.15; 6.35]$

Table II.4 – Mutant parameter sets
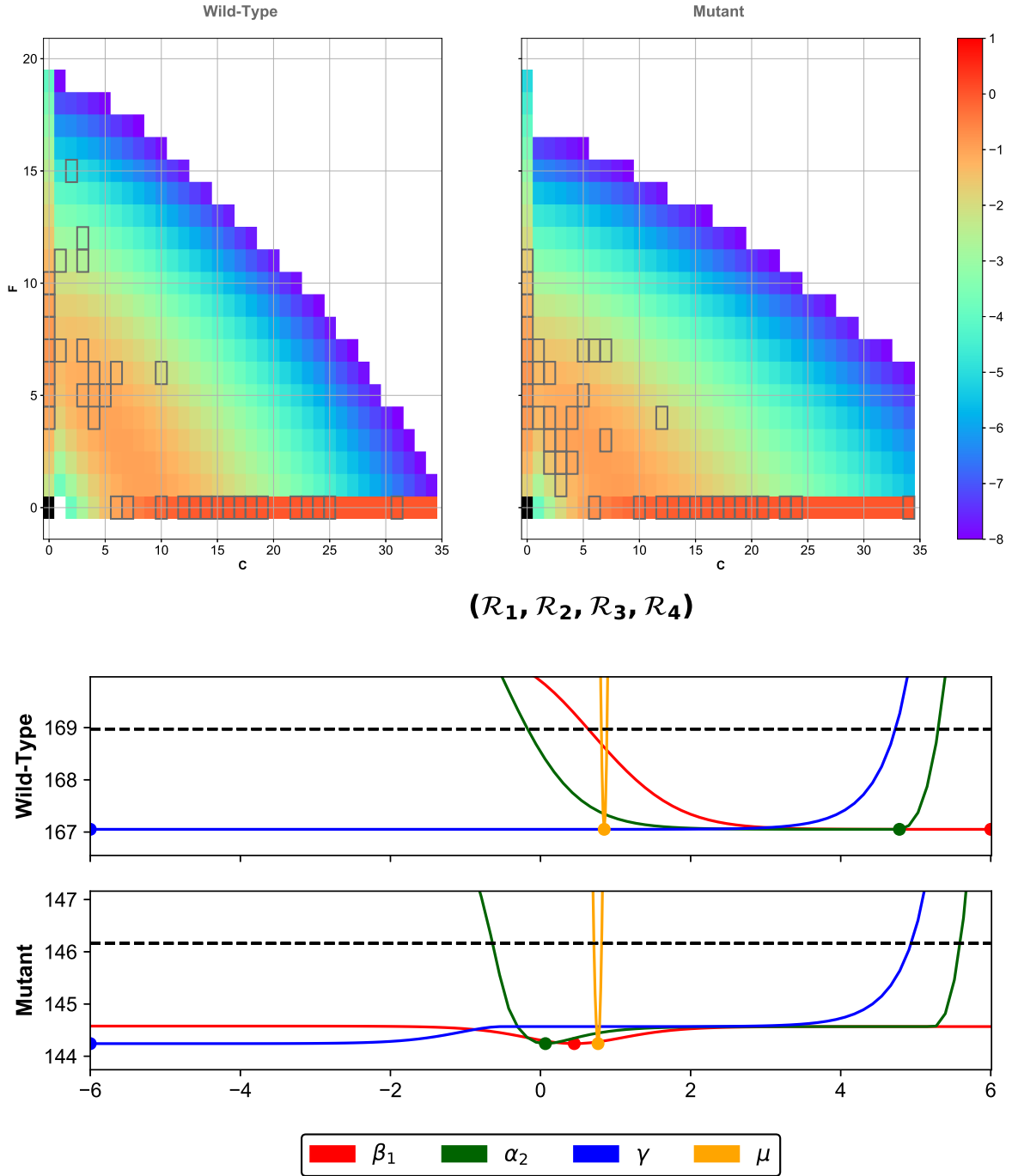
Fig. II.13 **Complete model: Best fit trajectories and PLE**. *Top panels: using Formula (II.38), we compute each probability $\mathbb{P}[F_c = f]$ for the complete model with the MLE $\hat{\theta}_m^l$, $l \in \mathbf{B}$ presented in Tables II.3 and II.4 (left panel: Wild-Type; right panel: Mutant). Each dark gray square corresponds to one data point in the experimental subsets $\mathbf{x}^l$, $l \in \mathbf{B}$. Middle and bottom panels: each panel represents the PLE, in log10 scale, obtained from the two experimental subsets (middle panel: Wild-Type; bottom panel: Mutant) and for parameters β_1, α_2, γ, μ (see the legend of Figure II.12). The dashed black line represents the 95%-statistical threshold, while each colored filled circle represents the optimum value of the likelihood.*
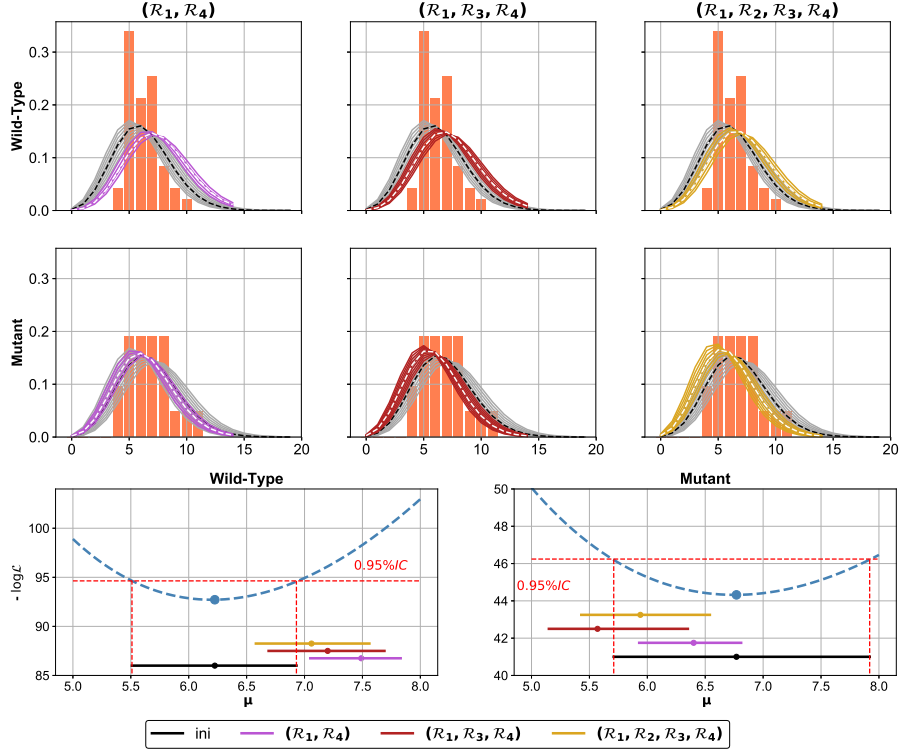
Fig. II.14 **Initial condition**. *Top and middle panels: experimental data histograms of the number of precursor cells in primordial follicles with inferred Poisson distributions. Histograms with coral-colored bars: initial precursor cell number in primordial follicles for Wild-Type x_{ini}^{WT} (top panels) and Mutant x_{ini}^{M} (middle panels) subsets. For subsets $l \in \mathbf{B}$ and submodels $(\mathcal{R}_1, \mathcal{R}_4)$ (left panels), $(\mathcal{R}_1, \mathcal{R}_3, \mathcal{R}_4)$ (center panels) and $(\mathcal{R}_1, \mathcal{R}_2, \mathcal{R}_3, \mathcal{R}_4)$ (right panels), we plot: in white dashed lines, the truncated Poisson distribution (II.40) with MLE $\hat{\mu}_m^l$; in colored solid lines: the truncated Poisson distribution (II.40) with μ in the confidence interval of $\hat{\mu}_m^l$; in black dashed lines: the truncated Poisson distribution (II.40) with MLE $\hat{\mu}_{ini}^l$; in gray solid lines, the truncated Poisson distribution (II.40) with μ in the confidence interval of $\hat{\mu}_{ini}^l$ (parameter values: $\hat{\mu}_{ini}^{WT} = 6.22 \in [5.54; 6.67]$, $\hat{\mu}_{ini}^{M} = 6.77 \in [5.75; 7.60]$). Bottom panels: negative log-likelihood function $\mathcal{L}_{ini}(\mathbf{x}_{ini}^l; \mu)$ and confidence intervals of $\hat{\mu}_{ini}^l$ and $\hat{\mu}_m^l$ (left panel: Wild-Type, right panel: Mutant). Cyan dashed lines: log-likelihood function $\mathcal{L}_{ini}(\mathbf{x}_{ini}^l; \mu)$; red dashed lines: 95% confidence interval; colored solid lines (resp. filled circles): confidence intervals of $\hat{\mu}_m^l$ (resp. $\hat{\mu}_m^l$ values) for each submodel.*
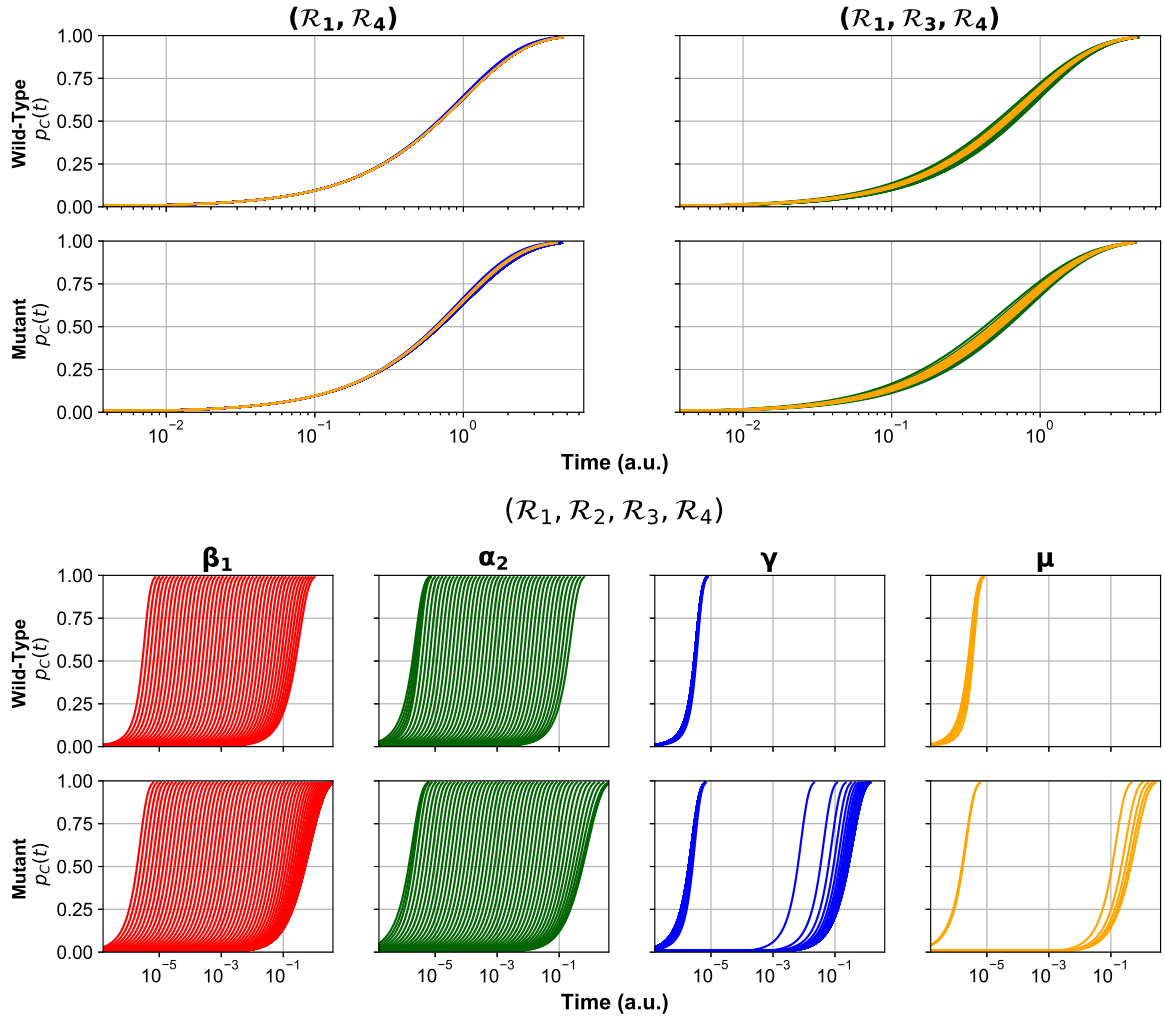
Fig. II.15 **Dynamics of the proportion of proliferative cells**. *For sub-model $(\mathcal{R}_1, \mathcal{R}_4)$ (top left panels), $(\mathcal{R}_1, \mathcal{R}_3, \mathcal{R}_4)$ (top right panels) and whole model $(\mathcal{R}_1, \mathcal{R}_2, \mathcal{R}_3, \mathcal{R}_4)$: $(\mathcal{R}_1, \mathcal{R}_3)$ (bottom panels), we plot the deterministic proportion of proliferative cells $p_C(t)$ computed from Eq. (II.5) with the fitted parameters lying in the MLE confidence interval $\hat{\theta}_m^l$ associated with each profile likelihood (see subsection II.3.2 for details). Blue lines: $p_C(t)$ with parameters $\hat{\theta}_m^l|\gamma$; yellow lines: $p_C(t)$ with parameters $\hat{\theta}_m^l|\mu$; green lines: $p_C(t)$ with parameters $\hat{\theta}_m^l|\alpha_2$; red lines: $p_C(t)$ with parameters $\hat{\theta}_m^l|\beta_1$.*
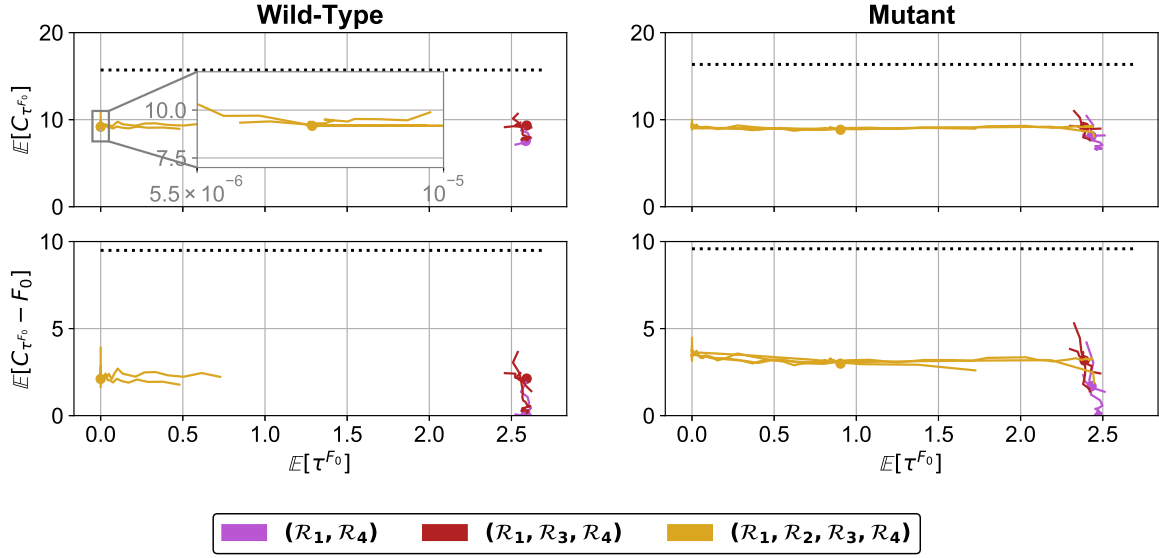
Fig. II.16 **Prediction of the mean number of proliferative cells and mean number of division events before extinction.** *We plot the mean number of proliferative cells at the extinction time* $\mathbb{E}\left[C_\tau^{F_0}\right]$ *(top panels), and the mean number of division events before extinction* $\mathbb{E}\left[C_\tau^{F_0} - F_0\right]$ *(bottom panels) as a function of the mean extinction time* $\mathbb{E}\left[\tau^{F_0}\right]$ *(left panels: Wild-Type; right panels: Mutant). For each parameter lying in the MLE confidence interval* $\hat{\theta}_m^l$, *we simulate 10,000 trajectories with the Gillespie algorithm, up to the extinction event* $\{F = 0\}$, *and compute* $\mathbb{E}\left[\tau^{F_0}\right]$, $\mathbb{E}\left[C_\tau^{F_0}\right]$ *and* $\mathbb{E}\left[C_\tau^{F_0} - F_0\right]$ *from standard empirical mean estimates. Colored solid lines:* $\mathbb{E}\left[C_\tau^{F_0}\right]$, $\mathbb{E}\left[C_\tau^{F_0} - F_0\right]$ *as a function of* $\mathbb{E}\left[\tau^{F_0}\right]$ *for parameters* $\hat{\theta}_m^l|p$ *and* $p \in \{\beta_1, \alpha_2, \gamma, \mu\}$ *associated with each profile likelihood (see subsection II.3.2 for details); filled circles:* $\hat{\theta}_m^l$, *for submodels* $\{(\mathcal{R}_1, \mathcal{R}_4), (\mathcal{R}_1, \mathcal{R}_3, \mathcal{R}_4),$ *and complete model* $(\mathcal{R}_1, \mathcal{R}_2, \mathcal{R}_3, \mathcal{R}_4)\}$. *Dotted black lines: standard empirical mean estimate of proliferative cell numbers (top panels) and division events (bottom panels) before extinction in the primary follicles (data set* $\{x^l, \text{ such that } f = 0\}$).

Model	Parameter	Wild-Type/Mutant	Dataset $\mathbf{x}_1$	Dataset $\mathbf{x}_2$
$(\mathcal{R}_1, \mathcal{R}_4)$	μ	0.015	0.005	0.01
	γ	0.12	0.01	0.06
$(\mathcal{R}_1, \mathcal{R}_3)$	μ	0.015	0.005	0.005
	α_2	0.04	0.01	0.01
$(\mathcal{R}_1, \mathcal{R}_2, \mathcal{R}_4)$	μ	0.015	0.01	0.015
	β_1	0.12	0.07	0.12
	γ	0.12	0.07	0.12
$(\mathcal{R}_1, \mathcal{R}_2, \mathcal{R}_3)$	μ	0.015	0.015	0.015
	β_1	0.12	0.12	0.12
	α_2	0.12	0.02	0.02
$(\mathcal{R}_1, \mathcal{R}_3, \mathcal{R}_4)$	μ	0.01	0.01	0.01
	α_2	0.08	0.01	0.01
	γ	0.08	0.01	0.01
$(\mathcal{R}_1, \mathcal{R}_2, \mathcal{R}_3, \mathcal{R}_4)$	μ	0.015	0.015	0.015
	β_1	0.12	0.12	0.12
	α_2	0.12	0.12	0.12
	γ	0.12	0.12	0.12

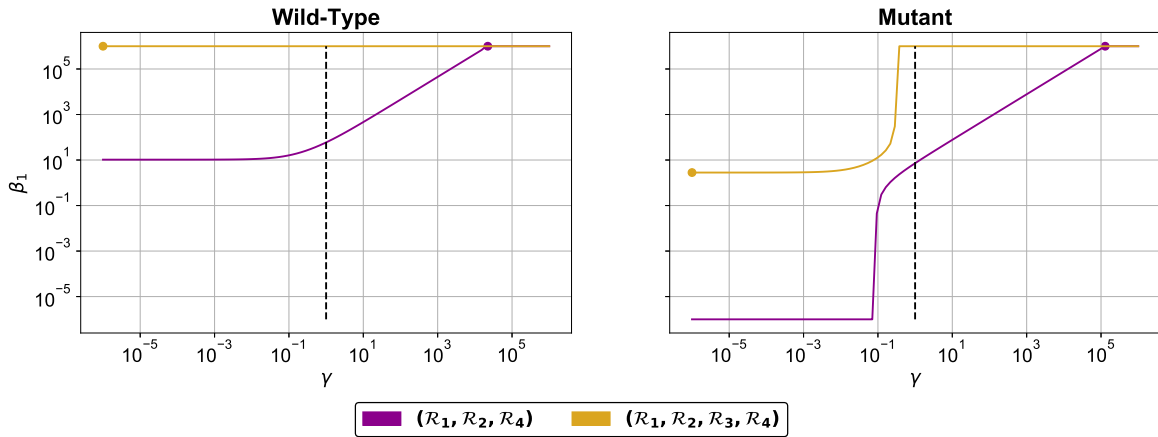Table II.5 – PLE parameter size-step

Fig. II.17 **Proliferation versus transition**. *For each subset (Wild-Type and Mutant), and for submodel* $(\mathcal{R}_1, \mathcal{R}_2, \mathcal{R}_4)$ *and complete model* $(\mathcal{R}_1, \mathcal{R}_2, \mathcal{R}_3, \mathcal{R}_4)$, *we represent the optimal value of* β_1 *along the PLE of* γ, $\widehat{(\beta_1)}_m^l|\gamma$ *(the PLE of* γ *is given by the blue lines in the top panels of Figure II.12 and bottom panels of Figure II.13).*

Chapter III

Modeling the compact growth phase
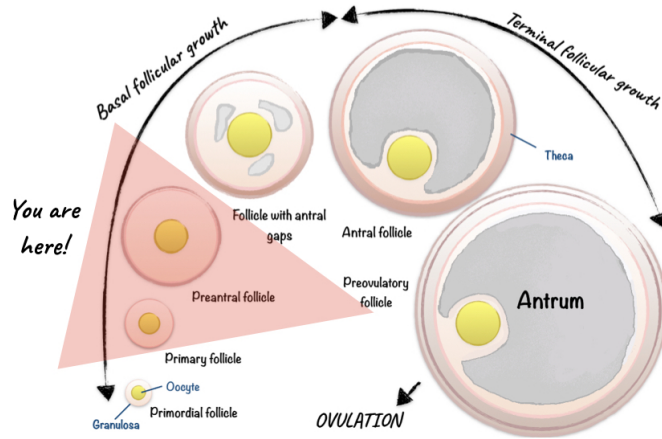
Before presenting the aforementioned work [33], we first introduce the model from which it was inspired.

III.1 Starting point: a non linear stochastic model for the coupled dynamics of the somatic cell population and oocyte

III.1.1 The [Clément-Michel-Monniaux-Stiehl] (CMMS) model [1]

The spatial heterogeneity of cell division favored by growth factors secreted by the oocyte has already been tackled in [1]. In this article, the authors have proposed a cell-based model written with the Poisson point measure formalism to represent the coupled dynamics of the somatic cells and oocyte. The cell population dynamics at time t is represented by the measure $Z_t = \sum_{k=1}^{N_t} \delta_{(X_k(t);A_k(t))}$, where N_t its associated number of somatic cells at time t. In other words, each cell k, represented by a dirac mass $\delta_{(X_k(t);A_k(t))}$, is characterized by its age
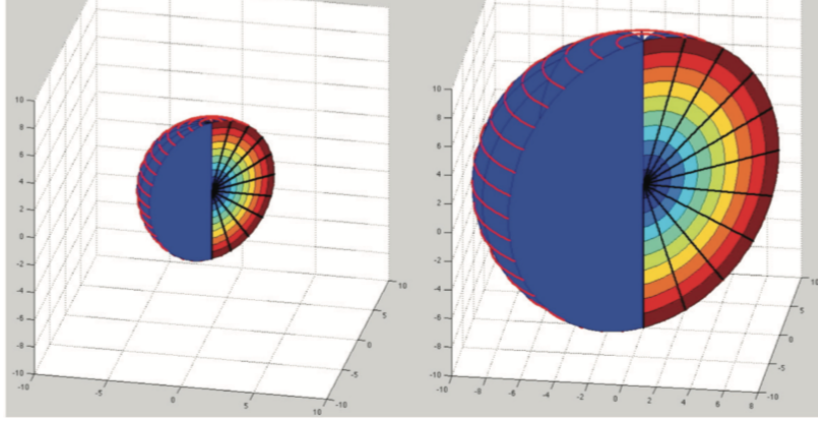
Fig. III.1 ***3D partition, extract from [1].*** *To evaluate the cell number in the different layers (rainbow color), the authors construct a layer "partition" of the space based on the spherical coordinates: the elements $\mathcal{L}_t^{(i,j,k)}(\omega)$ (Eq. (III.1)).*

$A_k(t)$ (continuous variable) and spatial position $X_k(t)$ (discrete triplet of variable (i,j,k), where i is the layer index, j the polar angle number and k the azimuth angle number). Specifically, the cells are distributed into limited-size subdomains $\mathcal{L}_t^{(i,j,k)}$ evolving with the oocyte growth and grouped by their layer index: each subdomain $\mathcal{L}_t^{(i,j,k)}$[1] is a partition of Layer i constructed from spherical coordinates

$$\mathcal{L}_t^{(i,j,k)}(\omega) := \{(r,\theta,\phi) \in [\frac{d_O(t,\omega)}{2} + 2(i-1)d_S, \frac{d_O(t,\omega)}{2} + 2id_S]$$
$$\times [j\pi\frac{j-1}{N}, \pi\frac{j}{N}] \times [-\pi + 2\pi\frac{k-1}{N}, [-\pi + 2\pi\frac{k}{N}]\}, \quad \text{(III.1)}$$

where $N \in \mathbb{N}^*$, d_O is the oocyte diameter whose growth law is given later and d_S is the somatic cell diameter. Layer i is defined as the union of all the partition sets $\mathcal{L}_t^{(i,j,k)}$ with the same layer index i:

$$\mathcal{L}_t^{(i)}(\omega) := \cup_{j,k\in[\![1,N]\!]}\mathcal{L}_t^{(i,j,k)}(\omega),$$

where $N_i \in \mathbb{N}^*$. Note that the volume layer $Vol_t^{(i,j,k)}$ increases with time with the same order $d_O(t,\omega)d_S^2$ as the oocyte diameter. The number of somatic cells located in Layer i evolves as $d_O(t,\omega)/d_S$.

To represent the impact of mitogenic factors diffusing instantaneously and isotropically from the oocyte on the cell cycle duration, each cell division occurs at a random time that follows an exponential like law of layer-dependent division rate $b(a) = 1 - \exp\left(-a/\theta_i\right)$ where θ_i is the average cell cyle duration in Layer i. In other words, the probability that a cell situated on Layer i is still not divided at age a verifies

$$\mathbb{P}\left[A_k(t) \geq a\right] = \exp\left(-a + \theta_i(1 - e^{-a/\theta_i})\right). \quad \text{(III.2)}$$

In addition, since the mitogenic factor concentration decreases radially, the cell cycle duration

---

[1]We slightly change the notation of subdomain $\mathcal{L}_t^{(j,i)}$ provided in [1] and take the one used in [3] (from the same author).

is supposed to increase with the Layer i coordinate. The authors state that:

$$\theta_i = \theta_1(1 + 2(i-1)\frac{d_S}{d_O}).$$

Cells may also move randomly between subdomains according to probabilities that take into account the overcrowding:

$$p(\mathcal{L}_t^{(i,j,k)}(\omega), Z_t, t) = \frac{1}{1 + \exp(-\frac{x_{ijk}-\mu}{\sigma})}.$$

The quantity $x_{ijk} = < Z_t, \mathcal{L}_t^{(i,j,k)} > \frac{Vol_S}{Vol_t^{(i,j,k)}}$, where $< Z_t, \mathcal{L}_t^{(i,j,k)} >$, is the cell number in subdomain $\mathcal{L}_t^{(i,j,k)}$ and Vol_S is the volume of a somatic cell. Parameter μ accounts fo the local overcrowding while σ is a variance that can be interpreted as the degree of tolerance to overcrowding.

The oocyte growth is represented by the following SDE:

$$d_O(t) = d_O(0) + \sum_{i \geq 1} \frac{\kappa_i}{\log_2(e)\theta_i} \int_0^t d_O^{(-4.1252)}(s) < Z_s^-, \mathcal{L}_{s-}^i > ds, \qquad \text{(III.3)}$$

where each κ_i weights to the contribution of the somatic cells on Layer i on the occyte growth. This model is non-linear hence, both numerical and analytical analyses are complex to perform.

III.1.2 From the [CMMS] model to our model

To obtain an analytically tractable problem, we first simplify the spatial structure of the CMMS model. On the basis of symmetry arguments, we reduce the three spatial dimensions $(r, \theta$ and $\phi)$ into one, the radial position, which amounts to spatially structuring the cells by their layer index. The main source of non-linearity of this model then comes from the spatial coupling between the somatic cells and the oocyte: the oocyte diameter growth is regulated by the amount of cells on the different layers (Eq. (III.3)) and the cell positions evolve with the oocyte diameter (layer capacity increasing with respect to time). We choose to follow solely the somatic cells dynamics and "linearize" the model by separating the dynamics of the somatic cells from the oocyte dynamics, also we do not impose a limit layer capacity. As a result, the cell size is not represented and we do not fix a maximum number of cells per layer: there is no notion of overcrowding. Finally, we consider a more general law b for the division rates than that one presented in Eq. (III.2) hence we do not prescribe any particular form. A specific choice will be made later in the calibration section and other options (continuous compactly supported functions) are studied by solving the inverse problem (Chapter 5).

To sum up, the main ingredients of our model are now the cell division modulated by an age- and layer-dependent rate, and inter-layer cell movements whose laws have not yet been defined. To help the formal analyzes, we make a last modification to the initial model: the daughter cells may move only immediately after their birth. We thus obtain a multitype Bellman-Harris model whose the numerical and analytical analyses can be made using the branching property.

This remaining part of this chapter is based on the published work

Frédérique Clément, Frédérique Robin, Romain Yvinec. *Analysis and calibration of a linear model for structured cell populations with unidirectional motion: Application to the morphogenesis of ovarian follicles.* published in SIAM J. Appl. Math., 2019, Vol. 79, No. 1, pp. 207-229 (see [33]).

III.2 Introduction

We study a multitype age dependent model in both a deterministic and stochastic framework to represent the dynamics of a population of cells distributed into successive layers. The model is a two dimensional structured model: cells are described by a continuous age variable and a discrete layer index variable. Cells may divide and move irreversibly from one layer to the next. The cell division rate is age and layer dependent, and is assumed to be bounded below and above. After division, the age is reset and the daughter cells either remain within the same layer or move to the next one. In its stochastic formulation, our model is a multitype Bellman-Harris branching process and in its deterministic formulation it is a multitype McKendrick–VonFoerster system.

The model enters the general class of linear models leading to Malthusian exponential growth of the population. In the partial differential equation (PDE) case, state-of-the-art-methods call to renewal equations system [18] or to an eigenvalue problem and general relative entropy techniques [149, 12] to show the existence of an attractive stable age distribution. Yet, in our case, the unidirectional motion prevents us from applying the Krein–Rutman theorem to solve the eigenvalue problem. As a consequence, we follow a constructive approach and explicitly solve the eigenvalue problem. On the other hand, we adapt entropy methods using weak convergences in $\mathbf{L}^1$ to obtain the large-time behavior and lower bound estimates of the speed of convergence towards the stable age distribution. In the probabilistic case, classical methods rely on renewal equations [65] and martingale convergences [150]. Using the same eigenvalue problem as in the deterministic study, we derive a martingale convergence giving insight into the large-time fluctuations around the stable state. Again, due to the lack of reversibility in our model, we cannot apply the Perron–Frobenius theorem to study the asymptotic of the renewal equations. Nevertheless, we manage to derive explicitly the stationary solution of the renewal equations for the cell number moments in each layer as in [65]. We recover the deterministic stable age distribution as the solution of the renewal equation for the mean age distribution.

The theoretical analysis of our model highlights the role of one particular layer: the leading layer characterized by a maximal intrinsic growth rate which turns out to be the Malthus parameter of the total population. The notion of a leading layer is a tool to understand qualitatively the asymptotic cell dynamics, which appears to operate in a multi-scale regime. All the layers upstream the leading one may extinct or grow with a rate strictly inferior to the Malthus parameter. The remaining downstream layers are driven by the leading layer: they grow exactly as the same rate as the Malthus parameter, which overcomes their intrinsic growth rates.

We then check and illustrate numerically our theoretical results. In the stochastic case, we use a standard implementation of an exact stochastic simulation algorithm. In the deterministic case, we design and implement a dedicated finite volume scheme adapted to the nonconservative form and dealing with proper boundary conditions. We verify that both the deterministic and stochastic simulated distributions agree with the analytical stable age distribution. Moreover, the availability of analytical formulas helps us to study the influence

of the parameters on the asymptotic proportion of cells, Malthus parameter, and stable age distribution.

Finally, we consider the specific application of ovarian follicle development inspired by the model introduced in [1] and representing the proliferation of somatic cells and their organization in concentric layers around the germ cell. While the original model is formulated with a nonlinear individual-based stochastic formalism, we design a linear version based on branching processes and endowed with a straightforward deterministic counterpart. We prove the structural parameter identifiability in the case of age independent division rates. Using a set of experimental biological data, we estimate the model parameters to fit the changes in the cell numbers in each layer during the early stages of follicle development. The main interest of our approach is to benefit from the explicit formulas derived in this paper to get insight on the regime followed by the observed cell population growth.

Beyond the ovarian follicle development, linear models for structured cell populations with unidirectional motion may have several applications in life science modeling, as many processes of cellular differentiation and/or developmental biology are associated with a spatially oriented development (e.g., neurogenesis on the cortex, intestinal crypt) or commitment to a cell lineage or fate (e.g., hematopoiesis, acquisition of resistance in bacterial strains).

The paper is organized as follows. In section 2, we describe the stochastic and deterministic model formulations and enunciate the main results. In section 3, we give the main proofs accompanied by numerical illustrations. Section 4 is dedicated to the application to the development of ovarian follicles. We conclude in section 5. Technical details and classical results are provided in appendix sections.

III.3 Model description and main results

III.3.1 Model description

We consider a population of cells structured by age $a \in \mathbb{R}_+$ and distributed into layers indexed from $j = 1$ to $j = J \in \mathbb{N}^*$. The cells undergo mitosis after a layer-dependent stochastic random time $\tau = \tau^j$, governed by an age-and-layer-dependent instantaneous division rate $b = b_j(a) : \mathbb{P}[\tau^j > t] = e^{-\int_0^t b_j(a)da}$. Each cell division time is independent from the other ones. At division, the age is reset and the two daughter cells may pass to the next layer according to layer-dependent probabilities. We note by $p_{2,0}^{(j)}$ the probability that both daughter cells remain on the same layer, $p_{1,1}^{(j)}$ and $p_{0,2}^{(j)}$, the probability that a single or both daughter cell(s) move(s) from layer j to layer $j + 1$, with $p_{2,0}^{(j)} + p_{1,1}^{(j)} + p_{0,2}^{(j)} = 1$. Note that the last layer is absorbing: $p_{2,0}^{(J)} = 1$. The dynamics of the model are summarized in Figure III.2.

Stochastic model
Each cell in layer j of age a is represented by a Dirac mass $\delta_{j,a}$ where $(j, a) \in \mathcal{E} := [\![1, J]\!] \times \mathbb{R}^+$. Let $\mathcal{M}_P$ be the set of point measures on $\mathcal{E}$:

$$\mathcal{M}_P := \left\{ \sum_{k=1}^N \delta_{j_k, a_k}, N \in \mathbb{N}^*, \forall k \in [\![1, N]\!], (j_k, a_k) \in \mathcal{E} \right\}.$$
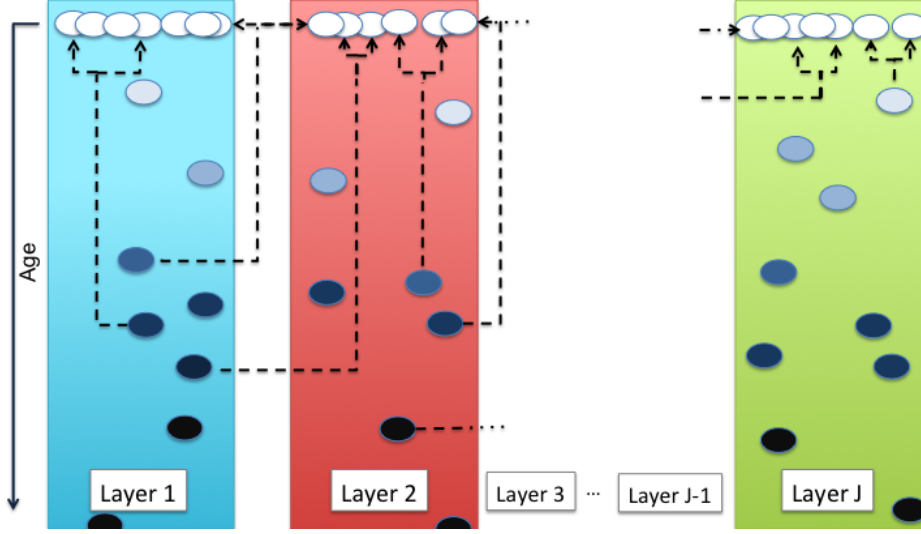
Fig. III.2   ***Model description.***   *Each cell ages until an age-dependent random division time τ^j. At division time, the age is reset and the two daughter cells may move only in a unidirectional way. When $j = J$, the daughter cells stay on the last layer.*

The cell population is represented for each time $t \geq 0$ by a measure $Z_t \in \mathcal{M}_P$:

$$Z_t = \sum_{k=1}^{N_t} \delta_{I_t^{(k)}, A_t^{(k)}}, \quad N_t := \ll Z_t, \mathbb{1} \gg = \sum_{j=1}^{J} \int_0^{+\infty} Z_t(dj, da).$$

N_t is the total number of cells at time t. On the probability space $(\Omega, \mathcal{F}, \mathbb{P})$, we define Q as a Poisson point measure of intensity $ds \otimes \#dk \otimes d\theta$, where ds and $d\theta$ are Lebesgue measures on $\mathbb{R}_+$ and $\#dk$ is a counting measure on $\mathbb{N}$. The dynamics of $Z = (Z_t)_{t \geq 0}$ is given by the following stochastic differential equation:

$$Z_t = \sum_{k=1}^{N_0} \delta_{I_0^{(k)}, A_0^{(k)}+t} + \int_{[0,t] \times \mathcal{E}} \mathbb{1}_{k \leq N_{s-}} R(k, s, Z, \theta) Q(ds, dk, d\theta)$$

where $R(k, s, Z, \theta) = (2\delta_{I_{s-}^{(k)}, t-s} - \delta_{I_{s-}^{(k)}, A_{s-}^{(k)}+t-s}) \mathbb{1}_{0 \leq \theta \leq m_1(s,k,Z)}$

$$+ (\delta_{I_{s-}^{(k)}, t-s} + \delta_{I_{s-}^{(k)}+1, t-s} - \delta_{I_{s-}^{(k)}, A_{s-}^{(k)}+t-s}) \mathbb{1}_{m_1(s,k,Z) \leq \theta \leq m_2(s,k,Z)} \quad \text{(III.4)}$$

$$+ (2\delta_{I_{s-}^{(k)}+1, t-s} - \delta_{I_{s-}^{(k)}, A_{s-}^{(k)}+t-s}) \mathbb{1}_{m_2(s,k,Z) \leq \theta \leq m_3(s,k,Z)}$$

and $m_1(s, k, Z) = b_{I_{s-}^{(k)}}(A_{s-}^{(k)}) p_{2,0}^{(I_{s-}^{(k)})}$, $m_2(s, k, Z) = b_{I_{s-}^{(k)}}(A_{s-}^{(k)})(p_{2,0}^{(I_{s-}^{(k)})} + p_{1,1}^{(I_{s-}^{(k)})})$,

$$m_3(s, k, Z) = b_{I_{s-}^{(k)}}(A_{s-}^{(k)}).$$

Deterministic model

The cell population is represented by a population density function $\rho := \left(\rho^{(j)}(t,a)\right)_{j \in [\![1,J]\!]} \in \mathbf{L}^1(\mathbb{R}_+)^J$ where $\rho^{(j)}(t,a)$ is the cell age density in layer j at time t. The population evolves

according to the following system of partial differential equations:

$$\begin{cases} \partial_t \rho^{(j)}(t,a) + \partial_a \rho^{(j)}(t,a) = -b_j(a)\rho^{(j)}(t,a) \\ \rho^{(j)}(t,0) = 2p_L^{(j-1)} \int_0^\infty b_{j-1}(a)\rho^{(j-1)}(t,a)da + 2p_S^{(j)} \int_0^\infty b_j(a)\rho^{(j)}(t,a)da \\ \rho(0,a) = \rho_0(a) \end{cases} \qquad \text{(III.5)}$$

where $\forall j \in [\![1, J-1]\!]$, $p_S^{(j)} = \frac{1}{2}p_{1,1}^{(j)} + p_{2,0}^{(j)}$, $p_L^{(j)} := \frac{1}{2}p_{1,1}^{(j)} + p_{0,2}^{(j)}$, $p_L^{(0)} = 0$ and $p_S^{(J)} = 1$. Here, $p_S^{(j)}$ is the probability that a cell taken randomly among both daughter cells, remains on the same layer and $p_L^{(j)} = 1 - p_S^{(j)}$ is the probability that the cell moves.

III.3.2 Hypotheses

Hypothesis III.1. *For all $j \in [\![1, J-1]\!]$, $p_S^{(j)}, p_L^{(j)} \in (0,1)$.*

Hypothesis III.2. *For each layer j, b_j is continuous bounded below and above:*

$$\forall j \in [\![1, J]\!], \quad \forall a \in \mathbb{R}_+, \quad 0 < \underline{b}_j \leq b_j(a) \leq \overline{b}_j < \infty \,.$$

Definition III.1. $\mathcal{B}_j$ *is the distribution function of τ^j $(\mathcal{B}_j(x) = 1 - e^{-\int_0^x b_j(a)da})$ and $d\mathcal{B}_j$ its density function $(d\mathcal{B}_j(x) = b_j(x)e^{-\int_0^x b_j(a)da})$.*

Hypothesis/Definition III.1. *(Intrinsic growth rate) The intrinsic growth rate λ_j of layer j is the solution of*

$$d\mathcal{B}_j^*(\lambda_j) := \int_0^\infty e^{-\lambda_j s} d\mathcal{B}_j(s)ds = \frac{1}{2p_S^{(j)}} \,.$$

Remark III.1. $d\mathcal{B}_j^*$ *is the Laplace transform of $d\mathcal{B}_j$. It is a strictly decreasing function and $(-\underline{b}_j, \infty) \subset \text{Supp}(d\mathcal{B}_j^*) \subset (-\overline{b}_j, \infty)$. Hence, $\lambda_j > -\overline{b}_j$. Moreover, note that $d\mathcal{B}_j^*(0) = \int_0^\infty d\mathcal{B}_j(x)dx = 1$. Thus, $\lambda_j < 0$ when $p_S^{(j)} < \frac{1}{2}$, $\lambda_j > 0$ when $p_S^{(j)} > \frac{1}{2}$ and $\lambda_j = 0$ when $p_S^{(j)} = \frac{1}{2}$. In particular, $\lambda_J > 0$ as $p_S^{(J)} = 1$.*

Remark III.2. *In the classical McKendrick–VonFoerster model (one layer), the population grows exponentially with rate λ_1 (see [26], Chap. IV). The same result is shown for the Bellman–Harris process in [65] (Chap. VI).*

Hypothesis/Definition III.2 (Malthus parameter)**.** *The Malthus parameter λ_c is defined as the unique maximal element taken among the intrinsic growth rates $(\lambda_j, j \in [\![1, J]\!])$ defined in (III.1). The layer such that the index $j = c$ is the leading layer.*

According to Remark III.1, λ_c is positive. We will need auxiliary hypotheses on λ_j parameters in some Theorems.

Hypothesis III.3. *All the intrinsic growth rate parameters are distinct.*

Hypothesis III.4. *For all $j \in [\![1, J]\!]$, $\lambda_j > -\liminf_{a \to +\infty} b_j(a)$.*

Hypothesis III.4 implies additional regularity for $t \mapsto e^{-\lambda_j t} d\mathcal{B}_j(t)$ (see proof in A.1.1):

Corollary III.1. *Under Hypotheses III.2 and III.4 and Hypothesis/Definition III.1, for all* $j \in [\![1, J]\!]$, $\forall k \in \mathbb{N}$,
$\int_0^\infty t^k e^{-\lambda_j t} d\mathcal{B}_j(t) dt < \infty$.

Stochastic initial condition

We suppose that the initial measure $Z_0 \in \mathcal{M}_P$ is deterministic. $(\mathcal{F}_t)_{t \in \mathbb{R}_+}$ is the natural filtration associated with $(Z_t)_{t \in \mathbb{R}_+}$ and Q.

Deterministic initial condition

We suppose that the initial population density ρ_0 belongs to $\mathbf{L}^1(\mathbb{R}_+)^J$.

III.3.3 Notation

Let $f, g \in \mathbf{L}^1(\mathbb{R}_+)^J$. We use for the scalar product:

- on $\mathbb{R}_+^J$, $f^T(a)g(a) = \sum_{j=1}^J f^{(j)}(a)g^{(j)}(a)$,

- on $\mathbf{L}^1(\mathbb{R}_+)$, $\langle f^{(j)}, g^{(j)} \rangle = \int_0^\infty f^{(j)}(a)g^{(j)}(a)da$, for $j \in [\![1, J]\!]$,

- on $\mathbf{L}^1(\mathbb{R}_+)^J$, $\ll f, g \gg = \sum_{j=1}^J \int_0^\infty f^{(j)}(a)g^{(j)}(a)da$.

Given a martingale $M = (M_t)_{t \geq 0}$, let $\langle M, M \rangle_t$ be its predictable quadratic variation at time t; remark that this notation is different from the scalar product on $\mathbf{L}^1(\mathbb{R}_+)$. We also introduce

$$B(a) = \text{diag}(b_1(a), ..., b_J(a)), \quad [K(a)]_{i,j} = \begin{cases} 2p_S^{(j)} b_j(a), & i = j, \quad j \in [\![1, J]\!] \\ 2p_L^{(j-1)} b_{j-1}(a), & i = j - 1, \quad j \in [\![2, J]\!] \end{cases}$$

We define the primal problem (P) as

$$\begin{cases} \mathcal{L}^P \hat{\rho}(a) = \lambda \hat{\rho}(a), \, a \geq 0 \\ \hat{\rho}(0) = \int_0^\infty K(a)\hat{\rho}(a)da \\ \ll \hat{\rho}, \mathbb{1} \gg = 1 \text{ and } \hat{\rho} \geq 0 \end{cases}, \quad \mathcal{L}^P \hat{\rho}(a) = -\partial_a \hat{\rho}(a) - B(a)\hat{\rho}(a), \tag{P}$$

and the dual problem (D) is given by

$$\begin{cases} \mathcal{L}^D \phi(a) = \lambda \phi(a), \, a \in \mathbb{R}_+^* \\ \ll \hat{\rho}, \phi \gg = 1 \text{ and } \phi \geq 0 \end{cases}, \quad \mathcal{L}^D \phi(a) = \partial_a \phi(a) - B(a)\phi + K(a)^T \phi(0). \tag{D}$$

III.3.4 Main results

a)   Eigenproblem approach

Theorem III.1 (Eigenproblem). *Under Hypotheses III.1, III.2, III.4 and, Hypotheses/Definitions III.1 and III.2, there exists a first eigenelement triple* $(\lambda, \hat{\rho}, \phi)$ *solution to equations (P) and (D) where* $\hat{\rho} \in \mathbf{L}^1(\mathbb{R}_+)^J$ *and* $\phi \in \mathcal{C}_b(\mathbb{R}_+)^J$. *In particular,* λ *is the Malthus parameter* λ_c *given in Definition III.2, and* $\hat{\rho}$ *and* ϕ *are unique.*

Beside the dual test function ϕ, we introduce other test functions to prove large-time convergence. Let $\hat{\phi}^{(j)}$, $j \in [\![1, J]\!]$ be a solution of

$$\partial_a \hat{\phi}^{(j)}(a) - (\lambda_j + b_j(a))\hat{\phi}^{(j)}(a) = -2p_S^{(j)} b_j(a)\hat{\phi}^{(j)}(0), \quad \hat{\phi}^{(j)}(0) \in \mathbb{R}_+^*. \tag{III.6}$$

Theorem III.2. *Under Hypotheses III.1, III.2, III.4 and Hypotheses/Definitions III.1 and III.2, there exist polynomials $(\beta_k^{(j)})_{1 \leq k \leq j \leq J}$ of degree at most $j - k$ such that*

$$\left\langle |e^{-\lambda_c t}\rho^{(j)}(t,\cdot) - \eta\hat{\rho}^{(j)}|, \hat{\phi}^{(j)} \right\rangle \quad \leq \quad \sum_{k=1}^{j} e^{-\mu_j t}\beta_k^{(j)}(t)\left\langle |\rho_0^{(k)} - \eta\hat{\rho}^{(k)}|, \hat{\phi}^{(k)} \right\rangle,$$

where $\eta := \ll \rho_0, \phi \gg$, $\mu_j := \lambda_c - \lambda_j > 0$ when $j \in [\![1, J]\!] \setminus \{c\}$ and $\mu_c := \underline{b}_c$. In particular, there exist a polynomial β of degree at most $J - 1$ and constant μ such that

$$\ll |e^{-\lambda_c t}\rho(t,\cdot) - \eta\hat{\rho}|, \hat{\phi} \gg \leq \beta(t)e^{-\mu t} \ll |\rho_0 - \eta\hat{\rho}|, \hat{\phi} \gg .$$

Using martingale techniques [150], we also prove a result of convergence for the stochastic process Z with the dual test function ϕ.

Theorem III.3. *Under Hypotheses III.1, III.2 and Hypotheses/Definitions III.1 and III.2, $W_t^{\phi} = e^{-\lambda_c t} \ll \phi, Z_t \gg$ is a square integrable martingale that converges almost surely and in $\mathbf{L}^2$ to a nondegenerate random variable W_{∞}^{ϕ}.*

b)   Renewal equation approach

Using generating function methods developed for multitype age dependent branching processes (see [65], Chap. VI), we write a system of renewal equations and obtain analytical formulas for the first two moments. We define $Y_t^{(j,a)} := \langle Z_t, \mathbb{1}_{j,\leq a} \rangle$ as the number of cells on layer j and of age less than or equal to a at time t, and $m_i^a(t)$ its mean starting from one mother cell of age 0 on layer 1:

$$m_j^a(t) := \mathbb{E}[Y_t^{(j,a)}|Z_0 = \delta_{1,0}].$$

Theorem III.4. *Under Hypotheses III.1, III.2, III.4 III.3, and Hypotheses/Definitions III.2, for all $a \geq 0$,*

$$\forall j \in [\![1, J]\!], \quad m_j^a(t)e^{-\lambda_c t} \to \widetilde{m}_j(a), \quad t \to \infty,$$

where $\widetilde{m}_j(a) =$

$$\begin{cases} 0, & j \in [\![1, c-1]\!], \\ \dfrac{\int_0^a \hat{\rho}^{(c)}(s)ds}{2p_S^{(c)}\hat{\rho}^{(c)}(0)\int_0^\infty sd\mathcal{B}_c(s)e^{-\lambda_c s}ds}, & j = c, \\ \dfrac{\int_0^a \hat{\rho}^{(j)}(s)ds}{2p_S^{(c)}\hat{\rho}^{(c)}(0)\int_0^\infty sd\mathcal{B}_c(s)e^{-\lambda_c s}ds} \displaystyle\prod_{k=1}^{c-1} \dfrac{2p_L^{(k)}d\mathcal{B}_k^*(\lambda_c)}{1 - 2p_S^{(k)}d\mathcal{B}_k^*(\lambda_c)}, & j \in [\![c+1, J]\!]. \end{cases}$$

c)   Calibration

We now consider a particular choice of the division rate:

Hypothesis III.5 (Age-independent division rate)**.** *For all $(j, a) \in \mathcal{E}$, $b_j(a) = b_j$.*

We also consider a specific initial condition with $N \in \mathbb{N}^*$ cells.

Hypothesis III.6 (First layer initial condition)**.** $Z_0 = N\delta_{1,0}.$

Then, integrating the deterministic PDE system (III.5) with respect to age or differentiating the renewal equation system (see (III.24)) on the mean number M, we obtain:

$$\begin{cases} \frac{d}{dt} M(t) = AM(t) \\ M(0) = (N, 0, ..., 0) \in \mathbb{R}^J \end{cases}, \quad [A]_{i,j} := \begin{cases} (2p_S^{(j)} - 1)b_j, & i = j, & j \in [\![1, J]\!], \\ 2p_L^{(j-1)} b_{j-1}, & i = j - 1, & j \in [\![2, J]\!]. \end{cases} \quad \text{(III.7)}$$

We prove the structural identifiability of the parameter set $\mathbf{P} := \{N, b_j, p_S^{(j)}, j \in [\![1, J]\!]\}$ when we observe the vector $M(t; \mathbf{P})$ at each time t.

Theorem III.5. *Under Hypotheses III.1, III.5 and III.6 and complete observation of system (III.7), the parameter set $\mathbf{P}$ is identifiable.*

We then perform the estimation of the parameter set $\mathbf{P}$ from experimental cell number data retrieved on four layers and sampled at three different time points (see Table III.1a). To improve practical identifiability, we embed biological specifications used in [1] as a recurrence relation between successive division rates:

$$b_j = \frac{b_1}{1 + (j - 1) \times \alpha}, \, j \in [\![1, 4]\!], \, \alpha \in \mathbb{R}.$$

We estimate the parameter set $\mathbf{P}_{exp} = \{N, b_1, \alpha, p_S^{(1)}, p_S^{(2)}, p_S^{(3)}\}$ using the D2D software [91] with an additive Gaussian noise model (see Figure III.3 and Table III.1b). An analysis of the profile likelihood estimate shows that all parameters except $p_S^{(2)}$ are practically identifiable (see Figure A.1b in Appendix subsection A.1.5).
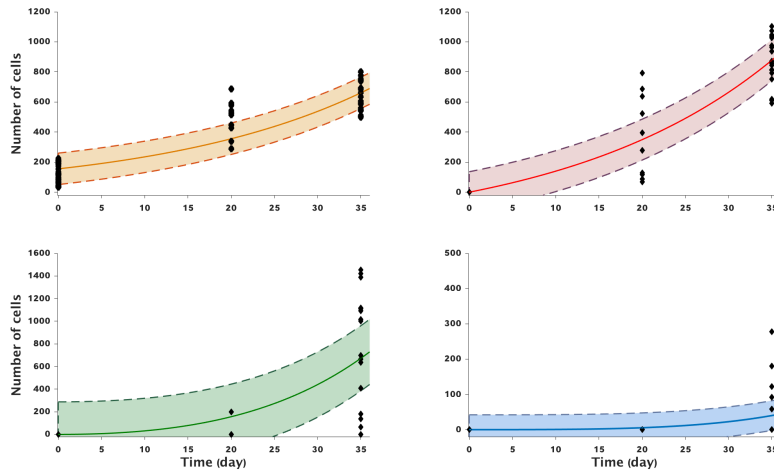

Fig. III.3   **Data fitting with model (III.7).** *Each panel illustrates the changes in the cell number in a given layer (top-left: Layer 1, top-right: Layer 2, bottom-left: Layer 3, bottom-right: Layer 4). The black diamonds represent the experimental data, the solid lines are the best fit solutions of (III.7) and the dashed lines are drawn from the estimated variance. The parameter values (Table III.1b) are estimated according to the procedure described in Appendix subsection A.1.5.*

III.4 Theoretical proof and illustrations

III.4.1 Eigenproblem

We start by solving explicitly the eigenproblem (P)–(D) to prove Theorem III.1.

Proof of Theorem III.1. According to Definition III.1, any solution of (P) in $\mathbf{L}^1(\mathbb{R}_+)^J$ is given by, $\forall j \in [\![1, J]\!]$,

$$\hat{\rho}^{(j)}(a) = \hat{\rho}^{(j)}(0)e^{-\lambda a}(\mathbb{1} - \mathcal{B}_j)(a) \,.$$

The boundary condition of the problem (P) gives us a system of equations for λ and $\hat{\rho}^{(j)}(0)$, $j \in [\![1, J]\!]$:

$$\hat{\rho}^{(j)}(0) \times (1 - 2p_S^{(j)}d\mathcal{B}_j^*(\lambda)) = 2p_L^{(j-1)}d\mathcal{B}_{j-1}^*(\lambda) \times \hat{\rho}^{(j-1)}(0) \,.$$

This system is equivalent to

$$C(\lambda)\hat{\rho}(0) = 0, \quad [C(\lambda)]_{i,j} = \begin{cases} 1 - 2p_S^{(j)}d\mathcal{B}_j^*(\lambda), & i = j, \quad j \in [\![1, J]\!], \\ 2p_L^{(j-1)}d\mathcal{B}_{j-1}^*(\lambda), & i = j - 1, \quad j \in [\![2, J]\!]. \end{cases}$$

Let $\Lambda := \{\lambda_j, j \in [\![1, J]\!]\}$. The eigenvalues of the matrix $C(\lambda)$ are $1 - 2p_S^{(j)}d\mathcal{B}_j^*(\lambda)$, $j \in [\![1, J]\!]$. Thus, if $\lambda \notin \Lambda$, according to Hypothesis/Definition III.1, 0 is not an eigenvalue of $C(\lambda)$ which implies that $\hat{\rho}(0) = 0$. As $\hat{\rho}$ satisfies both (III.4.1) and the normalization $\ll \hat{\rho}, \mathbb{1} \gg = 1$, we obtain a contradiction. So, necessary $\lambda \in \Lambda$.
We choose $\lambda = \lambda_c$ to be the maximum element of Λ according to Hypothesis/Definition III.2. Then, using (III.4.1) when $j = c$, we have:

$$\hat{\rho}^{(c)}(0) \times (1 - 2p_S^{(c)}d\mathcal{B}_c^*(\lambda_c)) = 2p_L^{(c-1)}d\mathcal{B}_{c-1}^*(\lambda_c) \times \hat{\rho}^{(c-1)}(0) \,.$$

Note that $1 - 2p_S^{(c)}d\mathcal{B}_c^*(\lambda_c) = 0$, so $\hat{\rho}^{(c-1)}(0) = 0$ and by backward recurrence using (III.4.1) from $j = c - 1$ to 1, it comes that $\hat{\rho}^{(j)}(0) = 0$ when $j < c$. By Hypothesis/Definition III.2, $\max(\Lambda)$ is unique. Thus, when $j > c$, $\lambda_j \neq \lambda_c$ and $1 - 2p_S^{(j)}d\mathcal{B}_j^*(\lambda_c) \neq 0$. Solving (III.4.1) from $j = c + 1$ to J, we obtain

$$\hat{\rho}^{(j)}(0) = \hat{\rho}^{(c)}(0) \times \prod_{k=c+1}^{j} \frac{2p_L^{(k-1)}d\mathcal{B}_{k-1}^*(\lambda_c)}{1 - 2p_S^{(k)}d\mathcal{B}_k^*(\lambda_c)}, \quad \forall j \in [\![c + 1, J]\!] \,.$$

We deduce $\hat{\rho}^{(c)}(0)$ from the normalization $\ll \hat{\rho}, \mathbb{1} \gg = 1$. Hence, $\hat{\rho}$ is uniquely determined by (III.4.1) together with the following boundary value:

$$\hat{\rho}^{(j)}(0) = \begin{cases} 0, & j \in [\![1, c - 1]\!], \\[2ex] \dfrac{1}{\sum_{j=c}^{J} \int_0^\infty \hat{\rho}^{(j)}(a)da \prod_{k=c+1}^{j} \frac{2p_L^{(k-1)}d\mathcal{B}_{k-1}^*(\lambda_c)}{1-2p_S^{(k)}d\mathcal{B}_k^*(\lambda_c)}}, & j = c, \\[3ex] \hat{\rho}^{(c)}(0) \displaystyle\prod_{k=c+1}^{j} \frac{2p_L^{(k-1)}d\mathcal{B}_{k-1}^*(\lambda_c)}{1 - 2p_S^{(k)}d\mathcal{B}_k^*(\lambda_c)}, & j \in [\![c + 1, J]\!]. \end{cases} \tag{III.8}$$

For the ODE system (D), any solution is given by, for $j \in [\![1, J]\!]$,

$$\phi^{(j)}(a) = \left[\phi^{(j)}(0) - 2(\phi^{(j)}(0)p_S^{(j)} + \phi^{(j+1)}(0)p_L^{(j)}) \int_0^a e^{-\lambda_c s}d\mathcal{B}_j(s)ds\right] e^{\int_0^a \lambda_c + b_j(s)ds} \,.$$

As $\int_0^a b_j(s)e^{-\int_0^s \lambda_c + b_j(u)du}ds$ is equal to $d\mathcal{B}_j^*(\lambda_c) - \int_a^\infty b_j(s)e^{-\int_0^s \lambda_c + b_j(u)du}ds$, we get

$$\phi^{(j)}(a) = \left[\phi^{(j)}(0) \left(1 - 2p_S^{(j)}d\mathcal{B}_j^*(\lambda_c) + 2p_S^{(j)}\int_a^{+\infty} b_j(s)e^{-\int_0^s \lambda_c + b_j(u)du}ds \right) \right.$$
$$\left. - \phi^{(j+1)}(0)\left(2p_L^{(j)}d\mathcal{B}_j^*(\lambda_c) - 2p_L^{(j)}\int_a^{+\infty} b_j(s)e^{-\int_0^s \lambda_c + b_j(u)du}ds \right) \right] e^{\int_0^a \lambda_c + b_j(s)ds}.$$

Searching for $\phi \in \mathcal{C}_b(\mathbb{R}_+)^J$, it comes that

$$\forall j \in [\![1, J]\!], \quad \phi^{(j)}(0)\left(1 - 2p_S^{(j)}d\mathcal{B}_j^*(\lambda_c) \right) - \phi^{(j+1)}(0)2p_L^{(j)}d\mathcal{B}_j^*(\lambda_c) = 0.$$

According to Hypothesis/Definition III.1, when $j = c$ in (III.4.1) we get $\phi^{(c+1)}(0) = 0$. Recursively, $\phi^{(j)}(0) = 0$ when $j > c$. Solving (III.4.1) from $j = 1$ to $c - 1$, we get

$$\forall j \in [\![1, c-1]\!], \quad \phi^{(j)}(0) = \phi^{(c)}(0) \times \prod_{k=j}^{c-1} \frac{2p_L^{(k-1)}d\mathcal{B}_{k-1}^*(\lambda_c)}{1 - 2p_S^{(k)}d\mathcal{B}_k^*(\lambda_c)}. \tag{III.9}$$

Again, we deduce $\phi^{(c)}(0)$ from the normalization $1 = \ll \hat{\rho}, \phi \gg = \langle \hat{\rho}^{(c)}, \phi^{(c)} \rangle$. Using Corollary III.1, we apply the Fubini theorem:

$$\phi^{(c)}(0) = \frac{1}{2\hat{\rho}^{(c)}(0)p_S^{(c)}\int_0^\infty \left(\int_a^{+\infty} e^{-\lambda_c s}d\mathcal{B}_c(s)ds \right)da} = \frac{1}{2\hat{\rho}^{(c)}(0)p_S^{(c)}\int_0^\infty se^{-\lambda_c s}d\mathcal{B}_c(s)ds}. \tag{III.10}$$

Hence, the dual function ϕ is uniquely determined by

$$\phi^{(j)}(a) = 2\left[p_S^{(j)}\phi^{(j)}(0) + p_L^{(j)}\phi^{(j+1)}(0) \right] \int_a^{+\infty} b_j(s)e^{-\int_a^s \lambda_c + b_j(u)du}ds. \tag{III.11}$$

together with the recurrence relation (III.9) and the boundary value (III.10) (ϕ is null on the layers downstream the leading layer, $j > c$). □

From Theorem III.1, we deduce the following bounds on ϕ (see proof in A.1.1).

Corollary III.2. *According to Hypothesis III.2 and Hypotheses/Definitions III.1 and III.2,*

$$\forall j \in [\![1, c]\!], \quad \frac{\underline{b}_j}{\lambda_c + \overline{b}_j} \le \frac{\phi^{(j)}(a)}{2[p_S^{(j)}\phi^{(j)}(0) + p_L^{(j)}\phi^{(j+1)}(0)]} \le 1. \tag{III.12}$$

To conclude this section, we also solve the additional dual problem on isolated layers which is needed to obtain the large-time convergence (see proof in A.1.1).

Lemma III.1. *According to Hypotheses III.2, III.4 and Hypothesis/Definition III.1, any solution $\hat{\phi}$ of (III.6) satisfies*

$$\forall j \in [\![1, J]\!], \quad \hat{\phi}^{(j)}(a) = 2p_S^{(j)}\hat{\phi}^{(j)}(0)\int_a^{+\infty} b_j(s)e^{-\lambda_j s - \int_a^s b_j(u)du}ds$$

and, $\forall a \in \mathbb{R}_+ \cup \{+\infty\}$, $\frac{\underline{b}_j}{\lambda_j + \overline{b}_j} \le \frac{\hat{\phi}^{(j)}(a)}{2p_S^{(j)}\hat{\phi}^{(j)}(0)} < +\infty$.

In what follows, we fix

$$\hat{\phi}^{(c)}(0) = \phi^{(c)}(0), \quad \forall j \in [\![1, c-1]\!] \quad \hat{\phi}^{(j)}(0) = \phi^{(j)}(0) + \frac{p_L^{(j)}}{p_S^{(j)}} \phi^{(j+1)}(0).$$

A first consequence is that $\hat{\phi}^{(c)} = \phi^{(c)}$ and, moreover, from Corollary III.2 and Lemma III.1, we have

$$\phi^{(j)}(a) \le \frac{\lambda_j + \overline{b}_j}{\underline{b}_j} \hat{\phi}^{(j)}(a). \tag{III.13}$$

III.4.2 Asymptotic study for the deterministic formalism

Adapting the method of characteristic, it is classical to construct the unique solution in $\mathcal{C}^1(\mathbb{R}_+, \mathbf{L}^1(\mathbb{R}_+)^J)$ of PDE (III.5) ([26], Chap. I). Let ρ be the solution of (III.5), $\hat{\rho}$ and ϕ given by Theorem III.1 and $\eta = \ll \rho_0, \phi \gg$. We define h as

$$h(t,a) = e^{-\lambda_c t} \rho(t,a) - \eta \hat{\rho}(a), \quad (t,a) \in \mathbb{R}_+ \times \mathbb{R}_+.$$

Following [149], we first show a conservation principle (see the proof in Appendix subsection A.1.1).

Lemma III.2 (Conservation principle)**.** *The function h satisfies the conservation principle*

$$\ll h(t,\cdot), \phi \gg = 0.$$

Second, we prove that h is solution of the following PDE system (see proof in Appendix subsection A.1.1).

Lemma III.3. *h is solution of*

$$\begin{cases} \partial_t |h(t,a)| + \partial_a |h(t,a)| + (\lambda_c + B(a)) |h(t,a)| = 0, \\ |h(t,0)| = |\int_0^{+\infty} K(a) h(t,a) da|. \end{cases}$$

Together with the above Lemmas III.1, III.2 and III.3, we now prove the following key estimates required for the asymptotic behavior.

Lemma III.4. *For all $j \in [\![1, J]\!]$, the component $h^{(j)}$ of h verifies the inequality*

$$\partial_t \left\langle |h^{(j)}(t,\cdot)|, \hat{\phi}^{(j)} \right\rangle \le \alpha_{j-1} \left\langle |h^{(j-1)}(t,\cdot)|, \hat{\phi}^{(j-1)} \right\rangle - \mu_j \left\langle |h^{(j)}(t,\cdot)|, \hat{\phi}^{(j)} \right\rangle + r_j(t), \tag{III.14}$$

where $\alpha_0 := 0$, for $j \in [\![1, J]\!]$, $\alpha_j := \frac{p_L^{(j)}}{p_S^{(j)}} \frac{\overline{b}_j}{\underline{b}_j} \frac{\hat{\phi}^{(j+1)}(0)}{\hat{\phi}^{(j)}(0)} (\lambda_j + \overline{b}_j)$ and

$$\mu_j = \begin{cases} \lambda_c - \lambda_j, & j \ne c \\ \underline{b}_c, & j = c \end{cases}, \quad r_j(t) := \begin{cases} 0, & j \ne c \\ \displaystyle\sum_{j=1}^{c-1} \frac{\lambda_j + \overline{b}_j}{\underline{b}_j} \left\langle |h^{(j)}(t,\cdot)|, \hat{\phi}^{(j)} \right\rangle, & j = c. \end{cases}$$

Proof of Lemma III.4. We remind the reader that $p_L^{(0)} = 0$ so that all the following computations are consistent with $j = 1$. Multiplying (III.3) by $\hat{\phi}$ and using (III.6), it comes for any

j

$$\begin{cases} \partial_t |h^{(j)}(t,a)| \hat{\phi}^{(j)}(a) + \partial_a |h^{(j)}(t,a)| \hat{\phi}^{(j)}(a) = -2p_S^{(j)} \hat{\phi}^{(j)}(0) b_j(a) |h^{(j)}(t,a)| + [\lambda_j - \lambda_c] |h^{(j)}(t,a)| \hat{\phi}^{(j)}(a), \\ \quad |h^{(j)}(t,0)| \hat{\phi}^{(j)}(0) = \hat{\phi}^{(j)}(0) | 2p_S^{(j)} \left\langle b_j, h^{(j)}(t,\cdot) \right\rangle + 2p_L^{(j-1)} \left\langle b_{j-1}, h^{(j-1)}(t,\cdot) \right\rangle |. \end{cases}$$
$$\tag{III.15}$$

As $\rho(t,\cdot)$ and $\hat{\rho}$ belong to $\mathbf{L}^1(\mathbb{R}_+)^J$ and $\hat{\phi}$ is a bounded function (from Lemma III.1) we deduce that $\ll h(t,\cdot), \hat{\phi} \gg < \infty$. Integrating (III.15) with respect to age, we have

$$\partial_t \left\langle |h^{(j)}(t,\cdot)|, \hat{\phi}^{(j)} \right\rangle \quad = \hat{\phi}^{(j)}(0) \left[|h^{(j)}(t,0)| - 2p_S^{(j)} \left\langle |h^{(j)}(t,\cdot)|, b_j \right\rangle \right] + (\lambda_j - \lambda_c) \left\langle |h^{(j)}(t,\cdot)|, \hat{\phi}^{(j)} \right\rangle .$$
$$\tag{III.16}$$

We deal with the first term in the right-hand side of (III.16). When $j \neq c$, using first the boundary value in (III.15), a triangular inequality and Lemma III.1, we get

$$\hat{\phi}^{(j)}(0) \left(|h^{(j)}(t,0)| - 2p_S^{(j)} \left\langle |h^{(j)}(t,\cdot)|, b_j \right\rangle \right) \leq \quad 2p_L^{(j-1)} \hat{\phi}^{(j)}(0) \left\langle |h^{(j-1)}(t,\cdot)|, b_{j-1} \right\rangle$$
$$\leq \quad \alpha_{j-1} \left\langle |h^{(j-1)}(t,\cdot)|, \hat{\phi}^{(j-1)} \right\rangle .$$

Thus, for $j \neq c$,

$$\partial_t \left\langle |h^{(j)}(t,\cdot)|, \hat{\phi}^{(j)} \right\rangle \quad \leq \quad \alpha_{j-1} \left\langle |h^{(j-1)}(t,\cdot)|, \hat{\phi}^{(j-1)} \right\rangle - \mu_j \left\langle |h^{(j)}(t,\cdot)|, \hat{\phi}^{(j)} \right\rangle .$$

When $j = c$, using the boundary value in (III.15) and a triangular inequality, we get

$$\partial_t \left\langle |h^{(c)}(t,\cdot)|, \hat{\phi}^{(c)} \right\rangle \quad \leq 2p_S^{(c)} \hat{\phi}^{(c)}(0) [| \left\langle h^{(c)}(t,\cdot), b_c \right\rangle | - \left\langle |h^{(c)}(t,\cdot)|, b_c \right\rangle]$$
$$+ 2p_L^{(c-1)} \hat{\phi}^{(c)}(0) | \left\langle h^{(c-1)}(t,\cdot), b_{c-1} \right\rangle |. \quad \text{(III.17)}$$

To exhibit a term $\left\langle |h^{(c)}(t,\cdot)|, \hat{\phi}^{(c)} \right\rangle$ in the right hand-side of (III.17), we need a more refined analysis. According to the conservation principle (Lemma III.2), for any constant γ (to be chosen later), we obtain

$$2p_S^{(c)} \hat{\phi}^{(c)}(0) | \left\langle h^{(c)}(t,\cdot), b_c \right\rangle | = \quad | 2p_S^{(c)} \hat{\phi}^{(c)}(0) \left\langle h^{(c)}(t,\cdot), b_c \right\rangle - \gamma \ll h(t,\cdot), \phi \gg |$$
$$\leq \quad | \left\langle h^{(c)}(t,\cdot), 2p_S^{(c)} \hat{\phi}^{(c)}(0) b_c - \gamma \phi^{(c)} \right\rangle | + \gamma \sum_{j=1}^{c-1} \left\langle |h^{(j)}(t,\cdot)|, \phi^{(j)} \right\rangle .$$

where we used a triangular inequality in the latter estimate. Moreover, according to (III.13), we have

$$\forall j \in [\![1, c-1]\!], \quad \left\langle |h^{(j)}(t,\cdot)|, \phi^{(j)} \right\rangle \quad \leq \quad \frac{\lambda_j + \bar{b}_j}{\underline{b}_j} \left\langle |h^{(j)}(t,\cdot)|, \hat{\phi}^{(j)} \right\rangle ,$$

and according to Corollary III.2,

$$\phi^{(c)}(a) \leq \frac{2p_S^{(c)} \phi^{(c)}(0)}{\underline{b}_c} b_c(a). \tag{III.18}$$

We want to find at least one constant γ such that for all $a \geq 0$, $2p_S^{(c)}\hat{\phi}^{(c)}(0)b_c(a) - \gamma\phi^{(c)}(a) > 0$. From (III.18), we choose $\gamma = \underline{b}_c$, and deduce from (III.4.2) and (III.4.2) that

$$2p_S^{(c)}\hat{\phi}^c(0)|\left\langle h^{(c)}(t,\cdot), b_c \right\rangle| \leq 2p_S^{(c)}\hat{\phi}^{(c)}(0)\left\langle |h^{(c)}(t,\cdot)|, b_c \right\rangle - \underline{b}_c\left\langle |h^{(c)}(t,\cdot)|, \phi^{(c)} \right\rangle$$
$$+ \underline{b}_c\sum_{j=1}^{c-1}\frac{\lambda_j + \overline{b}_j}{\underline{b}_j}\left\langle |h^{(j)}(t,\cdot)|, \hat{\phi}^{(j)} \right\rangle.$$

As before, using Lemma III.1, we obtain

$$2p_L^{(c-1)}\hat{\phi}^{(c)}(0)|\left\langle h^{(c-1)}(t,\cdot), b_{c-1} \right\rangle| \leq \alpha_{c-1}\left\langle |h^{(c-1)}(t,\cdot)|, \hat{\phi}^{(c-1)} \right\rangle.$$

Combining the latter inequality with (III.4.2) and (III.17), we deduce (III.14) for $j = c$. $\square$

We now have all of the elements to prove Theorem III.2.

Proof of Theorem III.2. We proceed by recurrence from the index $j = 1$ to J. For $j = 1$, we can apply Gronwall lemma in inequality (III.14) to get

$$\left\langle |h^{(1)}(t,\cdot)|, \hat{\phi}^{(1)} \right\rangle \leq e^{-\mu_1 t}\left\langle |h^{(1)}(0,\cdot)|, \hat{\phi}^{(1)} \right\rangle.$$

We suppose that for a fixed $2 \leq j \leq J$ and for all ranks $1 \leq i \leq j-1$, there exist polynomials $\beta_k^{(i)}$, $k \in [\![1, i]\!]$, of degree at most $i - k$ such that

$$\left\langle |h^{(i)}(t,\cdot)|, \hat{\phi}^{(i)} \right\rangle \leq \sum_{k=1}^{i}\beta_k^{(i)}(t)e^{-\mu_k t}\left\langle |h^{(k)}(0,\cdot)|, \hat{\phi}^{(k)} \right\rangle.$$

Applying this recurrence hypothesis in inequality (III.14) for j, there exist polynomials $\widetilde{\beta}_k^{(j)}(t)$ for $k \in [\![1, j-1]\!]$ (same degree than $\beta_k^{(j-1)}(t)$):

$$\partial_t \left\langle |h^{(j)}(t,\cdot)|, \hat{\phi}^{(j)} \right\rangle \leq \sum_{k=1}^{j-1}\widetilde{\beta}_k^{(j)}(t)e^{-\mu_k t}\left\langle |h^{(k)}(0,\cdot)|, \hat{\phi}^{(k)} \right\rangle - \mu_j\left\langle |h^{(j)}(t,\cdot)|, \hat{\phi}^{(j)} \right\rangle.$$

We get from a modified version of the Gronwall lemma (see Lemma A.1 in Appendix section):

$$\left\langle |h^{(j)}(t,\cdot)|, \hat{\phi}^{(j)} \right\rangle \leq \sum_{k=1}^{j}\beta_k^{(j)}(t)e^{-\mu_k t}\left\langle |h^{(k)}(0,\cdot)|, \hat{\phi}^{(k)} \right\rangle.$$

where $\beta_j^{(j)}$ is a constant and for $k \in [\![1, j-1]\!]$, $\beta_k^{(j)}$ is a polynomial of degree at most $(j-1-k)+1 = j-k$ (the degree only increases by 1 when $\mu_k = \mu_j$). This achieves the recurrence. $\square$

III.4.3 Asymptotic study of the martingale problem

The existence and uniqueness of the SDE (III.4) is proved in a more general context than ours in [85]. Following the approach proposed in [85], we first derive the generator of the process Z solution of (III.4). In this part, we consider $F \in \mathcal{C}^1(\mathbb{R}_+, \mathbb{R}_+)$ and $f \in \mathcal{C}_b^1(\mathcal{E}, \mathbb{R}_+)$.

Theorem III.6 (Infinitesimal generator of (Z_t))**.** *Under Hypotheses III.1 and III.2, the process Z defined in (III.4) and starting from Z_0 is a Markovian process in the Skorokhod space $\mathbb{D}([0,T], \mathcal{M}_P(\llbracket 1, J \rrbracket \times \mathbb{R}_+))$. Let $T > 0$, Z satisfies*

$$\mathbb{E}\big[\sup_{t \leq T} N_t\big] < \infty, \quad \mathbb{E}\big[\sup_{t \leq T} \ll a, Z_t \gg \big] < \infty, \tag{III.19}$$

and its infinitesimal generator is

$$\mathcal{G}F[\ll f, Z \gg] = \ll F'[\ll Z, f \gg]\partial_a f, Z \gg$$

$$+ \sum_{j=1}^{J} \int_0^\infty (F[\ll f, 2\delta_{j,0} - \delta_{j,a} + Z \gg] - F[\ll f, Z \gg])p_{2,0}^{(j)} b_j(a) Z(dj, da)$$

$$+ \sum_{j=1}^{J} \int_0^\infty (F[\ll f, \delta_{j,0} + \delta_{j+1,0} - \delta_{j,a} + Z \gg] - F[\ll f, Z \gg])p_{1,1}^{(j)} b_j(a) Z(dj, da)$$

$$+ \sum_{j=1}^{J} \int_0^\infty (F[\ll f, 2\delta_{j+1,0} - \delta_{j,a} + Z \gg] - F[\ll f, Z \gg])p_{0,2}^{(j)} b_j(a) Z(dj, da).$$

From this theorem, we derive the following Dynkin formula.

Lemma III.5 (Dynkin formula)**.** *Let $T > 0$. Under Hypotheses III.1 and III.2, $\forall t \in [0, T]$,*

$$F[\ll f, Z_t \gg] = F[\ll f, Z_0 \gg] + \int_0^t \mathcal{G}F[\ll f, Z_s \gg]ds + M_t^{F,f}$$

where $M^{F,f}$ is a martingale. Moreover,

$$\ll f, Z_t \gg = \ll f, Z_0 \gg + \int_0^t \ll \mathcal{L}^D f, Z_s \gg ds + M_t^f$$

where $\mathcal{L}^D$ the dual operator in (D) and M^f is a $\mathbf{L}^2$–martingale defined by

$$M_t^f = \int_0^t \ll B(\cdot)f(\cdot) - K(\cdot)^T f(0), Z_s \gg ds$$

$$+ \int\int_{[0,t]\times\mathcal{E}} \mathbb{1}_{k \leq N_{s^-}} \ll f, 2\delta_{I_{s^-}^{(k)},0} - \delta_{I_{s^-}^{(k)},A_{s^-}^{(k)}} \gg \mathbb{1}_{0 \leq \theta \leq m_1(s,k,Z)} Q(ds, dk, d\theta)$$

$$+ \int\int_{[0,t]\times\mathcal{E}} \mathbb{1}_{k \leq N_{s^-}} \ll f, \delta_{I_{s^-}^{(k)},0} + \delta_{I_{s^-}^{(k)}+1,0} - \delta_{I_{s^-}^{(k)},A_{s^-}^{(k)}} \gg \mathbb{1}_{m_1(s,k,Z) \leq \theta \leq m_2(s,k,Z)} Q(ds, dk, d\theta)$$

$$+ \int\int_{[0,t]\times\mathcal{E}} \mathbb{1}_{k \leq N_{s^-}} \ll f, 2\delta_{I_{s^-}^{(k)}+1,0} - \delta_{I_{s^-}^{(k)},A_{s^-}^{(k)}} \gg \mathbb{1}_{m_2(s,k,Z) \leq \theta \leq m_3(s,k,Z)} Q(ds, dk, d\theta)$$

with its predictable quadratic variation given by

$$\left\langle M^f, M^f \right\rangle_t = \int_0^t \Big[\sum_{j=1}^{J} \int_{\mathbb{R}_+} [\ll f, 2\delta_{j,0} - \delta_{j,a} \gg]^2 b_j(a) p_{2,0}^{(j)} Z_s(dj, da)$$

$$+ \sum_{j=1}^{J} \int_{\mathbb{R}_+} [\ll f, \delta_{j,0} + \delta_{j+1,0} - \delta_{j,a} \gg]^2 b_j(a) p_{1,1}^{(j)} Z_s(dj, da) \tag{III.20}$$

$$+ \sum_{j=1}^{J} \int_{\mathbb{R}_+} [\ll f, 2\delta_{j+1,0} - \delta_{j,a} \gg]^2 b_j(a) p_{0,2}^{(j)} Z_s(dj, da)\Big]ds.$$

The proofs of Theorem III.6 and Lemma III.5 are classical and provided in Appendix subsection A.1.2 for reader convenience. We now have all the elements to prove Theorem III.3.

Proof of Theorem III.3. We apply the Dynkin formula (III.5) with the dual test function ϕ and obtain

$$\ll \phi, Z_t \gg = \ll \phi, Z_0 \gg + \lambda_c \int_0^t \ll \phi, Z_s \gg ds + M_t^\phi.$$

As ϕ is bounded, $\ll \phi, Z_t \gg$ has finite expectation for all time t according to (III.19). Thus,

$$\mathbb{E}[\ll \phi, Z_t \gg] = \mathbb{E}[\ll \phi, Z_0 \gg] + \lambda_c \mathbb{E}[\int_0^t \ll \phi, Z_s \gg ds]. \qquad \text{(III.21)}$$

Using the Fubini theorem and solving equation (III.21), we obtain

$$\mathbb{E}[\ll \phi, Z_t \gg] = e^{\lambda_c t}\mathbb{E}[\ll \phi, Z_0 \gg] \Rightarrow \mathbb{E}[e^{-\lambda_c t}\ll \phi, Z_t \gg] = \mathbb{E}[\ll \phi, Z_0 \gg]. \quad \text{(III.22)}$$

Hence, $W_t^\phi = e^{-\lambda_c t} \ll \phi, Z_t \gg$ is a martingale. According to martingale convergence theorems (see Theorem 7.11 in [83]), W_t^ϕ converges to an integrable random variable $W_\infty^\phi \geq 0$, $\mathbb{P}$–p.s. when t goes to infinity. To prove that W_∞^ϕ is nondegenerated, we will show that the convergence holds in $\mathbf{L}^2$. Indeed, from the $\mathbf{L}^2$ convergence, we deduce the $\mathbf{L}^1$ convergence. Then, using almost sure convergence and applying the the dominated convergence theorem, we have

$$\mathbb{E}[W_\infty^\phi] = \mathbb{E}[\lim_{t\to\infty} W_t^\phi] = \lim_{t\to\infty} \mathbb{E}[W_t^\phi] = \mathbb{E}[W_0^\phi] > 0.$$

Consequently, W_∞^ϕ is nondegenerated. To show the $\mathbf{L}^2$ convergence, we compute the quadratic variation of W^ϕ. Applying the Ito formula (see [151] p. 78-81) with $F(t, \ll \phi, Z_t \gg) = e^{-\lambda_c t} \ll \phi, Z_t \gg$, we deduce

$$W_t^\phi = \ll \phi, Z_0 \gg + \int_0^t \left[\int_{\mathcal{E}} e^{-\lambda_c s}(\partial_a \phi^{(j)}(a) - \lambda_c \phi^{(j)}(a)) Z_s(dj, da)\right] ds$$

$$+ \int\int_{[0,t]\times\mathcal{E}} \mathbb{1}_{k\leq N_{s^-}} e^{-\lambda_c s} \ll \phi, 2\delta_{I_{s^-}^{(k)},0} - \delta_{I_{s^-}^{(k)},A_{s^-}^{(k)}} \gg \mathbb{1}_{0\leq\theta\leq m_1(s,k,Z)} Q(ds, dk, d\theta)$$

$$+ \int\int_{[0,t]\times\mathcal{E}} \mathbb{1}_{k\leq N_{s^-}} e^{-\lambda_c s} \ll \phi, \delta_{I_{s^-}^{(k)},0} + \delta_{I_{s^-}^{(k)}+1,0} - \delta_{I_{s^-}^{(k)},A_{s^-}^{(k)}} \gg \mathbb{1}_{m_1(s,k,Z)\leq\theta\leq m_2(s,k,Z)} Q(ds, dk, d\theta)$$

$$+ \int\int_{[0,t]\times\mathcal{E}} \mathbb{1}_{k\leq N_{s^-}} e^{-\lambda_c s} \ll \phi, 2\delta_{I_{s^-}^{(k)}+1,0} - \delta_{I_{s^-}^{(k)},A_{s^-}^{(k)}} \gg \mathbb{1}_{m_2(s,k,Z)\leq\theta\leq m_3(s,k,Z)} Q(ds, dk, d\theta).$$

As $\mathcal{L}^D \phi = \lambda_c \phi$, we have

$$\int_{\mathcal{E}} (\partial_a \phi^{(j)}(a) - \lambda_c \phi^{(j)}(a)) Z_s(dj, da) = \ll B(\cdot)\phi(\cdot) - K^T(\cdot)\phi(0), Z_s \gg.$$

Consequently, from (III.5), we deduce

$$W_t^\phi = \ll \phi, Z_0 \gg + \int_0^t e^{-\lambda_c s} dM_s^\phi. \qquad \text{(III.23)}$$

where the latter integral is defined path by path as a Stieltjes integral since M is a finite variation process (see 8.4, p.215 [83]). According to (III.20) and (III.23), we get

$$
\begin{aligned}
\left\langle W_\cdot^\phi, W_\cdot^\phi \right\rangle_t &= \int_0^t e^{-2\lambda_c s} d\left\langle M^\phi, M^\phi \right\rangle_s ds \\
&= \int_0^t e^{-2\lambda_c s}\left[\int_{\mathcal{E}} \left(p_{2,0}^{(j)}[\ll \phi, 2\delta_{j,0} - \delta_{j,a} \gg]^2 + p_{1,1}^{(j)}[\ll \phi, \delta_{j,0} + \delta_{j+1,0} - \delta_{j,a} \gg]^2\right.\right. \\
&\qquad\qquad\qquad\qquad \left.\left.+ p_{0,2}^{(j)}[\ll \phi, 2\delta_{j+1,0} - \delta_{j,a} \gg]^2\right) b_j(a) Z_s(dj, da)\right] ds\,.
\end{aligned}
$$

First, note that $\phi^{(j)}$ is null when $j \in [\![c+1, J]\!]$. Then, since $\phi^{(j)}$ is bounded upper and lower (see (III.12)) for all $j \in [\![1, c]\!]$ and b_j are bounded functions, we deduce that there exists a constant $K > 0$ such that

$$
\left\langle W^\phi, W^\phi \right\rangle_t \leq K \int_0^t e^{-2\lambda_c s} \left[\sum_{j=1}^c \int_0^{+\infty} \phi^{(j)}(a) Z_s(dj, da)\right] ds = K \int_0^t e^{-2\lambda_c s} \ll \phi, Z_s \gg ds\,.
$$

Then, taking expectation and using the Fubini theorem, we obtain :

$$
\mathbb{E}\left[\left\langle W^\phi, W^\phi \right\rangle_t\right] \leq K \int_0^t e^{-2\lambda_c s} \mathbb{E}\left[\ll \phi, Z_s \gg\right] ds\,.
$$

Using (III.22), we deduce that

$$
\mathbb{E}\left[\left\langle W^\phi, W^\phi \right\rangle_t\right] \leq K \int_0^t e^{-\lambda_c s} \mathbb{E}\left[\ll \phi, Z_0 \gg\right] ds \leq K \int_0^\infty e^{-\lambda_c s} \mathbb{E}\left[\ll \phi, Z_0 \gg\right] ds < \infty\,.
$$

Then, since W_t^ϕ is a $\mathbf{L}^2$–martingale, we deduce that $(W_t^\phi)^2 - \left\langle W^\phi, W^\phi \right\rangle_t$ is a martingale. Taking expectation and applying Doob's inequality (see Theorem 20 p.11, [151]), we deduce that, for all $T \geq 0$,

$$
\mathbb{E}[\sup_{t \leq T} \left(W_t^\phi\right)^2] \leq K \int_0^\infty e^{-\lambda_c s} \mathbb{E}\left[\ll \phi, Z_0 \gg\right] ds\,,
$$

so that $\mathbb{E}[\sup_{t<\infty} \left(W_t^\phi\right)^2] < \infty$. Since $\left(W_t^\phi\right)^2 \leq \sup_{t<\infty} \left(W_t^\phi\right)^2$, applying the dominated convergence theorem, we obtain the $\mathbf{L}^2$–convergence of W_t^ϕ. □

III.4.4 Asymptotic study of the renewal equations

We now turn to the study of renewal equations associated with the branching process Z. Following [65] (Chap. VI), we introduce generating functions that determine the cell moments. Throughout this subsection, we consider $a \in \mathbb{R}_+ \cup \{+\infty\}$. We recall that $Y_t^{(j,a)} = \langle Z_t, \mathbb{1}_j \mathbb{1}_{\leq a} \rangle$ and $Y_t^a = (Y_t^{(j,a)})_{j \in [\![1,J]\!]}$. For $\mathbf{s} = (s_1, ..., s_J) \in \mathbb{R}^J$ and $\mathbf{j} = (j_1, ..., j_J) \in \mathbb{N}^J$, we use classical vector notation $\mathbf{s}^{\mathbf{j}} = \prod_{i=1}^J s_i^{j_i}$.

Definition III.2. *We define $F^a[\mathbf{s}; t] = (F^{(i,a)}[\mathbf{s}; t])_{i \in [\![1,J]\!]}$ where $F^{(i,a)}$ is the generating function associated with Y_t^a starting with $Z_0 = \delta_{i,0}$:*

$$
F^{(i,a)}[\mathbf{s}; t] := \mathbb{E}[\mathbf{s}^{Y_t^a} | Z_0 = \delta_{i,0}]\,.
$$

We obtain a system of renewal equations for F and $M^a(t) := (\mathbb{E}[Y_t^{(j,a)}|Z_0 = \delta_{i,0}])_{i,j \in [\![1,J]\!]}$.

Lemma III.6 (Renewal equations for F)**.** *For $i \in [\![1,J]\!]$, $F^{(i,a)}$ satisfies*

$$\forall i \in [\![1,J]\!], \quad F^{(i,a)}[\mathbf{s};t] = (s_i \mathbb{1}_{t \le a} + \mathbb{1}_{t>a})(1 - \mathcal{B}_i(t)) + f^{(i)}(F^a[\mathbf{s},.]) * d\mathcal{B}_i(t)$$

where $f^{(i)}$ is given by $f^{(i)}(\mathbf{s}) := p_{2,0}^{(i)} s_i^2 + p_{1,1}^{(i)} s_i s_{i+1} + p_{0,2}^{(i)} s_{i+1}^2$.

Lemma III.7 (Renewal equations for M)**.** *For $(i,j) \in [\![1,J]\!]^2$, $M_{i,j}^a$ satisfies*

$$M_{i,j}^a(t) = \delta_{i,j}(1 - \mathcal{B}_i(t))\mathbb{1}_{t \le a} + 2p_S^{(i)} M_{i,j}^a * d\mathcal{B}_i(t) + 2p_L^{(i)} M_{i+1,j}^a * d\mathcal{B}_i(t) \,. \tag{III.24}$$

The proofs of Lemmas III.6 and III.7 are given in Appendix subsection A.1.2.

Theorem III.7. *Under Hypotheses III.1, III.2, III.4 and Hypotheses/Definitions III.2 and III.3,*

$$\forall i \in [\![1,J]\!], \quad \forall k \in [\![0,J-i]\!], \quad M_{i,i+k}^a(t) \sim \widetilde{M}_{i,i+k}(a)e^{\lambda_{i,i+k}t}, \quad t \to \infty$$

where $\lambda_{i,i+k} = \max\limits_{j \in [\![i,i+k]\!]} \lambda_j$,

$$\widetilde{M}_{i,i}(a) = \frac{\int_0^a (1 - \mathcal{B}_i(t))e^{-\lambda_i t}dt}{2p_S^{(i)} \int_0^\infty t d\mathcal{B}_i(t)e^{-\lambda_i t}dt} \tag{III.25}$$

and for $k \in [\![1,J-i]\!]$,

$$\widetilde{M}_{i,i+k}(a) = \begin{cases} \dfrac{2p_L^{(i)} d\mathcal{B}_i^*(\lambda_{i,i+k})}{1 - 2p_S^{(i)} d\mathcal{B}_i^*(\lambda_{i,i+k})} \widetilde{M}_{i+1,i+k}(a), & \text{if } \lambda_{i,i+k} \ne \lambda_i \,(i) \\[2ex] \dfrac{2p_L^{(i)} d\mathcal{B}_i^*(\lambda_i)}{2p_S^{(i)} \int_0^\infty t d\mathcal{B}_i(t)e^{-\lambda_i t}dt} \displaystyle\int_0^\infty M_{i+1,i+k}^a(t)e^{-\lambda_i t}dt, & \text{if } \lambda_{i,i+k} = \lambda_i \,(ii). \end{cases} \tag{III.26}$$

Proof. Let the mother cell index $i \in [\![1,J]\!]$. As no daughter cell can move upstream to its mother layer, the mean number of cells on layer $j < i$ is null (for all $t \ge 0$ and for $j < i$, $M_{i,j}^a(t) = 0$). We consider the layers downstream the mother one ($j \ge i$) and proceed by recurrence:

$$\mathcal{H}^k : \quad \forall i \in [\![1,J-k]\!], \; M_{i,i+k}^a(t) \sim \widetilde{M}_{i,i+k}(a)e^{\lambda_{i,i+k}t}, \text{ as } t \to \infty\,.$$

We first deal with $\mathcal{H}^0$. We consider the solution of (III.24) for $j = i$:

$$\forall t \in \mathbb{R}_+, \quad M_{i,i}^a(t) = (1 - \mathcal{B}_i(t))\,\mathbb{1}_{t \le a} + 2p_S^{(i)} M_{i,i}^a * d\mathcal{B}_i(t)\,.$$

We recognize a renewal equation as presented in [65](p.161, eq.(1)) for $M_{i,i}$, which is similar to a single type age-dependent process. The main results on renewal equations are recalled in Appendix subsection A.1.3. Here, the mean number of children is $m = 2p_S^{(i)} > 0$ and the lifetime distribution is $\mathcal{B}_i$. From Hypothesis III.2, we have

$$\int_0^\infty (1 - \mathcal{B}_i(t))\,\mathbb{1}_{t \le a}e^{-\lambda_i t}dt \le \frac{1}{\bar{b}_i} \int_0^\infty \mathbb{1}_{t \le a}d\mathcal{B}_i(t)e^{-\lambda_i t}dt \le \frac{1}{\bar{b}_i} \int_0^\infty d\mathcal{B}_i(t)e^{-\lambda_i t}dt < \infty$$

according to Hypothesis/Definition III.1. Thus, $t \mapsto \mathbb{1}_{t \leq a}\left(1 - \mathcal{B}_i(t)\right)e^{-\lambda_i t}$ is in $\mathbf{L}^1(\mathbb{R}_+)$. Using Hypothesis/Definition III.1 and Hypothesis III.4, we apply Corollary III.1 and Lemma A.3 in the Appendix subsection A.1.3 (see lemma 2 of [65], p.161) and obtain

$$M_{i,i}^a(t) \sim \widetilde{M}_{i,i}(a)e^{\lambda_i t}, \text{ as } t \to \infty, \text{ where } \widetilde{M}_{i,i}(a) = \frac{\int_0^a (1 - \mathcal{B}_i(t))e^{-\lambda_i t}dt}{2p_S^{(i)}\int_0^\infty t d\mathcal{B}_i(t)e^{-\lambda_i t}dt}.$$

Hence, $\mathcal{H}^0$ is verified. We then suppose that $\mathcal{H}^{k-1}$ is true for a given rank $k - 1 \geq 0$ and consider the next rank k. According to (III.24), $M_{i,i+k}^a$ is a solution of:

$$M_{i,i+k}^a(t) = 2p_S^{(i)}M_{i,i+k}^a * d\mathcal{B}_i(t) + 2p_L^{(i)}M_{i+1,i+k}^a * d\mathcal{B}_i(t). \tag{III.27}$$

We distinguish two cases : $\lambda_{i,i+k} \neq \lambda_i$ and $\lambda_{i,i+k} = \lambda_i$. We first consider $\lambda_{i,i+k} = \lambda_i$ and show that $f(t) = M_{i+1,i+k}^a * d\mathcal{B}_i(t)e^{-\lambda_i t}$ belongs to $\mathbf{L}^1(\mathbb{R}_+)$. Let $R > 0$. Using the Fubini theorem, we deduce that:

$$\int_0^R f(t)dt = \int_0^R \left[\int_u^R e^{-\lambda_i(t-u)}M_{i+1,i+k}^a(t-u)dt\right]e^{-\lambda_i u}d\mathcal{B}_i(u)du.$$

Applying a change of variable and using that $M_{i+1,i+k}^a(t) \geq 0$ for all $t \geq 0$, we have

$$\int_u^R e^{-\lambda_i(t-u)}M_{i+1,i+k}^a(t-u)dt \leq \int_0^R e^{-\lambda_i t}M_{i+1,i+k}^a(t)dt.$$

According to $\mathcal{H}^k$, we know that $M_{i+1,i+k}^a(t) \sim \widetilde{M}_{i+1,i+k}(a)e^{\lambda_{i+1,i+k}t}$ as $t \to \infty$. Then,

$$\int_0^R e^{-\lambda_i t}M_{i+1,i+k}^a(t)dt = \int_0^R e^{-\lambda_{i+1,i+k}t}M_{i+1,i+k}^a(t)e^{-(\lambda_i-\lambda_{i+1,i+k})t}dt \leq K\int_0^R e^{-(\lambda_i-\lambda_{i+1,i+k})t}dt \quad < \infty$$

when $R \to \infty$, as $\lambda_i = \lambda_{i,i+k} > \lambda_{i+1,i+k}$. Moreover, $\int_0^R e^{-\lambda_i u}d\mathcal{B}_i(u)du \leq d\mathcal{B}_i^*(\lambda_i) < \infty$ according to Hypothesis/Definition III.2. Finally, we obtain an estimate for $\int_0^R f(t)dt$ that does not depend on R. So, f is integrable. We can apply Lemma A.3 and deduce $M_{i,i+k}^a(t) \sim \widetilde{M}_{i,i+k}(a)e^{\lambda_{i,i+k}t}$, as $t \to \infty$, with $\widetilde{M}_{i,i+k}(a)$ given in (III.26)(ii).
We now consider the case $\lambda_{i,i+k} \neq \lambda_i$ and introduce the following notations :

$$\widehat{M}_{i,i+k}^a(t) = M_{i,i+k}^a(t)e^{-\lambda_{i,i+k}t}, \quad \widehat{d\mathcal{B}_i}(t) = \frac{d\mathcal{B}_i(t)}{d\mathcal{B}_i^*(\lambda_{i,i+k})}e^{-\lambda_{i,i+k}t}.$$

In this case, $\lambda_{i,i+k} > \lambda_i$, so that $2p_S^{(i)}d\mathcal{B}_i^*(\lambda_{i,i+k}) < 2p_S^{(i)}d\mathcal{B}_i^*(\lambda_i) = 1$. We want to apply Lemma A.4 (see lemma 4 of [65], p.163). We rescale (III.27) by $e^{-\lambda_{i,i+k}t}$ and obtain the following renewal equation for $\widehat{M}_{i,i+1}^a$:

$$\widehat{M}_{i,i+k}^a(t) = 2p_S^{(i)}d\mathcal{B}_i^*(\lambda_{i,i+k})\widehat{M}_{i,i+k}^a * \widehat{d\mathcal{B}_i}(t) + 2p_L^{(i)}M_{i+1,i+k}^a * d\mathcal{B}_i(t)e^{-\lambda_{i,i+k}t}.$$

We compute the limit of $f(t) = M_{i+1,i+k}^a * d\mathcal{B}_i(t)e^{-\lambda_{i,i+k}t}$:

$$f(t) = \int_0^\infty \mathbb{1}_{[0,t]}(u)M_{i+1,i+k}^a(t-u)e^{-\lambda_{i,i+k}(t-u)}e^{-\lambda_{i,i+k}u}d\mathcal{B}_i(u)du.$$

According to $\mathcal{H}^{k-1}$, $M_{i+1,i+k}^a(t) \sim e^{-\lambda_{i+1,i+k}t}\widetilde{M}_{i+1,i+k}(a)$. As $\lambda_{i,i+k} \neq \lambda_i$, we have $\lambda_{i,i+k} = \lambda_{i+1,i+k}$. Hence, $M_{i+1,i+k}^a(t)e^{-\lambda_{i,i+k}t}$ is dominated by a constant K such that $\int_0^\infty Ke^{-\lambda_{i,i+k}u}d\mathcal{B}_i(u)du <$

∞. We apply the Lebesgue dominated convergence theorem and obtain $\lim_{t\to\infty} f(t) = \widetilde{M}_{i+1,i+k}(a)d\mathcal{B}_i^*(\lambda_{i,i+k})$. Applying Lemma A.4, we obtain that:

$$\lim_{t\to\infty}\widehat{M}_{i,i+k}^a(t) = \frac{2p_L^{(i)}\widetilde{M}_{i+1,i+k}(a)d\mathcal{B}_i^*(\lambda_{i,i+k})}{1 - 2p_S^{(i)}d\mathcal{B}_i^*(\lambda_{i,i+k})} = \widetilde{M}_{i,i+k}(a),$$

and the recurrence is proved. □

We have now all the elements to prove Theorem III.4.

Proof of Theorem III.4. According to Theorem III.7, we have

$$\forall j \in [\![1,J]\!], \quad m_j^a(t) \sim \widetilde{M}_{1,j}(a)e^{\lambda_{1,j}t} \quad \text{as } t \to \infty. \tag{III.28}$$

When $j < c$, we deduce directly from (III.28) that $\tilde{m}_j(a) = 0$. We then consider the leading layer $j = c$. For $k \in [\![1, c-1]\!]$, $\lambda_{k,c} \neq \lambda_k$ so $\widetilde{M}_{k,c}(a)$ is related to $\widetilde{M}_{k+1,c}(a)$ by (III.26)(i). Thus, we obtain

$$\tilde{m}_c(a) = \prod_{m=1}^{c-1} \frac{2p_L^{(m)}d\mathcal{B}_m^*(\lambda_c)}{1 - 2p_S^{(m)}(d\mathcal{B}_m^*)(\lambda_c)}\widetilde{M}_{c,c}(a).$$

$\widetilde{M}_{c,c}(a)$ is given by (III.25) and we deduce $\tilde{m}_c(a)$. We turn to the layers $j > c$. For $k \in [\![1, c-1]\!]$, we have $\lambda_c = \lambda_{k,j} \neq \lambda_k$. We obtain from (III.26)(i)

$$\tilde{m}_j(a) = \prod_{m=1}^{c-1} \frac{2p_L^{(m)}d\mathcal{B}_m^*(\lambda_c)}{1 - 2p_S^{(m)}(d\mathcal{B}_m^*)(\lambda_c)}\widetilde{M}_{c,j}(a). \tag{III.29}$$

Then, as $\lambda_c = \lambda_{c,j}$, we use (III.26)(ii) and obtain:

$$\widetilde{M}_{c,j}(a) = \frac{2p_L^{(c)}d\mathcal{B}_c^*(\lambda_c)}{2p_S^{(c)}\int_0^\infty te^{-\lambda_c t}d\mathcal{B}_c(t)dt}\int_0^\infty M_{c+1,j}^a(t)e^{-\lambda_c t}dt. \tag{III.30}$$

Then, we apply the Laplace transform to (III.24) for $\alpha = \lambda_c$. Theorem III.7 and the fact that $\lambda_c = \lambda_{c,j}$ guarantee that we can apply the Laplace transform to (III.24) (see details in Appendix subsection A.1.3). We obtain

$$\int_0^\infty M_{c+1,j}^a(t)e^{-\lambda_c t}dt = \prod_{k=c+1}^{j-1}\frac{2p_L^{(k)}d\mathcal{B}_k^*(\lambda_c)}{1 - 2p_S^{(k)}d\mathcal{B}_k^*(\lambda_c)} \times \frac{\int_0^a \hat{\rho}^{(j)}(s)ds}{(1 - 2p_S^{(j)}d\mathcal{B}_j^*(\lambda_c)) \times \hat{\rho}^{(j)}(0)}. \tag{III.31}$$

Combining (III.29), (III.30) and (III.31) and the value of $\hat{\rho}^{(j)}(0)$ given in (III.8), we obtain $\tilde{m}_j(a)$. □

We also study the asymptotic behavior of the second moment in Appendix subsection A.1.3 (see Theorem A.1).

Remark III.3. *These results can be extended in a case when the mother cell is not necessary of age 0 (for the one layer case, see [65], p.153).*

Remark III.4. *Using the same procedure as in Theorem III.7, we can obtain a better estimate for the convergence of the deterministic solution ρ than that in Theorem III.2. Indeed, we can consider the study of $h(t,x) = e^{-\lambda_{1,j}t}\rho(t,x) - \eta\hat{\rho}_{1,j}(x)$ where $\hat{\rho}_{1,j}$ is the eigenvector of the subsystem composed of the jth first layer, and find the proper function $\phi_{1,j}$.*

III.4.5   Numerical illustration

We perform a numerical illustration with age independent division rates (which satisfy Hypothesis III.2). Figure III.4a illustrates the exponential growth of the number of cells, either for the original solution of the model (III.4) (left panel) or the renormalized solution (right panel), checking the results given in Theorems III.4 and A.1. Figure III.4b instantiates the effect of the parameters b_1 and $p_S^{(1)}$ on the leading layer (left panel) and the asymptotic proportion of cells (right panel). Note that the layer with the highest number of cells is not necessary the leading one. As can be seen in Figure III.5, the renormalized solutions of the SDE (III.4) and PDE (III.5) match the stable age distribution $\hat{\rho}$ (see Theorems III.1 and III.4). Asymptotically, the age distribution decreases with age, which corresponds to a proliferating pool of young cells, and is consistent with the fact that $\hat{\rho}^{(j)}$ is proportional to $e^{-\lambda_c a}\mathbb{P}[\tau^{(j)} > a]$. The convergence speeds differ between layers (here, the leading layer is the first one and the stable state of each layer is reached sequentially), corroborating the inequality given in Theorem III.2.

III.5 Parameter calibration

Throughout this part, we will work under Hypotheses III.1, III.5 and III.6. As a consequence, the intrinsic growth rate per layer can be computed easily:

$$\lambda_j = (2p_S^{(j)} - 1)b_j \in (-b_j, b_j) \quad \text{when } j < J.$$

III.5.1   Structural identifiability

We prove here the structural identifiability of our system following [98]. We start with a technical lemma.

Lemma III.8. *Let M be the solution of* (III.7)*. For any linear application $U : \mathbb{R}^J \to \mathbb{R}^J$, we have* $[\forall t, M(t) \in \ker(U)] \Rightarrow [U = 0]$.

Proof. Ad absurdum, if $U \neq 0$ and $M(t) \in \ker(U)$, for all t, then there exists a nonzero vector $u := (u_1, ..., u_J)$ such that for all t, $u^T M(t) = 0$. This last relation, evaluated at $t = 0$ and thanks to the initial condition of (III.7), implies $u_1 = 0$. Then, derivating M, solution of (III.7), we obtain
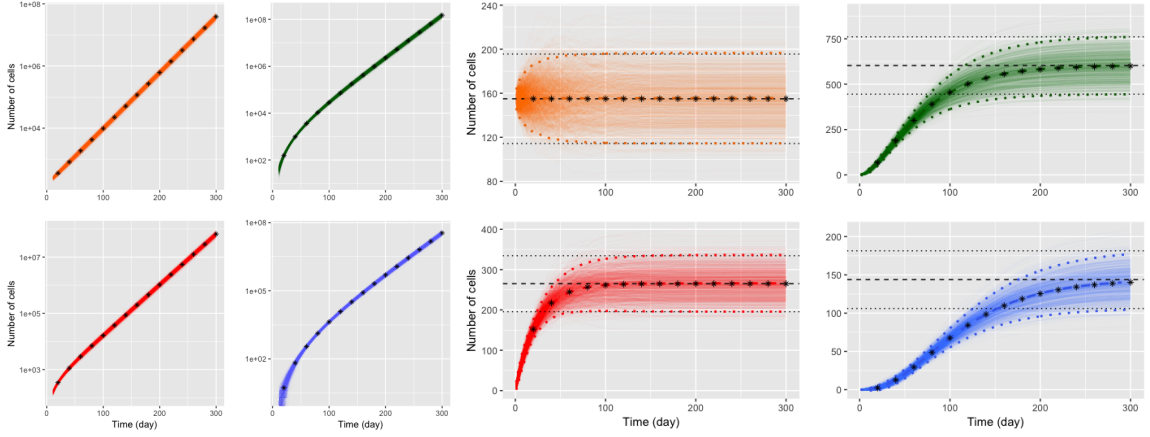
$$\frac{d}{dt}\sum_{j=2}^J u_j M^{(j)}(t) = 0 \quad \Rightarrow \quad \sum_{j=2}^J u_j[(b_{j-1} - \lambda_{j-1})M^{(j-1)}(t) + \lambda_j M^{(j)}(t)] = 0.$$

Again, at $t = 0$, we obtain $u_2(b_1 - \lambda_1) = 0$. Because $\lambda_1 \neq b_1$, $u_2 = 0$. Iteratively,
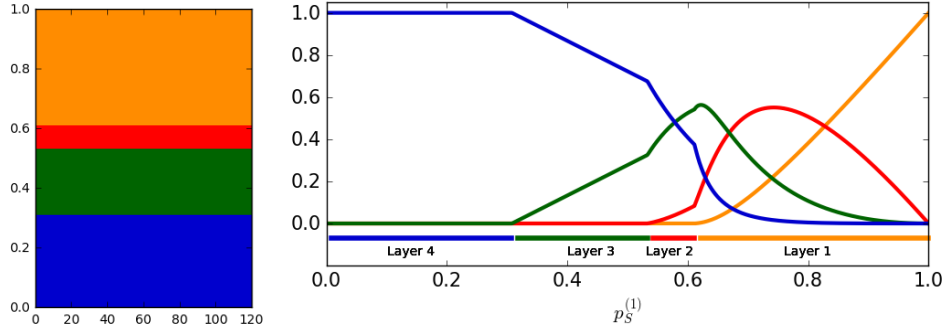
$$\forall j \in [\![2, J]\!], \quad u_j \prod_{k=1}^{j-1}(b_{k-1} - \lambda_{k-1}) = 0 \quad \Rightarrow u_j = 0.$$

We obtain a contradiction. $\square$

We can now prove Theorem III.5.

(a) *Exponential growth and asymptotic behavior*

(b) *Leading layer index and asymptotic proportion of cells*

Fig. III.4 **Exponential growth and asymptotic moments. Figure III.4a**: *Outputs of 1000 simulations of the SDE (III.4) according to Algorithm 3 with $p_S^{(j)}$, b_j given in Figure III.1b, $p_{1,1}^{(j)} = 0$ and $Z_0 = 155\delta_{1,0}$.* **Left panel:** *the solid color lines correspond to the outputs of the stochastic simulations while the black stars correspond to the numerical solutions of the ODE (III.7) with the initial number of cells on the first layer $N = 155$ (orange: Layer 1, red: Layer 2, green: Layer 3, blue: Layer 4).* **Right panel:** *the color solid lines correspond to the renormalization of the outputs of the stochastic simulations by $e^{-\lambda_c t}$. The black stars are the numerical solutions of the ODE (III.7). The color and black dashed lines correspond to the empirical means of the simulations and the analytical asymptotic means ($155\tilde{m}_j(\infty)$, Theorem III.4), respectively. The color and black dotted lines represent the empirical and analytical asymptotic 95% confidence intervals ($1.96\sqrt{v_j(\infty)}$, Corollary A.1), respectively.* **Figure III.4b**: *Leading layer index as a function of b_1 and $p_S^{(1)}$ (left panel) and proportion of cells per layer in asymptotic regime with respect to $p_S^{(1)}$ (right panel). In both panels, b satisfies (c)) and $p_S^{(j)} = -15 * p_L^{(1)} * (j-1)^2 - 110 * p_L^{(1)} * (j-1) + p_S^{(1)}$.*

Proof of Theorem III.5. According to [98], the system (III.7) is **P**-identifiable if, for two sets
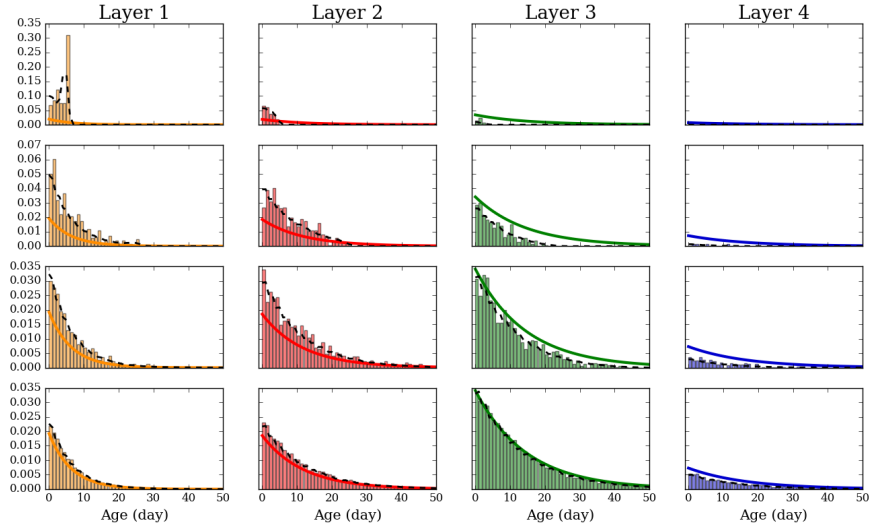
Fig. III.5 **Stable age distribution per layer.** *Age distribution at different times of one simulation of the SDE (III.4) and of the PDE (III.5) using the algorithms described in Appendix a) and b), respectively. We use the same parameters as in Figure III.4. From top to bottom: t = 5, 25, 50 and 100 days. The color bars represent the normalized stochastic distributions. The black dashed lines correspond to the normalized PDE distributions, the color solid lines to the stable age distributions $\hat{\rho}^{(j)}$, $j \in [\![1,4]\!]$. The details of the normalization of each lines are provided in A.1.4.*

of parameters $\mathbf{P}$ and $\widetilde{\mathbf{P}}$, $M(t; \mathbf{P}) = M(t; \widetilde{\mathbf{P}})$ implies that $\mathbf{P} = \widetilde{\mathbf{P}}$.

$$\forall t \geq 0, M(t; \mathbf{P}) = M(t; \widetilde{\mathbf{P}}) \Rightarrow \qquad\qquad \frac{d}{dt} M(t; \mathbf{P}) = \frac{d}{dt} M(t; \widetilde{\mathbf{P}})$$
$$\Rightarrow \qquad A_{\mathbf{P}} M(t; \mathbf{P}) = A_{\widetilde{\mathbf{P}}} M(t; \widetilde{\mathbf{P}}) = A_{\widetilde{\mathbf{P}}} M(t; \mathbf{P})$$
$$\Rightarrow \qquad\qquad\qquad (A_{\mathbf{P}} - A_{\widetilde{\mathbf{P}}}) M(t; \mathbf{P}) = 0$$

So, $M(t; \mathbf{P}) \in \ker(A_{\mathbf{P}} - A_{\widetilde{\mathbf{P}}})$ and, from Lemma III.8, we deduce that $A_{\mathbf{P}} = A_{\widetilde{\mathbf{P}}}$. Thus,

$$\begin{cases} (2p_S^{(j)} - 1)b_j = (2\widetilde{p}_S^{(j)} - 1)\widetilde{b}_j, & \forall j \in [\![1, J]\!], \\ 2p_L^{(j)} b_j = 2\widetilde{p}_L^{(j)} \widetilde{b}_j, & \forall j \in [\![1, J-1]\!]. \end{cases}$$

Using that $p_L^{(j)} = 1 - p_S^{(j)}$ and Hypothesis III.1, we deduce $\mathbf{P} = \widetilde{\mathbf{P}}$.   □

III.5.2 Biological application

We now consider the application to the development of ovarian follicles.

a)   Biological background

The ovarian follicles are the basic anatomical and functional units of the ovaries. Structurally, an ovarian follicle is composed of a germ cell, named oocyte, surrounded by somatic cells (see Figure III.6). In the first stages of their development, ovarian follicles grow in a compact

way, due to the proliferation of somatic cells and their organization into successive concentric layers starting from one layer at growth initiation up to four layers.
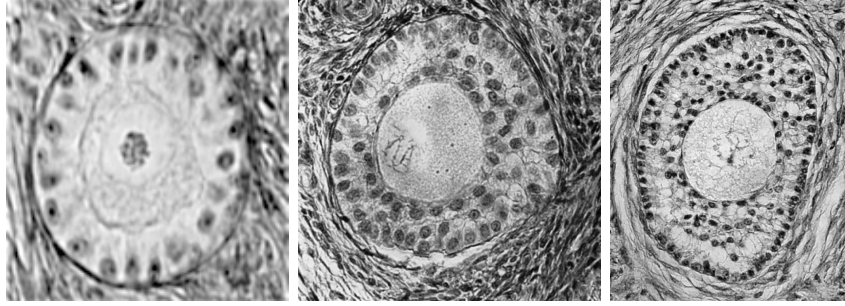

Fig. III.6 ***Histological sections of ovarian follicles in the compact growth phase.*** *Left panel: one-layer follicle, center panel: three-layer follicle, right panel: four-layer follicle. Courtesy of Danielle Monniaux.*

b)   Dataset description

We made use of a dataset providing us with morphological information at different development stages (oocyte and follicle diameter, total number of cells), and acquired from ex vivo measurements in sheep fetus [116]. In addition, from [121, 122], we can infer the transit times between these stages: it takes 20 days to go from one to three layers and 15 days from three to four layers. Hence (see Table III.1a), the dataset consists of the total numbers of somatic cells at three time points.

We next take advantage of the spheroidal geometry and compact structure of ovarian follicles to obtain the number of somatic cells in each layer. Spherical cells are distributed around a spherical oocyte by filling identical width layers one after another, starting from the closest layer to the oocyte. Knowing the oocyte and somatic cell diameter (d_O and d_s, respectively) and, the total number of cells N^{exp}, we compute the number of cells on the jth layer according to the ratio between its volume V^j and the volume of a somatic cell V^s:

INITIALIZATION: $j \leftarrow 1, V^s \leftarrow \frac{\pi d_s^3}{6}, N \leftarrow N^{exp}$

While $N > 0$:

$V^j \leftarrow \frac{\pi}{6} \left[(d_O + 2 * j * d_s)^3 - (d_O + 2 * (j-1) * d_s)^3 \right]$

$N_j \leftarrow \min(\frac{V^j}{V^s}, N), N \leftarrow N - N_j, j \leftarrow j + 1$

$J \leftarrow j - 1$

The corresponding dataset is shown in the four panels of Figure III.3.

c)   Parameter estimation

Before performing parameter estimation, we take into account additional biological specifications on the division rates. The oocyte produces growth factors whose diffusion leads to a decreasing gradient of proliferating chemical signals along the concentric layers, which results to the recurrence law (c)) similar as that initially proposed in [1]. Considering a regression

	$t = 0$	$t = 20$	$t = 35$
Data points (62)	34	10	18
Total cell number	113.89 ± 57.76	885.75 ± 380.89	2241.75 ± 786.26
Oocyte diameter (μm)	49.31 ± 8.15	75.94 ± 10.89	88.08 ± 7.43
Follicle diameter (μm)	71.68 ± 13.36	141.59 ± 17.11	195.36 ± 23.95

(a) **Summary of the dataset**

Layer j	$p_S^{(j)}$	b_j	λ_j
1	0.6806	0.1146	0.0414
2	0.4837	0.0435	-0.0014
3	0.9025	0.0269	0.02165
4	1	0.0194	0.0194

(b) **Estimated values of the parameters.**

Table III.1 – **Experimental dataset and estimated values of the parameters.** Table III.1b. The estimated value of α and the initial number of cells are $\alpha = 1.633$ and $N \approx 155$, respectively. For $j \geq 2$, the b_j parameter values (in blue) were computed using formula (c)). The λ_j values were computed using formula (III.5). The 95%-confidence intervals are $b_1 \in [0.0760; 0.1528]$, $\alpha \in [0.0231; 5.685]$, $N \in [126.4; 185.4]$, $p_S^{(1)} \in [0.6394; 0.7643]$, $p_S^{(2)} \in (0; 0.7914]$ and $p_S^{(3)} \in [0.6675; 0.9739]$.

model with an additive Gaussian noise, we estimate the model parameters to fit the changes in cell numbers in each layer (see Appendix subsection A.1.5 for details). The estimated parameters are provided in Table III.1b and the fitting curves are shown in Figure III.3. We compute the profile likelihood estimates [138] and observe that all parameters are practically identifiable except $p_S^{(2)}$ (Figure A.1a). In contrast, when we perform the same estimation procedure on the total cell numbers, most of the parameters are not practicality identifiable (dataset in Table III.1a, see detailed explanations in Appendix subsection A.1.5).

III.6 Conclusion

In this work, we have analyzed a multitype age-dependent model for cell populations subject to unidirectional motion, in both a stochastic and deterministic framework. Despite the nonapplicability of either the Perron–Frobenius or Krein–Rutman theorem, we have taken advantage of the asymmetric transitions between different types to characterize long time behavior as an exponential Malthus growth, and obtain explicit analytical formulas for the asymptotic cell number moments and stable age distribution. We have illustrated our results numerically, and studied the influence of the parameters on the asymptotic proportion of cells, Malthus parameter and stable age distribution. We have applied our results to a morphodynamic process occurring during the development of ovarian follicles. The fitting of the model outputs to biological experimental data has enabled us to represent the compact phase of follicle growth. Thanks to the flexibility allowed by the expression of morphodynamic laws in the model, we intend to consider other non-compact growth stages.

III.7 Complements on the dataset treatment (unpublished)

In this section, we give complements on the dataset treatment presented in subsection III.5.2 for which we need the number of cell per layer, which is not provided as such in the dataset.

We use the dataset composed of the three categories: "t=0", "t=20" and "t=35" (presented in section I.2.2), for which we have the total cell and layer number, and the oocyte and follicle diameter. Reconstructing the cell distribution into the different layers amounts to distributing objects of a given volume in a succession of nested hollow balls representing the layers. To reconstruct this information, we first recover the mean cell volume from the available information (oocyte and follicle diameter, and total cell number). To estimate the layer thickness, we model the cell volume considering two idealized, yet realistic, options: a sphere or a cube. To select among these two options, we made use of the observed number of layers.

Before starting, we first made the following assumptions:

i) all the somatic cells are incompressible and have the same volume V_S. Thus, all cell volume changes, such those induced by mitosis, are neglected.

ii) in the same way as in [1], the follicle and oocyte shapes can both be approximated by balls of diameter d_f and d_O, respectively.

iii) the cells are distributed compactly around the oocyte (no gap).

Applying assumptions ii) and iii), the somatic cell volume is deduced for each follicle $i \in [\![1, 101]\!]$ from the follicle and oocyte diameter and the total somatic cell number N_i by

$$(V_S)_i = \frac{4}{3}\pi \frac{(\frac{d_f}{2})_i^3 - (\frac{d_O}{2})_i^3}{N_i}. \tag{III.32}$$

We observe in Figure III.7 (right-panel) a large variability in the somatic cell volume distribution: it varies between 950 and 2,500 μm^3 and increases with the oocyte diameter. Due to this high variability, we decide to change course and model the volume of a somatic cell considering different realistic cell geometries.
Using the definition of an elementary volume, we first write the average somatic cell volume $(V_S)_i$ for each follicle of our dataset $i \in [\![1, 101]\!]$,

$$(V_S)_i = \int_0^{(d_S)_i} \int_0^{(\delta\theta)_i} \int_0^{(\delta\phi)_i} r^2 \sin(\theta) dr d\theta d\phi = \sigma_i(d_S)_i^3,$$

where $(\delta\theta)_i$ and $(\delta\phi)_i$ are constants that characterize the volume of a cell i. We merge these two constants into a single one: the constant σ_i, corresponding to the volume type constant (sphere or cube). We thus obtain an analytic formula linking the somatic cell volume $(V_S)_i$ to the layer tickness d_S. Note that we now only need to infer the layer tickness d_S and the

constant σ_i.

To that end, we consider two different options for the volume constant σ:

- 3D method (sphere): following [1], we suppose that a somatic cell is a sphere. Thus, we have

$$\frac{d_S}{2} = \sqrt[3]{\frac{3}{4\pi}V_S}.$$

(III.33)

- 3D method (cube): we suppose that a somatic cell is a cube. Thus, we have

$$d_S = \sqrt[3]{V_S}.$$

(III.34)

To choose between these two approaches, we compare the thickness d_S to that obtained with a 1D approach using the number of observed layers N_{layer}:

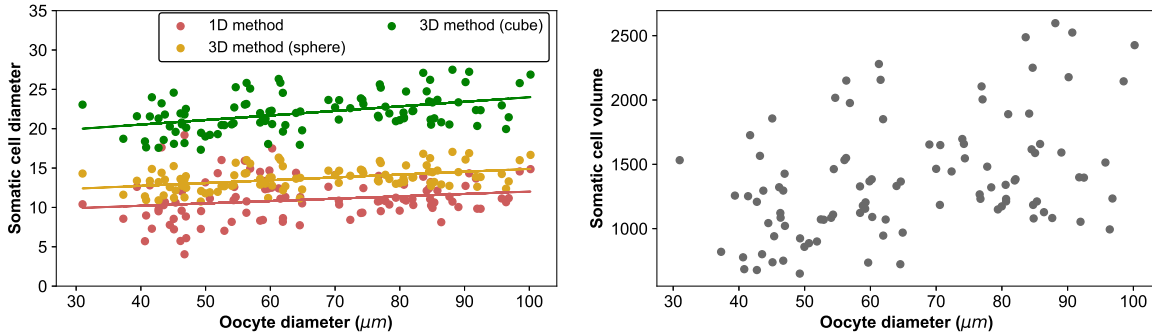- 1D method:

$$d_S = \frac{d_f - d_O}{2N_{layer}}.$$

(III.35)

Fig. III.7 **_Estimated somatic cell diameter and volume_**_. Right-panel: we apply Formula (III.32) and compute the somatic cell volume (in μm^3) for each follicle of our dataset. Left-panel: for each follicle in our dataset, we apply Formulas (III.33), (III.34) and (III.35) and represent the result with respect to the oocyte diameter (in μm). We then make a linear regression for each method (1D, sphere 3D and cube 3D) and obtain: 1D method: $\bar{d}_G = 9.11 \pm 1.00$ μm, $\alpha = 0.032 \pm 0.02$; 3D method (sphere): $\bar{d}_G = 11.30 \pm 1.00$ μm, $\alpha = 0.035 \pm 0.008$; 3D method (cube): $\bar{d}_G = 18.21 \pm 0.82$ μm, $\alpha = 0.058 \pm 0.012$._

We apply those three methods and show the results in Figure III.7 (left-panel). For the three methods, a small increase in the somatic cell diameter with respect to the oocyte is observed and is mostly due to the emergence of some gaps (antrum formation). The 1D method and the 3D method (sphere) lead to comparable results: the somatic cell diameter evolves between 9 and 11 μm, while this number evolves between 20 and 25 μm for the 3D method (cube). Among the two 3D methods, the sphere hypothesis gives more comparable results with our control method (1D) than the cube hypothesis, we thus select the 3D method (sphere). We turn now to the calibration of the somatic cell diameter d_S. Considering several values for d_S, cells were distributed among layers using the algorithm presented in subsection III.5.2
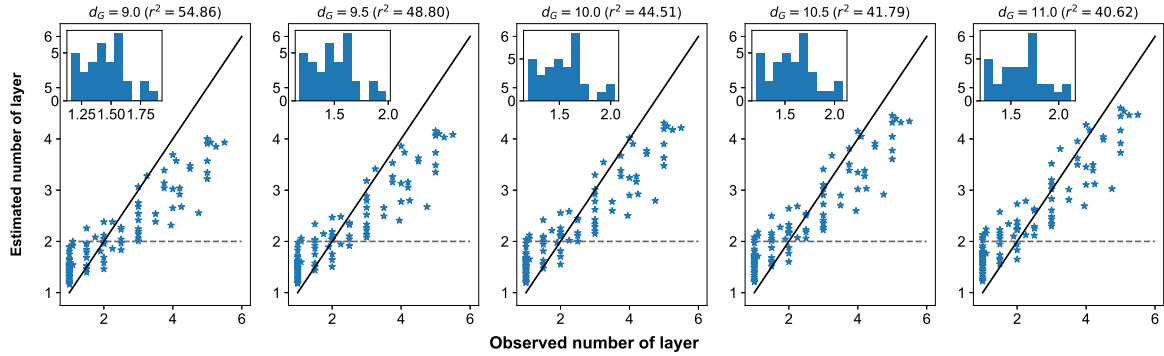
Fig. III.8 ***Assessment of the somatic cell diameter*** d_S***.*** *Using the algorithm presented in subsection III.5.2, we distribute cells among layers for each follicle $i \in [\![1, 101]\!]$ taking different values for d_S (9.0, 9.5, 10.0, 10.5 and 11.0). We then compute the number of layers obtained. In each case, we compute the least square error r^2 obtained between the estimated number of layers and the observed one. The horizontal dashed line corresponds to the threshold of two layers while the solid black line is the median line.*

for each follicle. From this, we deduce the estimated number of layers that we compare to the observed ones (least square error, see details in Figure III.8). We choose the d_S with the lowest r^2-values such that the follicles with less than 2 layers observed have less than 2 layers with our estimation procedure. We thus select $d_S = 9.5 \mu m$.

The cell distribution into the different layers is deduced from the layer thickness d_S and the somatic cell volume V_S: cells are distributed around a spherical oocyte by filling d_S–thick layers one after another, starting from the layer closest to the oocyte (see algorithm proposed in subsection III.5.2).

Chapter IV

Modeling the compact growth phase: complementary works

This chapter is dedicated to reflections that followed the work presented in the previous chapter (and published in [33]). We present two other approaches based on spatial models that could represent the coupled dynamics between the oocyte and the somatic cells.

IV.1 Back on the [CMMS] model

We first come back to the [CMMS] model (see subsection III.1.1) where the spatial cell position is represented by volume elements $(\mathcal{L}_t^{(i,j,k)})$. In this model, cells may be followed one by one and have a volume. However, the analysis of the CMMS model is complex due to its non-linearity. A first common practice consists in changing the scale that here can be either the population or the cell size scale.

This question has been tackled recently, in [3], in the course of this thesis, where the author investigates the large population and small cell size limits of the [CMMS] model. In addition, the existence of solutions of the [CMMS] model was also shown. We present below the results regarding the change of scales.

We recall that in the [CMMS] model, the locations of cells are given by their spherical coordinates $(r(t), \theta, \phi)$ with $r(t) \geqslant r_O(t)$ (the oocyte radius at time t). Note that the spatial component, r, is time-dependent here. To avoid coping with a moving state space, the author chooses an equivalent formalism: the cell location in the simplified model is (r, θ, ϕ) that corresponds to $(r - 1 + r_O(t), \theta, \phi)$ in space. The location of cells then belongs to the set $\mathcal{S} = \mathbb{R}^3 / B(0, 1)$, where $B(0, 1) = \{(r, \theta, \phi) : r < 1\}$.

Let ε be the diameter of a somatic cell. The i-th layer is then defined by

$$\mathcal{L}_i^\varepsilon = \{(r, \theta, \phi) \in \mathcal{S} : r \in [1 + (i-1)\varepsilon, 1 + i\varepsilon[\}.$$

In the same way as the [CMMS] model, the subdomains $\mathcal{L}_{i,j,k}^\varepsilon$ are defined as

$$\mathcal{L}_{i,j,k}^\varepsilon = \{(r, \theta, \phi) \in \mathcal{S} : r \in [1 + (i-1)\varepsilon, 1 + i\varepsilon[,$$
$$\theta \in \left[\pi \frac{j-1}{N}, \pi \frac{j}{N}\right[, \phi \in \left[-\pi + 2\frac{k-1}{N}\pi, -\pi + 2\frac{k}{N}\pi\right[\},$$

where $N \in \mathbb{N}^*$. For a given scaling population size $M \in \mathbb{N}^*$ and a cell size $\varepsilon > 0$, the whole population is represented by a point measure Z_t, $t \geq 0$,

$$Z_t^{M,\varepsilon}(da, dp) = \frac{1}{M} \sum_{n=1}^{N_t^{M,\varepsilon}} \delta_{(a_n^{M,\varepsilon}, x_n^{M,\varepsilon})} \in \mathcal{M}_P(\mathbb{R}_+ \times \mathcal{S}),$$

where $N_t^{M,\varepsilon}$ is the total cell number at time t. Each cell n is defined by its age $a_n^{M,\varepsilon} \in \mathbb{R}_+$ and spatial position $x_n^{M,\varepsilon} \in \mathcal{S}$ (and not an integer triplet (i, j, k) corresponding to the subdomain $\mathcal{L}_{i,j,k}^{\varepsilon}$).

In [3], the author (P. Michel) considers the limit of $(Z_t^{M,\varepsilon}(da, dp))_{\varepsilon, M}$ first when M goes to infinity and ε is fixed. From this law of large number, he obtains a PDE for all ε (weak limit). Then, taking ε goes to 0, he shows that the limit of this PDE is well-defined and is a weak solution of the following nonlinear partial differential equation:

$$\begin{cases} (\partial_t + \partial_a)\rho + \mathrm{div}\left[C\rho R\nabla(1 - R)\right] = 0, \ t > 0, \ a > 0, \ r > 1, \\ \rho|_{a=0} = 2\int_0^{+\infty} B(a, p)\rho(t, a, p)da, \\ \rho|_{t=0} = \rho_0, \\ \rho|_{r=1} = 1, \end{cases} \tag{IV.1}$$

with $C > 0$, and function $R = R\left(\int_{\mathbb{R}_+} \rho(t, a, p)da \frac{Vol_G(3r^2+6r+3)}{3r^2+6rr_O(t)+3r_O(t)^2}\right)$ is the cell displacement rate. The density function $\rho = \rho(t, a, p)$ represents the density of cells of age a and spatial position $p = (r, \theta, \phi) \in \mathcal{S}$ at time $t \geq 0$. The Dirichlet nonlocal boundary condition $\rho|_{a=0}$ represents the division events while the Dirichlet boundary condition $\rho|_{r=1}$ represents the fact that there is always cells on the boundary of the domain. Remark that in this model, the cell loss due to division does not appear directly on PDE (IV.1) but seems to be included in the divergence term (cell displacements).
The oocyte diameter verifies

$$r_O'(t) = (r_O(t))^\alpha \int_{\mathbb{R}_+ \times \mathcal{S}} \kappa(r)\rho(t, a, p)r^2 sin(\theta)da\, dr\, d\theta\, d\phi, \quad r_O(0) = r_0,$$

where $\kappa \in C_b^0(\mathbb{R}_+, \mathbb{R}_+)$ represents the growth factors secreted by the somatic cells.

One of the author's interesting conclusions is that there must be a balance between the renormalization of the number of cells M and the size of a cell ε. If the cell size is fixed, then the whole space is filled by cells when M goes to infinity while if the cells are too small and there is not enough of them (M too low), a concentrated mass can be observed on the boundary of the oocyte. However, according to the author, it is not completely clear that $(Z_t^{M,\varepsilon}(da, dp))_{\varepsilon, M}$ converges for all sequences of $(\varepsilon_k, M_k) \to (0, \infty)$, and it is still an open-question.

Inspiring from PDE (IV.1), which is a Keller-Segel type, we turn now to models built on the same formalism in the next subsection. We thus consider models where the cell volume is very small, such that a continuous model can be used.

IV.2 Mechanical spatial-structured model

At the follicle level, the cells form a cluster that can be assimilated to a growing fluid. This more or less incompressible fluid is maintained in a spherical shape by external forces acting on the outer wall of the follicle. It is also subjected to internal forces from the spherical oocyte: the oocyte exerts a radial pushing force throughout its growth. The dynamics of a follicle in the compact growth phase can be represented by two growing nested balls of same center: the inner ball is the oocyte while the hollow ball represents the somatic cells, which can be seen as an expanding fluid subjected to pressure forces from both inside and outside. We present this model in Figure IV.1. The oocyte is represented by the domain $\Omega_{\mathcal{O}}(t) = B_{r_O(t)}(O)$ corresponding to the inner ball of radius $r_O(t)$ (oocyte radius), and subjected to radial growth of speed $\vec{v}_{\mathcal{O}}(x,t) = \frac{d}{dt} r_O(t) \vec{e}_r$. The cells constituting the follicle are gathered within the domain $\Omega(t)$ (see Figure IV.1) such that the external forces are exerted on the free boundary $\partial\Omega(t) \backslash \partial\Omega_{\mathcal{O}}(t)$ while the internal forces are exerted on the pushing boundary $\partial\Omega_{\mathcal{O}}(t)$, which is the interface between the oocyte and the follicle.
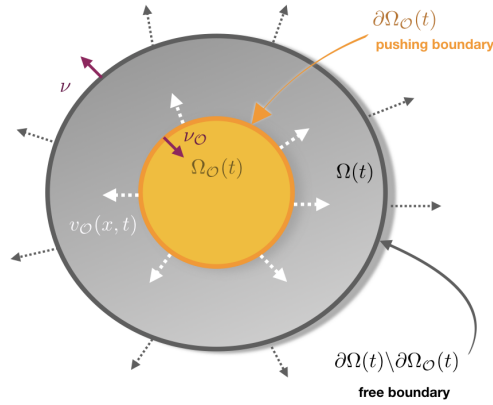

Fig. IV.1 *Spatial-structured model for the compact growth phase*

The hypothesis of incompressibility and compactness of cells naturally leads us to consider so-called free boundary problems such as the Hele-Shaw model.

a)   Free boundary problem: Hele-Shaw model

The Hele-Shaw model is a fluid mechanics model introduced in 1898 as part of a study on the modeling of the resistance surface between water and air. Nowadays, this model more generally describes the dynamics of the boundary between two incompressible and non-miscible fluids where one of them is passive. Even more recently, this model has attracted the attention of modellers working on the evolution of solid tumors, see for example [152, 153, 154].

In the simplest tumor growth models, the expansion of a spherical tumor is represented by cell division mechanisms regulated by nutrients from outside the tumor (external boundary). Since the fluid constituted by the tumor cells is assumed to be incompressible, the cell density is constant. The dynamics of the tumor is then represented by the pressure of the fluid p[1],

---

[1]It is a consequence of the Navier-Stokes equation, see for instance Chapter 0.2 of [155].

which can be linked to the velocity of the fluid via Darcy's law[2]. Fluid movement is induced by an increase in pressure by nutrient-modulated cell division (see Chapter 6 of [154]):

$$\begin{cases} -\Delta p = G(c(x,t)), x \in \Omega(t), \\ -\Delta c + \lambda c = 0, x \in \Omega(t), \\ p(x,t) = 0, x \in \partial\Omega(t), \\ c = c_b, x \in \partial\Omega(t). \end{cases}$$

where $G \in C^1$ is a positive function representing the net growth rate of cells as a function of available nutrients c. The parameter λ represents the consumption rate of nutrients. The nutriments diffuse from the external boundary of the tumor (blood concentration) at a constant concentration c_b up to the core of the tumor. The null Dirichlet boundary condition for the pressure implies that there are no cells outside domain $\Omega(t)$ (and therefore no movements). Assuming that for all $t \geq 0$, $\Omega(t) = B_{R(t)}(0)$ is the ball of radius $R(t)$ (tumor radius), one can deduce the law

$$\dot{R}(t) = \frac{S_{d-1}}{R(t)^{d-1}} \int_{\Omega(t)} G(c(x,t)dx),$$

where S_{d-1} denotes the constant linked to the sphere surface of dimension d. For example, $S_2 = 4\pi$. The detailed computation will be provided below. Such a formula is classical with those models. For instance, in [156], the authors also expressed the evolution of a tumor radius as a function that depends on the cell proliferation rate.

Inspired from this model, we consider the following Hele-Shaw like model for representing the follicle compact growth phase:

$$\begin{cases} -\Delta p(x) = b(x), x \in \Omega(t), \\ p(x,t) = 0, x \in \partial\Omega(t)\backslash\partial\Omega_{\mathcal{O}}(t), \\ v(x,t) \cdot \nu_{\mathcal{O}} = -\gamma\nabla p(x,t) \cdot \nu_{\mathcal{O}} = \vec{v}_{\mathcal{O}}(x,t) \cdot \nu_{\mathcal{O}}, x \in \partial\Omega_{\mathcal{O}}(t) \end{cases} \qquad \text{(IV.2)}$$

where:

- v is the velocity field of the cells (verifies the Darcy's law: $v = -\gamma\nabla p$),

- the sets $\Omega_{\mathcal{O}}(t)$ and $\Omega(t)$ are the spheres of radius $r_{\mathcal{O}}(t)$ and $r_{\mathcal{F}}(t) = r_{\mathcal{O}}(t) + r_{\mathcal{C}}(t)$, respectively.

- b is the net growth rate

The Dirichlet condition on the boundary $\partial\Omega(t)\backslash\partial\Omega_{\mathcal{O}}(t)$ represents a zero flux condition while the Neumann condition on the boundary $\partial\Omega_{\mathcal{O}}(t)$ represents the effect of the pushing boundary.

This model therefore explicitly re-introduces the effect of the oocte on the cells. To take into account the impact of cells on oocyte growth, a behavioural law could be added based on those proposed in [1].

Proposition IV.1. *Suppose that $\Omega(t) = B_{r_{\mathcal{F}}(t)}(t)$ such that $r_{\mathcal{F}}(t) < \infty$ and $\Omega_{\mathcal{O}}(t) = B_{r_{\mathcal{O}}(t)}(t)$, where $r_{\mathcal{F}}(t)$ and $r_{\mathcal{O}}(t)$ are the follicle and oocyte radius, respectively. Supposing that there exists a solution $p \in H^2(\Omega(t))$ of system (IV.2). Then,*

$$\frac{d}{dt}r_{\mathcal{F}}(t) \int_{\partial\Omega(t)\backslash\partial\Omega_{\mathcal{O}}(t)} dx = \gamma \int_{\Omega(t)} b(x)dx + \frac{d}{dt}r_{\mathcal{O}}(t) \int_{\partial\Omega_{\mathcal{O}}(t)} dx. \qquad \text{(IV.3)}$$

---

[2]The velocity field v is linked to the pressure field p by: $v = -\gamma\nabla p$, where γ is a diffusion constant.

Proof. Since $\Omega(t)$ is bounded and $p \in H^2(\Omega(t))$, we can integrate the Poisson equation of system (IV.2) on the whole domain $\Omega(t)$ and apply the Green formula[3]. We deduce that

$$- \int_{\Omega(t)} \Delta p(x) dx = - \int_{\partial\Omega(t)} \nabla p(x) \cdot \nu(x,t) dx$$

$$= - \int_{\partial\Omega(t) \backslash \partial\Omega_{\mathcal{O}}(t)} \nabla p(x) \cdot \nu(x,t) dx - \int_{\partial\Omega_{\mathcal{O}}(t)} \nabla p(x) \cdot \nu(x,t) dx.$$

Since $\nabla p(x) \cdot \nu(x,t) = -\frac{1}{\gamma} v(r_{\mathcal{F}}(t), t) = \frac{d}{dt} r_{\mathcal{F}}(t)$ on $\partial\Omega(t) \backslash \partial\Omega_{\mathcal{O}}(t)$ and $\nabla p(x) \cdot \nu(x,t) = -\frac{1}{\gamma} \vec{v}_{\mathcal{O}}(r_{\mathcal{O}}(t), t) \cdot \nu(x,t) = v_{\mathcal{O}}(r_{\mathcal{O}}(t), t)$ on $\partial\Omega_{\mathcal{O}}(t)$, we deduce first that:

$$- \int_{\Omega(t)} \Delta p(x) dx = \frac{1}{\gamma} v(r_{\mathcal{F}}(t), t) \int_{\partial\Omega(t) \backslash \partial\Omega_{\mathcal{O}}(t)} dx - \frac{1}{\gamma} v_{\mathcal{O}}(r_{\mathcal{O}}(t), t) \int_{\partial\Omega_{\mathcal{O}}(t)} dx.$$

then Formula (IV.3). $\qquad\square$

As we can expect, the follicle diameter evolves according to the oocyte diameter and the cell growth. The thickness of a follicle $e_{\mathcal{F}}(t) := r_{\mathcal{F}}(t) - r_{\mathcal{O}}(t)$ then verifies

$$\frac{d}{dt} e_{\mathcal{F}}(t) = \frac{1}{\int_{\partial\Omega(t) \backslash \partial\Omega_{\mathcal{O}}(t)} dx} \left[\gamma \int_{\Omega(t)} b(x) dx + \frac{d}{dt} r_{\mathcal{O}}(t) \left(\int_{\partial\Omega_{\mathcal{O}}(t)} dx - \int_{\partial\Omega(t) \backslash \partial\Omega_{\mathcal{O}}(t)} dx \right) \right].$$

Case study: negligible division speed

If the rate of cell division is negligible compared to the growth of the oocyte, the thickness of the follicle then verifies

$$\frac{d}{dt} e_{\mathcal{F}}(t) = \frac{d}{dt} r_{\mathcal{O}}(t) \left[\frac{\int_{\partial\Omega_{\mathcal{O}}(t)} dx}{\int_{\partial\Omega(t) \backslash \partial\Omega_{\mathcal{O}}(t)} dx} - 1 \right] = \frac{d}{dt} r_{\mathcal{O}}(t) \left[(\frac{r_{\mathcal{O}}(t)}{e_{\mathcal{F}}(t) + r_{\mathcal{O}}(t)})^{d-1} - 1 \right],$$

where d is the dimension of the space $\Omega(t) \subset \mathbb{R}^d$. Remark that the follicle thickness $e_{\mathcal{F}}$ is constant when $d = 1$. Supposing that the occyte radius is an increasing function, we also conclude that the follicle thickness $e_{\mathcal{F}}$ decreases if $d \geqslant 2$. These remarks can be interpreted as follows: in one dimension, the volume is linear while in more than two dimensions, the volume is a power of the dimension d. Thus, to maintain a constant cell density when $d \geqslant 2$, the follicle thickness has to decrease.

Case study: comparison with data

Formula (IV.3) is illustrated in Figure IV.2 for different parameter values. The green and dashed black lines illustrate the irrealistic case of no division: the thickness of the follicle decreases with the oocyte diameter. The colored lines represent other (more realistic) situations where there is cell divisions (see details in the legend). It can be seen that if the model with cell division (magenta and orange lines) seems to fit the data well for an oocyte diameter less than $100\mu m$, it does not predict the data for an oocyte diameter greater than $100\mu m$ (light blue data points). Actually, this is not surprising, these points correspond to follicles where an antrum has been observed, which implies to refine the model, for instance the incompressibility hypothesis.

---

[3]Green formula: For all $u \in H^2(\Omega), v \in H^1(\Omega)$, $\int_{\Omega} v\Delta u dx = - \int_{\Omega} \nabla u \cdot \nabla v dx + \int_{\partial\Omega} \frac{\partial u}{\partial n} v ds$, where H^1 and H^2 are Sobolev spaces [157].
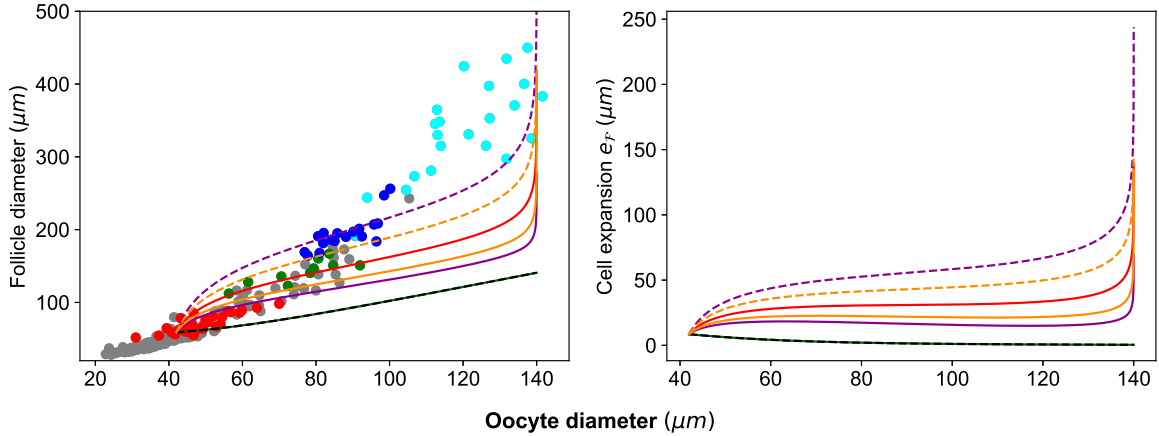
Fig. IV.2 **Illustration of Proposition IV.1 and application to data.** *We apply Proposition IV.1 for different parameter sets and we draw the follicle diameter $d_{\mathcal{F}}$ (left-panel) and the cell expansion $e_{\mathcal{F}}$ (right-panel) with respect to the oocyte diameter. In all cases, the oocyte radius $r_{\mathcal{O}}$ follows a logistic growth that verifies $r'_{\mathcal{O}}(t) = \alpha(r_{\mathcal{O}}(t) - 20)(r_{\mathcal{O}}(t) - 70)$. The black and green lines represent the case where there is no division ($b = 0$) such that either $\alpha = -0.0015$ (green line) or $\alpha = -0.001875$ (black dashed line). The red line corresponds to the parameter $\alpha = -0.0015$ and $b = 1$. The orange lines correspond to $b = 1$ and either $\alpha = -0.001875$ (dashed) or $\alpha = -0.0012$ (plain). The magenta lines correspond to $\alpha = -0.0015$ and either $b = 1.5$ (dashed) or $b = 0.67$ (plain). In the dataset presented in Chapter 1, we select follicles of Wild-Type genotype. The red, green and blue points correspond to the follicles distributed into the different times categories "t=0", "t=20" an "t=35" (presented in Table III.1a in Chapter 3, see details in section I.2.2). The light blue points are the follicles where an antrum has been observed. The grey points correspond to the remaining follicles that do not belong to any of the categories enunciated above.*

b) Link with the Keller-Segel model: from incompressible to compressible model

The link between incompressible and compressible cell dynamics models is still the subject of current researches, especially for tumor growth models that we continue to draw inspiration from (see for example [153, 158, 152]). Unlike incompressible cellular models, compressible models represent the dynamics of a cell density $u(x,t) \in [0.1]$ via a behavioural law (usually an advection-reaction equation) [159, 160, 156] such as

$$\partial_t u + \nabla \cdot (uv) = ub(c), x \in \mathbb{R}^d, t \geq 0, \text{ and } -\Delta c + \psi(u, c) = 0. \qquad \text{(IV.4)}$$

In the example above, cell dynamics is locally regulated by the presence of growth factors with a concentration of $c(x,t)$. The cells are always considered as a fluid whose speed v must be prescribed to be able to close the system. One possibility is to simultaneously apply Darcy's law and the following pressure law:

$$v = -\nabla p \text{ and } p(u) = u^{\gamma}.$$

Concretely, at each point of space, the cellular flow has for speed v which depends on the local cell density. Since $u(t, .)$ has values in $[0, 1]$, we find that the larger γ, the more homoge-

neous this velocity is and takes two values: 0 or 1 depending on whether there are cells or not.

We complete this model with a couple of Dirichlet boundary conditions: a boundary condition to model the oocyte growth and its secreted factors:

$$v(x,t) \cdot \nu_{\mathcal{O}} = \vec{v}_{\mathcal{O}}(x,t) \cdot \nu_{\mathcal{O}}, x \in \partial\Omega_{\mathcal{O}}(t),$$
$$c(x,t) = c_{\mathcal{O}}(x,t), x \in \partial\Omega_{\mathcal{O}}(t),$$

and zero-flux boundary conditions on the follicle border

$$v(x,t) \cdot \nu = 0, x \in \partial\Omega(t)\backslash\partial\Omega_{\mathcal{O}}(t),$$
$$c(x,t) = 0, x \in \partial\Omega(t)\backslash\partial\Omega_{\mathcal{O}}(t),$$

Thus, the main difference between our model and tumor growth models remains in the existence of the "pushing" boundary condition coming from the oocyte growth and the fact that the secreted factors come from the inside of the domain and not the outside.

From compressible to incompressible model. The asymptotic limit $\gamma \rightarrow +\infty$ can be viewed as an incompressible limit. We first explain formally the asymptotic limit: multiplying Eq. (IV.4) by $p'(u)$, we first obtain that:

$$\partial_t p'(u) - \nabla p(u) \cdot \nabla p(u) - up'(u)\Delta p(u) = up'(u)b(c).$$

Since from the pressure law, we have $up'(u) = \gamma p(u)$, we deduce

$$\partial_t p'(u) - \nabla p(u) \cdot \nabla p(u) - \gamma p(u)\Delta p(u) = \gamma p(u)b(c).$$

Taking $\gamma \rightarrow +\infty$, we obtain the Hele-Shaw model:

$$-\Delta p = b(c).$$

If there is no oocyte ($\Omega_{\mathcal{O}}(t) = \emptyset$), the asymptotic limit in our model is equivalent to that proved in [161] (see Theorem A.1). In our case, the pushing boundary introduces difficulties both for the theoretical analyses and the numerical simulations. The analysis of this model is thus an open-question that will be interesting to study. It will indeed provide information on the speed balance between the oocyte growth and the cell proliferation.

In Chapter 3, we have chosen to use a formalism where the spatial position of the cell is represented by a discrete index while we present here models where the spatial position of cells is continuous. The approach based on the incompressible-compressible limit seems to be interesting to be studied from many points of view: modeling, simulations, theoretical analyses, etc. It would also make it possible to take a step forward in the understanding of the coupling between oocyte growth and cell proliferation. Since these models are derived from fluid mechanical models, the Eulerian frame of reference[4] is used and it is not possible to follow a single cell trajectory.
Other approaches based on the Lagrangian frame of reference[5] can be used to complement

---

[4]The Eulerian frame of reference is a way of looking at fluid motion that focuses on specific locations in the space through which the fluid flows as time passes.

[5]The Lagrangian frame of reference is a way of looking at fluid motion where the observer follows an individual fluid parcel as it moves through space and time.

the cancer-like model and compare the results. Good examples of the Lagrangian frame of reference are stochastic processes such as the [CMMS] model [1] where the cells are defined by a spatial position (and an age). For example, the agent-based models, that are becoming more common in the modeling community, are relevant to represent morphogenesis mechanisms. The interested reader may refer to the reviews [162, 163]. The agent-based models tackle the question of the representation of the spatial position of a cell and the management of the space domain. Lattice-based models such as cellular automata are models where the domain is fixed while off-lattice models such as vertex models allows the domain to move according to cell dynamics.

Chapter V

Analysis and numerical simulation of an inverse problem for a structured cell population dynamics model

This chapter is based on the following article

> Frédérique Clément, Béatrice Laroche, Frédérique Robin, *Analysis and numerical simulation of an inverse problem for a structured cell population dynamics model.* Published in Mathematical Biosciences and Engineering, 2019, 16(4): 3018-3046 (see [164]).

Cell dynamics are classically investigated in the framework of structured populations, and especially of the McKendrick–VonFoerster model. The direct problem associated with the initial and extended formulations of this model has caught most of the attention, both on the theoretical ground (well-posedness, e.g. [27, 19]) and numerical ground (numerical approximation of the solutions, e.g. [32, 28, 29]). The inverse problems, intending to recover model functions, such as the death or division rate, from observable model outputs, have been much less studied [94, 95, 93, 101, 96], although they have a particular interest in a cell dynamics context, where *a priori* information on these rates are often quite poor.

In this work, we study and illustrate the well-posedness of a multiscale inverse problem (IP), defined from a multi-type version of the linear, age-structured formulation of the McKendrick–VonFoerster model, in the specific situation where cell death can only occur at the time of mitosis.

This problem has been initially motivated by a developmental biology issue, namely folliculogenesis, the process of growth and maturation of ovarian follicles. During the first development stages, the growth of ovarian follicles is mainly driven by the proliferation of the somatic cells surrounding the oocyte (egg cell), which progressively builds up several concentric cell layers. In this specific application [33], the cell type corresponds to the layer index, and the cell division rate is type-dependent. At the time of mitosis, cells are likely to move to the next layer (unidirectional motion), and the (layer-dependent) migration rate can be seen as the equivalent of a mitosis-induced death rate in the lower layer. As a consequence, the birth rate (boundary condition at birth with age $a = 0$) combines an intrinsic contribution from division and an extrinsic contribution from migration.

Beyond folliculogenesis, such a multi-type formulation can be applied to other cell processes with either spatially oriented development (e.g. cortical neurogenesis) or commitment to a

cell lineage or fate (e.g., hematopoiesis).

The multiscale character of the IP ensues from the fact that the observable data (total cell number on each layer) are available on the macroscopic scale and used to recover the microscopic functions entering the system of interconnected McKendrick–VonFoerster PDEs. More specifically, we consider here the problem of recovering the age-dependent division rates, and constant migration rates ruling the cell density in age on each layer, from the knowledge of the total cell number (zero-order moment of the density) on every layers.

In [33], we have tackled the simplified case of constant (yet layer-dependent) division rates. In this work, we extend the study to the case of compactly supported (lattice) division rates, in order to stick to a realistic interpretation of the division rate as a distribution of intermitotic times ; age is reset to zero at birth, there can be a minimal age compatible with division, and cells can become quiescent beyond a maximal age. We consider initial conditions corresponding either to a synchronized (Dirac mass) or non-synchronized cell population (Dirac comb or continuous function) on the first layer (all other layers are empty). If the well-posedness of the PDEs (V.1) for a $\mathbf{L}_1$ initial condition has been widely studied in the last decades (see for instance, [27, 19]), the case of Dirac measure initial conditions has been investigated only recently. For instance, in [34, 165], the authors have introduced the notion of measure solutions for the conservative renewal equation.

In the single layer (not multi-type) case, similar multiscale IP problems, dealing with an age-dependent reproduction rate have been studied [94, 93]. In [94], in the case of a strictly positive, reproduction-independent death rate resulting in an almost sure death before a maximal age L, the authors have shown, from the characteristic curves, that the birth rate (boundary condition) verifies a Volterra integral equation of the second kind, and then used the Fredholm alternative to further recover the reproduction rate. In [93], starting from the cumulative formulation (renewal equation), and assuming a non-lattice reproduction rate, the authors have studied both the case of reproduction-dependent and reproduction-independent death rate to recover the reproduction and death rates. In the reproduction-dependent (mitosis-dependent) case (see Theorem 4.3), using the Laplace transform, the authors have shown the IP well-posedness for an initial population synchronized at age 0 (Dirac mass). If, in addition, the total cell number can be expressed as a series of exponential functions, the IP well-posedness is also obtained for a non-synchronized initial population represented by a measure with support on $[0, 1]$ and no atom at 1.

Also, single-scale IP problems, where observation are available at the microscopic level, have been investigated in a similar age-structured framework [95, 97, 98] or in the size-structured framework [14, 44, 166]. In the semigroup framework, the problem of recovering the death rate from the knowledge of both the age distribution at two different time points and the reproduction rate is studied in [95]. A similar problem is considered in [98] from the observation of a truncated age distribution at any time. Finally, in a steady state configuration, given a rather mesoscopic observation, the distribution of intermitotic times, one can recover the mitosis-dependent death rate [97] from the eigenvalue problem, following the methodological principle introduced in [14, 44, 166].

This paper is organized as follows. In section 1, we present the direct problem (multi-type McKendrick–VonFoerster). Inspired from the single layer case [19], we propose a formal solution based on the characteristic curves, and use them to design a numerical scheme, as performed in [28]. We check our numerical scheme using the mass conservation property. In Section 2, using a Fredholm integral equation, we show the well-posedness of the IP in the

single layer case, when considering a continuous non-synchronized initial condition. Because of the mitosis-dependent death rate, the Fredholm alternative cannot be applied, and we use a constructive approach to obtain the lattice division rate from the knowledge of both the total cell number and a continuous (non-synchronized) initial condition. Then, we take advantage of the unidirectional motion and decompose the Jth layer model into J submodels, each corresponding to the single layer model with an additional extrinsic term in the boundary condition. We again derive a Fredholm integral equation for each submodel and deduce the well-posedness of the multi-type inverse problem. In section 3, we show the well-posedness of the IP in the single layer case, when considering Dirac masses as initial conditions. After constructing a solution from the characteristic lines, we still obtain a Fredholm integral equation. In each situation, we illustrate numerically our theoretical results. We conclude the paper by a Conclusion/Discussion section. Complements on the numerical scheme construction and the proofs can be found in the Appendix.

V.1 Model and discretized solutions

We recall the age and layer structured cell population model considered in [33]. Let $J \in \mathbb{N}^*$. The cell population is represented by a population density function $\rho := (\rho^{(j)}(t, a))_{j \in [\![1,J]\!]} \in \mathbf{L}_1(\mathbb{R}_+)^J$, where $\rho^{(j)}$ is the cell age density in layer j at time t such that ρ verifies, for all $j \in [\![1, J]\!]$, for all $t \in (0, +\infty)$,

$$\begin{cases} \partial_t \rho^{(j)}(t,a) + \partial_a \rho^{(j)}(t,a) = -b_j(a)\rho^{(j)}(t,a), \ a \in (0,\infty), \\ \rho^{(j)}(t, a = 0) = 2(1 - p_S^{(j-1)}) \int_0^{+\infty} b_{j-1}(a)\rho^{(j-1)}(t,a)(t,a)\, da + 2p_S^{(j)} \int_0^{+\infty} b_j(a)\rho^{(j)}(t,a)\, da, \\ \rho^{(j)}(0, a) = \psi_j(a), \quad a \in (0, +\infty), \end{cases}$$
(V.1)

where b_j are the division rate functions, and $\psi = (\psi_j)_{j \in [\![1,J]\!]}$ is the initial density such that for all $j \in [\![1, J]\!]$, $\psi_j \in \mathcal{C}_c(\mathbb{R}_+)$. For all $j \in [\![1, J]\!]$, the parameter $p_S^{(j)}$ is the probability that a cell taken randomly among both daughter cells, remains on its mother layer j. For all $j \in [\![1, J-1]\!]$, we take $p_S^{(j)} \in (0, 1)$. On the last layer, $p_S^{(J)} \in (0, 1]$. A natural choice in the multi-layer case is to consider $p_S^{(J)} = 1$ as in [33]. The division rate on each layer has a classical probabilistic interpretation [27, 94, 93, 97]: the probability that a cell born on the j-th layer has not yet divided at age α is

$$\exp\left(-\int_0^\alpha b_j(s)ds\right).$$

It follows that if $\int_0^{+\infty} b_j(s)ds = +\infty$, the cell divides almost surely, and conversely, if $\int_0^{+\infty} b_j(s)ds < +\infty$, a cell may never divide and become quiescent. This will happen in particular if b_j is a bounded, compactly supported function. We investigate the inverse problem associated with the model (V.1):

Definition V.1.

(IP) Given the initial condition ψ, the probability $p_S^{(J)}$ and the functions

$$m(t) := (m_j(t))_{j \in [\![1,J]\!]} \ \text{with} \ m_j(t) := \int_0^{+\infty} \rho^{(j)}(t,a)da,$$
(V.2)

defined for all $t \in [0, T)$, with $T > 0$, determine the functions b_j and the probabilities $p_S^{(j)}$, for all $j \in [\![1, J-1]\!]$, such that the direct problem (V.1) *is satisfied on $[0, T)$.*

The model is completed with a set of hypotheses on the division rate and initial conditions, formulated below.

Hypothesis V.1. *For all $j \in [\![1, J]\!]$, the division rates b_j are non-negative compactly supported functions: $b_j \in \mathcal{C}_c\left((A_j^{\min}, A_j^{\max}) \right)$, where $A_j^{\min}, A_j^{\max} \in \mathbb{R}_+ \cup \{0\} \cup \{+\infty\}$, such that $A_j^{\min} < A_j^{\max}$.*

For the single layer case, note that this hypothesis is more general than the one used either in [93] where the division rate function is supposed to be non-lattice or, in the steady state approach [97] where $A_1^{\max} = +\infty$.

Motivated by the biological process studied in [33], we consider that the system starts with all the layers empty, except the first one. We consider different types of initial conditions: either Dirac measures corresponding to a fully or partially synchronized population, or a continuous function corresponding to a non-synchronized population.
In case of a continuous initial condition, we assume that the following hypotheses are verified.

Hypothesis V.2. *For all $j \in [\![2, J]\!]$ and for all $a \in (0, +\infty)$, we have $\psi_j(a) = 0$ and $\psi_1 \in \mathcal{C}_c\left((a_{\min}^\psi, a_{\max}^\psi) \right)$, with $a_{\min}^\psi, a_{\max}^\psi \in \mathbb{R}_+$ such that $a_{\min}^\psi < a_{\max}^\psi$.*

If the initial condition is a Dirac measure or Dirac Comb, we assume that:

Hypothesis V.3. *For all $j \in [\![2, J]\!]$ and for all $a \in (0, +\infty)$, we have $\psi_j(a) = 0$. In addition, we suppose that there exist two sequences of $N + 1$ positive numbers, with $N \in \mathbb{N}$, $a = (a_i)_{i \in [\![0, N]\!]} \in \mathbb{R}_+^N \cup \{0\}$ and $\Psi = (\Psi_i)_{i \in [\![0, N]\!]} \in \mathbb{R}_+^N$ such that*

$$a_{\max}^\psi := a_0 > a_1 > ... > a_N =: a_{\min}^\psi.$$

Then, we define the initial condition on the first layer, for all $a \geq 0$, by

$$\psi_1(a) := \sum_{i=0}^{N} \Psi_i \delta_{a_i}(a). \tag{V.3}$$

Finally, to show the well-posedness of the inverse problem (IP), we will need two additional hypotheses on the b_j functions.

Hypothesis V.4. *For all $j \in [\![1, J]\!]$, the division rates b_j are analytic on their support sets.*

Hypothesis V.5. *The first division time on Layer 1 is larger than the age of the eldest cells at initial time: $A_1^{\min} \geq a_{\max}^\psi$.*

Hypothesis V.1 is quite natural from the biological viewpoint, whereas Hypotheses V.4 and V.5 are purely technical, yet easily fulfilled.
We follow the same approach as in [94, 95] and first solve the direct problem (V.1).

V.1.1 Formal solutions of the direct problem

Even if an explicit solution of the PDEs (V.1) cannot be obtained, one classical way to solve the direct problem when dealing with continuous initial conditions, is to use the method of characteristics [19, 27]. We integrate the PDEs (V.1) along the characteristics lines $a = a_0 + t$ and $t = t_0 + t$, where a_0 and t_0 are nonnegative constants. We get for all $j \in [\![1, J]\!]$ and for all $a \in (0, +\infty)$,

$$\rho^{(j)}(t, a) = \begin{cases} \psi_j(a-t)e^{-\int_{a-t}^{a} b_j(s)ds}, \ a \geq t \\ \rho^{(j)}(t-a, 0)e^{-\int_0^a b_j(s)ds}, \ a \leq t. \end{cases} \tag{V.4}$$

Hence, we obtain an expression for each $\rho^{(j)}$, for $j \in [\![1, J]\!]$, that depends on the initial density ψ_j, the division rate b_j, and the boundary condition $\rho^{(j)}$.

To close system (V.4), we need to get an explicit expression for the boundary condition. When $J = 1$, the boundary condition, classically called the birth rate, is solution of a renewal equation [93]. In our context, we can retrieve a similar renewal equation verified by the boundary condition:

$$\rho^{(j)}(t, 0) = h_j(t) + 2p_S^{(j)} \left(\int_0^t \rho^{(j)}(t-a, 0)b_j(a)e^{-\int_0^a b_j(s)ds}da + \int_t^{+\infty} \psi_j(a-t, 0)b_j(a)e^{-\int_{a-t}^a b_j(s)ds}da \right),$$

with $h_j(t) := 2(1 - p_S^{(j-1)}) \int_0^{+\infty} b_{j-1}(a)\rho^{(j-1)}(t, a)da$.

This equation is the deterministic counterpart of the renewal equation obtained from a stochastic equivalent model introduced in [33].

Figure V.1 illustrates the characteristic lines obtained from expression (V.4) with $J = 3$. Note that since all layers except the first are empty at initial time, a delay is needed for cells to enter the second and third layers.

V.1.2 Numerical scheme to simulate the direct problem

In this subsection, we propose a numerical scheme for the direct problem (V.1).

The main numerical difficulty associated with the hyperbolic PDEs (V.1) is the assessment of the boundary condition, which has been dealt with by several numerical methods, based either on the method of characteristics [32, 31, 28], escalator boxcar train [29] or finite volume method [33].

Given that our problem possibly involves a non-continuous initial condition (ψ_1), and lattice division rates, the method of characteristics is the most suitable one. In particular, the characteristics-based scheme ensures mass conservation during the transport phase by preventing numerical diffusion when $a < A_{\min}^j$.

In addition, we will see later that this approach helps designing a numerical scheme for solving the inverse problem (IP).

To obtain a discretized solution of the PDEs (V.1), we write the conservative law for a vector function $\tilde{\rho} = (\tilde{\rho}^{(j)})_{j \in [\![1,J]\!]}$, defined as: for all $j \in [\![1, J]\!]$, $t \in (0, +\infty)$ and $a \in (0, +\infty)$,

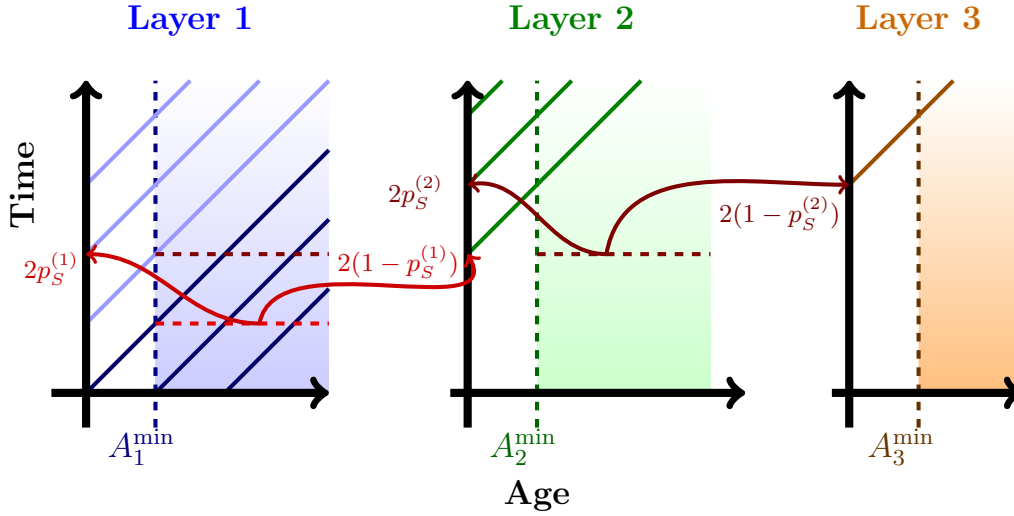$$\tilde{\rho}^{(j)}(t, a) := \rho^{(j)}(t, a) \exp\left(-\int_0^a b_j(s)ds \right).$$

Fig. V.1 ***Illustration of the PDEs*** (V.1) ***and the method of characteristics***. *Starting from Layer 1, since cells are aging, the density $\rho^{(1)}$ is transported along the characteristic lines $a = \tilde{a} + t$, for all $\tilde{a} \in (a_{\min}^{\psi}, a_{\max}^{\psi})$. Then, when a characteristic line enters the (lilac colored) division domain $[A_1^{\min}, A_1^{\max}]$, cells divide and the age is reset to zero. A proportion $2p_S^{(1)}$ of the new born cells remains on the mother layer (Layer 1) whereas the other proportion, $2(1 - p_S^{(1)})$, is sent to the second layer. The same mechanism is repeated from Layer 2 to Layer 3 and so on. Note that the motion is unidirectional: cells cannot go to layers of lower index than their mother.*

From the PDEs (V.1), we obtain directly that, for all $t \in (0, +\infty)$ and $a \in (0, +\infty)$,

$$\partial_t \tilde{\rho}^{(j)}(t, a) + \partial_a \tilde{\rho}^{(j)}(t, a) = 0. \tag{V.5}$$

We now have all the elements to design a numerical scheme.

First, we introduce the notations for the discretized solutions associated with the PDEs (V.1) over the time interval $[0, T]$.

We discretize both the age and time intervals with the same size step: $\Delta = \Delta t = \Delta a$, in order to be able to follow the characteristics. Let M be an integer such that $M \geq \lfloor \frac{a_{\max}^{\psi} + T}{\Delta} \rfloor$. We introduce the age grid points $a_n = n\Delta$, $n = 0, ..., M$ and the time grid points $t_k = k\Delta$, $k = 0, ..., \lfloor \frac{T}{\Delta} \rfloor$. We refer to the grid point a_n by the subscript n and to the time grid point t_k by the subscript k. Let $U_{k,n}^j$ be a numerical approximation to $\rho^{(j)}(t_k, a_n)$.

We have the following numerical algorithm whose local truncation error is $\mathcal{O}(\Delta)$, (see details in Appendix A.2.1):

$$U_{k+1,n}^j = U_{k,n-1}^j \exp\left(- \int_{a_{n-1}}^{a_n} b_j(s)ds\right), \tag{V.6}$$

$$U_{k+1,0}^j = 2(1-p_S^{(j-1)}) \sum_{n=\lfloor \frac{A_{\min}^{j-1}}{\Delta} \rfloor}^{\lfloor \frac{A_{\max}^{j-1}}{\Delta} \rfloor - 1} \left(1 - e^{-\int_{(n-1)\Delta}^{n\Delta} b_{j-1}(s)ds} \right) U_{k,n}^{j-1} + 2p_S^{(j)} \sum_{n=\lfloor \frac{A_{\min}^{j}}{\Delta} \rfloor}^{\lfloor \frac{A_{\max}^{j}}{\Delta} \rfloor - 1} \left(1 - e^{-\int_{(n-1)\Delta}^{n\Delta} b_j(s)ds} \right) U_{k,n}^j.$$

(V.7)

The reader can refer to [28] for a detailed proof of convergence in the single layer case. In the several layer case, the term corresponding to the intrinsic contribution could be dealt with in a similar way as in the single layer case, yet one should also control the order of the extrinsic term, which is beyond of the scope of this paper.

Remark V.1 (Mass conservation property)**.** *When $J = 1$ and $p_S^{(1)} = \frac{1}{2}$, we can observe that the mass conservation property is verified in the sense that*

$$\sum_{n=0}^M U_{k+1,n}^1 = \sum_{n=0}^M U_{k,n}^1.$$

V.2 Analysis of the inverse problem (IP) for continuous initial conditions

In this section, we analyse the inverse problem (IP) enunciated in Definition V.1 starting with the simplest case of a single layer and considering a compactly supported function as initial condition. We then extend our results to the general case of several layers.

V.2.1 Single layer case

In all this subsection, we fix $J = 1$ and consequently, to simplify notations, we drop the index layer so that for instance $\rho^{(1)}$ becomes ρ. We thus consider the following PDE, identical to the PDEs (V.1) with $J = 1$:

$$\begin{cases} \partial_t \rho(t,a) + \partial_a \rho(t,a) = -b(a)\rho(t,a), \ a \in (0,\infty), \\ \rho(t,a=0) = 2p_S \int_0^{+\infty} b(a)\rho(t,a)\,da, \\ \rho(0,a) = \psi(a), \quad a \in (0,+\infty), \end{cases}$$

(V.8)

Note that when $p_S = 1$, PDE (V.8) is the renewal equation. When $p_S < 1$, PDE (V.8) is similar to a McKendrick–VonFoerster equation in which the birth rate would be $2p_s$ times the death rate. We recall that according to the definition of (IP), $p_S = p_S^{(1)}(= p_S^{(J)})$ is assumed to be known while the division rate b is unknown.

a) Well-posedness of the inverse problem (IP)

We first show that the identification problem (IP) is equivalent to an inhomogeneous Fredholm integral equation.

Theorem V.1. *Under Hypotheses V.1 and V.2, and supposing that $p_S \neq \frac{1}{2}$, we define $f(t) := -\frac{1}{2p_S-1}m_1(t) + \frac{2p_S}{2p_S-1}m_1(0)$. Then, we have for all $t \in [0, A^{\min}]$*

$$f(t) = \int_{a_{\min}^\psi}^{a_{\max}^\psi} \psi(a)e^{-\int_a^{a+t} b(s)ds}\,da.$$

(V.9)

Before starting the proof of Theorem V.1, we will need the following lemma:

Lemma V.1. *Under the same hypotheses as Theorem V.1, we have for all $t \in [0, A^{\min}]$,*

$$m_1'(t) = \frac{2p_S - 1}{2p_S} \rho(t, 0) \tag{V.10}$$

Proof. Since both ψ and b are compactly supported, the total number of cells $m_1(t) = \int_0^{+\infty} \rho(t, a) da$ can be decomposed as the sum of the initial cells that have not yet divided and the cells born since time $t = A^{\min} - a_{\max}^\psi$:

$$m_1(t) = \underbrace{\int_{a_{\min}^\psi + t}^{a_{\max}^\psi + t} \rho(t, a) da}_{\text{initial cells}} + \underbrace{\int_0^{\min(A^{\min} - a_{\min}^\psi + t, 0)} \rho(t, a) da}_{\text{cells born since time } t = A^{\min} - a_{\max}^\psi}. \tag{V.11}$$

Using two changes of variables, the translation $s = a - a_{\min}^\psi - t$ and the homothetic transformation $s = \frac{a}{A^{\min} - a_{\min}^\psi + t}$, we can prove formula (V.10). Note that in the general case, corresponding here to $A^{\min} = a_{\min}^\psi = 0$ and $A^{\max} = a_{\max}^\psi = +\infty$, such changes of variables are not needed to obtain formula (V.10). The detailed proof is exposed in Appendix A.2.2. $\qquad\square$

We can now proceed to the proof of Theorem V.1.

Proof of Theorem V.1. To simplify the proof, we do not use expression (V.11) and instead, we write the total number of cells m_1 (eq. (V.2)) as the sum of the number of the remaining cells that have not divided yet and the cells born since time $t > 0$, according to the formal solution of ρ (V.4):

$$m_1(t) = \underbrace{\int_0^t \rho(t - a, 0) e^{-\int_0^a b(s) ds} da}_{\text{new born cells}} + \underbrace{\int_t^{t + a_{\max}^\psi} \psi(a - t) e^{-\int_{a-t}^a b(s) ds} da}_{\text{remaining mother cells}}.$$

We apply Lemma V.1, for all $t \geq 0$ and we obtain

$$m_1(t) = \frac{2p_S}{2p_S - 1} \int_0^t m_1'(t - a) e^{-\int_0^a b(s) ds} da + \int_t^{t + a_{\max}^\psi} \psi(a - t) e^{-\int_{a-t}^a b(s) ds} da.$$

We suppose that $t \leq A^{\min}$. Hence, the only cells that can divide are the cells present at initial time (mother cells). The newborn daughter cells have not yet had the time to divide (there are no grand-daughter cells). For all $t \in [0, A^{\min}]$,

$$\begin{aligned} m_1(t) &= \frac{2p_S}{2p_S - 1} \int_0^t m_1'(t - a) da + \int_t^{t + a_{\max}^\psi} \psi(a - t) e^{-\int_{a-t}^a b(s) ds} da \\ &= \frac{2p_S}{2p_S - 1} (m_1(t) - m_1(0)) + \int_t^{t + a_{\max}^\psi} \psi(a - t) e^{-\int_{a-t}^a b(s) ds} da. \end{aligned}$$

Since

$$\int_t^{t + a_{\max}^\psi} \psi(a - t) e^{-\int_{a-t}^a b(s) ds} da = \int_0^{a_{\max}^\psi} \psi(a) e^{-\int_a^{a+t} b(s) ds} da = \int_{a_{\min}^\psi}^{a_{\max}^\psi} \psi(a) e^{-\int_a^{a+t} b(s) ds} da,$$

the definition of f leads to the inhomogeneous Freholm integral equation (V.9). $\qquad\square$

Remark V.2. *Note that Theorem V.1 is defined on the time interval $[0, A^{\min}]$. During this interval, only the mother cells coming from the initial condition are dividing. Hence, we can extend this result to the time interval $[0, 2A^{\min} - a_{\max}^{\psi}]$ if $A^{\min} \geq a_{\max}^{\psi}$.*

Remark V.3 (Self-renewal case)**.** *Note that, if $p_S = \frac{1}{2}$, the identification problem is not well-posed so that alternative observation data should be used. Indeed, the total number of cells is constant along time whereas the solution of the inverse problem is based on changes in this number.*

Usually, the inhomogeneous Fredholm integral equation, which is a particular case of the Volterra integral equation, is studied in the case where the kernel is known. Here, we rather consider the inverse problem of reconstructing the kernel from function f and initial condition ψ.

Theorem V.2. *Under Hypotheses V.1, V.2, V.4 and V.5, the problem (IP) is well-posed.*

Proof. Applying Hypothesis V.5 to the Fredholm integral equation (V.9), we first deduce that, for all $t \in [0, A^{\min}]$,

$$f(t) = \int_{\mathbb{R}} \psi(a) \exp(-\int_{A^{\min}}^{a+t} b(s)ds)da.$$

Then, using the change of variables $u = a + t$, we obtain that

$$f(t) = \int_{\mathbb{R}} \psi(a-t) \exp(-\int_{A^{\min}}^{a} b(s)ds)da. \tag{V.12}$$

We can recognize a convolution product. However, since relation (V.12) is verified only for $t \in [0, A^{\min}]$, we cannot use the Laplace transform directly to separate function ψ from the age-dependent function $a \to \exp(-\int_{A^{\min}}^{a} b(s)ds)$. We rather introduce the truncated functions $\widetilde{f}$ and $\widetilde{b}$ such that:

$$\widetilde{f}(t) = f(t)\mathbf{1}_{[0,A^{\min})}(t) + f(A^{\min})\mathbf{1}_{[A^{\min},+\infty)}(t) \text{ and } \widetilde{b}(a) = b(a)\mathbf{1}_{[0,A^{\min}+a_{\max}^{\psi}]}(a). \tag{V.13}$$

In other words, function $\widetilde{f}$ coincides with function f on the interval $[0, A^{\min}]$, and function $\widetilde{b}$ coincides with function b on the interval $[0, A^{\min} + a_{\max}^{\psi}]$. Hence, we deduce from relations (V.12) and (V.13) that for all $t \geq 0$,

$$\widetilde{f}(t) = \int_{\mathbb{R}} \psi(a-t) \exp\left(-\int_{A^{\min}}^{a} \widetilde{b}(s)ds\right) da. \tag{V.14}$$

Since f, ψ and $g(a) := \exp(-\int_{A^{\min}}^{a} \widetilde{b}(s)ds)$ are constant beyond a given time/age, their associated Laplace transforms exist for all $p > 0$, so that we can apply a Laplace transform to relation (V.14), and deduce that, for all $p > 0$,

$$\mathcal{F}[\widetilde{f}](p) = \mathcal{F}[\widetilde{\psi}](p)\mathcal{F}[g](p), \tag{V.15}$$

where $\mathcal{F}[\widetilde{f}]$ is the Laplace transform associated with function f. From relation (V.15), we deduce the uniqueness of the Laplace transform of function g. From the injectivity property of the Laplace transform, we deduce the uniqueness of function g. From the bijectivity property of function g, we then deduce the uniqueness of function $\widetilde{b}$. Finally, from the uniqueness of function b on the interval $[0, A^{\min} + a_{\max}^{\psi}]$, we deduce from Hypothesis V.4 the uniqueness of function b on the whole interval $\mathbb{R}_+$. □

Remark V.4. *The results of Theorem V.2 can be extended to non-analytic b functions by piecewise reconstruction of b on its whole support $(A^{\min}, A^{\max})$. From the proof of Theorem V.2, we have the uniqueness of b on the interval $[0, A^{\min} + a_{\max}^{\psi}]$. Then, from the knowledge of b on the interval $[0, A^{\min} + a_{\max}^{\psi}]$ and remembering that the first newborn cells, born at time $2A^{\min} - a_{\max}^{\psi}$ (see Remark V.2) start to divide at time $t = 3A^{\min} - a_{\max}^{\psi}$, one can derive a Fredholm integral equation for $t \in [0, 3A^{\min} - a_{\max}^{\psi}]$, following the proof of Theorem V.1, hence deduce the uniqueness of b on the interval $[0, 2A^{\min} + a_{\max}^{\psi}]$. Repeating this operation as many times as needed, we finally obtain the uniqueness of function b on its whole support.*

While Theorem V.2 ensures the uniqueness of function b, it does not provide us with a tractable analytic formula to reconstruct it. This issue is addressed in the next paragraph.

b) Numerical procedure for non-synchronized populations

We finish the study of the inverse problem (IP) for the single layer case by proposing a numerical procedure to retrieve the division rate b from the total number of cells.
We assume that the initial condition ψ can be discretized using a time sequence $t_k = k\Delta$ and we aim to compute the $b(k\Delta)$ values.

The procedure is based on the fact that we use the same size step Δ for both the age and time grids. Let the initial sequence $\Psi = (\Psi_i)_{i \in [\![i_{\min}, i_{\max}]\!]}$ where $i_{\min} = \lfloor \frac{a_{\min}^{\psi}}{\Delta} \rfloor$ and $i_{\max} = \lfloor \frac{a_{\max}^{\psi}}{\Delta} \rfloor$.
Between $t = 0$ and $t = A^{\min} - a_{\max}^{\psi}$, cells are aging, hence PDE (V.8) is a pure transport equation. Then, at time $t = A^{\min} - a_{\max}^{\psi}$, the first division happens for cells that have reached age $A^{\min}$.

We fix the initial values of vector $b := (b_k)_{k \in [\![0,N]\!]}$ to zero. Each observation of the total number of cells at time t_k will be used to refresh one by one the value of vector b from left to right.
Using the numerical scheme (expressions (V.6) and (V.7)), we define the mass difference at time t_k by:

$$\mu_k := m(t_k) - \Delta \sum_{n=0}^{i_{\max}+k} U_{k,n}. \tag{V.16}$$

At time t_k, all the b_n for $n \in [\![0, i_{\max} + k - 1]\!]$ have been refreshed at time t_{k-1}, while the remaining values for indexes $n \in [\![i_{\max} + k, N]\!]$ are still zero. At this time t_k, the change in the mass difference can only come from the eldest cells indexed by $i_{\max} + k$. Hence, if $\mu_k = 0$, the eldest cells have not divided yet between t_{k-1} and t_k. Otherwise, if $\mu_k \neq 0$, a division has occurred. We recall the reader that p_S is the probability that at least one daughter cell remains on Layer 1. If $p_S < \frac{1}{2}$, this division results in a negative mass difference, otherwise, if $p_S > \frac{1}{2}$, it results in a positive mass difference.
To compute the $b_{i_{\max}+k}$, we use the mass difference definition (V.16) and the numerical scheme to write the mass balance conservation law:

$$m(t_k) = \Delta \underbrace{\sum_{n=0}^{i_{\max}+k-1} U_{k,n}}_{\text{remaining cells}} + \underbrace{\Delta U_{k-1,i_{\max}+k-1} e^{-\Delta b_{i_{\max}+k}} + 2 p_S \Delta (1 - e^{-\Delta b_{i_{\max}+k}}) U_{k-1,i_{\max}+k-1}}_{\text{dividing eldest cells}}.$$
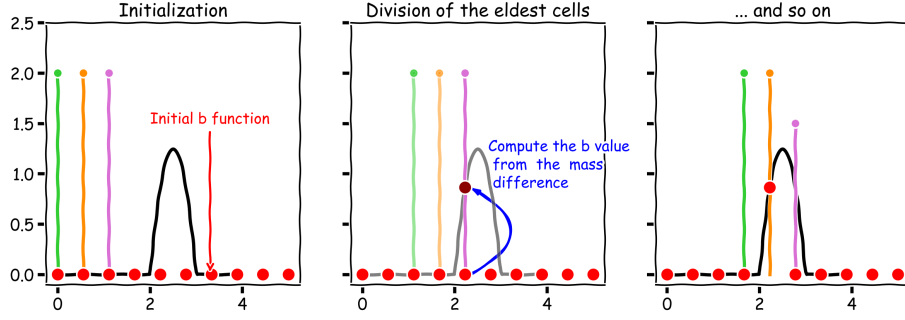
$$\tag{V.17}$$

Fig. V.2 **Illustration of Algorithm 2.** *Left panel: initial situation where all b values are set to zero (red dots). Each vertical colored segment corresponds to a Dirac mass $2\delta_{a_i}$, $i = 1, 2, 3$, of the initial Dirac comb condition (ψ). The black curve is the target b function. Middle panel: first occurrence of eldest cell division (initial ages a_3). The purple segment reaches the b function with aging at time t_k, hence the mass difference μ_k (formula (V.16)) is non-zero. Applying formula (V.18), we reconstruct the true $b[i_3 + k]$, where i_3 is the index of the discretized age a_3. Right-panel: continuation of the b updating from the same eldest cell (initial age a_3) at time $t_{k+1}, t_{k+2}, \ldots$*

Since at time t_k, $b_{i_{\max}+k}$ is zero before refreshing, we have from the numerical scheme (V.6) that $U_{k-1,i_{\max}+k-1} = U_{k,i_{\max}+k}$. Let $\tilde{u} := U_{k-1,i_{\max}+k-1}$. From the conservation law (V.17) and the μ_k definition (V.16), we deduce

$$\mu_k = -\Delta U_{k,i_{\max}+k} + \Delta(2p_S - 1)(1 - e^{-\Delta b_{i_{\max}+k}})\tilde{u} \Rightarrow b_{i_{\max}+k} = -\frac{\log(1 - x_k)}{\Delta}, \qquad \text{(V.18)}$$

with

$$x_k := \frac{\mu_k}{\Delta(2p_S - 1)\tilde{u}}.$$

These steps can be summarized by the following pseudo-code:

Initialization: give p_S, the total number of cells m and the time grid $t = (t_k)_{k \in [\![0,N]\!]}$;
Set $b_k = 0$, for all $k \in [\![0, N]\!]$;
for k *from* 0 *to* N **do**

    Compute $U_{k,n}$ with the numerical scheme (V.6) and (V.7);
    Compute the loss mass μ_k as defined in equation (V.16);
    if $|\mu_k| > 0$*:* **then**

        Compute $b[i_{\max} + k]$ using formula (V.18);
        Refresh the boundary condition and the eldest cells of age $i_{\max} + k$:

            • $U_{k,0} \leftarrow U_{k,0} + 2p_S U_{k,i}(1 - \exp(-\Delta b[i]))$

            • $U_{k,i} \leftarrow U_{k,i} \exp(-\Delta b[i])$

    end

end
Return vector b ;
Algorithm 2: Pseudo-code for the reconstruction of the b function from m and p_S.

We illustrate this method in Figure V.3 and in additional figures in Appendix A.2.3. Note that some instabilities appear in the case of the piecewise constant function (orange line) which may be due to its non-smooth character. We also performed a study on the sampling rate Δ (which appears to be in our case also the age size step) to get practical insight into the numerical convergence (stability) of the reconstruction of the estimated function with respect to Δ (see Figure A.3b in Appendix A.2.3).

V.2.2 Multi-layer case

We now consider the inverse problem (IP) with two layers (J = 2). We recall the reader that, in this case, we aim to determine all the division rates b_j, $j \in [\![1, J]\!]$ and the probability $p_S^{(j)}$, $j \in [\![1, J-1]\!]$ knowing the probability $p_S^{(J)}$ on Layer J, the initial condition ψ and the mean cell number of each layer m_j, $j \in [\![1, J]\!]$.

Theorem V.3. *Under the same hypotheses as Theorem V.2, the inverse problem (IP) is well-posed for $J = 2$.*

To prove Theorem V.3, we take advantages of the unidirectional motion of the model (V.1) and split the proof in two parts: the uniqueness of parameter $p_S^{(1)}$ and function b_1 (contribution of Layer 1), and the uniqueness of function b_2 (contribution of Layer 2). We start by the analysis of the first layer and get the following lemma:

Lemma V.2. *Under the same hypotheses as Theorem V.3, function b_1 and parameter $p_S^{(1)}$ verifying the inverse problem (IP) depend only on the total number of cells on Layer 1, m_1, and Layer 2, m_2, where m_1 and m_2 are defined by equation (V.2).*

Proof. The first cells coming from the initial condition ψ_1 enter Layer 2 at time $S_1 := A_1^{\min} - a_{\max}^{\psi}$ and start to divide at time $S_2 := A_2^{\min} + S_1$. Layer 2 is empty between $t = 0$ and $t = S_1$. From $t = S_1$ to $t = S_2$, the cells start to enter Layer 2 and are only aging. Hence, the cell density function on Layer 2, $\rho^{(2)}$, solution of the PDEs (V.1), verifies a transport equation with a source term at the boundary condition: for all $t \in [0, S_2]$,

$$\begin{cases} \partial_t \rho^{(2)}(t,a) + \partial_a \rho^{(2)}(t,a) = 0, \ a \in (0,\infty), \\ \rho^{(2)}(t,0) = 2p_S^{(1)} \displaystyle\int_0^{+\infty} b_1(a)\rho^{(1)}(t,a)\,da. \end{cases}$$

We first show that b_1 depends only on m_1 and m_2. We consider the sum of the cells on the two layers: $\rho = \rho^{(1)} + \rho^{(2)}$ and deduce from the PDEs (V.1) that

$$\partial_t \rho(t,a) + \partial_a \rho(t,a) = -b_1 \rho^{(1)}(t,a). \tag{V.19}$$

Since the b_1 function is non-zero on the interval $(A_1^{\min}, A_1^{\max})$, and the density function $\rho^{(2)}(t, \cdot)$ is non-zero on the interval $[0, t - S_1]$ for all $t \in (S_1, S_2)$, we deduce that $(A_1^{\min}, A_2^{\max}) \cap [0, t - S_1] = \emptyset$ when $t < S_1 + A_1^{\min}$. Hence, we can write using expression (V.19) that, for all $t \in (S_1, \min(S_1 + A_1^{\min}, S_2))$, $\partial_t \rho(t,a) + \partial_a \rho(t,a) = -b_1 \rho(t,a)$ and deduce that ρ is solution of the PDE:

$$\begin{cases} \partial_t \rho(t,a) + \partial_a \rho(t,a) = -b_1(a)\rho(t,a), & t \in (0, \min(S_1 + A_1^{\min}, S_2)), \ a \in (0, \infty), \\ \rho(t,0) = 2 \displaystyle\int_0^{+\infty} b_1(a)\rho(t,a)\,da, \\ \rho(0,a) = \psi(a), & a \in (0, +\infty), \end{cases}$$

(a) *Cell mean number m_1*

(b) *Estimated b functions*

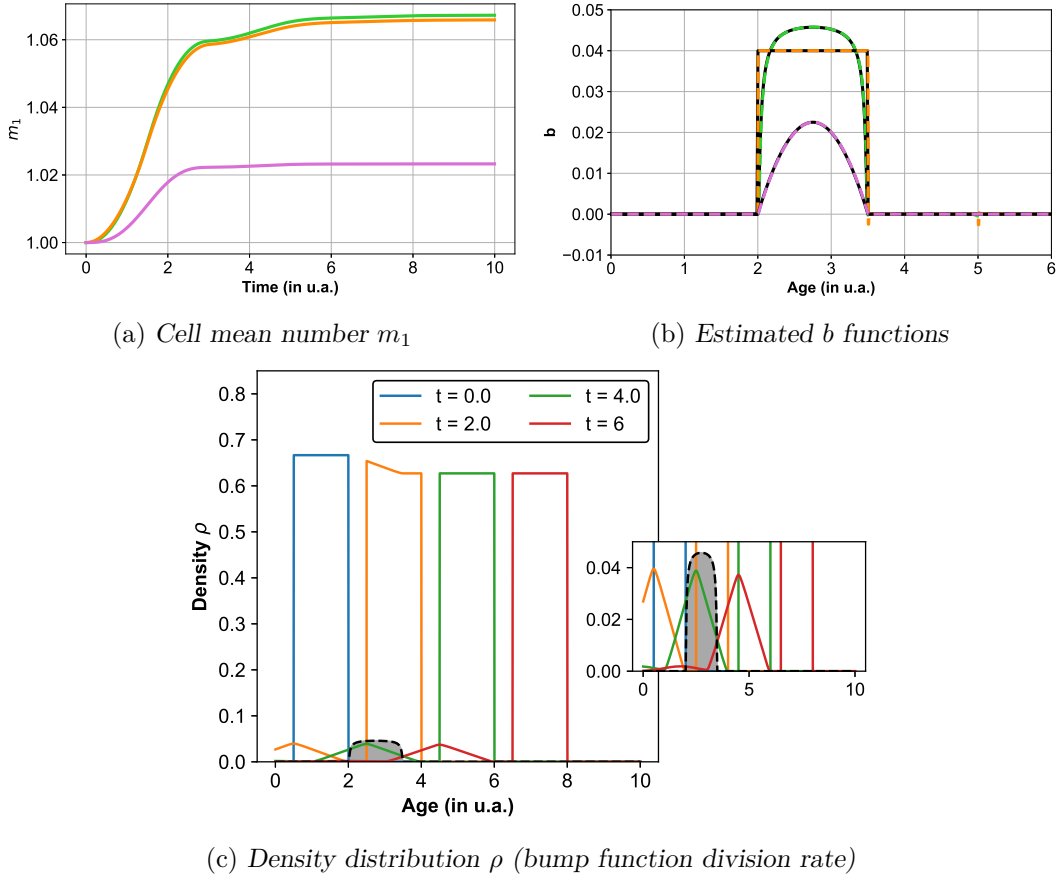(c) *Density distribution ρ (bump function division rate)*

Fig. V.3 **Illustration of the numerical procedure**. *Figure V.3a: we simulate m_1 using the numerical scheme for different b functions which are non-zero for all $a \in (2, 3.5)$: a bump function (green line) $b(a) = 0.05 \exp(\frac{0.05}{(a-2.75)^2-0.5625})$; a polynomial function (pink line) $b(a) = -0.004(a-2)(a-3.5)$ and a uniform function (orange line) $b(a) = \frac{2}{3}$. Figure V.3b: using Algorithm 2, we compute the b functions from the m_1 values. The estimated b functions are the dashed lines while the original functions are the black solid lines. Figure V.3c: we represent the simulated density distribution ρ at different time points ($t = 0, 0.5, 2, 3, 6$) for the bump b function (black dashed line) used in Figure V.3a. In all panels, $\Delta = 5*10e-3$, $\psi(a) = \mathbf{1}_{a \in [0.5,2]}(a)$ (piecewise function) and $p_S = 1$.*

Since this PDE is the same as PDE (V.8), we apply Theorem V.2 and deduce the uniqueness of b_1.

We turn now to the uniqueness of parameter $p_S^{(1)}$. Taking the derivative of both m_1 and m_2, for all $t \in [0, S_2]$, we obtain that:

$$m_1'(t) = (2p_S^{(1)} - 1) \int_0^{+\infty} b_1(a)\rho_1(t, a)\, da\,, \quad m_2'(t) = 2(1 - p_S^{(1)}) \int_0^{+\infty} b_1(a)\rho_1(t, a)\, da$$

As there exists at least one $t \in [0, S_2]$ such that $\int_0^{+\infty} b_1(a)\rho^{(1)}(t, a)\, da \neq 0$, we deduce, first,

$$m_1'(t)2(1 - p_S^{(1)}) = m_2'(t)(2p_S^{(1)} - 1),$$

and then the uniqueness of $p_S^{(1)}$. This ends the proof. $\qquad\qquad\square$

Inverse problem of an age structured population system with source term in the boundary condition

To show the uniqueness of function b_2, we first study the following inverse problem.
Let $\eta \in \mathbf{L}_1(\mathbb{R}_+)$, solution of the PDE

$$\begin{cases} \partial_t \eta(t, a) + \partial_a \eta(t, a) = -b(a)\eta(t, a), & t \in (0, \infty),\ a \in (0, \infty), \\ \eta(t, 0) = g(t) + 2 \int_0^{+\infty} b(a)\eta(t, a)\, da, \\ \eta(0, a) = \psi(a), \end{cases} \qquad (V.20)$$

with g a differentiable function on $\mathbb{R}_+$ supposed to be known and $\psi \in \mathcal{C}_c((a_{\min}^\psi, a_{\max}^\psi))$. We also suppose that $b \in \mathcal{C}_c((A^{\min}, A^{\max}))$ (Hypothesis V.1).
We investigate the inverse problem associated with the model (V.20):

$\widetilde{IP}$ Given the initial condition ψ, the function $\tilde{m}(t) := \int_0^{+\infty} \eta(t, a)da$ and the function g, both defined for all $t \in [0, T)$, with $T > 0$, determine function b such that the direct problem (V.20) is satisfied on $[0, T]$.

In the same way as in sub-section V.2.1, we can show that the inverse problem $\widetilde{IP}$ can be reformulated as a Fredholm integral equation

Lemma V.3. *Under Hypothesis V.1 and supposing that* $\psi \in \mathcal{C}_c((a_{\min}^\psi, a_{\max}^\psi))$, *we define* $f_2(t) := -\tilde{m}(t) + 2\tilde{m}(0) + \int_0^t g(a)da$. *Then, we have for all* $t \in [0, A^{\min}]$

$$f_2(t) = \int_{a_{\min}^\psi}^{a_{\max}^\psi} \psi(a)e^{-\int_a^{a+t} b(s)ds}da. \qquad (V.21)$$

Proof. In the same way as for the proof of Theorem V.3, we can write that

$$\tilde{m}(t) = \underbrace{\int_0^t \eta(t - a, 0)e^{-\int_0^a b(s)ds}da}_{\text{new born cells}} + \underbrace{\int_t^{t + a_{\max}^\psi} \psi(a - t)e^{-\int_{a-t}^a b(s)ds}da}_{\text{remaining mother cells}}. \qquad (V.22)$$

To obtain a relation between the boundary condition $\eta(t,0)$ on the one hand and, $\widetilde{m}(t)$ and $g(t)$ on the other hand, for all $t \geq 0$, we follow the same approach as in Lemma V.10 and get

$$\widetilde{m}(t) = \underbrace{\int_{a^\psi_{\min}+t}^{a^\psi_{\max}+t} \rho(t,a)da}_{\text{initial cells}} + \underbrace{\int_0^t \rho(t,a)da}_{\text{cells born}}.$$

Note that here the cells born are both coming from the source term g and the division rate b. Using the changes of variables $s = a - a^\psi_{\min} + t$ and $s = \frac{a}{t}$, we obtain that :

$$\widetilde{m}'(t) = -\int_0^{+\infty} b(a)\rho(t,a)da + \rho(t,0) = -\frac{\rho(t,0) - g(t)}{2} + \rho(t,0) \Rightarrow \rho(t,0) = 2\widetilde{m}'(t) - g(t).$$

If g is lattice, before using the changes of variables, the interval $(0,t)$ needs to be split in as many sub-intervals as necessary, so that the function is non-lattice.
Combining the expression of $\widetilde{m}'$ with expression (V.22) and using that $b \in \mathcal{C}_c((A^{\min}, A^{\max}))$, we deduce that, for all $t \in [0, A^{\min}]$,

$$\widetilde{m}(t) = 2\left[\widetilde{m}(t)\right]_0^t - \int_0^t g(a)da + \int_t^{t+a^\psi_{\max}} \psi(a-t)e^{-\int_{a-t}^a b(s)ds}da. \tag{V.23}$$

We finally deduce expression (V.21) from expression (V.23). □

Hence, since ψ is a compactly supported function, we deduce the well-posedness of the inverse problem $\widetilde{IP}$ from the application of Theorem V.2 with the suitable hypotheses.
We can now proceed to the proof of Theorem V.3.

Proof of Theorem V.3. The uniqueness of function b_1 and parameter $p_S^{(1)}$ is a consequence of Lemma V.2. We now prove the uniqueness of function b_2. Between $t = S_2$ and $t = S_3 := A_2^{\min} + S_2$, in the same way as in the single layer case, only cells born from Layer 1 mother cells can divide.
Let $g(t) := 2(1 - p_S^{(1)})\int_0^{+\infty} b_1(a)\rho_1(t,a) = \frac{2p_S^{(1)} - 1}{2p_S^{(1)}}m_1'(t)$, according to Lemma V.1. Since $p_S^{(1)}$ is known by definition of our inverse problem (IP), we deduce that g is entirely known. Then, for all $t \in (S_2, S_3)$, $\rho^{(2)}$ verifies

$$\begin{cases} \partial_t\rho^{(2)}(t,a) + \partial_a\rho^{(2)}(t,a) = -b_2\rho^{(2)}(t,a), \quad a \in (0,\infty), \\ \rho^{(2)}(t,0) = g(t) + 2\int_0^{+\infty} b_2(a)\rho^{(2)}(t,a)\,da, \\ \rho^{(2)}(S_2,a) = 2(1 - p_S^{(1)})\int_0^{+\infty} b_1(s)\rho_1(S_2 - a, s)ds, \end{cases}$$

Since this model is equivalent to PDE (V.20) (by performing a time translation $t - S_2$), we can apply Lemma V.3 and deduce that, for all $t \in (S_2, S_3)$,

$$f_2(t) = \int_{a^\psi_{\min}}^{a^\psi_{\max}} \rho^{(2)}(S_2,a)e^{-\int_a^{a+t} b_2(s)ds}da,$$

where $f_2(t) = -m_2(t) + 2m_2(0) + \int_0^t g(a)da = -m_2(t) + 2m_2(0) + \frac{2p_S^{(1)} - 1}{2p_S^{(1)}}(m_1(t) - m_1(0)$.
Here, the support of the initial condition $\rho^{(2)}(S_2,a)$ is $(0, A_2^{\min})$, so that Hypothesis V.5 is verified. Applying Theorem V.2, we deduce that b_2 is unique. This ends the proof. □

Using the unidirectional motion again, we can extend Theorem V.3 to the case of more than two layers, $N \geq 2$.

Remark V.5 (Self-renewal case)**.** *If we consider the case when the first layer is self-renewing (m_1 is constant), then since $m_1(t) = \bar{m}_1$ implies that $p_S^{(1)} = \frac{1}{2}$, we can nevertheless recover function b_2 (and $p_S^{(1)}$) using Theorem V.3.*

V.3 Analysis of the inverse problem (IP) for Dirac measure initial conditions

We turn now to the case of Dirac mass as initial condition. We suppose that the results proposed in [165, 34] for the renewal equation ($p_S = \frac{1}{2}$ and b non-lattice and bounded after a given age a^*) can be extended to our case ($p_S \in (0,1]$ and lattice function b). We also admit that the characteristic formula (V.4) is verified for the measure solutions $\mu_t \in \mathcal{M}(\mathbb{R}_+)$, the set of signed Borel measures on $\mathbb{R}_+$: for all $t \geq 0$, for all $a \geq 0$,

$$\mu_t(a) = \mathbf{1}_{[0,t]}(a)\mu_{t-a}(0)\exp\left(-\int_0^a b(u)du\right) + \mathbf{1}_{[t,+\infty)}(a)\psi(a-t)\exp\left(-\int_{a-t}^a b(u)du\right),$$

$$\mu_t(0) = 2p_S\int_{\mathbb{R}_+} b(a)d\mu_t(a), \quad \text{(V.24)}$$

in the sense that, for all $h \in \mathcal{C}_c(\mathbb{R}_+)$,

$$\int_{\mathbb{R}_+} h(a)d\mu_t(a) = \int_0^t \mu_{t-a}(0)\exp\left(-\int_0^a b(u)du\right)h(a)da + \int_t^{+\infty}\exp\left(-\int_{a-t}^a b(u)du\right)h(a)d\psi(a-t).$$
$$\text{(V.25)}$$

In the same way as for the continuous initial condition case, we derive the following equation, which is the formal analog of the Fredholm integral equation in Theorem V.1.

Theorem V.4. *Under Hypothesis V.1, and supposing that $\psi \in \mathcal{M}([a_{\min}^\psi, a_{\max}^\psi])$ and $p_S \neq \frac{1}{2}$, we define $f(t) := -\frac{1}{2p_S-1}m_1(t) + \frac{2p_S}{2p_S-1}m_1(0)$. Then, we have for all $t \in [0, A^{\min}]$*

$$f(t) = \int_{a_{\min}^\psi}^{a_{\max}^\psi}\exp\left(-\int_a^{a+t}b(s)ds\right)d\psi(a).$$

Proof. Taking $h(a) = b(a)$ in relation (V.25) , we deduce from formula (V.24) that for all $t \geq 0$,

$$\mu_t(0) = 2p_S\left[\int_0^t b(a)\mu_{t-a}(0)\exp\left(-\int_0^a b(u)du\right)da + \int_t^{+\infty}b(a)\exp\left(-\int_{a-t}^a b(u)du\right)d\psi(a-t)\right].$$

Then, since $t \in [0, A^{\min}]$, we deduce from Hypothesis V.1 that

$$\mu_t(0) = 2p_S\int_t^{+\infty}b(a)\exp\left(-\int_{a-t}^a b(u)du\right)d\psi(a-t) = 2p_S\int_0^{+\infty}b(s+t)\exp\left(-\int_s^{s+t}b(u)du\right)d\psi(s),$$
$$\text{(V.26)}$$

with the change of variables $s = a - t$. Then, using relation (V.26) in (V.25), we obtain that for all $h \in \mathcal{C}_c(\mathbb{R}_+)$,

$$\int_{\mathbb{R}_+} h(a) d\mu_t(a) = 2p_S \int_0^t \left[\int_0^{+\infty} b(s + t - a) \exp\left(- \int_s^{s+t-a} b(u) du \right) d\psi(s) \right] \exp\left(- \int_0^a b(u) du \right) h(a) da$$
$$+ \int_t^{+\infty} \exp\left(- \int_{a-t}^a b(u) du \right) h(a) d\psi(a - t). \quad \text{(V.27)}$$

Taking $h(a) = \mathbf{1}_{[0, a_{\max}^\psi + A^{\min}]}(a)$, we deduce from relation (V.27) that:

$$m(t) = 2p_S \int_0^t \left[\int_0^{+\infty} b(s + t - a) \exp\left(- \int_s^{s+t-a} b(u) du \right) d\psi(s) \right] \exp\left(- \int_0^a b(u) du \right) da$$
$$+ \int_t^{+\infty} \exp\left(- \int_{a-t}^a b(u) du \right) d\psi(a - t). \quad \text{(V.28)}$$

Since $t \in [0, A^{\min}]$, we have

$$\int_0^t \left[\int_0^{+\infty} b(s + t - a) \exp\left(- \int_s^{s+t-a} b(u) du \right) d\psi(s) \right] \exp\left(- \int_0^a b(u) du \right) da$$
$$= \int_0^t \left[\int_0^{+\infty} b(s + t - a) \exp\left(- \int_s^{s+t-a} b(u) du \right) d\psi(s) \right] da.$$

Then, applying first Fubini theorem then an integration by part, we deduce:

$$\int_0^t \left[\int_0^{+\infty} b(s + t - a) \exp\left(- \int_s^{s+t-a} b(u) du \right) d\psi(s) \right] da = \int_0^{+\infty} \left(1 - \exp\left(- \int_s^{s+t} b(u) du \right) \right) d\psi(s).$$
$$\text{(V.29)}$$

Using relation (V.29) in (V.28), we deduce that

$$m(t) = 2p_S \int_{\mathbb{R}_+} d\psi(s) - (2p_S - 1) \int_{\mathbb{R}_+} \exp\left(- \int_s^{s+t} b(u) du \right) d\psi(s)$$

and conclude. $\qquad \square$

Synchronized population

We consider a synchronized population $\psi(a) = \psi_0 \delta_{a_0}(a)$ ($N = 1$ in the definition of ψ (V.3)).

Corollary V.1 (Synchronized population)**.** *Under Hypotheses V.1 and V.3, we have, for all $t \in [0, A^{\min}]$,*

$$b(a_0 + t) = -\frac{f'(t)}{f(t)}. \quad \text{(V.30)}$$

Proof. Applying Theorem V.4 with $\psi(a) = \psi_0 \delta_{a_0}(a)$, we obtain for all $t \in [0, A^{\min}]$,

$$\psi_0 e^{- \int_{a_0}^{a_0+t} b(s) ds} = f(t).$$

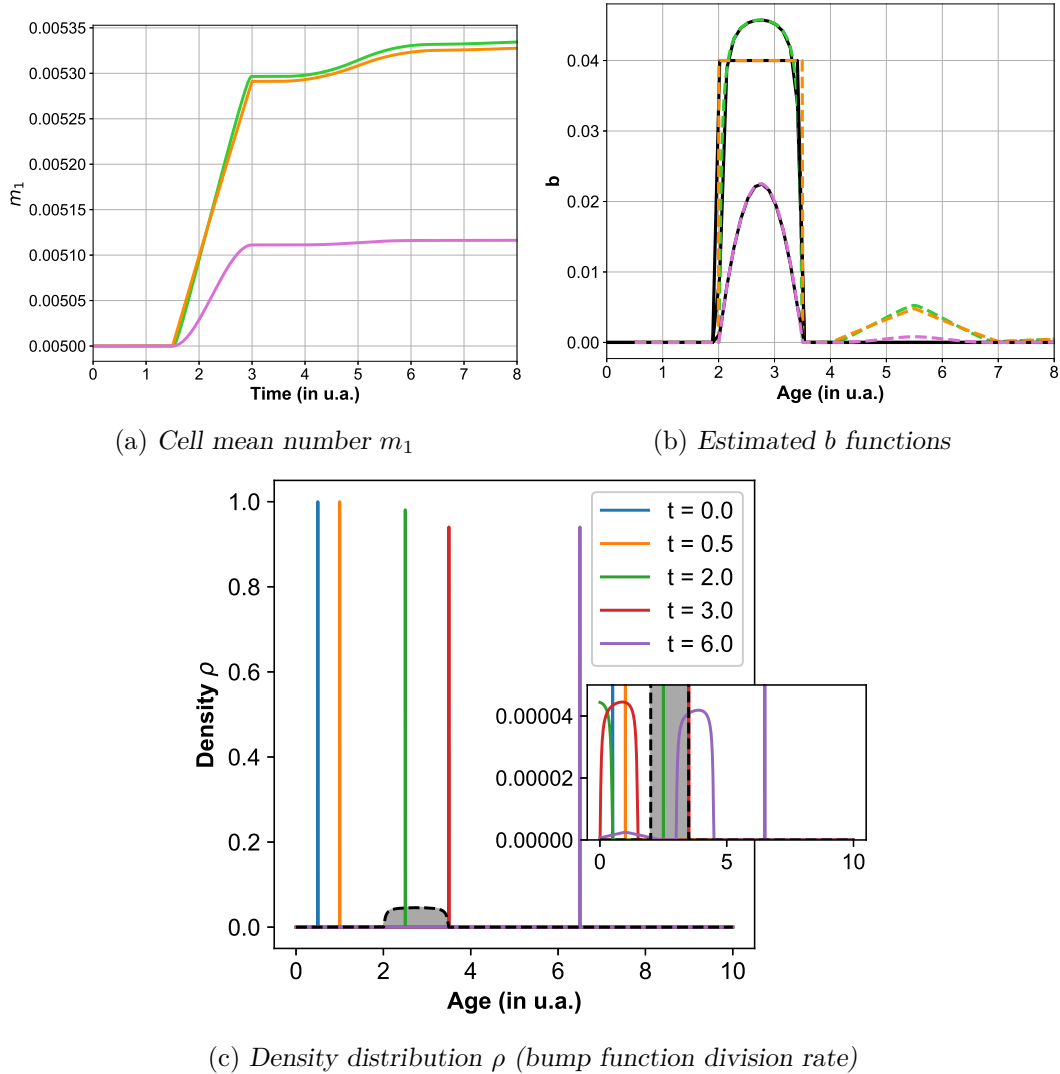Then, taking the logarithm function and taking the derivative with respect to time, we obtain formula (V.30). $\qquad \square$

(a) *Cell mean number m_1*

(b) *Estimated b functions*

(c) *Density distribution ρ (bump function division rate)*

Fig. V.4   *Illustration of Corollary V.1. Figure V.4a: in the same way as in Figure V.3, we simulate m_1 using the numerical scheme for the same b functions as in Figure V.3. Figure V.4b: applying formula (V.30), we compute the b functions from the m_1 values. The estimated b functions are the dashed lines while the original functions are the black solid lines. Figure V.4c: we represent the simulated density distribution ρ at different time points ($t = 0, 0.5, 2, 3, 6$) for the bump function (black dashed line) used in the Figure V.4a. In all panels, $\Delta = 5 * 10e - 3$, $\psi(a) = \delta_{0.5}(0)$ and $p_S = 1$.*

Corollary (V.1) is illustrated in Figure V.4 for different b functions. Between $t = 0$ and $t = 4$, the reconstructed b values in the three presented cases are identical to the expected ones. However, we can note that after $t = 4$, the reconstructed b values are no more consistent with the expected ones, which can be explained by the fact that formula (V.30) is verified only for $t \in [0, A^{\min}]$.

If $A^{\min} + a_0 \geq A^{\max}$ and p_S is known, we deduce the uniqueness of the b function from Corollary (V.1). In addition, we have an explicit formula to retrieve b from the observation

m_1 and the parameter p_S, as illustrated in Figure V.5. On the contrary, if $A^{\min} + a_0 < A^{\max}$, the b function can only be partially reconstructed on $[0, A^{\min} + a_0)$. In that case, the uniqueness is a consequence of the additional Hypothesis V.4.

Note that if Hypothesis V.5 is not verified, i.e. $a_0 > A^{\min}$, the b function can only be partially reconstructed as illustrated in Figure V.5.
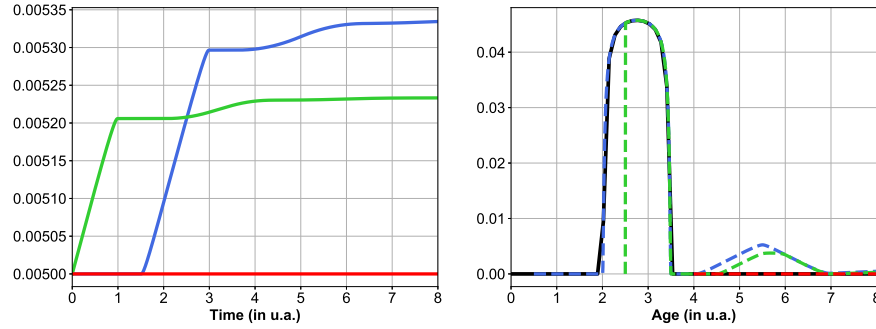
(a) *Complementary illustrations of Corollary V.1 for different initial conditions*
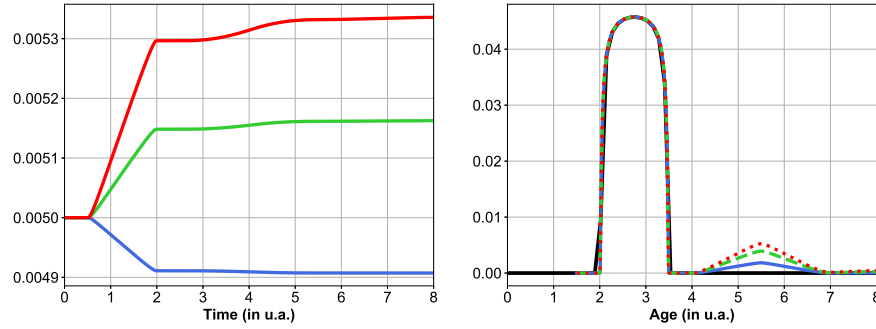
(b) *Complementary illustrations of Corollary V.1 for different p_S values*

Fig. V.5 *Complementary illustrations of Corollary V.1. We proceed in the same way as Figure V.4 using the bump function and for either different initial conditions (Figure V.5a): $\psi(a) = \delta_{0.5}(a)$ (blue line); $\psi(a) = \delta_{2.5}(a)$ (green line) and $\psi(a) = \delta_4(a)$ (red line), with $p_S = 1$, or different p_S values (Figure V.5b): $p_S = 0.35$ (blue line), $p_S = 0.75$ (green line) or $p_S = 1$ (red line), with $\psi(a) = \delta_{1.5}(a)$. In each subfigure, the left panel represents the mean cell number m_1 with respect to time, while the right panel represents the estimated b functions.*

Discrete non-synchronized population

We now consider a Dirac comb as initial condition: $\psi(a) = \displaystyle\sum_{i=0}^{N} \Psi_i \delta_{a_i}(a)$ with $N \geq 2$.

Corollary V.2 (Discrete non-synchronized population)**.** *Under Hypotheses V.1, V.3, V.4 and V.5, the problem (IP) is well-posed.*

Proof. To prove the uniqueness of the b function considering that the f function is known for all t, we proceed by induction and first prove that, for all $k \geq 0$,

$$f^{(k)}(t) = \phi_k(t)Q(t) + R^{(k)}(t) \tag{V.31}$$

with the series of functions ϕ_k defined as

$$\phi_{k+1}(t) = \phi_k'(t) - b(a_0 + t)\phi_k(t), \ \phi_0(t) = 1, \tag{V.32}$$

where $Q(t) := \Psi_0 \exp(-\int_{A^{\min}}^{a_0+t} b(s)ds)$ and $R(t) := \sum_{i=1}^{N} \Psi_i \exp(-\int_{A^{\min}}^{a_i+t} b(s)ds)$.
For $k = 0$, we apply Theorem V.4 and obtain that, for all $t \in [0, A^{\min}]$,

$$f(t) = \sum_{i=0}^{N} \Psi_i \exp\left(-\int_{a_i}^{a_i+t} b(s)ds\right) = \sum_{i=0}^{N} \Psi_i \exp\left(-\int_{A^{\min}}^{a_i+t} b(s)ds\right) = Q(t) + R(t). \tag{V.33}$$

Then, assuming that (V.31) is true up to rank k, we compute the time derivative of (V.31), so that for all $t \in [0, A^{\min}]$

$$f^{(k+1)}(t) = \phi_k'(t)Q(t) + \phi_k(t)Q'(t) + R^{(k+1)}(t) = \phi_{k+1}(t)Q(t) + R^{(k+1)}(t),$$

since $Q'(t) = -b(a_0 + t)Q(t)$ and ϕ_k satisfies (V.32). This ends the induction.

We can now turn to the well-posedness of the inverse problem (IP).
From Hypothesis V.5, we deduce that $A^{\min} > a_i$ for all $i \in [\![1, N]\!]$. Let us consider the positive time $\tau := A^{\min} - a_1$. Then, as $b \in \mathcal{C}_c\left((A^{\min}, A^{\max})\right)$ (Hypothesis V.1), we obtain that, for all $k > 0$,

$$R^{(k)}(\tau) = 0. \tag{V.34}$$

Then, from expression (V.33), we get

$$f(\tau) = \psi_0 \exp\left(-\int_{A^{\min}}^{a_0+\tau} b(s)ds\right) + \sum_{i=1}^{N} \Psi_i$$

hence $Q(\tau) = f(\tau) - \sum_{i=1}^{N} \Psi_i$. Combining this with (V.34) and (V.33), we deduce that, for all $k \geq 0$,

$$\phi_k(\tau) = \frac{f^{(k)}(\tau)}{f(\tau) - \sum_{i=1}^{N} \Psi_i}.$$

We thus deduce that, for all $k \geq 0$, $\phi_k(\tau)$ depends only on the f function and the initial condition ψ. From the recurrence relation (V.32), we have that ϕ_k depends on the $k - 1$ first derivatives of b. Hence, we deal with an invertible triangular system since the diagonal coefficients are equal to one, and we deduce the uniqueness of $b^{(k)}(a_0 + \tau)$ for each $k \geq 0$. We then deduce the uniqueness of b on its whole support, from Hypothesis V.4. $\qquad\square$

Using Corollary V.2, we can extend the results of Theorem V.3 to the case of Dirac measures initial conditions.

V.4 Conclusion

In this paper, we have analyzed an inverse problem associated with a multi-type version of the McKendrick–VonFoerster model, and consisting of retrieving the division rate functions b_j, and the probability of motion $p_S^{(j)}$, for $j \in [\![1, J-1]\!]$, from the knowledge on the total cell numbers on each layer. We chose to deal with compactly supported division rates, which account for both a recovery time after birth ($A^{\min}$) and a quiescent state beyond a given age ($A^{\max}$), and we have considered both synchronized or non-synchronized initial populations on

the first layer, and supposed that all other layers are empty at initial time. If no division has occurred at the initial time[1] ($A^{\min} - a_{\max}^{\psi} \geq 0$), the entire division rate can be reconstructed. This condition is encountered in the literature, see e.g. [98].

For continuous initial conditions, we have shown the well-posedness of the inverse problem, first in the single layer case (see Theorem V.2), and then in the several layer case (see Theorem V.3 [2]), after introducing a sequence of nested submodels with an additional source term due to migration in the boundary condition. Then, we show the same result in the single layer case for a discrete initial condition (Corollary V.1); we assume that the PDE (V.8) admits a measure solution, and construct this solution from the characteristic lines. Proving these latter assumptions is beyond the scope of this article and remains as an interesting open problem.

In the self-renewal case ($p_S^{(j)} = \frac{1}{2}$) for a layer j, the b_j function cannot be retrieved from the current observation (Remark V.3), even if the migration proportion parameters can be (Remark V.5). We speculate that supplying additional observation such as the age-weighted distribution ($\int_0^\infty a\rho^{(j)}(t,a)da$) could help to recover the identification property. In the cumulative formulation framework and suitable hypotheses, there is no particular difficulty with this case (see Theorem 4.3, [93]).

Instead of the total cell number, we could consider microscopic observation. In [95], the authors have shown, using a semi-group approach for the non-renewal version of the McKendrick–VonFoerster equation, that the death rate can be determined from observation of the age distribution at two time points including the initial time. Since, according to Lemma V.1, there is a link between the net birth function $\rho(t,0)$ and the total number of cells m_1, we expect to be able to obtain similar results.

Acknowledgments

---

[1]Additional (post-publication) comment: note that the hypothesis needed in Theorem V.1 can even be less restrictive than Hypothesis V.5. Indeed, the proof of Theorem V.1 only requires that there is no overlapping between the division times from different cell generations (mother, daughter, granddaughter cells etc).

[2]Additional (post-publication) comment: the proof is detailed in the case $J = 2$ with the natural choice $p_S^{(2)} = 1$. In the case $J > 2$, one would need to modify boundary condition (V.20) as $\eta(t,0) = g(t) + 2p_S^{(j)} \int_0^{+\infty} b(a)\eta(t,a)$ with $j > 1$. The following steps can be achieved in the same way with no more difficulty.

Chapter VI

Discussion and perspectives

In this thesis, we modeled two stages of the ovarian follicle development during its basal phase (follicle activation and compact growth) by combining stochastic and deterministic formalisms. We then analyzed these two models with complementary theoretical and numerical approaches and developed dedicated tools for this end. On the stochastic side, we proposed a rigourous numerical algorithm based on the truncated domain method and coupling techniques to compute some moments of a nonlinear stochastic process at the extinction time of a given cell population (Chapter 2). We studied the asymptotic behaviors of an age- and type- structured cell population (multi-type Bellman–Harris model) subject to unidirectional motion and derived explicit analytical formulas for the asymptotic cell number moments. On the deterministic side, we analyzed as well the asymptotic behavior of the deterministic counterpart of this model, which consists of a multi-type McKendrick–VonFoerster equation. Adapting the relative entropy method, we showed the existence of stable age state and obtained explicit analytical formulas (Chapter 3). We also studied the inverse problem related to our deterministic model for some division rates (continuous compactly supported functions) and different types of initial conditions (either compactly supported or Dirac measures)(Chapter 5). For both stochastic and deterministic frameworks, we simulated our models using classical algorithms (SSA algorithm [52] or Gillespie algorithm [61] for the stochastic models) or designing new ones (finite volume method in Chapter 3 and finite difference method based on the method of charateristics in Chapter 5). Finally, we calibrated our two models using a likelihood approach. To confront our dynamical models with rather "time-free" data, we either enriched the dataset with kinetics information (Chapter 3) or changed the time clock of our model (Chapter 2).

The two models presented have a common point: they both represent cell dynamics with unidirectional motion. This means that the cell dynamics of a population decomposed into J types evolves in a special way: a type-j cell can only be transformed or divide into one or more type-$\geqslant j$ cells. The transition rates between any two types may depend on the whole system, such as for the activation follicle model presented in Chapter 2. Unidirectionality is a pattern that can be found in other examples of cell biology: the immune system, neurogenesis [9], horizontal gene transfer [167], cell labeling in cell kinetics studies [168]. In particular, the non-local boundary condition of this model, associated with each cell division number i, only takes into account contributions of cells with cell division number $i-1$ (i.e. $p_S^{(j)} = 0$). etc. Very recently, the authors have analyzed in [167] the size dynamics of a population driven by horizontal gene transfer, birth and death mechanisms. The population is structured by a

trait taking a finite number of values. Using a large population analysis, they quantify the asymptotic dynamics of each subpopulation size on a logarithm scale.

The unidirectionnal aspect of our models was an advantage since it allowed us to decompose the global dynamics into subcategories, for example to prove asymptotic convergence results (Chapter 3) or to solve an inverse problem (Chapter 5). It also allowed us to divide the dynamics of the transitional system of the model presented in Chapter 2 into two parts: before and after the extinction of the precursor cell population. Depending on the behavior of the first compartment (extinction, explosion or constant), it is therefore possible to characterize the transient state of a cell population by providing characteristic times, which may be relevant in a developmental biology context. This aspect has been highlighted in [167] where the authors show the existence of "metastable" states: the asymptotic dynamics of their normalized process is characterized by a succession of deterministic time intervals (phases) delimited by changes of resident or dominant traits. As regards our Chapter 3 model, characteristic times could correspond to a time sequence $(t_j)_{j\in[\![1,J]\!]}$ such that the process $(\rho^{(i)}(t,\cdot))_{i\in[\![1,j]\!]}$ stabilizes around the stable age distribution $(\hat{\rho}^{(i)})_{i\in[\![1,j]\!]}$ during the time interval $[t_j, t_{j+1}]$. Other characteristic times can be designed and it is thus still an open interesting question.

In this thesis, we have chosen to use a formalism where the spatial position of the cell is represented by a discrete index, but a continuous index may be consider. For instance, the multi-type MK–VF version (discrete types) presented in Chapter 3 was studied in a case of continuous type variables in [48]. In this work, the authors extend the results proposed in [26] and show the asymptotic convergence in a case where the "birth matrix" is reducible and the "birth and death matrices" are non-smooth. A large population and size scale limit analysis of the [CMMS] model [1] has been done recently in [3] (see details in Chapter 4), where the author has obtained a Keller-Segel -like model. Suggestions for improvement were proposed in Chapter 4 based on cancer models that have been the subject of recent works, see for example [152, 154]. The approach based on the incompressible-compressible limit seems to be an interesting aspect to be studied from many points of view: modeling, simulations, theoretical analyses, etc. It would also make it possible to take a step forward in the understanding of the coupling between oocyte growth and cell proliferation.

To conclude, we have developed two numerical generators coupled with appropriate data fitting procedures, that simulate the cell number of an ovarian follicle during the early stages of its development (activation and compact growth phase) and enable us to reconstruct the follicle spatial structure. These numerical tools can be used to explore new approaches such as the incompressible-compressible limit, or be refined by adding ingredients: a finer calibration, a finer spatial structure representation, a better representation of cell interactions (oocyte-somatic cells, somatic cell-somatic cell) etc.

Appendix A

Appendix

A.1 Additionnal materials of Chapter 3

A.1.1 Supplemental proofs: deterministic model

Proof of Corollary III.1. According to Hypothesis III.4,

$$\exists A > 0, \, \epsilon > 0 \text{ such that } \forall a \geq A, \, b_j(a) + \lambda_j > \epsilon. \tag{A.1}$$

Let $k \in \mathbb{N}$. Using Hypothesis III.2, for all $t \geq A$, we have:

$$0 \leq t^k b_j(t) e^{-\int_0^t [b_j(s) + \lambda_j] \, ds} \leq \bar{b}_j t^k e^{-\int_0^A [b_j(s) + \lambda_j] \, ds} e^{-\int_A^t [b_j(s) + \lambda_j] \, ds}.$$

Then, using (A.1) we obtain:

$$0 \leq t^k b_j(t) e^{-\int_0^t [b_j(s) + \lambda_j] \, ds} \leq t^k K_{A,\epsilon} e^{-\epsilon t},$$

where $K_{A,\epsilon}$ is a constant given by $K_{A,\epsilon} := \bar{b}_j e^{-\int_0^A [b_j(s) + \lambda_j - \epsilon] \, ds}$. As $\epsilon > 0$, the function $t \mapsto t^k e^{-\epsilon t}$ is integrable on $\mathbb{R}_+$, and we deduce that $\int_A^{+\infty} t^k e^{-\lambda_j t} d\mathcal{B}_j(t) dt < \infty$. Using the continuity of b_j (Hypothesis III.2), we conclude that $t \mapsto e^{-\lambda_j t} d\mathcal{B}_j(t) dt$ is integrable on $\mathbb{R}_+$. $\qquad\square$

Proof of Corollary III.2. According to (III.11), we obtain:

$$\forall j \in [\![1, c]\!], \, \frac{\phi^{(j)}(a)}{2[p_S^{(j)} \phi^{(j)}(0) + p_L^{(j)} \phi^{(j+1)}(0)]} = \int_a^{+\infty} b_j(s) e^{-\int_a^s \lambda_c + b_j(u) du} ds \, .$$

According to Remark III.1 and Hypothesis/Definition III.2, we deduce that $\lambda_c > -\bar{b}_j$, $\forall j \in [\![1, J]\!]$. Hence, using also Hypothesis III.2, we have:

$$\frac{\phi^{(j)}(a)}{2[p_S^{(j)} \phi^{(j)}(0) + p_L^{(j)} \phi^{(j+1)}(0)]} \geq \underline{b}_j \int_a^{+\infty} e^{-(\lambda_c + \bar{b}_j)(s-a)} ds = \frac{\underline{b}_j}{\lambda_c + \bar{b}_j},$$

and reminding that $\lambda_c > 0$ (see remark III.1), we also obtain the right-side of (III.12):

$$\frac{\phi^{(j)}(a)}{2[p_S^{(j)}\phi^{(j)}(0) + p_L^{(j)}\phi^{(j+1)}(0)]} \leq \int_a^{+\infty} b_j(s)e^{-\int_a^s b_j(u)du}ds$$

$$= [-e^{-\int_a^s b_j(u)du}]_a^{+\infty} = 1.$$

$\square$

Proof of Lemma III.1. For $j \in [\![1, J]\!]$, any solution of (III.6) in $\mathbf{L}^1(\mathbb{R}_+)$ is given by:

$$\hat{\phi}^{(j)}(a) = \hat{\phi}^{(j)}(0)e^{\int_0^a[\lambda_j + b_j(s)]ds}[1 - 2p_S^{(j)}\int_0^a b_j(s)e^{-\int_0^s[\lambda_j + b_j(u)]du}ds].$$

According to Hypothesis/Definition III.1, $1 = 2p_S^{(j)}\int_0^{+\infty} b_j(s)e^{-\int_0^s[\lambda_j + b_j(u)]du}ds$, thus

$$\hat{\phi}^{(j)}(a) = 2p_S^{(j)}\hat{\phi}^{(j)}(0)\int_a^{+\infty} b_j(s)e^{-\int_a^s[\lambda_j + b_j(u)]du}ds.$$

Finally, according to Remark III.1, $\lambda_j > -\overline{b}_j$ and we obtain, using Hypothesis III.2,

$$\frac{\hat{\phi}^{(j)}(a)}{\hat{\phi}^{(j)}(0)} = 2p_S^{(j)}\int_a^{+\infty} b_j(s)e^{-\int_a^s[\lambda_j + b_j(u)]du}ds \geq 2p_S^{(j)}\underline{b}_j\int_a^{+\infty} e^{-(\lambda_j+\overline{b}_j)(s-a)}ds = 2p_S^{(j)}\frac{\underline{b}_j}{\lambda_j + \overline{b}_j}.$$

Then, we want to show that $\hat{\phi}^{(j)}(a) < \infty$ for all $a \in \mathbb{R}_+ \cup \{\infty\}$. Let

$$I(a) := \int_a^{+\infty} b_j(s)e^{-\int_0^s[\lambda_j + b_j(u)]du}ds.$$

Applying an integration by part to $I(a)$, we obtain that, for all $a \geq 0$,

$$I(a) = \left[e^{-\int_0^s[\lambda_j + b_j(u)]du}\right]_a^\infty - \lambda_j\int_a^\infty e^{-\int_0^s[\lambda_j + b_j(u)]du}ds.$$

Hypothesis/Definition III.1 and Hypothesis III.2 imply that, for all $a \geq 0$, $\int_a^\infty e^{-\int_0^s[\lambda_j + b_j(s)]ds} < \infty$ and so,
$\lim_{s \to 0} e^{-\int_0^s[\lambda_j + b_j(u)]du} = 0$. Thus, we have:

$$I(a) = e^{-\int_0^a[\lambda_j + b_j(u)]du} - \lambda_j\int_a^\infty e^{-\int_0^s[\lambda_j + b_j(u)]du}ds. \tag{A.2}$$

Multiplying (A.2) by $e^{\int_0^a[\lambda_j + b_j(u)]du}$, we deduce:

$$\frac{\hat{\phi}^{(j)}(a)}{2p_S^{(j)}\hat{\phi}^{(j)}(0)} = 1 - \lambda_j\int_a^\infty e^{-\int_a^s[\lambda_j + b_j(u)]du}ds. \tag{A.3}$$

If $\lambda_j \geq 0$, we deduce directly from (A.3) that, for all $a \in \mathbb{R}_+ \cup \{\infty\}$, $\frac{\hat{\phi}^{(j)}(a)}{2p_S^{(j)}\hat{\phi}^{(j)}(0)} \leq 1$. We assume that $\lambda_j < 0$. Using Hypothesis III.4, we deduce that there exists constants $A > 0$ and $\epsilon > 0$ such that

$$\forall a \geq A, \quad \lambda_j + b_j(a) > \epsilon > 0.$$

Hence, with $C = \frac{-\lambda_j}{\epsilon} > 0$, we have:

$$\forall a \geq A, \quad -\lambda_j \leq C(\lambda_j + b_j(a)).$$

Applying this inequality to (A.3), we obtain:

$$\forall a \geq A, \quad \frac{\hat{\phi}^{(j)}(a)}{2p_S^{(j)}\hat{\phi}^{(j)}(0)} \leq 1 + C \int_a^\infty [\lambda_j + b_j(s)]e^{-\int_0^s [\lambda_j + b_j(u)]du}ds \times e^{\int_0^a [\lambda_j + b_j(s)]ds}.$$

Again, using Hypothesis/Definition III.1 and Hypothesis III.2, we obtain:

$$\int_a^\infty [\lambda_j + b_j(s)]e^{-\int_0^s [\lambda_j + b_j(u)]du}ds = \left[-e^{-\int_0^s [\lambda_j + b_j(u)]du}\right]_a^\infty = e^{-\int_0^a [\lambda_j + b_j(u)]du}.$$

We deduce

$$\forall a \geq A, \quad \frac{\hat{\phi}^{(j)}(a)}{2p_S^{(j)}\hat{\phi}^{(j)}(0)} \leq 1 + C.$$

As $\hat{\phi}^{(j)}$ is continuous, we conclude that

$$\forall a \in \mathbb{R}_+ \cup \{+\infty\}, \quad \frac{\hat{\phi}^{(j)}(a)}{2p_S^{(j)}\hat{\phi}^{(j)}(0)} < \infty.$$

$\square$

Proof of Lemma III.2. Deriving $\ll e^{-\lambda_c t}\rho(t,\cdot), \phi \gg$ with respect to t, we obtain

$$\frac{d}{dt} \ll e^{-\lambda_c t}\rho(t,\cdot), \phi \gg = -e^{-\lambda_c t} \ll (\lambda_c \mathbb{1} + \mathcal{B} + \partial_a)\rho(t,\cdot), \phi \gg.$$

By integration by part and using that $\rho \in \mathbf{L}^1(\mathbb{R}_+)^J$ and $\phi \in \mathcal{C}_b^1(\mathbb{R}_+)^J$, we have

$$\ll \partial_a\rho(t,\cdot), \phi \gg = -\rho(t,0)^T\phi(0) - \ll \rho(t,\cdot), \partial_a\phi \gg,$$

and we deduce

$$\frac{d}{dt} \ll e^{-\lambda_c t}\rho(t,\cdot), \phi \gg = e^{-\lambda_c t}\left[\rho(t,0)^T\phi(0)+ \ll \rho(t,\cdot), \partial_a\phi \gg - \ll (\lambda_c \mathbb{1} + \mathcal{B})\rho(t,\cdot), \phi \gg\right].$$

As we have $(\lambda_c \mathbb{1} + \mathcal{B})^T = (\lambda_c \mathbb{1} + \mathcal{B})$, it comes

$$\ll \rho(t,\cdot), \partial_a\phi \gg - \ll (\lambda_c \mathbb{1} + \mathcal{B})\rho(t,\cdot), \phi \gg = \ll \rho(t,\cdot), \partial_a\phi - (\lambda_c \mathbb{1} + \mathcal{B})\phi \gg.$$

Then, using that $\mathcal{L}^D\phi = \lambda_c\phi$, we deduce $(\partial_a - \lambda_c \mathbb{1} - \mathcal{B})\phi = -K(\cdot)^T\phi(0)$. Thus,

$$\frac{d}{dt} \ll e^{-\lambda_c t}\rho(t,\cdot), \phi \gg = e^{-\lambda_c t}\left[\rho(t,0)^T\phi(0)- \ll \rho(t,\cdot), K(\cdot)^T\phi(0) \gg\right].$$

Note that $\ll \rho(t,\cdot), K(\cdot)^T\phi(0) \gg = \ll K(\cdot)\rho(t,\cdot), \phi(0) \gg = \rho(t,0)^T\phi(0)$. Consequently,

$$\frac{d}{dt} \ll e^{-\lambda_c t}\rho(t,\cdot), \phi \gg = 0.$$

Hence,

$$\forall t, \quad \ll e^{-\lambda_c t}\rho(t,\cdot), \phi \gg = \ll \rho_0(\cdot), \phi \gg = \eta.$$

Thanks to the renormalization $\ll \hat{\rho}, \phi \gg = 1$, we obtain the conservation principle:

$$\ll e^{-\lambda_c t}\rho(t,\cdot) - \eta\hat{\rho}, \phi \gg = \ll e^{-\lambda_c t}\rho(t,\cdot), \phi \gg - \eta \ll \hat{\rho}, \phi \gg = 0.$$

$\square$

Proof of Lemma III.3. From the linearity of the system, it can be easily shown that h is solution of

$$\begin{cases} \partial_t h(t,a) + \partial_a h(t,a) + [\lambda_c + B(a)]h(t,a) = 0, & t \geq 0, \quad a \geq 0, \\ h(t,a=0) = \int_0^\infty K(a)h(t,a)da. \end{cases}$$

Let f be a derivable function. Applying the chain rules, it comes, for $j \in [\![1,J]\!]$,

$$\begin{aligned} \partial_t f[h^{(j)}(t,a)] + \partial_a f[h^{(j)}(t,a)] &= f'(h^{(j)}(t,a))[\partial_t h^{(j)}(t,a) + \partial_a h^{(j)}(t,a)] \\ &= -[\lambda_c + b_j(a)] \times h^{(j)}(t,a)f'(h^{(j)}(t,a)). \end{aligned}$$

For $f(x) = |x|$, $f'(x) = \frac{|x|}{x}$, we deduce

$$\partial_t |h^{(j)}(t,a)| + \partial_a |h^{(j)}(t,a)| = -[\lambda_c + b_j(a)]|h^{(j)}(t,a)|.$$

$\square$

Lemma A.1. *[Modified Grönwall lemma] Let $N \in \mathbb{N}^*$. Suppose that $\forall i \in [\![1,N]\!]$, there exist $\kappa_i \in \mathbb{R}_+^*$, $\gamma \in \mathbb{R}_+^*$ and P_i polynomials of degree $\alpha_i \in \mathbb{N}$ such that*

$$F'(t) \leq \sum_{i=1}^N P_i(t)e^{-\kappa_i t} - \gamma F(t).$$

Then,

$$F(t) \leq Ke^{-\gamma t} + \sum_{i=1}^N \widetilde{P}_i(t)e^{-\kappa_i t},$$

where K is a constant and for all $i \in [\![1,N]\!]$, $\widetilde{P}_i$ is a polynomial of degree $\widetilde{\alpha}_i \leq \alpha_i + 1$.

Proof. Note that $\frac{d}{dt}(e^{\gamma t}F(t)) = (F'(t) + \gamma F(t)) \times e^{\gamma t}$. Hence,

$$\frac{d}{dt}(e^{\gamma t}F(t)) \leq \sum_{i=1}^N P_i(t)e^{(-\kappa_i + \gamma)t}.$$

Then, integrating on the interval $[0,t]$, we obtain

$$e^{\gamma t}F(t) - F(0) \leq \sum_{i=1}^N \widetilde{P}_i(t)e^{(\gamma - \kappa_i)t} + K.$$

Hence

$$F(t) \leq (F(0) + K)e^{-\gamma t} + \sum_{i=1}^N \widetilde{P}_i(t)e^{-\kappa_i t},$$

where K is a constant and for all $i \in [\![1,N]\!]$, $\widetilde{P}_i$ a polynomial of degree $\widetilde{\alpha}_i \leq \alpha_i + 1$ (the degree increases when $\gamma = \kappa_i$). $\square$

A.1.2 Supplemental proofs: Stochastic model

For any $f : (t,a) \mapsto (f_t^{(j)}(a))_{j \in [\![1,J]\!]} \in \mathcal{B}_b^1(\mathbb{R}_+ \times \mathbb{R}_+, \mathbb{R})^J$ (the space product of the set of bounded functions with bounded derivatives), we note ∂_1 and ∂_2 respectively its derivative with respect to time (t) and age (a).

Lemma A.2. *Let* $F \in \mathcal{C}^1(\mathbb{R}, \mathbb{R})$, $f \in \mathcal{B}_b^1(\mathbb{R}_+ \times \mathbb{R}_+, \mathbb{R})^J$.

$$F[\ll Z_t, f_t \gg] = F[\ll f_0, Z_0 \gg] + \int_0^t \ll \partial_1 f_s + \partial_2 f_s, Z_s \gg F'[\ll f_s, Z_s \gg] ds$$

$$+ \int_{[0,t] \times \mathcal{E}} \left[\mathbb{1}_{k \leq N_{s-}} \left(F[\ll f_s, 2\delta_{I_{s-}^{(k)},0} - \delta_{I_{s-}^{(k)}, A_{s-}^{(k)}} + Z_{s-} \gg] - F[\ll f_s, Z_{s-} \gg] \right) \mathbb{1}_{0 \leq \theta \leq m_1(s,k,Z)} \right.$$

$$+ \left(F[\ll f_s, \delta_{I_{s-}^{(k)}+1,0} + \delta_{I_{s-}^{(k)},0} - \delta_{I_{s-}^{(k)}, A_{s-}^{(k)}} + Z_{s-} \gg] - F[\ll f_s, Z_{s-} \gg] \right) \mathbb{1}_{m_1(s,k,Z) \leq \theta \leq m_2(s,k,Z)}$$

$$+ \left. \left(F[\ll f_s, 2\delta_{I_{s-}^{(k)}+1,0} - \delta_{I_{s-}^{(k)}, A_{s-}^{(k)}} + Z_{s-} \gg] - F[\ll f_s, Z_{s-} \gg] \right) \mathbb{1}_{m_2(s,k,Z) \leq \theta \leq m_3(s,k,Z)} \right] Q(ds, dk, d\theta).$$

Proof. We integrate f_t against the measure Z_t

$$\ll Z_t, f_t \gg = \sum_{k=1}^{N_0} f_t^{(I_0^{(k)})}(A_0^{(k)} + t)$$

$$+ \int_{[0,t] \times \mathcal{E}} \left[\mathbb{1}_{k \leq N_{s-}} \left(2f_t^{(I_{s-}^{(k)})}(t-s) - f_t^{(I_{s-}^{(k)})}(A_{s-}^{(k)} + t - s) \right) \mathbb{1}_{0 \leq \theta \leq m_1(s,k,Z)} \right.$$

$$+ \left(f_t^{(I_{s-}^{(k)})}(t-s) + f_t^{(I_{s-}^{(k)}+1)}(t-s) - f_t^{(I_{s-}^{(k)})}(A_{s-}^{(k)} + t - s) \right) \mathbb{1}_{m_1(s,k,Z) \leq \theta \leq m_2(s,k,Z)}$$

$$+ \left. \left(2f_t^{(I_{s-}^{(k)}+1)}(t-s) - f_t^{(I_{s-}^{(k)})}(A_{s-}^{(k)} + t - s) \right) \mathbb{1}_{m_2(s,k,Z) \leq \theta \leq m_3(s,k,Z)} \right] Q(ds, dk, d\theta).$$

Derivating $f_t^{(j)}[a + t - s]$, we obtain

$$\frac{d}{dt} \left[f_t^{(j)}[a + t - s] \right] = \partial_1 f_t^{(j)}[a + t - s] + \partial_2 f_t^{(j)}[a + t - s]$$

$$\Rightarrow \int_s^t \frac{d}{du} \left[f_u^{(j)}[a + u - s] \right] du = \int_s^t \left[\partial_1 f_u^{(j)}[a + u - s] + \partial_2 f_u^{(j)}[a + u - s] \right] du$$

$$\Rightarrow f_t^{(j)}[a + t - s] = f_s^{(j)}[a] + \int_s^t \left[\partial_1 f_u^{(j)}[a + u - s] + \partial_2 f_u^{(j)}[a + u - s] \right] du.$$

Then, replacing j by the index $I_{s^-}^{(k)}$ and a by $A_{s^-}^{(k)}$ or 0, it comes

$$\ll Z_t, f_t \gg = \sum_{k=1}^{N_0} f_0^{(I_0^{(k)})}(A_0^{(k)}) + T_0 + T_1 + T_2 + T_3$$

$$+ \int_{[0,t]\times\mathcal{E}} \mathbb{1}_{k \leq N_{s^-}} \left[\left(2f_s^{(I_{s^-}^{(k)})}(0) - f_s^{(I_{s^-}^{(k)})}(A_{s^-}^{(k)}) \right) \mathbb{1}_{0 \leq \theta \leq m_1(s,k,Z)} \right.$$

$$+ \left(f_s^{(I_{s^-}^{(k)})}(0) + f_s^{(I_{s^-}^{(k)}+1)}(0) - f_s^{(I_{s^-}^{(k)})}(A_{s^-}^{(k)}) \right) \mathbb{1}_{m_1(s,k,Z) \leq \theta \leq m_2(s,k,Z)}$$

$$\left. + \left(2f_s^{(I_{s^-}^{(k)}+1)}(0) - f_s^{(I_{s^-}^{(k)})}(A_{s^-}^{(k)}) \right) \mathbb{1}_{m_2(s,k,Z) \leq \theta \leq m_3(s,k,Z)} \right] Q(ds, dk, d\theta),$$

where

$$T_0 = \sum_{k=1}^{N_0} \int_0^t \left[\partial_1 f_u^{(I_0^{(k)})}(A_0^{(k)} + u) + \partial_2 f_u^{(I_0^{(k)})}(A_0^{(k)} + u) \right] du,$$

$$T_1 = \int_{[0,t]\times\mathcal{E}} \mathbb{1}_{k \leq N_{s^-}} \int_s^t \left[2\partial_1 f_u^{(I_{s^-}^{(k)})}(u - s) + 2\partial_2 f_u^{(I_{s^-}^{(k)})}(u - s) - \partial_1 f_u^{(I_{s^-}^{(k)})}(A_{s^-}^{(k)} + u - s) \right.$$

$$\left. - \partial_2 f_u^{(I_{s^-}^{(k)})}(A_{s^-}^{(k)} + u - s) \mathbb{1}_{0 \leq \theta \leq m_1(s,k,Z)} \right] du\, Q(ds, dk, d\theta)$$

$$T_2 = \int_{[0,t]\times\mathcal{E}} \mathbb{1}_{k \leq N_{s^-}} \int_s^t \left[\partial_1 f_u^{(I_{s^-}^{(k)})}(u - s) + \partial_1 f_u^{(I_{s^-}^{(k)}+1)}(u - s) + \partial_2 f_u^{(I_{s^-}^{(k)})}(u - s) \right.$$

$$+ \partial_2 f_u^{(I_{s^-}^{(k)}+1)}(u - s) - \partial_1 f_u^{(I_{s^-}^{(k)})}(A_{s^-}^{(k)} + u - s)$$

$$\left. - \partial_2 f_u^{(I_{s^-}^{(k)})}(A_{s^-}^{(k)} + u - s) \mathbb{1}_{m_1(s,k,Z) \leq \theta \leq m_2(s,k,Z)} \right] du\, Q(ds, dk, d\theta),$$

and

$$T_3 = \int_{[0,t]\times\mathcal{E}} \mathbb{1}_{k \leq N_{s^-}} \int_s^t \left[2\partial_1 f_u^{(I_{s^-}^{(k)}+1)}(u - s) + 2\partial_2 f_u^{(I_{s^-}^{(k)}+1)}(u - s) - \partial_1 f_u^{(I_{s^-}^{(k)})}(A_{s^-}^{(k)} + u - s) \right.$$

$$\left. - \partial_2 f_u^{(I_{s^-}^{(k)})}(A_{s^-}^{(k)} + u - s) \mathbb{1}_{m_2(s,k,Z) \leq \theta \leq m_3(s,k,Z)} \right] du\, Q(ds, dk, d\theta).$$

As the partial differential of each $f^{(j)}$ are uniformly bounded, we can apply the Fubini theorem on T_0, T_1, T_2 and T_3:

$$T_0 = \int_0^t \ll \partial_1 f_u + \partial_2 f_u, \sum_{k=1}^{N_0} \delta_{I_0^{(k)}, A_0^{(k)} + u} \gg du,$$

$$T_1 = \int_0^t \left[\ll \partial_1 f_u + \partial_2 f_u, \int_0^u \int_{\mathcal{E}} \mathbb{1}_{k \leq N_{s-}} \left(2\delta_{I_{s-}^{(k)}, u-s} - \delta_{I_{s-}^{(k)}, A_{s-}^{(k)} + u-s} \right) \mathbb{1}_{0 \leq \theta \leq m_1(s,k,Z)} Q(ds, dk, d\theta) \gg \right] du,$$

$$T_2 = \int_0^t \left[\ll \partial_1 f_u + \partial_2 f_u, \int_0^u \int_{\mathcal{E}} \mathbb{1}_{k \leq N_{s-}} \left(\delta_{I_{s-}^{(k)}, u-s} + \delta_{I_{s-}^{(k)} + 1, u-s} \right. \right.$$
$$\left. \left. - \delta_{I_{s-}^{(k)}, A_{s-}^{(k)} + u-s} \right) \mathbb{1}_{m_1(s,k,Z) \leq \theta \leq m_2(s,k,Z)} Q(ds, dk, d\theta) \gg \right] du,$$

$$T_3 = \int_0^t \left[\ll \partial_1 f_u + \partial_2 f_u, \int_0^u \int_{\mathcal{E}} \mathbb{1}_{k \leq N_{s-}} \left(2\delta_{I_{s-}^{(k)+1}, u-s} - \delta_{I_{s-}^{(k)}, A_{s-}^{(k)} + u-s} \right) \mathbb{1}_{m_2(s,k,Z) \leq \theta \leq m_3(s,k,Z)} Q(ds, dk, d\theta) \gg \right.$$

Finally, using the stochastic differential equation (III.4)

$$T_0 + T_1 + T_2 + T_3 = \int_0^t \ll \partial_1 f_u + \partial_2 f_u, Z_u \gg du.$$

Consequently, we obtain

$$\ll f_t, Z_t \gg = \ll f_0, Z_0 \gg + \int_0^t \ll \partial_1 f_s + \partial_2 f_s, Z_s \gg ds$$

$$+ \int_{[0,t] \times \mathcal{E}} \mathbb{1}_{k \leq N_{s-}} \left[\ll f_s, 2\delta_{I_{s-}^{(k)}, 0} - \delta_{I_{s-}^{(k)}, A_{s-}^{(k)}} \gg \mathbb{1}_{0 \leq \theta \leq m_1(s,k,Z)} \right.$$

$$+ \ll f_s, \delta_{I_{s-}^{(k)}, 0} + \delta_{I_{s-}^{(k)} + 1, 0} - \delta_{I_{s-}^{(k)}, A_{s-}^{(k)}} \gg \mathbb{1}_{m_1(s,k,Z) \leq \theta \leq m_2(s,k,Z)}$$

$$\left. + \ll f_s, 2\delta_{I_{s-}^{(k)} + 1, 0} - \delta_{I_{s-}^{(k)}, A_{s-}^{(k)}} \gg \mathbb{1}_{m_2(s,k,Z) \leq \theta \leq m_3(s,k,Z)} \right] Q(ds, dk, d\theta),$$

which gives us Lemma A.2 for $F(x) = x$. We conclude by applying the Ito's formula (see [151], p.68-70). $\square$

We introduce the sequence of stopping times ξ_N.

Definition A.1. *Let ξ_N a sequence of stopping times defined as*

$$\xi_N = \sup \left(t : N_t < N, \quad \ll a, Z_t \gg < N \right).$$

Proof of Hypothesis III.6. We first start by showing (III.19).

$$N_t = N_0 + \int_{[0,t] \times \mathcal{E}} \mathbb{1}_{k \leq N_{s-}} \mathbb{1}_{0 \leq \theta \leq b_{I_{s-}^{(k)}}(A_{s-}^{(k)})} Q(ds, dk, d\theta).$$

Thus,

$$\sup_{s \leq t \wedge \xi_N} N_s \leq N_0 + \int_0^{t \wedge \xi_N} \int_{\mathcal{E}} \mathbb{1}_{k \leq N_{s-}} \mathbb{1}_{0 \leq \theta \leq \bar{b}} Q(ds, dk, d\theta),$$

where $\bar{b} := \sup_{j \in [\![0,J]\!]} \bar{b}_j$. Taking the expectation and using the Poisson measure properties, we obtain

$$\mathbb{E}[\sup_{s \leq t \wedge \xi_N} N_s] \leq \mathbb{E}[N_0] + \bar{b}\mathbb{E}\left[\int_0^{t \wedge \xi_N} N_s ds\right] \leq \mathbb{E}[N_0] + \bar{b}\mathbb{E}\left[\int_0^{t \wedge \xi_N} \sup_{u \leq s \wedge \xi_N} N_u ds\right].$$

Hence,

$$\mathbb{E}[\sup_{s \leq t \wedge \xi_N} N_s] \leq \mathbb{E}[N_0] + \bar{b}\mathbb{E}\left[\int_0^t \sup_{u \leq s \wedge \xi_N} N_u ds\right].$$

By Fubini theorem, we deduce that

$$\mathbb{E}[\sup_{s \leq t \wedge \xi_N} N_s] \leq \mathbb{E}[N_0] + \bar{b} \int_0^t \mathbb{E}\left[\sup_{u \leq s \wedge \xi_N} N_u\right] ds.$$

Applying Grönwall lemma, we deduce for all $t \leq T$ that

$$\mathbb{E}[\sup_{s \leq t \wedge \xi_N} N_s] \leq \mathbb{E}[N_0] e^{\bar{b}t}.$$

Hence,

$$\mathbb{E}[\sup_{t \leq T \wedge \xi_N} N_t] \leq \mathbb{E}[N_0] e^{\bar{b}T} \quad < \infty.$$

Using the same method, we also deduce that $\mathbb{E}[\sup_{t \leq T} \ll a, Z_t \gg] < \infty$.

Then, we use the same approach as [84] (Theorem 2.2.8) to compute the infinitesimal generator of Z_t, denoted by $\mathcal{G}$. By construction, $(Z_t)_{t \in \mathbb{R}_+}$ is a markovian process of $\mathbb{D}([0,T], \mathcal{M}_P([\![1,J]\!] \times \mathbb{R}_+))$. Let $f \in \mathbf{C}_b^1(\mathcal{E}, \mathbb{R})$, by definition, $\mathcal{G}F := \lim_{t \to 0} \frac{d}{dt} \mathbb{E}[F[\ll f, Z_t \gg]]$. Taking the expectation of the expression of $\ll f, Z_{t \wedge \xi_N} \gg$ given in lemma A.2, we obtain

$$\mathbb{E}\left[F[\ll f, Z_{t \wedge \xi_N} \gg]\right] = \mathbb{E}\left[F[\ll f, Z_0 \gg]\right]$$
$$+ \mathbb{E}\left[\int_0^{t \wedge \xi_N} \ll \partial_a f, Z_s \gg F'[\ll f, Z_s \gg] ds\right] + \mathbb{E}\left[\chi^{f,F}(t \wedge \xi_N, Z)\right],$$

where

$$\chi^{f,F}(t, Z) := \int_0^t \int_{\mathcal{E}} \Big[(F[\ll f, 2\delta_{j,0} - \delta_{j,a} + Z_s \gg] - F[< f, Z_s >]) p_{2,0}^{(j)}$$
$$+ (F[< f, \delta_{j+1,0} + \delta_{j,0} - \delta_{j,a} + Z_s >] - F[\ll f, Z_s \gg]) p_{1,1}^{(j)}$$
$$+ (F[< f, 2\delta_{j+1,0} - \delta_{j,a} + Z_s >]$$
$$- F[< f, Z_s >]) p_{0,2}^{(j)} \Big] b_j(a) Z_s(dj, da) ds.$$

We have the following estimates,

$$\mathbb{E}\left[\chi^{f,F}(t \wedge \xi_N, Z)\right] \leq 2\mathbb{E}\left[\sup_{t \leq T} N_t\right] T \|F\|_\infty \bar{b},$$

$$\mathbb{E}[\int_0^{t \wedge \xi_N} \ll \partial_a f_s, Z_s \gg F'[\ll f, Z_s \gg] ds] \leq \mathbb{E}[\sup_{t \leq T} N_t] T \times \|\partial_a f\|_\infty \times \|F'\|_\infty.$$

Those bounds are independent of N thanks to (III.19), so that we may let N goes to infinity. Moreover,

$$\frac{d}{dt}\int_0^t \ll \partial_a f, Z_s \gg F'[\ll f, Z_s \gg]ds = \ll \partial_a f, Z_t \gg F'[\ll f, Z_t \gg]$$

which is also dominated by $\mathbb{E}[\sup_{t \leq T} N_t] \times \|\partial_a f\|_\infty \times \|F'\|_\infty$. Also,

$$
\begin{aligned}
\frac{\partial}{\partial t}\chi(t, Z_t) = \int_{\mathcal{E}} &\Big[(F[< f, 2\delta_{j,0} - \delta_{j,a} + Z_t >] - F[< f, Z_t >]) \, p_{2,0}^{(j)} \\
&+ (F[\ll f, \delta_{j+1,0} + \delta_{j,0} - \delta_{j,a} + Z_t \gg] - F[\ll f, Z_t \gg]) \, p_{1,1}^{(j)} \\
&+ (F[\ll f, 2\delta_{j+1,0} - \delta_{j,a} + Z_t \gg] - F[\ll f, Z_t \gg]) \, p_{0,2}^{(j)} \Big] b_j(a) Z_t(dj, da).
\end{aligned}
$$

$|\frac{\partial}{\partial t}\chi(t, Z_t)|$ is dominated $\mathbb{P}$-p.s by $2\mathbb{E}[\sup_{t \leq T} N_t]\|F\|_\infty \bar{b}$. We can thus apply the differentiating theorem under the integral sign $\mathbb{E}$ and conclude. $\qquad\square$

Proof of Lemma III.5. Introducing the compensated Poisson measure $\tilde{Q}$, $\tilde{Q}(ds, dk, d\theta) := Q(ds, dk, d\theta) - dsdkd\theta$, we define the process:

$$
\begin{aligned}
M_t^{F,f} := \int\int_{[0, t\wedge\xi_N]\times\mathcal{E}} \mathbb{1}_{k<N_{s-}} \Big[&\Big(F[\ll f, 2\delta_{I^k_{s-},0} - \delta_{I^k_{s-},A^k_{s-}} + Z_{s-} \gg] - F[\ll f, Z_{s-} \gg]\Big) \mathbb{1}_{0\leq\theta\leq m_1(s,k,Z)} \\
+ &\Big(F[\ll f, \delta_{I^k_{s-}+1,0} + \delta_{I^k_{s-},0} - \delta_{I^k_{s-},A^k_{s-}} + Z_{s-} \gg] - F[\ll f, Z_{s-} \gg]\Big) \mathbb{1}_{m_1(s,k,Z)\leq\theta\leq m_2(s,k,Z)} \\
+ &\Big(F[\ll f, 2\delta_{I^k_{s-}+1,0} - \delta_{I^k_{s-},A^k_{s-}} + Z_{s-} \gg] - F[\ll f, Z_{s-} \gg]\Big) \mathbb{1}_{m_2(s,k,Z)\leq\theta\leq m_3(s,k,Z)} \Big] \tilde{Q}(ds, dk, d\theta).
\end{aligned}
$$

We can verify that $M_t^{F,f}$ is a martingale as an integral against a compensated Poisson measure. Then, applying Lemma A.2 and the definition of the generator given in theorem III.6, we show that

$$M_t^{F,f} = F[\ll f, Z_t \gg] - F[\ll f, Z_0 \gg] - \int_0^t \mathcal{G}F[\ll f, Z_s \gg]ds. \qquad (A.4)$$

We turn now to the computation of the quadratic variation and use the same approach as in [79]. We apply (A.4) for $F(x) = x^2$. Note that we cannot use directly this result as $x \mapsto x^2$ is not bounded and we need to first use a localizing sequence (see [83] p. 382, theorem 13.14). We obtain that

$$
\begin{aligned}
&\ll f, Z_t \gg^2 - \ll f, Z_0 \gg^2 - \int_0^t 2 \ll f, Z_s \gg \times \ll \partial_a f, Z_s \gg ds \\
&- \int_0^t \sum_{j=1}^J \int_{\mathbb{R}_+} \Big[\Big(\ll f, 2\delta_{j,0} - \delta_{j,a} + Z_s \gg^2 - \ll f, Z_s \gg^2\Big) b_j(a) p_{2,0}^{(j)} \\
&- \Big(\ll f, \delta_{j,0} + \delta_{j+1,0} - \delta_{j,a} + Z_s \gg^2 - \ll f, Z_s \gg^2\Big) b_j(a) p_{1,1}^{(j)} Z_s(dj, da) \\
&- \Big(\ll f, 2\delta_{j+1,0} - \delta_{j,a} + Z_s \gg^2 - \ll f, Z_s \gg^2\Big) b_j(a) p_{0,2}^{(j)} Z_s(dj, da)ds \Big]
\end{aligned} \qquad (A.5)
$$

is a martingale. Then, applying (A.4) for $F(x) = x$ (using a localizing sequence again), we get that

$$\ll f, Z_t \gg \;=\; \ll f, Z_0 \gg + \int_0^t \ll \partial_a f, Z_s \gg ds$$

$$+ \int_0^t \Big[\sum_{j=1}^J \int_{\mathbb{R}_+} \ll f, 2\delta_{j,0} - \delta_{j,a} \gg b_j(a) p_{2,0}^{(j)} Z_s(dj, da)\Big] ds$$

$$+ \int_0^t \Big[\sum_{j=1}^J \int_{\mathbb{R}_+} \ll f, \delta_{j,0} + \delta_{j+1,0} - \delta_{j,a} \gg b_j(a) p_{1,1}^{(j)} Z_s(dj, da)\Big] ds$$

$$+ \int_0^t \Big[\sum_{j=1}^J \int_{\mathbb{R}_+} \ll f, 2\delta_{j+1,0} - \delta_{j,a} \gg b_j(a) p_{0,2}^{(j)} Z_s(dj, da)\Big] ds + M_t^f$$

is a semi-martingale. Applying the Ito formula (see [151], p. 78-79), we obtain

$$\ll f, Z_t \gg^2 \;-\; \ll f, Z_0 \gg^2 - \int_0^t 2 \ll f, Z_s \gg \times \ll \partial_a f, Z_s \gg ds$$

$$+ \sum_{j=1}^J \int_{\mathbb{R}_+} (2 \ll f, Z_s \gg \times \ll f, 2\delta_{j,0} - \delta_{j,a} \gg) b_j(a) p_{2,0}^{(j)} Z_s(dj, da)$$

$$+ \sum_{j=1}^J \int_{\mathbb{R}_+} (2 \ll f, Z_s \gg \times \ll f, \delta_{j,0} + \delta_{j+1,0} - \delta_{j,a} \gg) b_j(a) p_{1,1}^{(j)} Z_s(dj, da) \qquad \text{(A.6)}$$

$$+ \sum_{j=1}^J \int_{\mathbb{R}_+} (2 \ll f, Z_s \gg \times \ll f, 2\delta_{j+1,0} - \delta_{j,a} \gg) b_j(a) p_{0,2}^{(j)} Z_s(dj, da)\Big] ds$$

$$- \left\langle M^f, M^f \right\rangle_t$$

is a martingale. We consider the jump corresponding to the case when the two daughter cells remain on their mother layer. Note that

$$\ll f, 2\delta_{j,0} - \delta_{j,a} + Z_s \gg^2 - \ll f, Z_s \gg^2 = 2 \ll f, Z_s \gg \times \ll f, 2\delta_{j,0} - \delta_{j,a} \gg + \ll f, 2\delta_{j,0} - \delta_{j,a} \gg^2 .$$

We proceed similarly for the two other jumps. Applying the Doob-Meyer theorem ([151], p. 106), we deduce the quadratic variation $\left\langle M^f, M^f \right\rangle_t$ comparing (A.5) and (A.6). $\qquad\square$

A.1.3 Supplemental proofs: Moment study

Generating functions

Proof of Lemma III.6. Let $a \geq 0$. Remind that the generating function is given by

$$F^{(i,a)}[\mathbf{s}; t] = \sum_{\mathbf{k} \in \mathbb{N}^J} \mathbf{s}^{\mathbf{k}} \mathbb{P}\big[Y_t^a = \mathbf{k} | Z_0 = \delta_{i,0}\big].$$

Let $i \in [\![1, J]\!]$ and $\mathbf{j}, \mathbf{k} \in \mathbb{N}^J$. We note $P_{\mathbf{j},\mathbf{k}}^a(t) := \mathbb{P}\big[Y_t^a = \mathbf{k} | Z_0 = \sum_{i=1}^J j_i \delta_{i,0}\big]$. We write the backward equation for the probability $P_{e_i,\mathbf{k}}^a(t) := \mathbb{P}\big[Y_t^a = \mathbf{k} | Z_0 = \delta_{i,0}\big]$. Starting from a single mother cell of age 0 and layer i, there are three possibilities at time t: (i) the cell has not divided and $t \leq a$, (ii) the cell has not divided and $t > a$, and (iii) the cell has divided. Thus,

$$P_{e_i,\mathbf{k}}^a(t) = \big(\delta_{e_i,\mathbf{k}} \mathbb{1}_{t \leq a} + \delta_{\mathbf{0},\mathbf{k}} \mathbb{1}_{t > a}\big) \mathbb{P}[\tau^{(i)}(a_0 = 0) \geq t]$$

$$+ \int_0^t [p_{2,0}^{(i)} P_{2e_i,\mathbf{k}}^a(t - y) + p_{1,1}^{(i)} P_{e_i+e_{i+1},\mathbf{k}}^a(t - y) + p_{0,2}^{(i)} P_{2e_{i+1},\mathbf{k}}^a(t - y)] d\mathcal{B}_i(y) dy \quad \text{(A.7)}$$

where $\mathbb{P}[\tau^{(i)}(a_0 = 0) \geq t] = e^{-\int_0^t b_i(s)ds}\mathbb{1}_{t \geq 0} = 1 - \mathcal{B}_i(t)$.

Applying the branching property, we have for all $y \in [0, t]$, for all $i \in [\![1, J]\!]$

$$P^a_{2e_i,\mathbf{k}}(y) = \sum_{\mathbf{k}_1, \mathbf{k}_2 / \mathbf{k}_1 + \mathbf{k}_2 = \mathbf{k}} [P^a_{e_i,\mathbf{k}_1}(y) P^a_{e_i,\mathbf{k}_2}(y)],$$

and also, for all $i \in [\![1, J-1]\!]$,

$$P^a_{e_i+e_{i+1},\mathbf{k}}(y) = \sum_{\mathbf{k}_1, \mathbf{k}_2 / \mathbf{k}_1 + \mathbf{k}_2 = \mathbf{k}} P^a_{e_{i+1},\mathbf{k}_1}(y) P^a_{e_i,\mathbf{k}_2}(y).$$

Hence, we can rewrite the expression of

$$A_t := \int_0^t [p^{(i)}_{2,0} P^a_{2e_i,\mathbf{k}}(t-y) + p^{(i)}_{1,1} P^a_{e_i+e_{i+1},\mathbf{k}}(t-y) + p^{(i)}_{0,2} P^a_{2e_{i+1},\mathbf{k}}(t-y)]d\mathcal{B}_i(y)dy$$

as

$$A_t = p^{(i)}_{2,0} \int_0^t \sum_{\mathbf{k}_1, \mathbf{k}_2 / \mathbf{k}_1 + \mathbf{k}_2 = \mathbf{k}} P^a_{e_i,\mathbf{k}_1}(t-y) P^a_{e_i,\mathbf{k}_2}(t-y)d\mathcal{B}_i(y)dy$$

$$+ p^{(i)}_{1,1} \int_0^t \sum_{\mathbf{k}_1, \mathbf{k}_2 / \mathbf{k}_1 + \mathbf{k}_2 = \mathbf{k}} P^a_{e_{i+1},\mathbf{k}_1}(t-y) P^a_{e_i,\mathbf{k}_2}(t-y)d\mathcal{B}_i(y)dy$$

$$+ p^{(i)}_{0,2} \int_0^t \sum_{\mathbf{k}_1, \mathbf{k}_2 / \mathbf{k}_1 + \mathbf{k}_2 = \mathbf{k}} P^a_{e_{i+1},\mathbf{k}_1}(t-y) P^a_{e_{i+1},\mathbf{k}_2}(t-y)d\mathcal{B}_i(y)dy.$$

Note that

$$\sum_{\mathbf{k} \in \mathbb{N}^J} \mathbf{s}^{\mathbf{k}} P^a_{2e_i,\mathbf{k}}(t-y) = \sum_{\mathbf{k} \in \mathbb{N}^J} \mathbf{s}^{\mathbf{k}} \sum_{\mathbf{k}_1, \mathbf{k}_2 / \mathbf{k}_1 + \mathbf{k}_2 = \mathbf{k}} P^a_{e_i,\mathbf{k}_1}(t-y) P^a_{e_i,\mathbf{k}_2}(t-y)$$

$$= \sum_{\mathbf{k} \in \mathbb{N}^J} \sum_{\mathbf{k}_1 = 0}^{\mathbf{k}} \mathbf{s}^{\mathbf{k}_1} P^a_{e_i,\mathbf{k}_1}(t-y) \mathbf{s}^{\mathbf{k}-\mathbf{k}_1} P^a_{e_i,\mathbf{k}-\mathbf{k}_1}(t-y).$$

We note $\sum_{\mathbf{k}_1=0}^{\mathbf{k}}$ the sum of all the $\mathbf{k}_1 \in \mathbb{N}^J$ vectors such that $\mathbf{k}_1 \leq \mathbf{k}$ component by component. We have

$$\sum_{\mathbf{k} \in \mathbb{N}^J} \mathbf{s}^{\mathbf{k}} P^a_{2e_i,\mathbf{k}}(t-y) = \sum_{\mathbf{k} \in \mathbb{N}^J} \sum_{\mathbf{k}_1 = 0}^{\mathbf{k}} \mathbf{s}^{\mathbf{k}_1} P^a_{e_i,\mathbf{k}_1}(t-y) \mathbf{s}^{\mathbf{k}-\mathbf{k}_1} P^a_{e_i,\mathbf{k}-\mathbf{k}_1}(t-y)$$

$$= \sum_{\mathbf{k}_1 \in \mathbb{N}^J} \mathbf{s}^{\mathbf{k}_1} P^a_{e_i,\mathbf{k}_1}(t-y) \sum_{\mathbf{k} \geq \mathbf{k}_1} \mathbf{s}^{\mathbf{k}-\mathbf{k}_1} P^a_{e_i,\mathbf{k}-\mathbf{k}_1}(t-y)$$

$$= (\sum_{\mathbf{k}_1 \in \mathbb{N}^J} \mathbf{s}^{\mathbf{k}_1} P^a_{e_i,\mathbf{k}_1}(t-y))(\sum_{\mathbf{k}_2 \in \mathbb{N}^J} \mathbf{s}^{\mathbf{k}_2} P^a_{e_i,\mathbf{k}_2}(t-y)).$$

Hence,

$$\sum_{\mathbf{k} \in \mathbb{N}^J} \mathbf{s}^{\mathbf{k}} P^a_{2e_i,\mathbf{k}}(t-y) = (F^{(i,a)}[\mathbf{s}; t-y])^2. \tag{A.8}$$

In the same way, we also obtain

$$\sum_{\mathbf{k} \in \mathbb{N}^J} \mathbf{s}^{k} P^a_{e_i+e_{i+1},k}(t-y) = F^{(i,a)}[\mathbf{s}; t-y] F^{(i+1,a)}[\mathbf{s}; t-y]$$

and

$$\sum_{\mathbf{k}\in\mathbb{N}^J} \mathbf{s}^{\mathbf{k}} P^a_{2e_{i+1},\mathbf{k}}(t-y) = (F^{(i+1,a)}[\mathbf{s};t-y])^2. \tag{A.9}$$

Finally, multiplying (A.7) by $\mathbf{s}^{\mathbf{k}}$, summing on $\mathbf{k}\in\mathbb{N}^J$ and applying (A.8)-(A.9), we obtain:

$$\forall i\in[\![1,J]\!], F^{(i,a)}[\mathbf{s};t] = (s_i\mathbb{1}_{t\leq a}+\mathbb{1}_{t>a})(1-\mathcal{B}_i(t))+\int_0^t f^{(i)}(F[\mathbf{s};t-y])d\mathcal{B}_i(y)dy.$$

$\square$

First moments

Proof of Lemma III.7. By classical property, $M^a_{i,j}(t) = \frac{\partial}{\partial s_j}F^{(i,a)}[s;t]\big|_{\mathbf{s}=1}$. From (III.6) it comes that

$$\frac{\partial}{\partial s_j}F^{(i,a)}[s;t] = \delta_{i,j}(1-\mathcal{B}_{i,i}(t))\mathbb{1}_{t\leq a}+\int_0^t \frac{\partial}{\partial s_j}f^{(i)}[F^a(s,y)]d\mathcal{B}_i(t-y)dy$$

where

$$\frac{\partial}{\partial s_j}f^{(i)}[F^a(s,t)] = 2p^{(i)}_{2,0}F^{(i,a)}[s;t]\frac{\partial}{\partial s_j}F^{(i,a)}[s;t]+2p^{(i)}_{0,2}F^{(i+1,a)}[s;t]\frac{\partial}{\partial s_j}F^{(i+1,a)}[s;t]$$

$$+p^{(i)}_{1,1}\big[F^{(i+1,a)}[s;t]\frac{\partial}{\partial s_j}F^{(i,a)}[s;t]+F^{(i,a)}[s;t]\frac{\partial}{\partial s_j}F^{(i+1,a)}[s;t]\big].$$

For $\mathbf{s}=1$, knowing that $F^{(i,a)}(1,t)=1$, we get

$$M^a_{i,j}(t) = \delta_{i,j}(1-\mathcal{B}_i(t))\mathbb{1}_{t\leq a}$$

$$+\int_0^t \big[2p^{(i)}_{2,0}M^a_{i,j}(y)+p^{(i)}_{1,1}[M^a_{i,j}(y)+M^a_{i+1,j}(y)]+2p^{(i)}_{0,2}M^a_{i+1,j}(y)\big]d\mathcal{B}_i(t-y))dy$$

which can be rewritten as

$$M^a_{i,j}(t) = \delta_{i,j}(1-\mathcal{B}_i(t))\mathbb{1}_{t\leq a}+\big[2p^{(i)}_S M^a_{i,j}+2p^{(i)}_L M^a_{i+1,j}\big]*d\mathcal{B}_i(t).$$

$\square$

Harris lemmas

We recall some results on the renewal theory presented in [65], p.161-163.
Let G be a distribution function on $(0,\infty)$ with the additional assumption $G(0+)=0$. We consider the renewal equation

$$K(t) = f(t)+m\int_0^t K(t-u)dG(u) = f(t)+mK*G(t)$$

where m is a positive constant representing the mean number of children, f is a continuous function representing a source term and G is the life time distribution. In addition, we suppose that G is not lattice.

Lemma A.3 (Harris's lemma 2, p.161)**.** *Suppose that there exists a Malthus parameter α such that $m\int_0^\infty e^{-\alpha t}dG(t)=1$, and that the following conditions also hold:*

(a) $f(t)e^{-\alpha t}$ *is a continuous function such that* $f(t)e^{-\alpha t} \in \mathbf{L}^1(\mathbb{R}_+)$.

(b) $\int_0^\infty t^2 dG(t) < \infty$.

Then, $K(t) \sim n_f e^{\alpha t}$, *where*

$$n_f = \frac{\int_0^\infty f(t)e^{-\alpha t}dt}{m \int_0^\infty te^{-\alpha t}dG(t)}.$$

Lemma A.4 (Harris's lemma 4, p.163)**.** *Suppose that* $m < 1$ *and* $\lim_{t\to\infty} f(t) = c$. *then* $K(t) \to \frac{c}{1-m}$.

Additional computation details for the proof of Hypothesis III.4

We detail how to obtain Formula (III.31). We first take the Laplace transform of (III.24) for $\alpha = \lambda_c$ for $i = c + 1$ and $j \in [\![c+1, J]\!]$. We distinguish the case $i = j$ from the others. If $j = c + 1$, we obtain

$$\int_0^\infty M_{j,j}^a(t)e^{-\lambda_c t}dt = \frac{1}{\hat{\rho}^{(j)}(0)} \int_0^a \hat{\rho}^{(j)}(t)dt + 2p_S^{(j)} \int_0^\infty \left[\int_0^t d\mathcal{B}_j(t-u)M_{j,j}^a(u)du\right] e^{-\lambda_c t}dt.$$

By the Laplace transform property for the convolution, we deduce that

$$\int_0^\infty \left[\int_0^t d\mathcal{B}_j(t-u)M_{j,j}^a(u)du\right] e^{-\lambda_c t}dt = d\mathcal{B}_j^*(\lambda_c) \int_0^\infty M_{j,j}^a(t)e^{-\lambda_c t}dt,$$

hence

$$\int_0^\infty M_{j,j}^a(t)e^{-\lambda_c t}dt = \frac{1}{\hat{\rho}^{(j)}(0)} \int_0^a \hat{\rho}^{(j)}(t)dt + 2p_S^{(j)}d\mathcal{B}_j^*(\lambda_c) \int_0^\infty M_{j,j}^a(t)e^{-\lambda_c t}dt$$

$$= \frac{1}{\hat{\rho}^{(j)}(0) \times (1 - 2p_S^{(j)}d\mathcal{B}_j^*(\lambda_c))} \int_0^a \hat{\rho}^{(j)}(t)dt.$$

When $j > c + 1$, we have:

$$\int_0^\infty M_{c+1,j}^a(t)e^{-\lambda_c t}dt = 2p_S^{(c+1)}d\mathcal{B}_{c+1}^*(\lambda_c) \int_0^\infty M_{c+1,j}^a(t)e^{-\lambda_c t}dt + 2p_L^{(c+1)}d\mathcal{B}_j^*(\lambda_c) \int_0^\infty M_{c+2,j}^a(t)e^{-\lambda_c t}dt.$$

Hence,

$$\int_0^\infty M_{c+1,j}^a(t)e^{-\lambda_c t}dt = \frac{2p_L^{(c+1)}}{1 - 2p_S^{(c+1)}d\mathcal{B}_{c+1}^*(\lambda_c)} \int_0^\infty M_{c+2,j}^a(t)e^{-\lambda_c t}dt.$$

Here, we obtain a recurrence formula between $\int_0^\infty M_{c+1,j}^a(t)e^{-\lambda_c t}dt$ and $\int_0^\infty M_{c+2,j}^a(t)e^{-\lambda_c t}dt$, and we obtain (III.31).

Second moments

Definition A.2. *Let* $a \geq 0$. *We define the second moment*

$$L^a(t) := (\mathbb{E}[(Y_t^{(a,j)})^2 | Z_0 = \delta_{i,0}])_{i,j\in[\![1,J]\!]}.$$

Lemma A.5. $L^a(t)$ *is solution of the renewal equation:* $\forall (i,j) \in [\![1,J]\!]^2$,

$$
\begin{aligned}
L^a_{i,j}(t) = \quad & \delta_{i,j}(1 - \mathcal{B}_i(t))\mathbb{1}_{t \leq a} + [2p_S^{(i)} L^a_{i,j} + 2p_L^{(i)} L^a_{i+1,j}] * d\mathcal{B}_i(t) \\
& + [2p_{2,0}^{(i)}(M^a_{i,j})^2 + 2p_{1,1}^{(i)} M^a_{i,j} M^a_{i+1,j} + 2p_{0,2}^{(i)}(M^a_{i+1,j})^2] * d\mathcal{B}_i(t).
\end{aligned}
\tag{A.10}
$$

Proof of Lemma (A.5). Note that $\frac{\partial^2}{\partial s_j} F^{(i,a)}[s;t]|_{\mathbf{s}=1} = L^a_{i,j}(t) - M^a_{i,j}(t)$. We derive (A.1.3) with respect to s_j and obtain:

$$
\frac{\partial^2}{\partial s_j^2} F^{(i,a)}[\mathbf{s};t] = \int_0^t \frac{\partial}{\partial s_j^2} f^{(i)}(F^a[\mathbf{s},u]) d\mathcal{B}_i(t-u) du
$$

where

$$
\begin{aligned}
\frac{\partial^2}{\partial s_j^2} f^{(i)}(F^a[\mathbf{s},t]) = 2p_{2,0}^{(i)} & \left(F^{(i,a)}[\mathbf{s};t] \frac{\partial^2}{\partial s_j} F^{(i,a)}[\mathbf{s};t] + (\frac{\partial}{\partial s_j} F^{(i,a)}[\mathbf{s};t])^2 \right) \\
+ 2p_{0,2}^{(i)} & \left(F^{(i+1,a)}[\mathbf{s};t] \frac{\partial^2}{\partial s_j} F^{(i+1,a)}[\mathbf{s};t] + (\frac{\partial}{\partial s_j} F^{(i+1,a)}[\mathbf{s};t])^2 \right)
\end{aligned}
$$

$$
+ p_{1,1}^{(i)} \left(F^{(i+1,a)}[\mathbf{s};t] \frac{\partial^2}{\partial s_j} F^{(i,a)}[\mathbf{s};t] + 2\frac{\partial}{\partial s_j} F^{(i,a)}[\mathbf{s};t] \frac{\partial}{\partial s_j} F^{(i+1,a)}[\mathbf{s};t] + F^{(i,a)}[\mathbf{s};t] \frac{\partial^2}{\partial s_j} F^{(i+1,a)}[\mathbf{s};t] \right).
$$

When $\mathbf{s} = 1$, we get

$$
\begin{aligned}
L^a_{i,j}(t) - M^a_{i,j}(t) = 2p_{2,0}^{(i)} & \left(L^a_{i,j} - M^a_{i,j} + (M^a_{i,j})^2 \right) * d\mathcal{B}_i(t) + 2p_{0,2}^{(i)} \left(L^a_{i+1,j} - M^a_{i+1,j} + (M^a_{i+1,j})^2 \right) * d\mathcal{B}_i(t) \\
& + p_{1,1}^{(i)} \left(L^a_{i,j} - M^a_{i,j} + 2M^a_{i,j} M^a_{i+1,j} + L^a_{i+1,j} - M^a_{i+1,j} \right) * d\mathcal{B}_i(t).
\end{aligned}
$$

Using the system of equations (III.24), we deduce (A.10). $\qquad \square$

Theorem A.1. *Under the same hypotheses as in Hypothesis III.4, and supposing that for all $i \in [\![1,J]\!], \lambda_i > 0$, we have, for all $a \geq 0$:*

$$
\forall i \in [\![1,J]\!], \quad \forall k \in [\![0, J-i]\!] \quad L^a_{i,i+k}(t) \sim \widetilde{L}_{i,i+k}(a) e^{2\lambda_{i,i+k} t}, \ as \ t \to \infty
$$

such that

$$
\widetilde{L}_{i,i}(a) = \frac{2p_{2,0}^{(i)} d\mathcal{B}_i^*(2\lambda_i)(\widetilde{M}^a_{i,i})^2}{1 - 2p_S^{(i)} d\mathcal{B}_i^*(2\lambda_i)},
$$

and for $k \in [\![1, J-i]\!]$,

$$
\widetilde{L}_{i,i+k}(a) =
\begin{cases}
\dfrac{2p_{2,0}^{(i)} (\widetilde{M}^a_{i,i+k})^2 d\mathcal{B}_i^*(2\lambda_{i,i+k})}{1 - 2p_S^{(i)} d\mathcal{B}_i^*(2\lambda_{i,i+k})} + l_{i,i+k}(a), & if \ \lambda_{i,i+k} \neq \lambda_i \\[3mm]
\dfrac{2p_{2,0}^{(i)} (\widetilde{M}^a_{i,i+k})^2 d\mathcal{B}_i^*(2\lambda_{i,i+k})}{1 - 2p_S^{(i)} d\mathcal{B}_i^*(2\lambda_{i,i+k})}, & if \ \lambda_{i,i+k} = \lambda_i
\end{cases}
$$

where

$$
l_{i,i+k}(a) = \frac{\left[\widetilde{L}_{i+1,i+k}(a) + 2p_{1,1}^{(i)} \widetilde{M}^a_{i,i+k} \widetilde{M}^a_{i+1,i+k} + 2p_{0,2}^{(i)} (\widetilde{M}^a_{i+1,i+k})^2 \right] d\mathcal{B}_i^*(2\lambda_{i,i+k})}{1 - 2p_S^{(i)} d\mathcal{B}_i^*(2\lambda_{i,i+k})}.
$$

Proof. Let $a \geq 0$. We introduce the following notations

$$\widehat{L}^a_{i,i+k}(t) = L^a_{i,i+k}(t)e^{-2\lambda_{i,i+k}t}, \quad \widehat{d\mathcal{B}_i}(t) = \frac{d\mathcal{B}_i(t)}{d\mathcal{B}^*_i(2\lambda_{i,i+k})}e^{-2\lambda_{i,i+k}t}.$$

We use the same approach as that performed for the proof of Hypothesis III.4, and proceed by recurrence:

$$\mathcal{H}^k: \quad \forall i \in [\![1, J-k]\!], \ L^a_{i,i+k}(t) \sim \widetilde{L}^a_{i,i+k}e^{2\lambda_{i,i+k}t}, \text{ as } t \to \infty.$$

When $k = 0$, according to (A.10) $L^a_{i,i}$ is solution of the renewal equation:

$$L^a_{i,i}(t) = (1 - \mathcal{B}_i(t))\,\mathbb{1}_{t \leq a} + 2p^{(i)}_{2,0}(M^a_{i,i})^2 * d\mathcal{B}_i(t) + 2p^{(i)}_S L^a_{i,i} * d\mathcal{B}_i(t). \tag{A.11}$$

We rescale (A.11) by $e^{-2\lambda_i t}$ and obtain:

$$\widehat{L}^a_{i,i}(t) = e^{-2\lambda_i t}\left[(1 - \mathcal{B}_i(t))\,\mathbb{1}_{t \leq a} + 2p^{(i)}_{2,0}(M^a_{i,i})^2 * d\mathcal{B}_i(t)\right] + 2p^{(i)}_S d\mathcal{B}^*_i(2\lambda_i)\widehat{L}^a_{i,i} * \widehat{d\mathcal{B}_i}(t).$$

Note that as $2\lambda_i > \lambda_i > 0$, we have $2p^{(i)}_S d\mathcal{B}^*_i(2\lambda_i) < 1$, so that we can use Lemma A.4. We compute the limit of the source term :

$$\lim_{t \to \infty} e^{-2\lambda_i t}\left[(1 - \mathcal{B}_i(t))\,\mathbb{1}_{t \leq a} + 2p^{(i)}_{2,0}(M^a_{i,i})^2 * d\mathcal{B}_i(t)\right].$$

From Hypothesis III.2, we have:

$$\int_0^\infty (1 - \mathcal{B}_i(t))\,\mathbb{1}_{t \leq a}e^{-\lambda_i t}dt \leq \frac{1}{b_i}\int_0^\infty d\mathcal{B}_i(t)e^{-\lambda_i t}dt < \infty.$$

Thus, $(1 - \mathcal{B}_i(t))\,\mathbb{1}_{t \leq a}e^{-\lambda_i t} \in \mathbf{L}^1(\mathbb{R}_+)$ and, $\lim_{t \to \infty} e^{-\lambda_i t}[1 - \mathcal{B}_i(t)] = 0$. Using the hypothesis $\lambda_i > 0$, we obtain that $\lim_{t \to \infty} e^{-2\lambda_i t}[1 - \mathcal{B}_i(t)] = 0$. Then,

$$e^{-2\lambda_i t}(M^a_{i,i})^2 * d\mathcal{B}_i(t) = \int_0^\infty \mathbb{1}_{[0,t]}(M^a_{i,i}(t-u)e^{-\lambda_i(t-u)})^2 d\mathcal{B}_i(u)e^{-2\lambda_i u}du.$$

Using Hypothesis III.4, we have $M^a_{i,i}(t) \sim e^{\lambda_i t}\widetilde{M}_{i,i}(a)$, as $t \to \infty$. Applying Lebesgue dominated convergence theorem, we obtain

$$\lim_{t \to \infty} e^{-2\lambda_i t}(M^a_{i,i})^2 * d\mathcal{B}_i(t) = (\widetilde{M}_{i,i}(a))^2 d\mathcal{B}^*_i(2\lambda_i).$$

Then, applying Lemma A.4, we deduce:

$$L^a_{i,i}(t) \sim \widetilde{L}_{i,i}(a)e^{2\lambda_i t}, \text{ as } t \to \infty, \text{ where } \widetilde{L}_{i,i}(a) = \frac{2p^{(i)}_{2,0}d\mathcal{B}^*_i(2\lambda_i)(\widetilde{M}_{i,i}(a))^2}{1 - 2p^{(i)}_S d\mathcal{B}^*_i(2\lambda_i)}.$$

Hence, $\mathcal{H}^0$ is true. Then, we suppose that $\mathcal{H}^{k-1}$ holds and we show $\mathcal{H}^k$. According to (A.10), we write the equation for $L^a_{i,i+k}$ and rescale it by $e^{-2\lambda_{i,i+k}t}$:

$$\widehat{L}^a_{i,i+k}(t) = 2p^{(i)}_S d\mathcal{B}^*_i(2\lambda_{i,i+k})\widehat{L}^a_{i,i+k} * \widehat{d\mathcal{B}_i}(t) + e^{-2\lambda_{i,i+k}t}2p^{(i)}_L L^a_{i+1,i+k} * d\mathcal{B}_i(t)$$
$$+ e^{-2\lambda_{i,i+k}t}\left[2p^{(i)}_{2,0}(M^a_{i,i+k})^2 + 2p^{(i)}_{1,1}M^a_{i,i+k}M^a_{i+1,i+k} + 2p^{(i)}_{0,2}(M^a_{i+1,i+k})^2\right] * d\mathcal{B}_i(t).$$

Here, $m = 2p_S^{(i)} d\mathcal{B}_i^*(2\lambda_{i,i+k}) < 1$, so that we can use Lemma A.4. We first compute the limit of $e^{-2\lambda_{i,i+k}t} L_{i+1,i+k}^a * d\mathcal{B}_i(t)$ when t goes to infinity when either $\lambda_{i,i+k} = \lambda_i$ or $\lambda_{i,i+k} \neq \lambda_i$. We start with the case $\lambda_{i,i+k} \neq \lambda_i$ (so, $\lambda_{i,i+k} = \lambda_{i+1,i+k}$). For all $t \geq 0$, we have

$$e^{-2\lambda_{i,i+k}t} L_{i+1,i+k}^a * d\mathcal{B}_i(t) = d\mathcal{B}_i^*(2\lambda_{i,i+k}) \int_0^\infty \mathbb{1}_{[0,t]} e^{-2\lambda_{i,i+k}(t-u)} L_{i+1,i+k}^a(t-u) \widehat{d\mathcal{B}_i}(u) du.$$

According to $\mathcal{H}^{k-1}$, we know that $L_{i+1,i+k}^a(t) \sim \widetilde{L}_{i+1,i+k}(a) e^{2\lambda_{i,i+k}t}$. We deduce with a Lebesgue dominated convergence theorem that

$$\lim_{t \to \infty} e^{-2\lambda_{i,i+k}t} L_{i+1,i+k}^a * d\mathcal{B}_i(t) = d\mathcal{B}_i^*(2\lambda_{i,i+k}) \widetilde{L}_{i+1,i+k}(a).$$

We apply the same method as above for the other terms of the source term. Hypothesis III.4 gives us that $M_{i,i+k}^a \sim e^{\lambda_{i,i+k}t} \widetilde{M}_{i,i+k}(a)$ and $M_{i+1,i+k}^a \sim e^{\lambda_{i,i+k}t} \widetilde{M}_{i+1,i+k}(a)$. Using Lebesgue dominated convergence theorem, we obtain:

$$\lim_{t \to \infty} e^{-2\lambda_{i,i+k}t} \left[2p_{2,0}^{(i)} (M_{i,i+k}^a)^2 + 2p_{1,1}^{(i)} M_{i,i+k}^a M_{i+1,i+k}^a + 2p_{0,2}^{(i)} (M_{i+1,i+k}^a)^2 \right] * d\mathcal{B}_i(t)$$
$$= \left[2p_{2,0}^{(i)} (\widetilde{M}_{i,i+k}(a))^2 + 2p_{1,1}^{(i)} \widetilde{M}_{i,i+k}(a) \widetilde{M}_{i+1,i+k}(a) + 2p_{0,2}^{(i)} (\widetilde{M}_{i+1,i+k}(a))^2 \right] d\mathcal{B}_i^*(2\lambda_{i,i+k}).$$

We then consider the case $\lambda_{i,i+k} = \lambda_i > \lambda_{i+1,i+k}$ and start by computing the limit of $e^{-2\lambda_{i,i+k}t} L_{i+1,i+k}^a * d\mathcal{B}_i(t)$.

$$e^{-2\lambda_{i,i+k}t} L_{i+1,i+k}^a * d\mathcal{B}_i(t) = d\mathcal{B}_i^*(2\lambda_{i,i+k}) e^{-2(\lambda_{i,i+k}-\lambda_{i+1,i+k})t} \int_0^\infty \mathbb{1}_{[0,t]} e^{-2\lambda_{i+1,i+k}(t-u)} L_{i+1,i+k}^a(t-u) \widehat{d\mathcal{B}_i}(u) du.$$

Using $\mathcal{H}^{k-1}$ and Lebesgue dominated convergence theorem, we first obtain that

$$\lim_{t \to \infty} \int_0^\infty \mathbb{1}_{[0,t]} e^{-2\lambda_{i+1,i+k}(t-u)} L_{i+1,i+k}^a(t-u) \widehat{d\mathcal{B}_i}(u) du = d\mathcal{B}_i^*(2\lambda_{i+1,i+k}) \widetilde{L}_{i+1,i+k}(a) < \infty,$$

hence,

$$\lim_{t \to \infty} e^{-2\lambda_{i,i+k}t} L_{i+1,i+k}^a * d\mathcal{B}_i(t) = 0.$$

Then, Hypothesis III.4 give us that $M_{i,i+k}^a \sim e^{\lambda_{i,i+k}t} \widetilde{M}_{i,i+k}(a)$ and $M_{i+1,i+k}^a \sim e^{\lambda_{i+1,i+k}t} \widetilde{M}_{i+1,i+k}(a)$. Using similar methods, we obtain:

$$\lim_{t \to \infty} e^{-2\lambda_{i,i+k}t} \left[2p_{2,0}^{(i)} (M_{i,i+k})^2 + 2p_{1,1}^{(i)} M_{i,i+k} M_{i+1,i+k} + 2p_{0,2}^{(i)} (M_{i+1,i+k})^2 \right] * d\mathcal{B}_i(t)$$
$$= 2p_{2,0}^{(i)} (\widetilde{M}_{i,i+k})^2 d\mathcal{B}_i^*(2\lambda_{i,i+k}).$$

We conclude by applying Lemma A.4 that $\mathcal{H}^k$ holds. □

Variance

Definition A.3. *We write $v_j^a(t)$, the variance of $Y_t^{(j,a)}$ starting from a mother cell on the first layer such that:*

$$v_j^a(t) = \mathbb{E}[(Y_t^{(j,a)})^2 | Z_0 = \delta_{1,0}] - \mathbb{E}[Y_t^{(j,a)} | Z_0 = \delta_{1,0}]^2.$$

We study the asymptotic behavior of the variance $v_j^a(t)$ when the first layer is the leading one.

Corollary A.1. *Let $a \geq 0$. Under the same hypotheses as in Hypothesis A.1 and supposing that $c = 1$, we have*

$$\forall k \in [\![1, J]\!] \quad v_j^a(t) \sim \widetilde{v}_j(a)e^{2\lambda_c t}, \ as \ t \to \infty$$

where

$$\widetilde{v}_j(a) = \widetilde{L}_{1,j}(a) - (m_j(a))^2 = \left[\frac{2p_{2,0}^{(1)}d\mathcal{B}_1^*(2\lambda_1)}{1 - 2p_S^{(1)}d\mathcal{B}_1^*(2\lambda_1)} - 1 \right] (m_j(a))^2.$$

Proof. Let $a \geq 0$. According to Hypothesis A.1 and using that $c = 1$, we have:

$$\forall j \in [\![1, J]\!], \quad L_{1,j}^a(t) \sim \widetilde{L}_{1,j}(a)e^{2\lambda_1 t}, \quad as \ t \to \infty.$$

Using Hypothesis III.4 and A.1, we deduce for all $j \in [\![1, J]\!]$:

$$\widetilde{v}_j(a) = \widetilde{L}_{1,j}(a) - (m_j(a))^2 = \left[\frac{2p_{2,0}^{(1)}d\mathcal{B}_1^*(2\lambda_1)}{1 - 2p_S^{(1)}d\mathcal{B}_1^*(2\lambda_1)} - 1 \right] (m_j(a))^2.$$
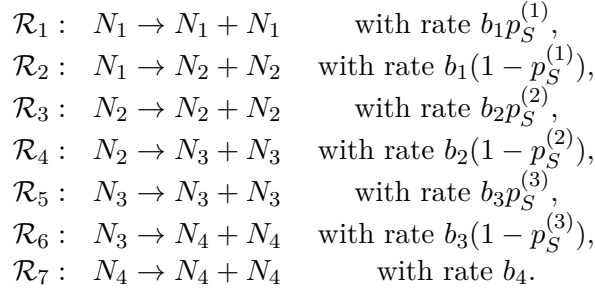
$\square$

a) Stochastic simulation procedures

Markov case

Considering a markovian case, we simulate the process Z_t solution of the SDE (III.4) with the Gillespie algorithm. We use the package StochSS [169].

We consider that for each layer $j \in [\![1, 3]\!]$, $p_{1,1}^{(j)} = 0$. Hence, $p_{2,0}^{(j)} = p_S^{(j)}$ and $p_{0,2}^{(j)} = 1 - p_S^{(j)}$. Considering a system with 4 layers, our system is ruled by the 7-th reactions below:

$$
\begin{aligned}
\mathcal{R}_1 &: \quad N_1 \to N_1 + N_1 & \text{with rate } b_1 p_S^{(1)}, \\
\mathcal{R}_2 &: \quad N_1 \to N_2 + N_2 & \text{with rate } b_1(1 - p_S^{(1)}), \\
\mathcal{R}_3 &: \quad N_2 \to N_2 + N_2 & \text{with rate } b_2 p_S^{(2)}, \\
\mathcal{R}_4 &: \quad N_2 \to N_3 + N_3 & \text{with rate } b_2(1 - p_S^{(2)}), \\
\mathcal{R}_5 &: \quad N_3 \to N_3 + N_3 & \text{with rate } b_3 p_S^{(3)}, \\
\mathcal{R}_6 &: \quad N_3 \to N_4 + N_4 & \text{with rate } b_3(1 - p_S^{(3)}), \\
\mathcal{R}_7 &: \quad N_4 \to N_4 + N_4 & \text{with rate } b_4.
\end{aligned}
$$

General case

We simulate our process using the algorithm 3, on a predefine time horizon $T_{\max}$.

b) Deterministic simulation protocol

To solve numerically the problem (III.5), we design a dedicated finite volume scheme adapted to the non-conservative form with proper boundary conditions. We define the time step Δt and the age step Δa. The time discretization is defined by

$$t_0 = 0, \quad t_{n+1} = t_n + \Delta t, \quad \text{for } n = 0, ..., N_t$$

where $(N_t + 1)\Delta t$ is the time horizon of the simulation. Similarly, N_a is the number of cells[1] in the domain. The cells $\mathcal{C}_i$ are indexed by a rational number i ($\frac{1}{2}, \frac{3}{2}$, etc.) with $i \in [\![\frac{1}{2}, N_a - \frac{1}{2}]\!]$.

---

[1]The cell is here the standard name used for each elementary volume in the framework of finite volume methods.

Define a sequence $\mathcal{S}$ of cells of a given age and layer;
Simulate the time of division of each cell in $\mathcal{S}$;
while $t < T_{\max}$ **do**

> Select the next cell m that will divide. l^m is its layer index and a^{l^m} is the age at division.;
>
> Randomly draw the layer of its daughters cell l^{d_1} and l^{d_2} according to the probabilities $p_{2,0}^{(l^m)}$, $p_{1,1}^{(l^m)}$ and $p_{2,0}^{(l^m)}$.;
>
> Randomly draw the next time of division of daughter cell d_1 according to its layer index l^{d_1}. ;
>
> Randomly draw the next time of division of daughter cell d_2 according to its layer index l^{d_2}. ;
>
> Add d_1 and d_2 into the sequence $\mathcal{S}$. ;
>
> $t \leftarrow t + t^m$;

end

Algorithm 3: Simulation stochastic process

The edges of each cell are located at $a_{i-\frac{1}{2}} = (i - \frac{1}{2})\Delta a$ and $a_{i+\frac{1}{2}} = (i + \frac{1}{2})\Delta a$ (remark that $\Delta a = a_{i+\frac{1}{2}} - a_{i-\frac{1}{2}}$ and $a_0 = 0$). As age and time evolve at the same speed, we chose N_a such that $t_{N_t} - a_{\max}^0 < N_a \Delta a$ where $a_{\max}^0$ is the maximal age of the initial distribution.

Let $j \in [\![1, J]\!]$. We define $P_{n,i}^j$ as the mean value of the density $\rho^{(j)}$ in cell $\mathcal{C}_i$ at time t_n:

$$P_{n,i}^j := \frac{1}{\Delta a} \int_{a_{i-\frac{1}{2}}}^{a_{i+\frac{1}{2}}} \rho^{(j)}(t_n, a)\, da\,.$$

We integrate the equation $\partial_t \rho^{(j)} + \partial_a \rho^{(j)} = -b_j \rho^{(j)}$ with respect to age in cell $\mathcal{C}_i$ and obtain:

$$\frac{d}{dt} \int_{a_{i-\frac{1}{2}}}^{a_{i+\frac{1}{2}}} \rho^{(j)}(t, a)\, da = -\rho^{(j)}(t, a_{i+\frac{1}{2}}) + \rho^{(j)}(t, a_{i-\frac{1}{2}}) - \int_{a_{i-\frac{1}{2}}}^{a_{i+\frac{1}{2}}} b_j(a)\rho^{(j)}(t, a)\, da.$$

Then, we suppose that all b_js functions are regular enough so that we can approximate b_j, for all $j \in [\![1, J]\!]$ on each cell $\mathcal{C}_i$ by their mean value $\bar{b}_j^i$. We obtain:

$$\frac{d}{dt} \int_{a_{i-\frac{1}{2}}}^{a_{i+\frac{1}{2}}} \rho^{(j)}(t, a)\, da = -\rho^{(j)}(t, a_{i+\frac{1}{2}}) + \rho^{(j)}(t, a_{i-\frac{1}{2}}) - \bar{b}_j^i \int_{a_{i-\frac{1}{2}}}^{a_{i+\frac{1}{2}}} \rho^{(j)}(t, a)\, da.$$

We approximate the derivative in time with a finite difference scheme:

$$\frac{d}{dt} \int_{a_{i-\frac{1}{2}}}^{a_{i+\frac{1}{2}}} \rho^{(j)}(t_n, a)\, da = \frac{1}{\Delta t}\left[\int_{a_{i-\frac{1}{2}}}^{a_{i+\frac{1}{2}}} \rho^{(j)}(t_{n+1}, a)da - \int_{a_{i-\frac{1}{2}}}^{a_{i+\frac{1}{2}}} \rho^{(j)}(t_n, a)da \right] + \mathcal{O}(\Delta t)$$

and we deduce:

$$\frac{\Delta a}{\Delta t}\left[P_{n+1,i}^j - P_{n,i}^j \right] = -\rho^{(j)}(t, a_{i+\frac{1}{2}}) + \rho^{(j)}(t, a_{i-\frac{1}{2}}) - \bar{b}_j^i \Delta a P_{n,i}^j.$$

The edge terms $\rho^{(j)}(t, a_{i+\frac{1}{2}})$ and $\rho^{(j)}(t, a_{i-\frac{1}{2}})$ correspond to the fluxes that cross the boundaries of cell $\mathcal{C}_i$. When $i = \frac{1}{2}$, the boundary condition of equation (III.5) gives us the value of

this term:

$$\rho^{(j)}(t_n, a_0) = 2p_S^{(j)} \int_0^\infty b_j(a)\rho^{(j)}(t_n, a)da + 2(1 - p_S^{(j-1)}) \int_0^\infty b_{j-1}(a)\rho^{(j-1)}(t_n, a)da$$

$$= 2p_S^{(j)} \sum_i \int_{\mathcal{C}_i} b_j(a)\rho^{(j)}(t_n, a)da + 2(1 - p_S^{(j-1)}) \sum_i \int_{\mathcal{C}_i} b_{j-1}(a)\rho^{(j-1)}(t_n, a)da$$

$$= 2p_S^{(j)} \Delta t \sum_i \bar{b}_i P_{n,i}^j + 2(1 - p_S^{(j-1)})\Delta t \sum_i \bar{b}_i^{j-1} P_{n,i}^{j-1}.$$

When $i \neq \frac{1}{2}$, we approximate each term $\rho^{(j)}(t_n, a_{i+\frac{1}{2}})$ by

$$\rho^{(j)}(t_n, a_{i+\frac{1}{2}}) = P_{n,i+\frac{1}{2}}^j + \mathcal{O}(\Delta a).$$

Hence, we obtain the following numerical scheme:

$$P_{n+1,i}^j = \left[1 - \bar{b}_i^j \Delta t - \frac{\Delta t}{\Delta x}\right] P_{n,i}^j + \frac{\Delta t}{\Delta x} P_{n,i-1}^j$$

$$P_{n+1,\frac{1}{2}}^j = \left[1 - \bar{b}_{\frac{1}{2}}^j \Delta t - \frac{\Delta t}{\Delta x}\right] P_{n,\frac{1}{2}}^j + 2s_j \Delta t \sum_i \bar{b}_i P_{n,i}^j + 2(1 - s_{j-1})\Delta t \sum_i \bar{b}_i^{j-1} P_{n,i}^{j-1}.$$

A.1.4 Construction of Figure III.5

In this part, we give some details about the construction of figure III.5. We simulate the SDE (III.4) using the algorithm 3 and the PDE (III.5) using the algorithm described in the subsection below (see b)) taking $\Delta a = 9.5 \times 10e - 3$ and $\Delta t = 10e - 4$.

We discretized the age according to a sequence of integers $k \in [\![1, 50]\!]$. Let $j \in [\![1, J]\!]$ be a layer index. The color bar associated with age k for the jth layer corresponds to the total number of cells on the jth layer of age $a \in [k, k+1)$ renormalized by the total number of cells:

$$\frac{<< Z_t, \mathbb{1}_{j,k\leq a<k+1} >>}{<< Z_t, \mathbb{1} >>}.$$

The dashed black line with the age k for the jth layer corresponds to:

$$\frac{\int_k^{k+1} \rho^{(j)}(t, a)da}{\sum_{j=1}^4 \int_0^{+\infty} \rho^{(j)}(t, a)da} \sim \frac{\sum_{i=\lfloor\frac{k}{\Delta x}\rfloor}^{\lfloor\frac{k+1}{\Delta x}\rfloor - 1} P_{n,i}^j}{\sum_{j=1}^4 \sum_i P_{n,i}^j}.$$

The color solid lines which represent the stable distribution $\hat{\rho}$ and compute their value at each age point k by

$$\frac{\int_k^{k+1} \hat{\rho}^{(j)}(a)da}{\sum_{j=1}^4 \int_0^{+\infty} \hat{\rho}^{(j)}(a)da}.$$

A.1.5 Parameter estimation procedure

Using the software D2D [91], we estimate the parameters of our model, using an additive Gaussian noise statistical model (standard least squares likelihood). The standard deviation and the initial number N of cells on the first layer are also estimated. To investigate the practical identifiability, we compute the profile likelihood estimate (PLE) [138]. We observe that all the parameters are practically identifiable except the probability of staying on the second layer $p_S^{(2)}$ (see Figure A.1a). In contrast, most of the parameters are not practically identifiable when we consider the total number of cells as the observable function $(\sigma(t;p) = \sum_{j=1}^{J} M^{(j)}(t;p)$, Figure A.1b).

A.2 Additionnal materials of Chapter 5

A.2.1 Numerical scheme

Proof. Let $j \in [\![1, J]\!]$. From the transport equation (V.5) and applying an Euler explicit scheme for the differential operators ∂_a and ∂_t, we have, for all $k > 0$,

$$\frac{\tilde{\rho}^{(j)}(t_{k+1}, a_n) - \tilde{\rho}^{(j)}(t_k, a_n)}{\Delta} + \frac{\tilde{\rho}^{(j)}(t_k, a_{n+1}) - \tilde{\rho}^{(j)}(t_k, a_n)}{\Delta} + \mathcal{O}(\Delta) = 0.$$

We deduce first that

$$\tilde{\rho}^{(j)}(t_{k+1}, a_n) \approx \tilde{\rho}^{(j)}(t_k, a_{n-1}).$$

Then, applying the $\tilde{\rho}^{(j)}$ definition, we deduce the relation for $U_{k,n}^j$ (V.6). We now tackle the boundary condition. Taking advantage of the unidirectional motion, we proceed by recurrence starting with layer 1:

$$\rho^{(1)}(t, 0) = 2p_S^{(1)} \int_{A_{\min}^1}^{A_{\max}^1} b_1(a)\rho^{(1)}(t, a)\, da.$$

Since $b_1(a)\rho^{(1)}(t, a) = -\partial_t\rho^{(1)}(t, a) - \partial_a\rho^{(1)}(t, a)$, we deduce that

$$\rho^{(1)}(t, 0) = -2p_S^{(1)} \int_{A_{\min}^1}^{A_{\max}^1} \partial_t\rho^{(1)}(t, a)\, da + 2p_S^{(1)}\rho^{(1)}(t, (A_{\min}^1)^+) - 2p_S^{(1)}\rho^{(1)}(t, (A_{\max}^1)^-).$$

Applying an Euler implicit scheme to the differential operator ∂_t, we obtain

$$\rho^{(1)}(t_{k+1}, 0) = 2p_S^{(1)}\rho^{(1)}(t_{k+1}, (A_{\min}^1)^+) - 2p_S^{(1)}\rho^{(j)}(t_{k+1}, (A_{\max}^1)^-) - 2p_S^{(1)} \int_{A_{\min}^1}^{A_{\max}^1} \left(\frac{\rho^{(1)}(t_{k+1}, a) - \rho^{(1)}(t_k, a)}{\Delta} \right) da + \mathcal{O}$$

$$\tag{A.12}$$

We discretize the integral using a classical left rectangle rule where the integral $\int_{a_k}^{a_{k+1}} g(a)da$ is approximated by $(a_{k+1} - a_k)g(a_k)$, and obtain the following formula:

$$\int_{A_{\min}^1}^{A_{\max}^1} \rho^{(1)}(t_{k+1}, a)da = \Delta \sum_{n=\lfloor \frac{A_{\min}^1}{\Delta} \rfloor}^{\lfloor \frac{A_{\max}^1}{\Delta} \rfloor - 1} \rho^{(1)}(t_{k+1}, a_n) + \mathcal{O}(\Delta^2). \tag{A.13}$$

Combining expressions (A.12) and (A.13), we deduce that

$$\rho^{(1)}(t_{k+1}, 0) = 2p_S^{(1)}\rho^{(1)}(t_{k+1}, A_{\min}^j) - 2p_S^{(1)}\rho^{(1)}(t_{k+1}, A_{\max}^1) - 2p_S^{(1)} \sum_{n=\lfloor \frac{A_{\min}^1}{\Delta} \rfloor}^{\lfloor \frac{A_{\max}^1}{\Delta} \rfloor - 1} \left(\rho^{(1)}(t_{k+1}, a_n) - \rho^{(1)}(t_k, a_n) \right) + \mathcal{O}(\Delta).$$
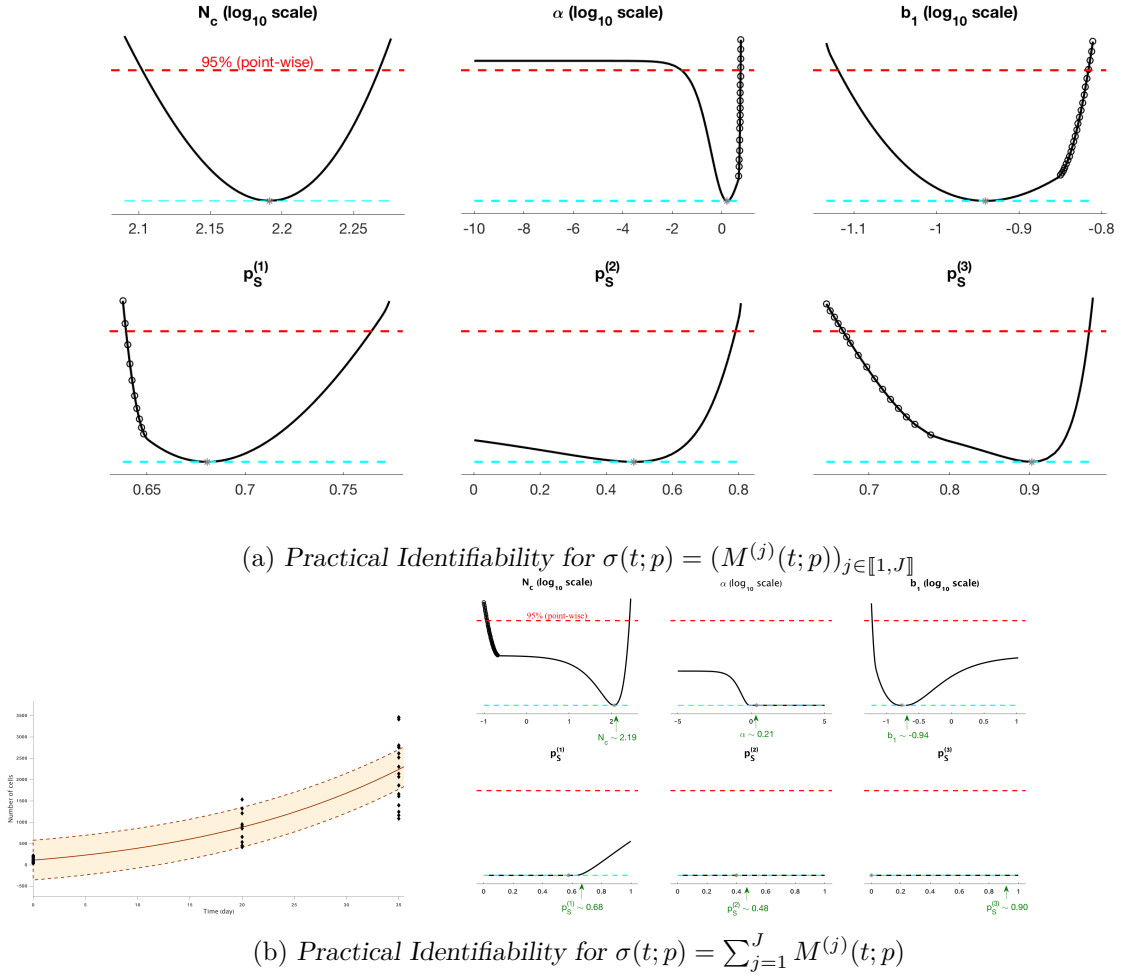
(a) *Practical Identifiability for* $\sigma(t;p) = (M^{(j)}(t;p))_{j\in[\![1,J]\!]}$

(b) *Practical Identifiability for* $\sigma(t;p) = \sum_{j=1}^{J} M^{(j)}(t;p)$

Fig. A.1 **Practical Identifiability**. **Figure A.1a** *Profile likelihood estimate (PLE) for each parameter in the set* $\mathbf{P}_{exp} = \{N, b_1, \alpha, p_S^{(1)}, p_S^{(2)}, p_S^{(3)}\}$ *when the observation function is* $\sigma(t;p) = (M^{(j)}(t;p))_{j\in[\![1,J]\!]}$. *The red dashed lines correspond to the 95%-statistical threshold while the blue dashed lines correspond to the optimum value of the likelihood.* **Figure A.1b** *Parameter estimation results for* $\sigma(t;p) = \sum_{j=1}^{J} M^{(j)}(t;p)$. **Left panel**: *Data fitting model with model (III.7). The black diamonds represent the experimental data (total number of cells), the solid line is the best fit solution of (III.7) and the dashed lines are drawn from the estimated variance.* **Left panel**: *Profile likelihood estimates of each parameter in the set* P_{exp}.

We define $U_{n,0}^1$ as follow

$$U_{k+1,0}^1 = 2p_S^{(1)} U_{k+1,\lfloor\frac{A_{\min}^1}{\Delta}\rfloor}^1 - 2p_S^{(1)} U_{k+1,\lfloor\frac{A_{\max}^1}{\Delta}\rfloor}^1 - 2p_S^{(1)} \sum_{n=\lfloor\frac{A_{\min}^1}{\Delta}\rfloor}^{\lfloor\frac{A_{\max}^1}{\Delta}\rfloor-1} \left(U_{k+1,n}^1 - U_{k,n}^1\right)$$

$$= -2p_S^{(1)} \sum_{n=\lfloor\frac{A_{\min}^1}{\Delta}\rfloor+1}^{\lfloor\frac{A_{\max}^1}{\Delta}\rfloor} U_{k+1,n}^1 + 2p_S^{(1)} \sum_{n=\lfloor\frac{A_{\min}^1}{\Delta}\rfloor}^{\lfloor\frac{A_{\max}^1}{\Delta}\rfloor-1} U_{k,n}^1.$$

Using $U_{k+1,n}^1$ definition (V.6), we deduce that

$$U_{k+1,0}^1 = 2p_S^{(1)} \sum_{n=\lfloor \frac{A_{\min}^1}{\Delta} \rfloor}^{\lfloor \frac{A_{\max}^1}{\Delta} \rfloor - 1} \left(1 - e^{-\int_{(n-1)\Delta}^{n\Delta} b_1(s)ds} \right) U_{n,k}^1.$$

We now consider the case $j > 1$:

$$\rho^{(j)}(t,0) = 2(1 - p_S^{(j-1)}) \int_{A_{\min}^{j-1}}^{A_{\max}^{j-1}} b_{j-1}(a)\rho^{(j-1)}(t,a)\, da + 2p_S^{(j)} \int_{A_{\min}^j}^{A_{\max}^j} b_j(a)\rho^{(j)}(t,a)\, da.$$

We use the same approach to discretize the two integrals in the right-hand side of the equation above and obtain expression (V.7). □

A.2.2 Complement of proofs

Proof of Lemma V.1. Taking the derivative of expression (V.11), we obtain

$$m_1'(t) = \frac{d}{dt} \int_{a_{\min}^\psi + t}^{a_{\max}^\psi + t} \rho(t,a)da + \frac{d}{dt} \int_0^{\min(0, A^{\min} - a_{\max}^\psi + t)} \rho(t,a)da. \tag{A.14}$$

Since the boundaries of the two right hand-side terms of expression (A.14) depend on time, changes of variables are required to proceed to the derivation.
We first start by the term corresponding to the remaining cells. Applying the change of variables $s = a - a_{\min}^\psi - t$, we deduce that, for all $t \geq 0$,

$$\frac{d}{dt} \int_{a_{\min}^\psi + t}^{a_{\max}^\psi + t} \rho(t,a)da = \frac{d}{dt} \int_0^{a_{\max}^\psi - a_{\min}^\psi} \rho(t, s + a_{\min}^\psi + t)ds$$

$$= \int_0^{a_{\max}^\psi - a_{\min}^\psi} \left[\partial_t\rho(t, s + a_{\min}^\psi + t) + \partial_a\rho(t, s + a_{\min}^\psi + t) \right] ds = \int_{a_{\min}^\psi + t}^{a_{\max}^\psi + t} \partial_t\rho(t,a)da + [\rho(t,a)]_{a_{\min}^\psi + t}^{a_{\max}^\psi + t}, \tag{A.15}$$

applying first the chain rule then the reverse change of variables $a = s + a_{\min}^\psi + t$.

We turn now to the term representing the cells born since time $t = A^{\min} - a_{\max}^\psi$. For all $t > A^{\min} - a_{\max}^\psi$, we apply the change of variables $a = s(A^{\min} - a_{\max}^\psi + t)$ and obtain,

$$\int_0^{A^{\min} - a_{\max}^\psi + t} \rho(t,a)da = (A^{\min} - a_{\max}^\psi) \int_0^1 \rho(t, s(A^{\min} - a_{\max}^\psi + t))ds.$$

Taking the derivative of this expression and using the chain rule, we obtain:

$$\frac{d}{dt} \int_0^{A^{\min} - a_{\max}^\psi + t} \rho(t,a)da = \int_0^1 \rho(t, s(A^{\min} - a_{\max}^\psi + t))ds$$

$$+ (A^{\min} - a_{\max}^\psi + t) \int_0^1 \left[\partial_t\rho(t, s(A^{\min} - a_{\max}^\psi + t)) + s\partial_a\rho(t, s(A^{\min} - a_{\max}^\psi + t)) \right] ds. \tag{A.16}$$

Using an integration by part, we first deduce that

$$(A^{\min}-a^\psi_{\max}+t)\int_0^1 s\partial_a\rho(t,s(A^{\min}-a^\psi_{\max}+t))ds = \Big[s\rho(t,s(A^{\min}-a^\psi_{\max}+t))\Big]_0^1 - \int_0^1 \rho(t,s(A^{\min}-a^\psi_{\max}+t))ds. \tag{A.17}$$

Combining expressions (A.16) and (A.17), we deduce that

$$\frac{d}{dt}\int_0^{A^{\min}-a^\psi_{\max}+t}\rho(t,a)da = (A^{\min}-a^\psi_{\max}+t)\int_0^1 \partial_t\rho(t,s(A^{\min}-a^\psi_{\max}+t))ds + \rho(t,A^{\min}-a^\psi_{\max}+t)$$

$$= \int_0^{A^{\min}-a^\psi_{\max}+t}\partial_t\rho(t,a)da + \rho(t,A^{\min}-a^\psi_{\max}+t), \tag{A.18}$$

using the reverse change of variables $s = \frac{a}{a^\psi_{\max}+t}$.

Finally, combining expressions (A.15) and (A.18), we deduce, for all $t > A^{\min}-a^\psi_{\max}$,

$$m_1'(t) = \int_{a^\psi_{\min}+t}^{a^\psi_{\max}+t}\partial_t\rho(t,a)da + [\rho(t,a)]_{a^\psi_{\min}+t}^{a^\psi_{\max}+t} + \int_0^{A^{\min}-a^\psi_{\max}+t}\partial_t\rho(t,a)da + \rho(t,A^{\min}-a^\psi_{\max}+t). \tag{A.19}$$

From PDEs (V.1), we can write that

$$\int_{a^\psi_{\min}+t}^{a^\psi_{\max}+t}\partial_t\rho(t,a)da = -\int_{a^\psi_{\min}+t}^{a^\psi_{\max}+t}b(a)\rho(t,a)da - [\rho(t,a)]_{a^\psi_{\min}+t}^{a^\psi_{\max}+t} \tag{A.20}$$

and

$$\int_0^{A^{\min}-a^\psi_{\max}+t}\partial_t\rho(t,a)da = -\int_0^{A^{\min}-a^\psi_{\max}+t}b(a)\rho(t,a)da - [\rho(t,a)]_0^{A^{\min}-a^\psi_{\max}+t}. \tag{A.21}$$

Using expressions (A.20) and (A.21), we deduce from expression (A.19), that for all $t > A^{\min}-a^\psi_{\max}$,

$$m_1'(t) = -\int_0^{+\infty}b(a)\rho(t,a)da + \rho(t,0) = \frac{2p_S-1}{2p_S}\rho(t,0).$$

We complete the proof by considering the case when $t \in [0, A^{\min}-a^\psi_{\max}]$. In that case, no division has occurred, hence for all $t \in [0, A^{\min}-a^\psi_{\max}]$, $\rho(t,0) = \int_0^{\min(0,A^{\min}-a^\psi_{\max}+t)}\rho(t,a)da = 0$. In the same way as previously, we obtain that for all $t \in [0, A^{\min}-a^\psi_{\max}]$,

$$m_1'(t) = -\int_{a^\psi_{\min}+t}^{a^\psi_{\max}+t}b(a)\rho(t,a)da = 0 = \frac{2p_S-1}{2p_S}\rho(t,0),$$

since the intersection of the support of b, $(A^{\min}, A^{\max})$, and the interval $[a^\psi_{\min}+t, a^\psi_{\max}+t]$ is empty when $t \in [0, A^{\min}-a^\psi_{\max}]$. This ends the proof. $\qquad\square$

A.2.3 Complementary illustrations of Algorithm

We observe that the numerical convergence rate is faster, in both the L^∞ and L^2 relative error norms, in the case of a polynomial b function, as well as in the L^2 norm in the case of a bump function, compared to the other cases. The convergence pattern differs according to the norm both in the bump and piecewise constant cases. A plateau is reached for relatively high values of Δ in the case of a bump function and L^∞ norm.
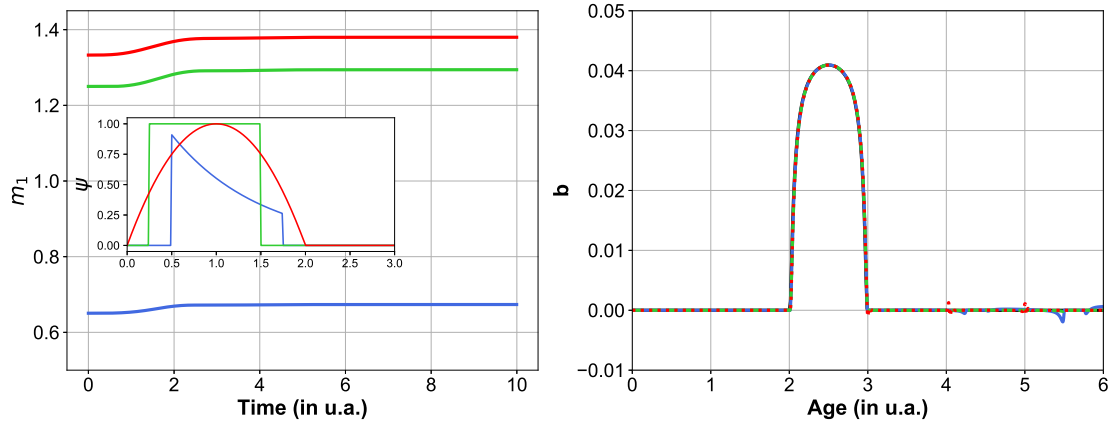
(a) *Complementary illustrations of Corollary V.1 for different initial conditions*
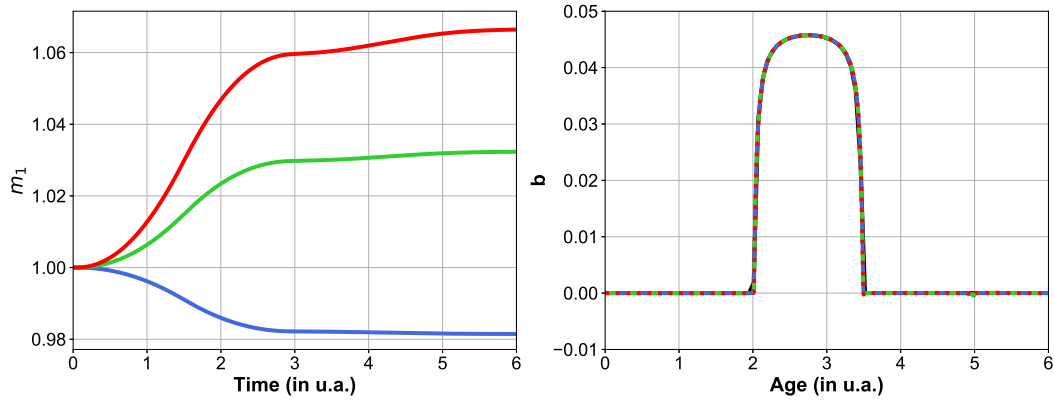

(b) *Complementary illustrations of Corollary V.1 for different p_S values*

Fig. A.2 **Complementary illustrations of Algorithm 2**. *We proceed in the same way as in Figure V.3 using the bump function and for either different initial conditions (Figure A.2a): $\psi(a) = 1.5\exp(-a)\mathbf{1}_{[0.5,1.75]}(a)$(blue line); $\psi(a) = \mathbf{1}_{[0.25,1.5]}(a)$(green line) and $\psi(a) = a(a-2)\mathbf{1}_{[0.,2.]}(a)$(red line), with $p_S = 1$, or different p_S values (Figure A.2b): $p_S = 0.35$ (blue line), $p_S = 0.75$ (green line) or $p_S = 1$ (red line), with $\psi(a) = \mathbf{1}_{[0.5,2]}(a)$.*
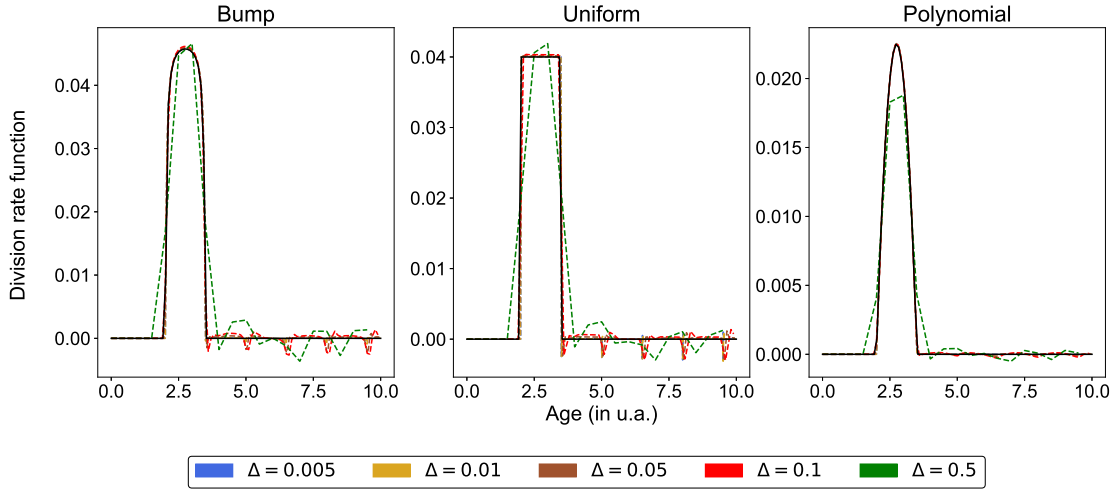
(a) *Estimated b function*
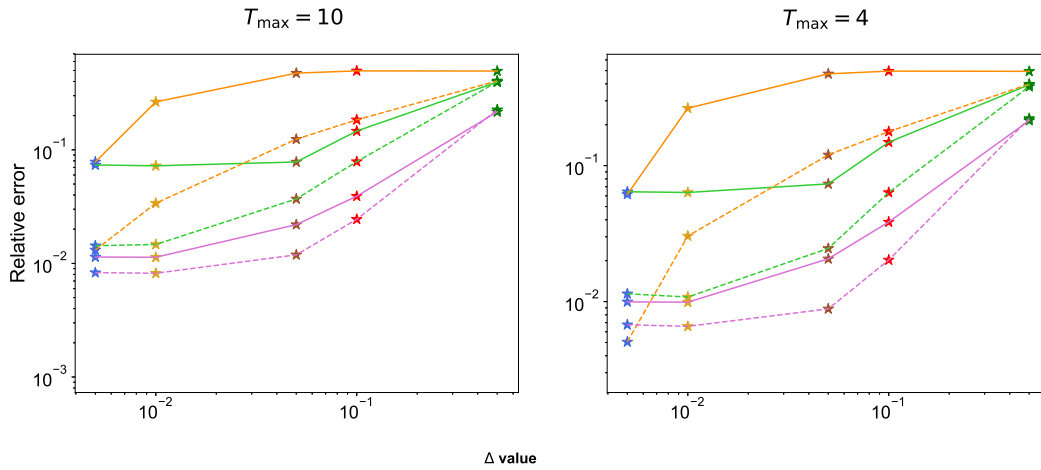
(b) *Relative error analysis*

Fig. A.3 ***Sensitivity of the reconstruction algorithm to the observation sampling rate***. *We simulate m_1 using the numerical scheme for the same division rates function, initial condition and p_S parameter as in Figure V.3 with $\Delta = 5 \times 10^{-3}$. We thus obtain two vectors of size K: the discretized $m_1^K = (m_1^k)_{k=0,...,K-1}$ vector and its associated time vector $t^K = (t_k)_{k=0,...,K-1}$. For Δ chosen in the grid of increasing step sizes $\Delta \in \{0.005, 0.01, 0.05, 0.1, 0.5\}$, we extract from vectors m_1^K and t^K the sub-vectors $m_1^{K_\Delta}$ and t^{K_Δ} such that $t_1^{K_\Delta} = k\Delta$. Then, we apply Algorithm 2 and deduce the estimated b^Δ function from $m_1^{K_\Delta}$ (Figure A.3a). Figure A.3b: we compute the relative L^2 and L^∞ errors (dashed and solid lines, respectively) by comparing each estimated b^Δ functions to the original b functions computed with the finest step size. Pink lines: polynomial b function, orange lines: uniform b function, green lines: bump b function. Each colored star represents the relative error obtained for a given Δ value.*

Bibliography

[1] F. Clément, P. Michel, D. Monniaux & T. Stiehl; «Coupled Somatic Cell Kinetics and Germ Cell Growth: Multiscale Moded-Base Insight on Ovarian Follicular Development»; Multiscale Model. Simul. **11**, p. 719–746 (2013). VIII, 2, 32, 39, 81, 89, 90, 93, 98, 113, 115, 116, 122, 126, 150

[2] G. Box; «Science and Statistics»; Journal of the American Statistical Association **71**, p. 791—-799 (1976). 1

[3] P. Michel; «Large population and size scale limit of a stochastic particle model»; Mathematical Models and Methods in Applied Sciences **27**, p. 581–615 (2017). 2, 90, 119, 120, 150

[4] T. Malthus; *An essay on the principle of population* (J. Johnson, London) (1798). 2

[5] A. Lotka; «Contribution to the Theory of Periodic Reaction»; J.Phys.Chem. **14**, p. 271–274 (1910). 3

[6] V. Volterra; «Variazioni e fluttuazioni del numero d'individui in specie animali conviventi»; Mem. Acad. Lincei Roma. **2**, p. 31–113 (1926). 3

[7] R. Antia, C. Bergstrom, S. Pilyugin, S. M. Kaech & R. Ahmed; «Models of CD8+ Responses: 1. What is the Antigen-independent Proliferation Program»; Journal of Theoretical Biology **221**, p. 585–598 (2003). 3

[8] F. Crauste, J. Mafille, L. Boucinha, S. Djebali, O. Gandrillon, J. Marvel & C. Arpin; «Identification of nascent memory CD8 T cells and modeling of their ontogeny»; Cell Systems **4**, p. 306–317 (2017). 3

[9] B. Freret-Hodara, Y. Cui, A. Griveau, L. Vigier, Y. Arai, J. Touboul & A. Pierani; «Enhanced Abventricular Proliferation Compensates Cell Death in the Embryonic Cerebral Cortex»; Cereb. Cortex **27** (2016). 3, 44, 149

[10] F. Clément, M.-A. Gruet, P. Monget, M. Terqui, E. Jolivet & D. Monniaux; «Growth kinetics of the granulosa cell population in ovarian follicles: an approach by mathematical modelling»; Cell.Prolif. **30**, p. 255–570 (1997). 3, 39

[11] P. Michel; *Principe d'entropie relative généralisée et dynamique de populations structurées*; Phd thesis; Université Paris-Dauphine, Paris 9 (2005). 4, 12

[12] B. Perthame; *Transport equations in biology* (Birkhäuser Verlag, Basel) (2007); ISBN 978-3-7643-7842-4. 4, 5, 12, 92

[13] O. Perron; «Zur Theorie der Matrices»; Mathematische Annalen **64**, p. 248—-263 (1907). 4

[14] B. Perthame & J. P. Zubelli; «On the inverse problem for a size-structured population model»; Inverse Problems **23**, p. 1037 (2007). 5, 29, 128

[15] D. Serre; *Matrices, Theory and Applications* (Springer-Verlag New York, Inc) (2002). 5, 6

[16] J. M. Cushing; *An introduction to structured population dynamics*; tome 71 (SIAM) (1998). 7, 8

[17] E. Stadler; «Eigensolutions and spectral analysis of a model for vertical gene transfer of plasmids»; J. Math. Biol. (2018). 7, 12

[18] J. A. Metz & O. Diekmann; *The dynamics of physiologically structured populations*; tome 68 (Springer-Verlag) (1986). 8, 9, 10, 12, 92

[19] B. L. Keyfitz & N. Keyfitz; «The McKendrick partial differential equation and its uses in epidemiology and population study»; Math. Comput. Model. **26**, p. 1–9 (1997). 8, 9, 127, 128, 131

[20] A. McKendrick; «Applications of mathematics to medical problems»; Proceedings of the Edinburgh Mathematical Society **44**, p. 98–130 (1926). 8

[21] H. Von Foerster; «Some remarks on changing populations»; The Kinetics of Cell Proliferation **44**, p. 382–407 (1959). 8

[22] N. Echenim, D. Monniaux, M. Sorine & F. Clément; «Multi-scale modeling of the follicle selection process in the ovary.»; Mathematical biosciences **198**, p. 57–79 (2005). 8, 39

[23] N. Echenim, F. Clément & M. Sorine; «Multiscale modeling of follicular ovulation as a reachability problem.»; Multiscale Model. Simul. **13**, p. 895–912 (2007). 8, 39

[24] P. Michel; «Multiscale modeling of follicular ovulation as a mass and maturity dynamical system»; Multiscale Model. Simul. **9**, p. 282–313 (2011). 8, 39

[25] P. Leslie; «On the use of matrices in certain population mathematics»; Biometrika **33**, p. 183–212 (1945). 8

[26] G. F. Webb; *Theory of nonlinear age-dependent population dynamics* (Marcel Dekker, New York) (1985). 9, 95, 101, 150

[27] M. E. Gurtin & R. C. MacCamy; «Non-linear age-dependent population dynamics»; Arch. Rational Mech. Anal. **54**, p. 281–300 (1974). 9, 127, 128, 129, 131

[28] C. Chiu; «Nonlinear age-dependent models for prediction of population growth»; Math. Biosci. **99**, p. 119–133 (1990). 9, 127, 128, 131, 133

[29] A. M. de Roos; «Numerical methods for structured population models: the Escalator Boxcar Train»; Numer. Methods Partial Differential Equations **4**, p. 173–195 (1988). 9, 127, 131

[30] P. Gwiazda, K. Kropielnicka & A. Marciniak-Czochra; «The escalator boxcar train method for a system of aged-structured equations»; ArXiv (2015). 9

[31] M. Iannelli, T. Kostova & F. A. Milner; «A fourth order method for numerical integration of age and size structured population models»; Numer. Methods Partial Differential Equations **25**, p. 918–930 (2009). ISSN 1098-2426. 9, 131

[32] L. M. Abia, O. Angulo & J. C. López-Marcos; «Age-structured population models and their numerical solution»; Ecol. Modell. **188** (2005). 9, 127, 131

[33] F. Clément, F. Robin & R. Yvinec; «Analysis and calibration of a linear model for structured cell populations with unidirectional motion : Application to the morphogenesis of ovarian follicles»; SIAM J. Appl. Math. p. in press (2019). 9, 28, 89, 92, 119, 127, 128, 129, 130, 131

[34] P. Gabriel; «Measure solutions to the Conservative Renewal Equation»; ESAIM: Proc. Surveys **62**, p. 68–78 (2018). 9, 128, 142

[35] K. Kuritz, D. Stöhr, N. Pollak & F. Allgöwer; «On the relationship between cell cycle analysis with ergodic principles and age-structured cell population models»; Journal of Theoretical Biology **414**, p. 91–102 (2017). 9

[36] P. Gwiazda & E. Wiedmemann; «Generalized Entropy Method for the Renewal Equation with Measure Data»; arXiv **414** (2016). 9

[37] P. Gwiazda & E. Wiedmemann; «Relative entropy method for measure solutions of the growth-fragmentation equation»; SIAM J. Math. Anal. **5**, p. 5811–5824 (2018). 9

[38] P. Gwiazda, J. Jabloński, A. Marciniak-Czochra & A. Ulikowska; «Analysis of particle methods for structured population models with nonlocal boundary term in the framework of bounded Lipschitz distance»; Numerical Methods for Partial Differential Equations **30**, p. 1797–1820 (2014). 9

[39] J. A. Carrillo, P. Gwiazda, K. Kropielnicka & A. Marciniak-Czochra; «The escalator boxcar train method for a system of aged-structured equations in the space of measures»; ArXiv (2018). 9

[40] F. Sharpe & A. Lotka; «A Problem in age distribution.»; Phil. Mag. **21**, p. 435–438 (1911). 9

[41] G. Webb; «A semigroup proof of the Sharpe-Lotka theorem»; Infinite-Dimensional Systems, Lecture Notes in Mathematics **1076**, p. 254–268 (1984). 9, 10

[42] W. Feller; «On the integral equation of renewal theory»; AMS **12**, p. 243—-267 (1941). 9, 21

[43] P. Gabriel; «Équations structurées en dynamique des populations»; Cours de l'Ecole Normale Supérieur de Cachan (2013). 11, 12

[44] M. Doumic, B. Perthame & J. P. Zubelli; «Numerical solution of an inverse problem in size-structured population dynamics»; Inverse Problems **25** (2009). 12, 29, 128

[45] T. Lepoutre; *Analyse et modélisation de phénomènes de croissance et mouvement issus de la biologie.*; Phd thesis; Université Pierre et Marie Curie, Paris 6 (2009). 12

[46] P. Gabriel & H. Martin; «Steady distribution of the incremental model for bacteria proliferation»; J. Math. Biol. **14** (2019). 12

[47] M. Doumic; «Analysis of a Population Model Structured by the Cells Molecular Content»; Math. Model. Nat. Phenom. **2** (2007). 12

[48] S. Méléard, M. Rera & T. Roget; «The bd-model of ageing: from individual-based dynamics to evolutive differential inclusions»; arXiv (2018). 12, 150

[49] J. Almquist, L. Bendrioua, C. Beck Adiels, M. Goksör, S. Hohmann & M. Jirstrand; «A Nonlinear Mixed Effects Approach for Modeling the Cell-To-Cell Variability of Mig1 Dynamics in Yeast»; PLoS ONE (2015). 12

[50] M. Karlsson, D. L. Janzén, L. Durrieu, A. Colman-Lerner, M. C. Kjellsson & G. Cedersund; «Nonlinear mixed-effects modelling for single cell estimation: when, why, and how to use it»; BMC Systems Biology (2015). 12

[51] D. Wilkinson; *Stochastic Modelling for Systems Biology, Second Edition*; Texts in Applied Mathematics (CRC Press) (2011). 12, 44

[52] D. F. Anderson & T. G. Kurtz; *Stochastic analysis of biochemical systems*; tome 1 (Springer) (2015). 13, 14, 15, 19, 48, 149

[53] S. Watanabe; «On discontinuous additive functionals and Lévy measures of a Markov process»; Japan.J.Maths **34** (1964). 15

[54] P. Brémaud; *Markov chains: Gibbs fields, Monte Carlo simulation, and queues*; *Texts in Applied Mathematics*, tome 31 (Springer Science & Business Media) (2013); ISBN 0-387-98509-3. 15, 16, 48

[55] V. Bansaye & S. Méléard; *Stochastic models for structured populations* (Springer) (2015). 16, 17, 23, 24

[56] D. Kendall; «Stochastic processes and population growth»; Journal of the Royal Statistical Society, Series B (Methodological) **11**, p. 230—-282 (1949). 16

[57] W. Feller; «On the Integro-Differential Equations of Purely Discontinuous Markoff Processes»; TAMS **48**, p. 488—-515 (1940). 16

[58] B. Munsky & M. Khammash; «The finite state projection algorithm for the solution of the chemical master equation»; J. Chem. Phys. **124**, p. 044 104 (2006). 18, 46, 62, 80

[59] J. Kuntz; *Deterministic approximation schemes with computable errors for the distributions of Markov chains*; Phd thesis; Imperial College London (2017). 18, 46, 62, 80

[60] J. Kuntz, P. Thomas, G.-B. Stan & M. Barahona; «The exit time finite state projection scheme: bounding exit distributions and occupation measures of continuous-time Markov chains»; (2019). 18

[61] D. GILLESPIE; «A general method for numerically simulating the stochastic time evolution of chemical reactions»; J. Comput. Phys. **22**, p. 403–434 (1976). ISSN 0021-9991. 19, 69, 149

[62] M. KIMMEL & D. E. AXELROD; *Branching processes in biology (Interdisciplinary Applied Mathematics)*; 2ᵉ édition (Springer N.Y.) (2002). 19

[63] M. KIMMEL & D. AXELROD; *Branching processes in biology*; 19 (Springer-Verlag) (2015). 19, 20, 44

[64] K. B. ATHREYA & P. E. NEY; *Branching processes*; tome 196 (Springer Science & Business Media) (2012). 19

[65] T. E. HARRIS; *The theory of branching processes* (Springer-Verlag) (1963). 19, 21, 22, 44, 92, 95, 97, 106, 107, 108, 109, 162

[66] T. E. HARRIS; *The theory of branching processes* (Courier Corporation) (2002). 20

[67] V. VATUTIN, E. DYAKONOVA, P. JAGERS & S. SAGITOV; «A decomposable branching process in a markovian environment»; International Journal of Stochastic Analysis **2012** (2012). 21

[68] «Limit theorems for decomposable branching processes in a random environment»; **52**. 21

[69] V. VATUTIN & S. SAGITOV; «A decomposable critical branching process with two types of particles»; Trudy Mat. Inst. Steklov. **177**, p. 3–20 (1986). 21

[70] V. VATUTIN; «The structure of decomposable reduced branching processes. II. functionals limits theorems»; Theory Proba. Appl. **60**, p. 103–119 (2016). 21

[71] R. BELLMAN & T. HARRIS; «On the theory of age-dependent stochastic branching process»; PNAS **34**, p. 601—-604 (1948). 21

[72] R. BELLMAN & T. HARRIS; «On age-dependent branching process»; AM **55**, p. 280—-295 (1952). 21

[73] C. J. MODE; «A multidimensional age-dependent branching process with applications to natural selection. I»; Math. Biosci. **3**, p. 1–18 (1968). 21

[74] C. J. MODE; «A multidimensional age-dependent branching process with applications to natural selection. II»; Mathematical Biosciences **3**, p. 231–247 (1968). 21

[75] K. CRUMP & C. J. MODE; «An general age-dependent branching process I»; Journal of mathematical analysis and applications **24**, p. 494—-508 (1969). 21

[76] K. CRUMP & C. J. MODE; «An general age-dependent branching process II»; Journal of mathematical analysis and applications **25**, p. 8—-17 (1969). 21

[77] K. CRUMP & C. J. MODE; «An age-dependent branching process with correlations among sister cells»; Journal of Applied Probability **6**, p. 205—-210 (1969). 23

[78] N. Fournier & S. Méléard; «A microscopic probabilistic description of a locally regulated population and macroscopic approximations»; The Annals of Applied Probability **14**, p. 1880—-1919 (2004). 23

[79] N. Champagnat, R. Ferrière & S. Méléard; «From individual stochastic processes to macroscopic models in adaptive evolution»; Stoch. Models **24**, p. 2–44 (2008). ISSN 1532-6349. 23, 159

[80] N. Champagnat, R. Ferrière & S. Méléard; «Unifying evolutionary dynamics: from individual stochastic processes to macroscopic models»; Theoretical Population Biology **69**, p. 297–321 (2006). ISSN 0040-5809. 23

[81] G. Berzunza, A. Sturm & A. Winter; «Trait-dependent branching particle systems with competition and multiple offspring»; ArXiv (2018). 23

[82] F. Campillo, N. Champagnat & C. Fritsch; «Links between deterministic and stochastic approaches for invasion in growth-fragmentation-death models.»; Journal of Mathematical Biology **73**, p. 1781–1821 (2016). 23, 25

[83] F. C. Klebaner; *Introduction to stochastic calculus with applications*; 3e édition (Imperial College Press, London UK) (2012). 24, 25, 105, 106, 159

[84] V. C. Tran; *Modèles particulaires stochastiques pour des problèmes d'évolution adaptative et pour l'approximation de solutions statistiques*; Thèse de doctorat; Université de Nanterre-Paris X (2006). 24, 158

[85] V. Tran; «Large population limit and time behaviour of a stochastic particle model describing an age-structured population»; ESAIM: Probability and Statistics **12**, p. 345–386 (2008). 25, 103

[86] A. Raue, V. Becker, U. Klingmüller & T. J.; «Identifiability and observability analysis for experimental design in nonlinear dynamical models.»; Chaos **20** (2010). 26, 27, 28

[87] S. Cole, H. Chu & S. Greeland; «Maximum Likelihood, Profile Likelihood, and Penalized Likelihood: A Primer»; American Journal of Epidemiology **179**, p. 252–260 (2014). 27

[88] S. Cole, H. Chu & S. Greeland; «Maximum Likelihood, Profile Likelihood, and Penalized Likelihood: A Primer»; Applied Statistic **37**, p. 87–94 (1988). 27

[89] S. Murphy & A. Van der Vaart; «On Profile Likelihood»; Journal of the American Statistical Association **95**, p. 449–465 (2000). 27

[90] S. Quinn, T. Harris & D. Bacon; «Notes on likelihood intervals and profiling»; Communications in Statistics **29**, p. 109–129 (2000). 27

[91] A. Raue, B. Steiert, M. Schelker, C. Kreutz, T. Maiwald, H. Hass, J. Vanlier, C. Tönsing, L. Adlung, R. Engesser, W. Mader, T. Heinemann, J. Hasenauer, M. Schilling, T. Höfer, E. Klipp, F. Theis, U. Klingmüller, B. Schöberl & J. Timmer; «Data2Dynamics: a modeling environment tailored to parameter estimation in dynamical systems»; Bioinformatics **31**, p. 3558–3560 (2015). ISSN 1367-4803. 27, 98, 170

[92] S. HROSS & J. HASENAUER; «Analysis of CFSE time-series data using division- age- and label-strutured population models.»; Bioinformatics **32**, p. 2321–2329 (2016). 27

[93] M. GYLLENBERG, A. OSIPOV & L. PIVRINTA; «The inverse problem of linear age-structured population dynamics»; J. Evol. Equ. **2**, p. 223–239 (2002). 27, 29, 127, 128, 129, 130, 131, 147

[94] W. RUNDELL; «Determining the birth function for an age structured population»; Math. Popul. Stud. **1**, p. 377–395 (1989). 27, 29, 127, 128, 129, 130

[95] W. RUNDELL; «Determining the death rate for an age-structured population from census data»; SIAM J. Appl. Math. **53**, p. 1731–1746 (1993). 27, 29, 127, 128, 130, 147

[96] A. J. LOTKA; «On an integral equation in population analysis»; Ann. Math. Stat. **10**, p. 144–161 (1939). 27, 29, 127

[97] P. GABRIEL, S. P. GARBETT, V. QUARANTA, D. R. TYSON & G. F. WEBB; «The contribution of age structure to cell population responses to targeted therapeutics»; J. Theor. Biol. **311**, p. 19–27 (2012). 27, 29, 128, 129, 130

[98] A. PERASSO & U. RAZAFISON; «Identifiability problem for recovering the mortality rate in an age-structured population dynamics model»; Inverse Probl. Sci. Eng. **24**, p. 711–728 (2016)ISSN 1741-5977. 28, 110, 111, 128, 147

[99] H. KUNZE & E. VRSCAY; «Solving inverse problems for ordinary differential equations using the Picard contraction mapping»; Inverse Problems **15**, p. 745–770 (1999). 28

[100] H. KUNZE, J. HICKEN & E. VRSCAY; «Inverse problems for ODEs using contraction maps and suboptimality of the 'collage method'»; Inverse Problems **20** (2004). 28

[101] A. J. LOTKA; «The structure of a growing population»; Hum. Biol. **3**, p. 459–493 (1931). 29, 127

[102] H. SAWYER, P. SMITH, D. HEATH, J. JUENGEL, S. WAKEFIELD & K. MCNATTY; «Formation of ovarian follicles during fetal development in sheep»; Biol. Reprod. **66**, p. 1134–1150 (2002). 29, 38, 44

[103] «Développement folliculaire ovarien et ovulation chez les mammifères»; **22**. 30, 32

[104] D. MONNIAUX, V. CADORET, F. CLÉMENT, R. DALBIES-TRAN, S. ELIS, S. FABRE, V. MAILLARD, P. MONGET & S. UZBEKOVA; «Folliculogenesis»; dans I. HUHTANIEMI & L. MARTINI (rédacteurs), «Encyclopedia of Endocrine Diseases (Second Edition)», p. 377–398 (Elsevier) (2018); ISBN 978-0-12-801238-3. 29, 31, 43

[105] D. MONNIAUX; «Factors influencing establishment of the ovarian reserve and their effects on fertility»; Anim. Reprod. **15**, p. 635–647 (2018). 29, 38, 44

[106] D. MONNIAUX, F. CLÉMENT, R. DALBIÈS-TRAN, A. ESTIENNE, S. C. M. FABRE & P. MONGET.; «The ovarian reserve of primordial follicles and the dynamic reserve of antral growing follicles : what is the link ?»; Biology of reproduction **90** (2014). 29, 32, 34

[107] D. M. D. R. M.-A. Driancourt, A. Gougeon & C. Thibault.; «Folliculogénése et ovulation»; dans C. Thibault & M. Levasseur (rédacteurs), «La reproduction chez les mammiféres et l'homme», p. 317—-347 (INRA) (2001). 30, 31

[108] P. Reddy, W. Zheng & K. Liu; «Mechanisms maintaining the dormancy and survival of mammalian primordial follicles»; Trends Endocrinol. Metab. **21**, p. 96–103 (2010). 31, 44

[109] W. Wallace & T. Kelsey; «Human ovarian reserve from conception to the menopause»; PLos ONE **5**, p. e8772 (2010). 31

[110] J. Kerr, L. Brogan, M. Myers, K. Hutt, T. Mladenovska, S. Ricardo, K. Hamza, C. Scott, A. Strasser & J. Findlay; «The primordial follicle reserve is not renewed after chemical or γ-irradiation mediated depletion.»; Reproduction **143**, p. 469—-476 (2012). 31

[111] P. Monget, J. Bobe, A. Gougeon, S. Fabre, D. Monniaux & R. Dalbiès-Tran; «The ovarian reserve in mammals: a functional and evolutionary perspective»; Molecular and Cellular Endocrinology **356**, p. 2–12 (2012). 31

[112] A. Durlinger, P. Kramer, B. Karels, F. de Jong, J. Uilenbroeck, J. Grootegoed & A. Themmen; «Control of Primordial Follicle Recruitment by Anti-Müllerian Hormone in the Mouse Ovary»; Endocrinology **140**, p. 5789—-5796 (1999). 31

[113] C. Ruoss, A. Tadros, T. O'Shea, J. McFarlane & G. Almahbobi; «Ovarian follicle development in Booroola sheep exhibiting impaired bone morphogenetic protein signalling pathway»; Reproduction **138**, p. 689–696 (2009). 31

[114] H. Picton; «Activation of follicle development: the primordial follicle»; Theriogenology **55**, p. 1193 – 1210 (2001). 32, 44

[115] J. Fortune; «The early stages of follicular development: activation of primordial follicles and growth of preantral follicles»; Anim. Reprod. Sci. **78**, p. 135 – 163 (2003). 32, 44

[116] T. Lundy, P. Smith, A. O'connell, N. L. Hudson & K. P. McNatty; «Populations of granulosa cells in small follicles of the sheep ovary»; J Reprod Fertil **115**, p. 251–262 (1999). 33, 34, 36, 38, 44, 45, 67, 113

[117] T. Wilson, X. Wu, J. Juengel, I. Ross, J. Lumsden, E. Lord, K. Dodds, G. Walling, J. Mcewan, A. O'connell, K. Mcnatty & G. Montgomery; «Highly Prolific Booroola Sheep Have A Mutation In The Intracellular Kinase Domain Of Bone Morphogenetic Protein Ib Receptor (Alk-6) That Is Expressed In Both Oocytes And Granulosa Cells.»; Biol. Reprod. **64**, p. 1225–1235 (2001). 33, 67

[118] T. Pedersen & H. Peters; «Proposal for a classification of oocytes and follicles in the mouse ovary.»; J Reprod Fertil. **17**, p. 555–557 (1968). 34

[119] R. Braw-Tal & S. Yossefi; «Studies in vivo and in vitro on the initiation of follicle growth in the bovine ovary»; J. Reprod. Fertil. **109**, p. 165–171 (1997). 34, 44, 67

[120] K. McNatty, P. Smith, N. Hudson, D. Heath, D. Tisdall, W. O & R. Braw-Tal; «Development of the sheep ovary during fetal and early neonatal life and the effect of fecundity genes»; J. Reprod. Fertil. Suppl. **49**, p. 123–135 (1995). 35, 37

[121] P. Smith, W.-S. O, N. L. Hudson, L. Shaw, D. A. Heath, L. Condell, D. J. Phillips & K. P. McNatty; «Effects of the Booroola gene (FecB) on body weight, ovarian development and hormone concentrations during fetal life»; J Reprod Fertil **98**, p. 41–54 (1993). ISSN 1470-1626, 1741-7899. 35, 113

[122] P. Smith, R. Braw-Tal, K. Corrigan, N. L. Hudson, D. A. Heath & K. P. Mc-Natty; «Ontogeny of ovarian follicle development in Booroola sheep fetuses that are homozygous carriers or non-carriers of the FecB gene»; J Reprod Fertil **100**, p. 485–490 (1994). 35, 113

[123] L. P. Cahill & P. Mauleon; «A study of the population of primordial and small follicles in the sheep»; Journal of reproduction and fertility **61**, p. 201–206 (1981). 38

[124] A. R. Clark & J. Kruger; «Mathematical modeling of the female reproductive system: from oocyte to delivery»; WIREs Syst Biol Med p. 9:e13532 (2017). 39

[125] F. Clément & D. Monniaux; «Multiscale modelling of ovarian follicular selection»; Prog. Biophys. Mol. Biol. **113**, p. 398–408 (2013). 39

[126] F. Clément, F. Robin & R. Yvinec; «Stochastic nonlinear model for somatic cell population dynamics during ovarian follicle activation»; arXiv . 43

[127] P. Getto & A. Marciniak-Czochra; «Mathematical modelling as a tool to understand cell self-renewal and differentiation»; Methods Mol. Biol. **1293**, p. 247–266 (2015). 44

[128] T. Stiehl & A. Marciniak-Czochra; «Stem cell self-renewal in regeneration and cancer: Insights from mathematical modeling»; Methods Mol. Biol. **5**, p. 112–120 (2017). 44

[129] L. Pujo-Menjouet; «Blood cell dynamics: half of a century of modelling»; Math. Model. Nat. Phenom. **11**, p. 92–115 (2016). 44

[130] R. Darling & A. Siegert; «The first passage problem for a continuous markov process»; Ann. Math. Statist. **24**, p. 624–639 (1953). 44

[131] N. Van Kampen; *Stochastic processes in physics and chemistry*; tome 1 (Elsevier) (1992). 44

[132] T. Chou & M. D'Orsogna; «First Passage Problems in Biology»; dans «First-passage phenomena and their Applications», p. 306–345 (World Scientific) (2014). 44

[133] M. Castro, M. López-García, C. Lythe & C. Molina-París; «First passage events in biological systems with non-exponential inter-event times»; Sci. Rep. **8**, p. 15 054 (2018). 44

[134] C. Marr, M. Strasser, M. Schwarzfischer, T. Schroeder & F. Theis; «Multi-scale modeling of GMP differentiation based on single-cell genealogies»; FEBS J. **279**, p. 3488–500 (2012). 44

[135] I. Glauche, M. Cross, R. Loeffler & I. Roeder; «Lineage specification of hematopoietic stem cells: mathematical modeling and biological implications»; Stem Cells **25**, p. 1791–1799 (2007). 44

[136] A. Gougeon & G. Chainy; «Morphometric studies of small follicles in ovaries of women at different ages»; J. Reprod. Fertil. **81**, p. 433–442 (1987). 44, 67

[137] S. Meredith, G. Dudenhoeffer & K. Jackson; «Classification of small type B/C follicles as primordial follicles in mature rats»; J. Reprod. Fertil. **119**, p. 43–48 (2000). 44, 67

[138] A. Raue, C. Kreutz, T. Maiwald, J. Bachmann, M. Schilling, U. Klingmöller & J. Timmer; «Structural and practical identifiability analysis of partially observed dynamical models by exploiting the profile likelihood»; Bioinformatics **25**, p. 1923–1929 (2009). ISSN 1367-4803. 44, 67, 71, 72, 114, 170

[139] P. Da Silva-Buttkus, G. Jayasooriya, J. Mora, M. Mobberley, T. Ryder, M. Baithun, J. Stark, S. Franks & K. Hardy; «Effect of cell shape and packing density on granulosa cell proliferation and formation of multiple layers during early follicle development in the ovary»; J. Cell Sci. **121**, p. 3890–3900 (2008). 45

[140] D. Monniaux; «Driving folliculogenesis by the oocyte-somatic cell dialog: Lessons from genetic models»; Theriogenology **86**, p. 41–53 (2016). 45

[141] H. Zhang, S. Risal, N. Gorre, K. Busayavalasa, X. Li, Y. Shen, B. Bosbach, M. Brännström & K. Liu; «Somatic cells initiate primordial follicle activation and govern the development of dormant oocytes in mice»; Curr. Biol. **24**, p. 2501–2508 (2014). ISSN 0960-9822. 45

[142] P. Knight & C. Glister; «TGF-beta superfamily members and ovarian follicle development.»; Reproduction **132**, p. 191–206 (2006). 45

[143] K. Reader, L. Haydon, R. Littlejohn, J. Juengel & K. McNatty; «Booroola BMPR1B mutation alters early follicular development and oocyte ultrastructure in sheep»; Reprod. Fertil. Dev. **24**, p. 353–361 (2012). 45

[144] D.-E. Gratie, B. Iancu & I. Petre; «ODE analysis of biological systems»; dans «Formal Methods for Dynamical Systems», p. 29–62 (Springer) (2013). 46

[145] D. Gillespie; «Approximate accelerated stochastic simulation of chemically reacting systems»; J. Chem. Phys. **115**, p. 1716–1733 (2001). 47

[146] R. Storn & K. Price; «Differential evolution – a simple and efficient heuristic for global optimization over continuous spaces»; J. Global Optim. **11**, p. 341–359 (1997). https://doi.org/10.1023/A:1008202821328. 71

[147] K. Burnham & D. Anderson; *Model selection and multimodel inference: a practical information theoretic approach*; 2e édition (Springer-Verlag New York) (2003). 76, 77

[148] F. Clément, F. Robin & R. Yvinec; «Analysis and Calibration of a Linear Model for Structured Cell Populations with Unidirectional Motion: Application to the Morphogenesis of Ovarian Follicles»; SIAM J. Appl. Math. **79**, p. 207–229 (2019). 81

[149] P. MICHEL, S. MISCHLER & B. PERTHAME; «General relative entropy inequality: an illustration on growth models»; J. Math. Pures Appl. **84**, p. 1235–1260 (2005). ISSN 0021-7824. 92, 101

[150] P. JAGERS & F. C. KLEBANER; «Population-size-dependent and age-dependent branching processes»; Stochastic Process. Appl. **87**, p. 235–254 (2000). 92, 97

[151] P. E. PROTTER; *Stochastic Integration and Differential Equations*; 2ᵉ édition (Appl. Math. (N.Y.) 21, Springer-Verlag, Berlin) (2004); ISBN 978-3-662-10061-5. 105, 106, 157, 160

[152] B. PERTHAME, F. QUIRÓS & J. VÁZQUEZ; «The Hele–Shaw asymptotics for mechanical models of tumor growth»; Arch. Rational Mech. Anal. **212**, p. 93–127 (2014). 121, 124, 150

[153] A. MELLET, B. PERTHAME & F. QUIRÓS; «A Hele–Shaw problem for tumor growth»; Journal of Functional Analysis **273**, p. 3061–3093 (2017). 121, 124

[154] B. PERTHAME; *Some mathematical models of tumor growth* (Lectures at Université Pierre et Marie Curie) (2016). 121, 122, 150

[155] V. RUNGE; *Éléments d'analyse et de contrôle dans le problème de Hele–Shaw*; Thèse de doctorat; École doctorale InfoMaths ED512, École Centrale de Lyon (2014). 121

[156] H. BYRNE & M. CHAPLAIN; «Growth of nonnecrotic tumors in the presence and absence of inhibitors.»; Math Biosci. **130**, p. 151–81 (1995). 122, 124

[157] G. ALLAIRE; *Analyse numérique et optimisation, Une introduction à la modélisation mathématique et à la simulation numérique* (Ecole Polytechnique) (2013). 123

[158] S. MOTSCH & D. PEURICHARD; «From short-range repulsion to Hele-Shaw problem in a model of tumor growth»; J. Math. Biol. p. 1–30 (2017). 124

[159] X. CHEN & A. FRIEDMAN; «A free boundary problem for an elliptic-hyperbolic system: an application to tumor growth»; SIAM J. Math. Anal. **35**, p. 974—-986 (2003). 124

[160] S. CUI & A. FRIEDMAN; «A hyperbolic free boundary problem modeling tumor growth»; INTERFACES AND FREE BOUNDARIES **5**, p. 159—-182 (2003). 124

[161] B. PERTHAME, F. QUIRÓS & J. VÁZQUEZ; «The Hele–Shaw asymptotics for mechanical models of tumor growth»; Arch. Rational Mech. Anal. **212**, p. 93—-127 (2014). 125

[162] P. VAN LIEDEKERKE, M. M. PALM, N. JAGIELLA & D. DRASDO; «Simulating tissue mechanics with agent-based models: concepts, perspectives and some novel results»; Computational Particle Mechanics **2**, p. 401–444 (2015). 126

[163] D. IBER, S. TANAKA, P. FRIED, P. GERMANN & D. MENSHYKAU; «Simulating tissue morphogenesis and signaling»; dans N. C. (EDS) TISSUE MORPHOGENESIS. (rédacteur), «Methods in Molecular Biology (Methods and Protocols)», , tome 1189p. 323–338 (2014). 126

[164] F. Clément, B. Laroche & F. Robin; «Analysis and numerical simulation of an inverse problem for a structured cell population dynamics model»; Mathematical Biosciences and Engineering **16**, p. 3018–3046 (2019). 127

[165] P. Gwiazda, T. Lorenz & A. Marciniak-Czochra; «A nonlinear structured population model: Lipschitz continuity of measure-valued solutions with respect to model ingredients»; J. Differ. Equ. **248**, p. 2703–2735 (2010). 128, 142

[166] T. Bourgeron, M. Doumic & M. Escobedo; «Estimating the division rate of the growth-fragmentation equation with a self-similar kernel»; Inverse Problems **30**, p. 025 007 (2014). 128

[167] N. Champagnat, S. Méléard & V. Tran; «Stochastic analysis of emergence of evolutionary cyclic behavior in population dynamics with transfer»; ArXiv (2019). 149, 150

[168] P. Metzger, J. Hasenauer & F. Allgower; «Modeling and analysis of division-, age-, and label-structured cell populations»; Proceedings of 9th International Workshop on Computational Systems Biology p. 55—-58 (2012). 149

[169] B. Drawert, A. Hellander, B. Bales, D. Banerjee, G. Bellesia, B. J. D. Jr, G. Douglas, M. Gu, A. Gupta, S. Hellander, C. Horuk, D. Nath, A. Takkar, S. Wu, P. Lötstedt, C. Krintz & L. R. Petzold; «Stochastic simulation service: bridging the gap between the computational expert and the biologist»; PLoS Comput. Biol. **12**, p. e1005 220 (2016). ISSN 1553-7358. 167